UNIVERSITY OF SOUTHAMPTON

FACULTY OF NATURAL AND ENVIRONMENTAL SCIENCE

Ocean and Earth Science

Volume 1 of 1

High-Resolution Records of Deglaciation and Palaeomagnetism in the Late-Quaternary Sediments of Windermere, UK

by

Rachael Avery

Thesis for the degree of Doctor of Philosophy

September 2017

UNIVERSITY OF SOUTHAMPTON

ABSTRACT

FACULTY OF NATURAL AND ENVIRONMENTAL SCIENCE

Palaeoclimate

Thesis for the degree of Doctor of Philosophy

HIGH-RESOLUTION RECORDS OF DEGLACIATION AND PALAEOMAGNETISM IN THE LATE-QUATERNARY SEDIMENTS OF WINDERMERE, UK

by Rachael Sarah Avery

Windermere, in the Lake District, UK, is a glacial ribbon lake that has accumulated sediment since its exposure after the retreat of the British and Irish Ice Sheet (BIIS). A coring campaign by the British Geological Survey in partnership with the University of Southampton has recovered a suite of sediment cores from Windermere, which document lacustrine sedimentation from ~15 ka to the present day.

The varved nature of some of the sediments has offered the opportunity to investigate the nature and timing of events in the northern UK over the Lateglacial (~14.7 – 11.7 ka BP). In particular, the placement of Windermere between continental Europe and Greenland provided the impetus to investigate the laminations further, with the possibility that climatic leads and lags across the region may be identified should the chronology prove robust enough. Also, the seismic work already carried out in Windermere implied that the initial retreat of ice from the lake during the last deglaciation was fairly rapid, and the recovery of the cores was intended in part to test this claim using suspected varves recovered. A third possibility, once the cores had been recovered and other investigations were underway (prior to this study), was that the palaeomagnetic nature of the sediment may be ascertained and the UK palaeomagnetic master curve of Turner & Thompson (1981; obtained in part from Windermere sediments) may be updated and extended using newer measurement and dating techniques.

A suite of techniques were used to analyse the cores, including (but not limited to) scanning electron microscope imagery of resin-embedded thin sections, Itrax XRF core scanning, palaeomagnetic measurements, and grain size analysis.

The upper part of the varve sequence is more organic-rich and was radiocarbon-dated to provide a Holocene (~11.7 ka – present) age-depth model. Palaeomagnetic measurements from the Holocene were placed on this age-depth model and stacked to form a new Holocene geomagnetic palaeosecular variation curve for the UK, WINPSV-12K. The pre-Holocene (~15 – 11.7 ka BP) sediments were not suitable for palaeomagnetic stack creation, thus the original UK master curve of Turner & Thompson (1981) was not able to be extended.

The pre-Holocene (~15 – 11.7 ka BP) sediments of Windermere yield several sequences of annually laminated sediments, or varves. The lowermost varves represent a period of ~250 yr prior to the onset of the Lateglacial Interstadial (~14.7 – 12.9 ka BP), and document ice retreat of the Lake District ice cap (which had separated from the receding British and Irish Ice Sheet) up the North Basin of the lake. The final collapse of the Trout Beck valley glacier occurred in 36-40 vyr. Seismic reflection imaging indicates the possibility of a further >40 m of varves in the South Basin.

The Younger Dryas-age (~12.9 – 11.7 ka BP) sediment sequences of the South Basin are interrupted by large mass transport deposits. The Younger Dryas-age varves in the North Basin appear to predominantly nival (i.e. snowmelt-induced) in style. The early Younger Dryas-age varves exhibit evidence of stormy conditions (e.g. bioturbation from wind mixing), as reported from other North Atlantic- influenced sites. The later varves show higher instances of less-bioturbated varves and more precipitation (i.e. thicker varves), as the sea ice extent decreased and the polar front-related storm tracks moved north of the UK. Our results show the potential for construction of precise annually resolved record throughout the Younger Dryas interval.

Spectral analysis of selected varve sequences from the pre-Interstadial period (pre- ~14.7 ka BP) and the Younger Dryas age (~12.9 – 11.7 ka BP) sediments shows that interannual variability between 2 – 4 yr, often associated with the Quasi-Biennial Oscillation and teleconnections of El Niño-La Niña events, was ubiquitously present. Interannual variability in the 4 – 7 yr band was however absent in the pre-Interstadial sequence but present in the Younger Dryas sequences, in keeping with current thinking that variability in El Niño strength was damped prior to ~14 ka BP.

This study has shown that Windermere is a site sensitive to regional climatic and geomagnetic variability, and the annual resolution of the pre-Holocene sediments has afforded many insights into the deglacial history of the Lake District.

Table of Contents

List of Tables

List of Figures

DECLARATION OF AUTHORSHIP

I, RACHAEL S. AVERY

declare that this thesis and the work presented in it are my own and has been generated by me as the result of my own original research.

High-Resolution Records of Deglaciation and Palaeomagnetism in the Late-Quaternary Sediments of Windermere, UK

I confirm that:

1. This work was done wholly or mainly while in candidature for a research degree at this University;
2. Where any part of this thesis has previously been submitted for a degree or any other qualification at this University or any other institution, this has been clearly stated;
3. Where I have consulted the published work of others, this is always clearly attributed;
4. Where I have quoted from the work of others, the source is always given. With the exception of such quotations, this thesis is entirely my own work;
5. I have acknowledged all main sources of help;
6. Where the thesis is based on work done by myself jointly with others, I have made clear exactly what was done by others and what I have contributed myself;
7. Parts of this work have been published as: Avery, R. S., Xuan, C., Kemp, A. E. S., Bull, J. M., Cotterill, C. J., Fielding, J. J., Pearce, R. B., and Croudace, I. W. (2017), A new Holocene record of geomagnetic secular variation from Windermere, UK. Earth and Planetary Science Letters, 477C (2017) pp. 108-122, DOI 10.1016/j.epsl.2017.08.025

Signed: RACHAEL AVERY

Date: 14/03/2018

Acknowledgements

Financial Support

This project was funded by a British Geological Survey BUFI studentship (reference S243) in collaboration with the University of Southampton.

This work was supported by the NERC Radiocarbon Facility NRCF010001 (allocation numbers 1856.1014 and 1736.1013).

Information, advice, guidance, and technical help

Firstly, I would like to thank my supervisors Alan Kemp, Jon Bull, Carol Cotterill, and Chuang Xuan for all of their technical advice, pastoral help, general guidance, fieldwork assistance, draft comments, patience, and so much more. I would also like to thank Richard Pearce for his help with everything SEM and lab related.

Thanks also go to Suzanne MacLachlan and the BOSCORF staff. Kate Davis and Barry Marsh have been invaluable in all things photography related. Ian Croudace orchestrated the lead and caesium dating of some of the cores, which has been invaluable. Matt Cooper, Charlie Thompson, and Ross Williams have also assisted in various forms of lab work.

I would like to thank Pete Langdon, Pete Morgan, Hayley Goodes, and Alistair Monteith for their help with my search for tephra both in terms of helping me learn my way around the Geography labs, procedures, and equipment; and in terms of helping me to learn what to look for in the microscope! Pete Langdon (and his family) and Pete Morgan were a real help on the fieldwork coring our Low Wray Bay cores, providing equipment and in-the-field help.

In the Lake District itself, I would like to thank the Lake Wardens for their practical assistance, as well as the staff at the Freshwater Biological Association and Ben James, the skipper of the RV John Lund. Special thanks go to Liz Haworth whose extraordinary knowledge of the Lake District has been particularly useful.

At the BGS, I would like to thank Tom Bradwell and Emrys Philips in particular for their technical expertise, patience, and encouragement; and Melanie Leng for providing useful data. Thanks also go to all those (in particular Claire Mellet, Emrys Philips, and Carol Cotterill) who helped me feel welcome and comfortable during my stay in Edinburgh.

I am also grateful to Callum, Ellie, Amber, and Charlotte for their work on the Windermere sediments for their MSci Geology projects.

This project could not have been completed without the magnificent efforts of Bob Jones, John Ford, and Dan Doran in the sectioning lab, producing all of those thin sections!

My thanks go out to Helen Miller, whose previous work on Windermere has provided a solid bedrock for my own work, who helped with lots of the early fieldwork and core processing, and whose encouragement and advice from back in my first year has been appreciated more and more as I've progressed through this project. You were right: I did get through it.

Finally, thank you to Steve Bohaty and Bernd Zolitschka who examined this thesis and conducted my viva, and who provided many constructive comments.

Personal Support

Firstly, I would like to thank James Fielding, colleague on my sister-project, office-mate, and a good friend. He has been my lab partner and fieldwork partner, conference-buddy, and a source of humour for all occasions. I think we have both helped each other and it was great to collaborate with such a genuinely lovely person.

I would also like to thank my other office-mates who have been a source of humour, comfort, writing-advice, IT help, and company. In particular, Cat and Manon have really helped through low periods and have been a great source of solace, laughter, and houmous.

So many other friends have been important in so many ways, whether it was getting me into bouldering, or inviting me to social events, or just listening to me vent. Thank you all, you are too many to name!

Thanks also to my family for always being there and for giving me a space in which there was no pressure to have to be good at anything, or even mention work. It is worth more than you know.

Finally, David. Without you, I don't know how I would have got through this. You've been there with something to comfort my every crisis of confidence, illness, homesickness, lab failure, and frustration. You've helped me laugh more, not to take work home with me, and to learn about the world in different ways, and I will be forever grateful.

Definitions and Abbreviations

AF: Alternating field

AMO: Atlantic Multidecadal Oscillation

AMOC: Atlantic Meridional Overturning Circulation

AMS: Accelerator Mass Spectrometry

AO: Arctic Oscillation

ARM: Anhysteretic Remanent Magnetisation

ARMacq: acquired Anhysteretic Remanent Magnetisation

As: Arsenic

BGS: British Geological Survey

BIIS: British-Irish Ice Sheet

BOSCORF: British Ocean Sediment Core Research Facility

BSEI: Backscatter electron image

BVG: Borrowdale Volcanic Group

Ca: Calcium

cal yr BP: calendar years before present (where 'present' is defined as 1950 AD)

^{12}C, ^{13}C, and ^{14}C: Isotopes of carbon with 6, 7, and 8 neutrons respectively

CIS: Core Imaging System

CTS: Covered thin section

CO_2: Carbon dioxide

Cs: Caesium

DC: Direct current

D-O: Dansgaard-Oeschger

DI: De-ionised

EDS: Energy-dispersive X-ray spectroscopy

ENSO: El Niño – Southern Oscillation

Fe: Iron

GAD: Geocentric Axial Dipole

G-IG: Glacial-interglacial

GI: Greenland Interstadial

GIS: Geographical Information System

GPS: Global positioning system

GS: Greenland stadial

HCl: Hydrochloric acid

HNO_3: Nitric acid

HS: Heinrich Stadial

IODP: Integrated Ocean Drilling Program

IRM: Isothermal Remanent Magnetisation

K: potassium

kcps: kilocounts per second

LGM: Last Glacial Maximum

LLS: Loch Lomond Stadial

LoI: Loss on ignition

LWB: Low Wray Bay

MDF: Median Destruction Field

Mn: Manganese

MTD: Mass transport deposit

MTM: Multi-taper method

NAO: North Atlantic Oscillation

NERC: Natural Environment Research Council

NH: Northern Hemisphere

NNA: Northern North Atlantic

NRCF: National Radiocarbon Facility

NRM: Natural Remanent Magnetisation

OSL: Optically-stimulated luminescence

Pb: Lead

PDO: Pacific Decadal Oscillation

PSD: Pseudo-single domain

PSV: Palaeosecular Variation

PTS: Polished thin section

QBO: Quasi-Biennial Oscillation

ROI: Region(s) of interest

RPI: Relative Palaeointensity

RPM: Revolutions per minute

S: Sulphur

SEM: Scanning Electron Microscope

SF: Seismic Facies

SH: Southern Hemisphere

SHED: Schmidt-Hammer Exposure Dating

Si: Silica

SPT: Sodium polytungstate

Sr: Strontium

SRM: Superconducting Rock Magnetometer

Ti: Titanium

VGP: Virtual Geomagnetic Pole

VSM: Vibrating Sample Magnetometer

Vyr: Varve year

WI: Windermere Interstadial

XRD: X-ray diffraction

YD: Younger Dryas

XRF: X-ray fluorescence

1. Introduction

This thesis investigates a suite of sediment cores recovered from Windermere, UK, which record sedimentation into the lake since the retreat of the British-Irish Ice Sheet. Much Quaternary research is focussed on the nature and timing of rapid climate changes, and the cores from Windermere are able to provide new insights into the rapidity of initial ice retreat in the catchment, the landscape of the Younger Dryas (GS-1, Loch Lomond Stadial), and lake events in the Lateglacial Interstadial. Data from the cores are also used to produce a new, well-dated, Holocene palaeomagnetic reference curve that may aid regional stratigraphic correlations. In this chapter the climatic context of the studied period is introduced, an overview of the lake coring programs given, and the aims and structure of this thesis are outlined.

1.1 Climatic Setting

1.1.1 Glacial-Interglacial Cycles

The Cenozoic has seen a gradual long-term decrease in global temperatures and carbon dioxide (CO_2) levels, culminating in the relatively rapid shorter-term temperature and CO_2 cycles of the Pleistocene and Holocene (Beerling and Royer, 2011; Zachos et al., 2008). Each full cycle, known as a glacial-interglacial (G-IG) cycle, comprised a slower descent into colder, CO_2-poor conditions, and a rapid resurgence into warmer, CO_2-richer conditions (Lisiecki and Raymo, 2005). This pattern emerged at 2.73 Ma with each G-IG cycle lasting around 41 kyr, likely paced with the Milankovitch obliquity cycles. At 1.25 – 0.9 Ma the periodicity shifted to ~100 kyr. The G-IG cycles intensified over the course of the Pleistocene with cycles in the last 700 ka exhibiting CO_2 levels of 280-300 ppm (known as 'pre-industrial') during the Interglacials and 180 ppm during the Glacials (Barnola et al., 1987). Interglacial periods were largely similar to today's climate (prior to anthropogenic global warming), whilst glacial periods were characterised by the growth of large ice sheets over large high- and mid-latitude continental areas including North America, Russia, and Europe, and a drop in global temperature (Hughes et al., 2016).

The primary underlying driver for G-IG cycles is thought to be insolation (solar radiation reaching the planet's surface) in the Northern Hemisphere, with interglacials mainly coinciding with periods of higher summer Northern Hemisphere insolation. Temperature

and summer insolation in the Southern Hemisphere are out of phase (Berger and Loutre, 1991; Kawamura et al., 2007). The fluctuations in ice-sheet volume exhibit a saw-toothed pattern, with full-glacial periods lasting 40-100 kyr and the interglacial periods lasting only 5-40 kyr (Lisiecki and Raymo, 2005). The quasi-100 kyr periodicity is only weakly linked with the eccentricity cycle (period 100 & 400 kyr; the ellipticity of Earth's orbit) and more strongly associated with every fourth or fifth precession cycle (period 19 & 23 kyr; the orientation of Earth's rotational axis) (Maslin and Ridgwell, 2005). The exact reason for this transition in the nature of nonlinear Earth-system feedbacks and ice-sheet response to insolation is still unknown, although it is likely that changes in ocean circulation and deep-ocean carbon storage played a significant role in driving pCO_2 variations (e.g. Lear et al., 2016). Each G-IG cycle has resulted in mass migrations and extinctions (or retreats to refugia) of both marine and terrestrial macro- and microfauna including the migration and evolution of hominids (e.g. Frumkin et al., 2011; Médail and Diadema, 2009).

1.1.2 The Last Glacial Cycle

Ice sheets from each successive glaciation have eroded most of the evidence of their predecessors, so the record from last glacial period is the best preserved and yields the most internal detail. The last G-IG cycle followed the pattern of the previous cycles with stepped glaciation followed by rapid deglaciation (Lisiecki and Raymo, 2005). Present in each G-IG cycle are several smaller millennial-scale temperature and CO_2 features. In the Greenland ice-core records of the last glacial cycle, there are several warm-cool oscillations known as Dansgaard-Oeschger cycles. It is thought that these were present in other G-IG cycles too, but the Greenland ice cores do not extend beyond the last glacial cycle (Rasmussen et al., 2016). Dansgaard-Oeschger cycles identified in the Greenland ice cores, and the Nordic Sea and North Atlantic, exhibit a saw-tooth shape with a rapid warming phase of only a few decades to warm Interstadial conditions, followed by a stepped cooling phase over a much longer period and a rapid drop to cold Stadial conditions (Johnsen et al., 1992). During many of these stadials, massive discharges from the Laurentide Ice Sheet led to the deposition of ice-rafted debris in the North Atlantic known as Heinrich layers (Bond and Lotti, 1995). The stadials in which Heinrich events occur are commonly referred to as Heinrich Stadials (Sanchez Goñi and Harrison, 2010).

During the last glacial period as temperatures dropped, ice sheets gradually spread over much of the Arctic Ocean and Northern Hemisphere continents to the mid-latitudes (Hughes et al., 2016). The increase in terrestrial ice volume, as inferred by both

geomorphological evidence and benthic oxygen isotope data, caused sea level to drop by 120 m (Rohling et al., 1998). In addition, the presence of the ice sheets- up to a few km thick- diverted the polar jet stream and perturbed regional hydrological cycles (Shinn and Barron, 1989). The last glacial period culminated in the Last Glacial Maximum (LGM) which occurred in the Northern Hemisphere between 26.5 and 19 ka (Clark et al., 2009). At the LGM the ice sheets covered parts of Europe (Ehlers et al., 2011), and the British-Irish ice sheet covered most of the UK (C. D. Clark et al., 2012).

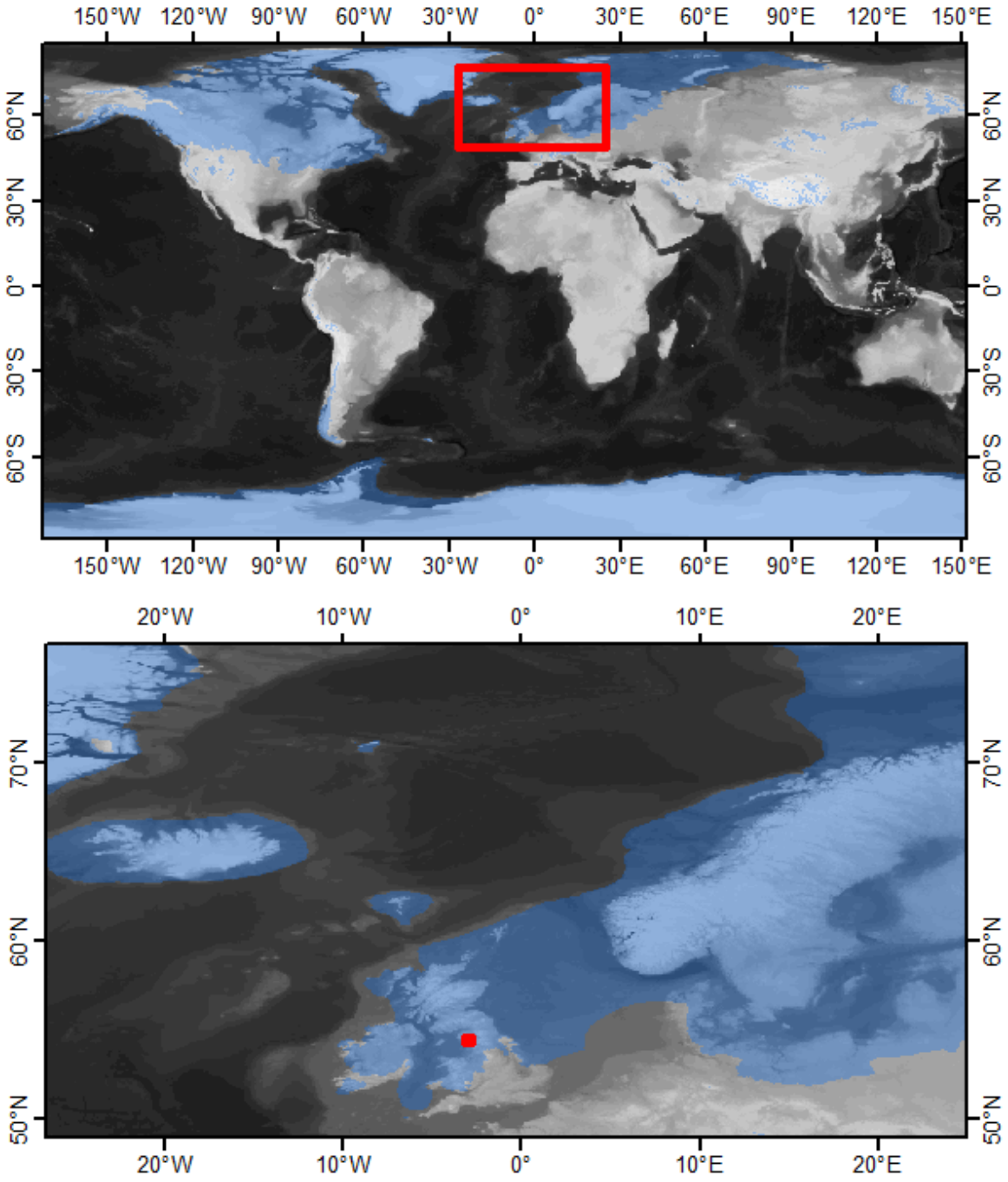

Figure 1.1 Extent of Last Glacial Maximum ice globally (top) and in the region surrounding the study area (bottom). Topography and bathymetry shown as greyscale; red dot in bottom panel indicates location of study area. Semi-transparent blue overlay indicates ice sheet extent. The data was produced by (Ehlers et al., 2011)

1.1.3 Deglaciation of the Northern Hemisphere

1.1.3.1 The Northern Hemisphere and Europe

After 19-23 ka the climate in Europe and North America rapidly warmed and the ice sheets began to retreat; the Laurentide ice sheet had reduced to a fraction of its size by 8 ka BP, and the Eurasian ice sheets had effectively disappeared around 9.6 (Fennoscandian) and 15 (British-Irish) ka BP (Clark et al., 2009). Several abrupt climate shifts occurred during the rapid deglaciation between 19 and ~11.7 ka (Lowe et al., 2008), most notably a relatively rapid widespread deglaciation accelerated by an abrupt warming to the Lateglacial Interstadial (GI-1; Bølling-Allerød) at around 14.7 cal ka BP (the Greenland-based event stratigraphy of which is split into 5 minor warm and cool phases (Björck et al., 1998)). Temperature and circulation changes in the deep North Atlantic Ocean which likely triggered the abrupt Bølling-Allerød warming have been detected as early as 15.6 cal ka BP (Thiagarajan et al., 2014). The interval between 18 ka BP and the onset of GI-1 is referred to as Heinrich Stadial 1 (HS1), and is punctuated at around 16.1 cal ka BP with the coldest North Atlantic conditions occurring after this (Broecker and Putnam, 2012). The warming occurred across Europe (e.g. van der Hammen, 1951), but has also been detected in Lake El'gygytygyn in North-Eastern Siberia (Asikainen et al., 2007). In Hässeldala, Sweden, reconstructed July temperatures increase between 14.1 and 13.1 cal ka BP (Wohlfarth et al., 2016). A similar, shorter period occurred in North America called the Two Creeks interval (Kaiser, 1994). In all type locations, the Interstadial is characterised by the presence of macrofossils associated with warmer and wetter conditions than the previous Stadial, although deuterium records from Hässeldala in Sweden and Meerfelder Maar in Germany indicate that the Interstadial was more humid in Germany than Sweden (Wohlfarth et al., 2016). In the Southern Hemisphere, there are records showing cooling at this time, indicative of the bipolar see-saw driven by the Atlantic Meridional Overturning Circulation (AMOC) (Shakun and Carlson, 2010).

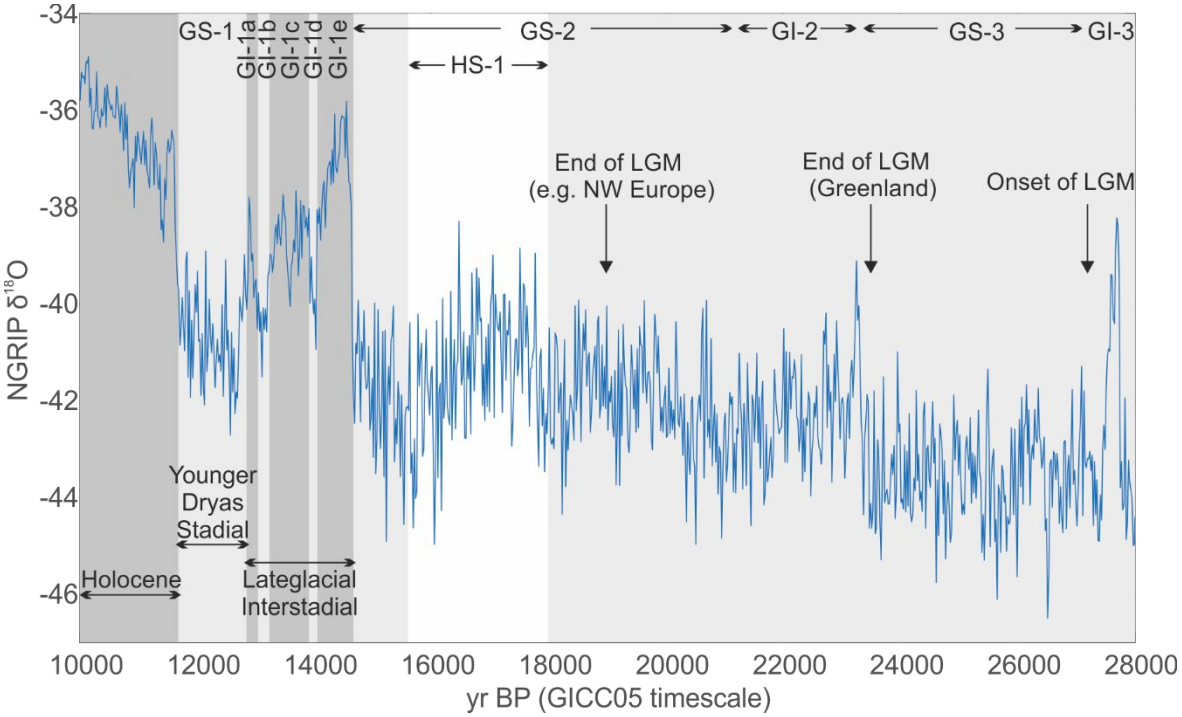

Figure 1.2 NGRIP $\delta^{18}O$ data demonstrating the phases within the last deglaciation. Note that the Greenland record is not applicable to all of Europe in detail and that the event timings will be different due to climate diachroneity, but the major climate events of the deglaciation are evident. GS: Greenland Stadial; GI: Greenland Interstadial; HS: Heinrich Stadial; LGM: Last Glacial Maximum. Higher $\delta^{18}O$ values in ice indicate higher air temperature at the ice surface. Data from (NGRIP Dating Group 2006).

A brief hydroclimatic cooling and drying occurred at about 12.9. cal ka BP (GS-1, Younger Dryas, Loch Lomond Stadial), which was essentially restricted to the Northern Hemisphere (the Southern Hemisphere becoming warmer and wetter). Although the average global temperature decreased by ~0.6 ^{o}C during this period, regional manifestations differed and the bipolar see-saw was active (Shakun and Carlson, 2010). This brief Northern Hemisphere return to cold conditions during the overall warming is associated with a combination of slowing of the AMOC, negative radiative forcing, and changed atmospheric circulation (Renssen et al., 2015). There was cooling of 2-3 ^{o}C across most of continental Europe and 8 ^{o}C in Greenland and offshore Canada, but evidence from around the British Isles is less clear with a possible small warming offshore Ireland (Shakun and Carlson, 2010). The start of the Younger Dryas appears to have occurred 100-250 years earlier in Greenland than anywhere else, with northern Ireland cooling next and followed by Scandinavia and Western continental Europe (Muschitiello and Wohlfarth, 2015; Wohlfarth et al., 2016). The Stadial is reported to have a bipartite structure in Europe and the North Atlantic, with the first part of the Younger Dryas being colder and drier and the second part warming and wettening somewhat (Bakke et al., 2009). The transition between these two phases is shown to be rapid but diachronous across the region, as the polar front shifted northwards from northern Iberia and the Alps to its present location south of Greenland (Lane et al., 2013).

The transition from the Younger Dryas to the early Holocene was rapid. GS-1 (broadly equivalent to the YD but bounded by changes in deuterium excess in Greenland ice rather than terrestrial Scandinavian environmental changes (Lohne et al., 2013)) shows an abrupt change in ocean mode (recorded by deuterium excess) in the North Atlantic occurring in just 1-3 years. Environmental changes (as recorded in Greenland) occurred over ~60 years (Steffensen et al., 2008). Terrestrial climate amelioration in southern Scandinavia (i.e. the end of the YD) occurred about 100 years after the GS-1 ended, over 30-50 years (Lohne et al., 2013), although data from Hässeldala in Sweden finds warmer and wetter conditions precede Holocene warming in Greenland by ~200 years.

1.1.3.2 The UK and the Lake District

The British and Irish Ice Sheet melted from the British Isles from 23 cal ka BP with occasional lobular re-advances during the overall retreat. Many reconstructions show the Lake District to have been glaciated at 18 ka BP, but deglaciated at 17 ka BP (C. D. Clark et al., 2012; Ehlers et al., 2011; Hughes et al., 2016, 2011). However, there is a paucity of dates around the north of England between the estimated 18 ka BP and 17 ka BP glaciation lines (Hughes et al., 2016)) meaning that in many modelled glacial reconstructions, radiocarbon dates obtained in 1977 from older methods- although since recalibrated- (Coope and Pennington, 1977; Knight, 2001; personal recalibration) are a main source of data in reconstructions. Optically-stimulated luminescence (OSL) dating from near Morecambe Bay gives this area is ice-free by 19.3 $\pm$ 0.3 ka BP, whilst Schmidt-Hammer exposure dating (SHED) shows the inland Lake District uplands as exposed by ~16.5 ka BP (Tomkins et al., 2016). The Windermere ^{14}C ice-free date is given as ~17.7 cal ka BP (Coope and Pennington, 1977), but this date is now considered too old due to old carbon in the catchment (Wilson and Lord, 2014). It is reasonable to suggest that Lingmell Col in the southwest Lake District (750 m asl) was exposed at 17.3 $\pm$ 1.1 cal ka BP (Ballantyne et al., 2009), and that Windermere was ice-free by 14.7 cal ka BP (the widely-accepted start of the Lateglacial Interstadial across Europe).

The period between 14.7 and 12.9 cal ka BP (location-dependent) was much warmer and wetter than the previous stadial, and is known generally as the Lateglacial Interstadial. In the UK it is known as the Windermere Interstadial (Coope and Pennington, 1977), in terrestrial northern Europe as the Bølling-Allerød, and in the Greenland ice core chronology as GI-1 (Lowe et al., 2008).

In Wales the landscape was dominated by Juniper scrub and Birch woodland (Walker et al., 2003b). Mean July temperature during the early part of the Interstadial is thought to have been around 20 °C, followed by stepped reductions throughout the Interstadial causing reductions in the Juniper then Birch woodlands (Walker et al., 2003a). In the Scottish Highlands, ice caps existed throughout this period (Bradwell et al., 2008), and exposure dating in the central Lake District and Northwest Scotland also provides evidence for some possible ice persistence in the early Interstadial (McCarroll et al., 2010). Sorrel and Mugwort grew in Northern Scotland, succeeded by Sedge, Crowberry, and sparse Juniper (Pennington, 1977). In east Yorkshire, the Interstadial was characterised by delayed-onset Juniper then Birch woodland (Walker et al., 1993). Windermere itself has been given as the type location for this particular climate interval in the UK (Coope and Pennington, 1977).

In the UK, the Loch Lomond Stadial (the UK equivalent of the YD) occurred around 12.9 cal ka BP. The Loch Lomond Stadial in the UK was characterised by re-nucleation of ice in Wales, the Scottish Highlands, and the Lake District (Golledge, 2010; Hughes, 2009; Sissons, 1980). The Highland ice cap is thought to have been thick but spatially limited, with some surrounding icefields (Golledge, 2010). Originally it was thought there were just a few valley and cirque glaciers in the Lake District re-glaciation (Sissons, 1980), but subsequent detailed geomorphological mapping in selected areas of the Lake District has found clear evidence of summit icefields and outlet glaciers, and overall more ice than Sissons' original interpretation (Brown et al., 2011; McDougall, 2013, 2001). Mean July temperatures in Wales are thought to have been around 10-11 °C (Walker et al., 2003a). Scottish Highland glaciers which had reached their maximum extent by 12.4 cal ka BP were all in retreat by 12.1 cal ka BP, several hundred years before the abrupt warming at the start of the Holocene (Ballantyne, 2012), and it is not unreasonable to suggest that similar trends were present in the uplands of Northern England and Wales.

1.1 Windermere

Windermere (Figure 1.3), situated in the southeast of the English Lake District, is a north-south trending glacial ribbon lake in a steep-sided pre-glacial river valley overdeepened by successive glaciations (Pennington and Pearsall, 1973; Pinson et al., 2013). Windermere is a spoke in the radial drainage of the Lake District (Mitchell, 1956). The lake is 17 km long with a maximum width of 1.5 km, an elevation of 39 m above Ordnance Datum Newlyn, and a present maximum water depth of 62 m (Lowag et al., 2012; Miller et al., 2013).

Windermere drains a catchment of 242 km^2 (Miller et al., 2013) with Ordovician Borrowdale Volcanic Group bedrock in the north and Windermere Supergroup (Silurian mudstones and siltstones) in the south. A bedrock high separates Windermere into a north and South Basin, and a sill dams the lake in the south forcing drainage to the west into the River Leven (Wilson, 1987). (Modern lake outflow is now also controlled by a weir). Windermere in its present form has been accumulating sediment since the lake became exposed after the retreat of the British-Irish Ice Sheet c. 17 ka (Ballantyne et al., 2009; Coope and Pennington, 1977).

Windermere's location near the west coast of England gives it an Atlantic-influenced climate with the prevailing weather coming from the west. Windermere is favourably located in the North-Atlantic-Europe region, being set between the North Atlantic and Europe and between Mediterranean and Scandinavian latitudes. There is diachroneity between climate records from across this region, for example between the Greenland ice cores and varved Meerfelder Maar sediment cores in Germany (Lane et al., 2013).

Windermere has been the subject of research for several decades. Many suites of short (gravity) cores have been recovered from Windermere covering sediments from the last deglaciation and associated pollen and diatom assemblages (Coope and Pennington, 1977; Pennington, 1947, 1943). Lakebed samples have also been used to shed light on modern lake pollution and fish ecology (Miller et al., 2014b, 2014c). Windermere's sediments were used to produce a Holocene palaeosecular magnetic variation (PSV) curve for the UK (Thompson and Turner, 1979; Turner and Thompson, 1982, 1981), dated using bulk radiocarbon samples. This curve has been used in Holocene PSV studies across Europe and North America as a dated stratigraphic tool, and in PSV models (e.g. Barletta et al., 2010; Korte et al., 2011; Sagnotti et al., 2011; Snowball et al., 2007). The lake was also successfully used as a test site for new, high-resolution seismic equipment by the University of Southampton (Lowag et al., 2012; Pinson et al., 2013; Vardy et al., 2010).

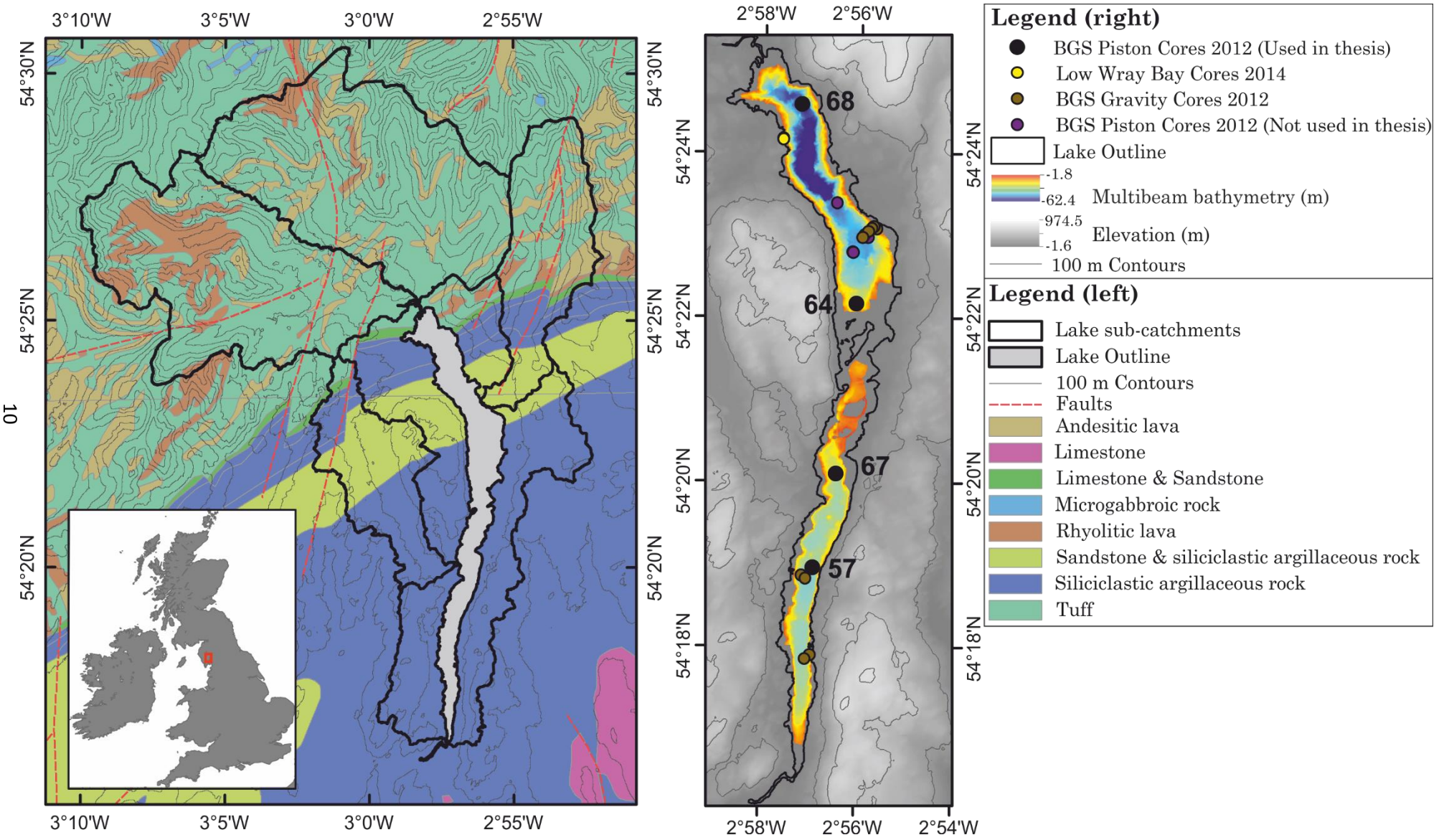
3°10'W
3°5'W
3°0'W
2°55'W
54°30'N
54°25'N
54°20'N
2°58'W
2°56'W
2°54'W
54°24'N
54°22'N
54°20'N
54°18'N
68
64
67
57
Legend (right)
BGS Piston Cores 2012 (Used in thesis)
Low Wray Bay Cores 2014
BGS Gravity Cores 2012
BGS Piston Cores 2012 (Not used in thesis)
Lake Outline
-1.8
-62.4
Multibeam bathymetry (m)
974.5
-1.6
Elevation (m)
100 m Contours
Legend (left)
Lake sub-catchments
Lake Outline
100 m Contours
Faults
Andesitic lava
Limestone
Limestone & Sandstone
Microgabbroic rock
Rhyolitic lava
Sandstone & siliciclastic argillaceous rock
Siliciclastic argillaceous rock
Tuff

Figure 1.3: Left: Windermere and its catchment, showing bedrock geology and 100 m contours. Left inset: The British Isles, with the location of Windermere shown as a small black box. Right: Locations of cores taken, along with multibeam bathymetry (rainbow) and topography (greyscale and contours).

1.2 Varves: an Introduction

Varves were first defined as annually-deposited proglacial clays (de Geer, 1912), but 'varve' is now taken to mean any annually-deposited sediment or sedimentary rock with a clear seasonal signal. Varves may form in both lacustrine and marine settings, but marine varves are rare. There are three common varve types: biogenic, endogenic and clastic varves (Zolitschka, 2007). Biogenic varves form from organic matter produced by seasonal biological productivity, while endogenic varves are formed from the settling of chemically precipitated minerals. Clastic varves are formed from minerogenic sediment entering a lake, mainly by fluvial or atmospheric processes, and settling on the lakebed. Many varves are a combination of these three types. Although there are thousands of lakes globally, the formation of varves is relatively uncommon, requiring both strong seasonality of one or more depositional processes and preservation of lakebed microstructure (e.g. little to no bioturbation)(Zolitschka, 2007).

Early varve study focussed on cross-correlating glacial varve sequences in order to track ice retreat during the last deglaciation on the east coast of Sweden (de Geer, 1912) and in New England (Antevs, 1928, 1922) . Thinking that varve thickness variations were controlled principally by solar cycles modulating ice melt, De Geer and colleagues tried to cross-correlate varve sequences from the Americas and central Asia (e.g. De Geer, 1937). However, his incorrect cross-correlations led to varves being largely discredited as a sound climate indicator for several decades until varves became a useful tool for studying anthropogenic impacts on lakes (e.g. Tolonen & Jaakkola, 1983). Varves also became important for calibration of radiocarbon ages and for dating of events such as volcanic eruptions (Bronk Ramsey et al., 2012; Lane et al., 2015).

For clastic varves to form, the sedimentation pattern within the lake must exhibit strong seasonality (Chutko and Lamoureux, 2008; O'Sullivan, 1983). This may be controlled by seasonal changes in sediment delivery to the lake, by seasonal depositional controls within the lake, or a combination thereof (Smith and Ashley, 1985). In addition the settling processes within the lake must be efficient enough that most –if not all- of the sediment delivered in a given year will also settle that year. Varve preservation is especially

promoted in stratified water with little influence from waves, currents, and bioturbation (e.g. Smith et al., 2004; Besonen et al., 2008; Cook et al., 2009), and which is protected from one-off events such as slides and turbidity currents. Absence of abiotic microstructure disturbances such as gas bubbles and microseismicity also promote varve preservation (Zolitschka et al., 2015).

Varves may record a variety of modulations on sedimentation including land use, pollution, climate variation, and erosion. Information on the nature of each year's sedimentation may be extracted from each varve in a sequence to produce time series of interannual sedimentation variation. Inferences may then be made on the interannual controls on sedimentation, taking into account both the lake catchment morphology and processes (including land-use changes) and wider regional climate fluctuations. In addition, if a sequence of varves can be shown to be continuous (with no hiatuses or major erosion) and can be dated, it is possible to count the varves in the sequence to build an absolute chronology for the lake (Francus et al., 2008). Even without dates, a 'floating' chronology may be constructed for relative ages. Independent dating methods such as palaeomagnetic studies and tephrochronology can constrain the age of a floating varve chronology (Zolitschka, 2007; Zolitschka et al., 2000).

A proglacial or periglacial clastic varve comprises an annual couplet, with a coarser layer at the varve's base overlain by a finer layer (Ashley, 1975, 1972) (Figure 1.4). The coarse layer is deposited during the melt season while the fine material remains in suspension until fluvial processes cease in the winter and the water column becomes calm enough for clay-grade material to settle (Figure 1.5). The coarse layer may comprise several separate fining-upwards depositional events from throughout the melt season and from late-summer rainfall. Windermere has previously been found to contain laminated sediments from Low Wray Bay, a shallow (~4 m) bay in the North Basin (Pennington, 1947, 1943). However, there has been no in-depth study of the deep-depocentre varves of the lake.

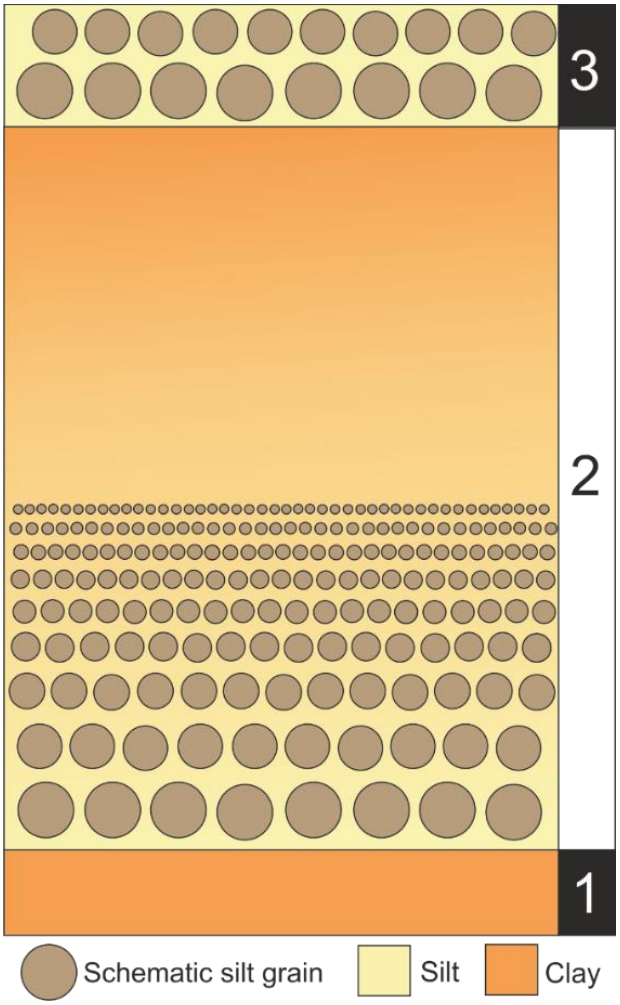

Figure 1.4 Schematic of a simple, glaciolacustrine varve. Yellow and orange represent silt and clay matrix respectively. Brown circles represent variation in silt grain size (not to scale). White and black numbered boxes (right) indicate sequential varves.

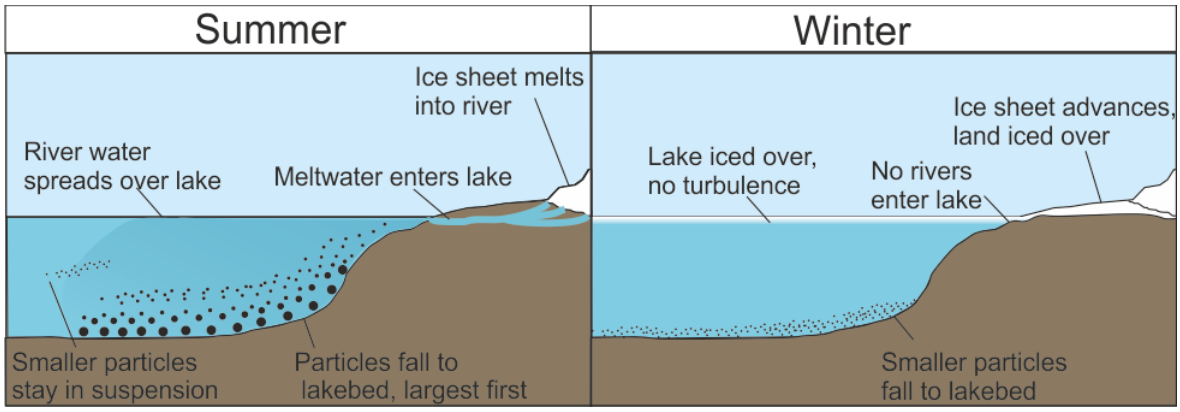

Figure 1.5 Proglacial varve formation

The nature and thickness of each varve or varve sequence depends on the bedrock geology, sediment supply and transport mechanisms, depositional controls and post-deposition conditions. The relationship between the climate or environmental signal can be complex: for example in a proglacial environment, interannual air temperature variability may in fact

affect both the release of sediment from under the glacier and also the stratification, biodiversity and chemical conditions of the lake (Hodder et al., 2007).

1.2.1 Supply and transport

In proglacial and periglacial environments, sediment supply from within the catchment may be bedrock erosion by glacial processes (ice sheet or glacier activity) or regolith activation by snowmelt, precipitation events, aeolian activity, or a combination of the above.

1.2.1.1 Glacial

Summer temperature-controlled glacier activity in a proglacial setting largely controls sediment supply (Desloges, 1994), while sediment transport may be in the form of short-lived meltwater streams. Glacier position controls sediment availability (Blass et al., 2003)- both through variations in the area of exposed available sediment and through variable sediment release from summer glacier melt events. Contemporary glacier recession (Green Lake catchment British Columbia, Canada) has been observed to drive sediment delivery events to the lake (Menounos, 2006; Schiefer et al., 2006).

Within the glacier itself, the sediment is transported either by subglacial meltwater or less commonly by ice shear and released at the edge of the glacier (Hodder, Gilbert, & Desloges, 2007 and references therein). The highest sedimentation rates on decadal to centennial timescales are thought to be associated with both rapid ice advance and also initial glacier recession from maximum ice extent (Leonard, 1997). Understanding the timing and magnitude sediment release from lake-proximal glaciers is key to correctly interpreting ice-proximal proglacial varve thickness records (Hodder et al., 2007).

1.2.1.2 Nival

In non-glacier-fed High Arctic lakes it is the spring snow melt which provides the dominant mechanism for both sediment release and transport (Hardy, 1996; Leemann and Niessen, 1994). Several studies have found that a large proportion of sediment is discharged within the early part of the melt season (Cockburn and Lamoureux, 2008; Cuven et al., 2011; Hardy, 1996; Lewis et al., 2005; Menounos and Clague, 2008) over a period of several days during the peak melt, sometimes with a diurnal cycle visible in the sediment (Lewis et al., 2005).

1.2.1.3 Pluvial

Rainfall events are most influential and common in late summer or autumn (Desloges and Gilbert, 1994; Menounos and Clague, 2008) after the initial snow (or ice) melt and often occur when the initial silt package has largely settled (Blass et al., 2003; Hardy, 1996). Rainfall events have the potential to mobilise high sediment yields and may even contribute the highest proportion of sediment to a varve, although preceding conditions such as soil moisture or permafrost presence may modulate the sediment response to rainfall significantly (Lapointe et al., 2012; Lewis et al., 2012). Rainstorm events may be seen in the varve as slightly coarser silt bands towards the top of the silt package, but in particularly intense or sustained rainstorms enough sediment may be mobilised and transported to create a sustained turbidity current in the lake, causing the rainfall layer within the varve to have its own compound laminations (Hardy, 1996; Schiefer et al., 2006). Alternatively the rainfall layer may be seen as a graded bed due to intense stream discharge (Francus et al., 2008), or a series of poorly-sorted coarse-grained sublaminae (Cuven et al., 2010). Rainfall may also mobilise sediment leading to non-erosive, angular, non-fluvial sand grain layers which may be hyper-concentrated density flows (Francus et al., 2008).

1.2.1.4 Aeolian

A minor form of sediment transport is aeolian. Although very small particles will be supplied to the lake throughout the year, these grains may only enter the water in the ice-free months. This may lead to an influx of aeolian grains from the lake-ice surface just after melting, although usually these grains would not be large enough to warrant attention. However, larger coarse silt to sand-sized grains are distinguishable as aeolian due to their angular shape and more isolated natures, often found at the top of the silt layer or within the clay cap (Francus et al., 2008). They are either isolated grains if delivered to the lake in the ice-free season or as a thin horizon if the grains had dropped from melting lake-surface ice in the summer. A lack or shortage of snow covering the sediment source material is conducive to aeolian erosion (Cuven et al., 2010)

In practice, most lake systems are mixed and varves may contain signals from all of the above sources.

1.2.2 Deposition & preservation

Subsequent to sediment entering the lake, it can be deposited in a number of ways depending on the water column structure and chemistry of the lake, and the lakebed topography.

Sediment-laden water is usually denser than the lake water so enters the lake towards the lake bed and continues along the lake bed (Hodder et al., 2007). It is likely that the clay particles of the winter varve cap are deposited on the lakebed by flocculation rather than single-particle settling in order to allow for each year's clay to settle over the course of a winter season (Hodder, 2009).

There exists within-lake variation in depostitional patterns of sediment. A less-stable environment and fluctuating water levels and ice proximity may lead to poorly-formed or inconsistent laminations, especially in more ice-proximal or shallow locations (Cook et al., 2009). Larger particles settling into poorly-consolidated sediment, or sediment settling in locations prone to bioturbation, are also likely to form poor laminations (Francus et al., 2008). Lake water-depth influences varve deposition, preservation, or thickness (Zolitschka, 1996).

1.2.3 Graded Beds and Turbidites

One-off storms or increased runoff, catchment instability and slope failure (e.g. slumps) can produce massive or graded beds which may be erosive (Zolitschka, 1996), and mass transport deposits which can be from a few millimetres up to several metres thick (These are found in the Windermere cores). Graded beds form from a single, short-lived depositional event or event suite and interrupt the normal sedimentation pattern, are usually thicker than mm-scale laminae, and often have coarser grains at the base (Francus et al., 2008). Events causing graded beds may produce erosive deposits proximal to the lake inflow but a subannual layer within a varve in an inflow-distal depocentre (Schiefer, 2006).

Graded beds in glacierised catchments may be associated with rapid glacier recession or particularly intense snowmelt conditions (Menounos, 2006). Sediment can be 'dumped' in a flood event triggered by extreme rainfall, and in a glacierised catchment this is likely to be autumn or late-summer rainstorms (Menounos, 2006).

Turbidites (delivered by turbidity currents (Zolitschka, 1996)) are often the result of subaqueous slumping (Cockburn and Lamoureux, 2007) arising from catchment instability

and sometimes triggered by intense rainfall (Francus, 2002). Sublaminae within turbidites may arise from sediment pulsing in a single turbidity current, currents from minor discharge peaks within the flood period, or alternatively from fluctuations in sediment-laden current direction through the period. A turbidite base is generally poorly sorted and coarse grained whereas the finer material is deposited afterwards through particle settling (Reading, 1996).

1.2.4 Interpreting a varve: catchment and climate

When interpreting varve properties it is important to consider what processes have dominantly contributed to the formation of the varves in question.

Many studies find that varve thickness and grain size- in both glaciated and unglaciated catchments- may be related to summer temperature during the ice and/or snow melt season, controlling the runoff energy and volume and thus lake sediment delivery (e.g. Cook et al., 2009; Francus, 2002; Hambley and Lamoureux, 2006; Hardy, 1996; Hughen et al., 2000; Schiefer et al., 2006; Smith et al., 2004; Zolitschka, 1996). In some unglaciated catchments, sediment delivery to the lake is dominated by the amount of snow on the ground over winter, somewhat controlled by winter temperature (Cockburn and Lamoureux, 2008, 2007; Cuven et al., 2011; Hambley and Lamoureux, 2006). Colder winter temperatures can delay the spring melt and shorten the melt season such that the snow is all melted in a briefer, more intense period leading to higher melt energy and greater sediment transfer (Hodder et al., 2007).

For varve records that do not have weather station or sediment trap data, it is necessary to infer the processes leading to varve formation from comparisons with other catchments with as similar hydrological conditions as possible. The validity of the necessary assumption that certain processes within similar catchments lead to the same varve types is questionable but ultimately unquantifiable.

1.3 Previous and ongoing work on Windermere by the University of Southampton

This study is part of a wider project studying Windermere. Here, other aspects of the wider project are listed for reference.

- Several seismic investigations into the sub-bottom of the lake took place in 2007 and 2011, imaging lake-bed moraines, lakebed depocenters, and Younger Dryas-age mass transport deposits (Lowag et al., 2012; Pinson et al., 2013; Vardy et al., 2010).
- The PhD thesis of Helen Miller (Miller, 2014) investigated several different aspects of Windermere. Chapter 2 presented a 1:10000 map of the geomorphological features and sedimentary processes shaping the landscape in and around Windermere (Miller et al., 2013). Chapter 3 details the sediment coring which took place in 2012, upon which this study and that of J. James Fielding (2017) is based. Chapter 4 presents a record of pollution at the top of Core 68 using Itrax XRF data (Miller et al., 2014b). Chapter 5 presents an interpretation of the glacial and paraglacial history of the Trout Beck Valley, based on till orientation and LiDAR and multibeam imagery on a catchment scale (Miller et al., 2014a). Chapter 6 presents an investigation into the spawning habits of Arctic Charr (*Salvelinus alpinus*) and the conditions of their spawning grounds, in comparison with qualitatively-described spawning conditions from over 50 years ago (Miller et al., 2014c).
- The PhD thesis of J. James Fielding (Fielding, 2017) investigates the Holocene sediments of Windermere, based on a piston core (Core 68) discussed in this thesis, and on several additional gravity cores taken to recover the sediment-water interface. Chapter 2 focusses on a mass transport deposit found in the uppermost sediments of the gravity cores, and relates it to the 1979 Carlisle earthquake (This chapter is currently in revision at the Journal of the Geological society of London). Chapter 3 uses geochemical analysis of the gravity cores to understand sediment pollution in Windermere since the 1800's. Chapter 4 focusses on diatom blooms identified with a scanning electron microscope and compares these blooms with records from the Freshwater Biological Association, in order to understand seasonal cycles of lake ventilation and geochemical focussing. Chapter 5 focusses on the entirety of the Holocene record using the piston core, including a pilot pollen study, a Chironomid study, and the use of geochemical analyses to identify redox changes and mass transport deposits.
- Future work is also planned for the current cores to look in much more detail at the sections of sediment that correspond with the Lateglacial ('Windermere') Interstadial, including detailed pollen and Chironomid work.

1.4 Objectives of this Study

The overarching objective was to use sediment cores acquired from Windermere (coring details may be found in Section 2.1) to develop new insights into the deglaciation of Windermere and place this in the context of the deglacial history of the British and Irish Ice Sheet and North Atlantic climate change. To this end, several sub-objectives have been identified:

- To provide a chronology and develop age models for the cores using the full range of available methods including radiocarbon dating, tephra, varve counts, and palaeomagnetic methods.
- To construct a new palaeomagnetic secular variation (PSV) record from the four main Windermere cores with a view to updating the UK PSV curve of Turner and Thompson (1981), and to provide another stratigraphic method of dating and correlating the four cores throughout their length.
- To analyse and synthesise the overall stratigraphy and sedimentology of the deglacial sediments in order to reconstruct and correlate the key climatic transitions and processes operating during deglaciation.
- To develop varve chronologies in order to improve understanding of the timing of the different phases of the Lateglacial period.
- To analyse time series of varves and develop records of seasonal through centennial scale and examine evidence for variations in the drivers of interannual variability during deglaciation.

By synthesis of all available data, to produce a new model for the deglaciation of Windermere and relate this to the overall deglacial history of the North Atlantic region.

It should be noted that although the original aim with the palaeomagnetic investigations was to provide a PSV curve for the entire length of the four cores, mineralogical and sedimentological factors meant that the pre-Holocene sediments did not provide reliable palaeomagnetic data (see Section 3.5.1 and Figure 3.12 for more details). The result is that only the Holocene part of the PSV curve is presented in Chapter 3, and that PSV could not be used as an additional age constraint in the pre-Holocene sediments.

1.5 Thesis Overview

Chapter 2 presents an overview of the methods used to analyse the cores. In addition, the overall core stratigraphy is described, and a broad core chronology is introduced. Each sedimentary unit in the pre-Holocene part of the cores is shown and described. A synthesis of varve formation is also given.

Chapter 3 presents a new Holocene palaeomagnetic secular variation curve from sediment in Windermere for the Holocene. This new curve updates the UK master curve of 1981, providing a well-dated palaeomagnetic reference curve for climate-independent dating of regional sediment archives.

Chapter 4 presents a sedimentological investigation into the varved sediments of Windermere that formed prior to the onset of the Lateglacial Interstadial. The thickness of suitable varve sequences has been measured, and the implications for the deglaciation of the Windermere valley is discussed.

Chapter 5 presents a sedimentological investigation into the varved sediments of Windermere that formed after the Lateglacial Interstadial, during the Loch Lomond Stadial. The thickness of suitable varve sequences has been measured, and the implications for the nature of environmental change during the stadial is discussed.

Chapter 6 presents a short time series analysis study of varve thicknesses from both the pre- and post-Interstadial varve sequences, and discusses the interannual variations of the varves in terms of climatic oscillations.

Chapter 7 summarises the conclusions and advocates future work in the field.

Appendix A details the sampling and subsampling of the cores, and detailed methods of core processing and analysis.

2. Methods

In this chapter, an overview of coring, core-processing, and macro-scale stratigraphy is given.

2.1 Coring

2.1.1 Piston Coring

A multibeam bathymetry site survey coupled with chirp, parametric, and multi-channel boomer seismic reflection surveys were used to identify sediment depocentres which would provide sediment deposits representative of catchment processes ancient and modern (Lowag et al., 2012; Miller et al., 2013; Vardy et al., 2010). Many depocentres were found to contain several distinct seismic units which were identified as representing the Holocene, Younger Dryas, the Lateglacial Interstadial, and initial BIIS retreat (Pinson et al., 2013).

Several sediment cores were subsequently collected using both a Uwitec piston corer and Uwitec gravity corer in 2012 as part of a coring campaign by the British Geological Survey (BGS) and the University of Southampton (Miller, 2014). In total, 18 cores were collected in 2012 from a variety of locations within the lake including deep (>20 m water depth) sub-basins, a headscarp, and shallower locations. This was the first instance of piston coring in deep (>20 m water depth) water in Windermere, giving rise to previously unseen sediment sequences. Gravity cores were also collected in 2014 in order to recover the sediment-water interface in the locations of some of the piston cores.

Piston cores were acquired in 2 m sequential sections with 9 cm diameter core barrels. The piston core sections were then cut into 1 m sections and split lengthways into working and archive halves. Four ~6-10 m long cores with the highest deposition rates and longest timespans of the core suite were selected for detailed study in this thesis (Table 2.1).

Basin	Core ID	Core name for thesis	UTM co-ordinates, 30 N	Co-ordinates (decimal degrees)	Core length (m)	Water depth (m)

North	+54-03/68 PC	Core 68	502900, 6029136	54.40996 N, -2.95532 E	10	53.7
North	+54-03/64 PC	Core 64	504184, 6024657	54.36969 N, -2.93560 E	8	25.6
South	+54-03/67 PC	Core 67	503763, 6020830	54.33530 N, -2.94213 E	8	26.9
South	+54-03/57 PC	Core 57	503267, 6018702	54.31618 N, -2.94978 E	6	37.3

Table 2.1: Details of the four piston cores used in this study that were taken in April 2012.

2.1.2 Gravity Coring

The piston coring process summarised above is prone to sediment loss at the very tops of the cores, such that the sediment-water interface and some amount of sediment below this was lost in 2012. In order to recover this missing sediment, fieldwork was carried out in May 2014 to collect a suite of gravity cores that preserved the sediment-water interface. A gravity core was collected at the site of each of the four main long cores (Cores 57, 67, 64, and 68), and towards the mouth confluence of the inflow rivers Rothay and Brathay, Cunsey Beck, and Pull Wyke.

The North Basin cores were taken from the *RV John Lund* using a 9 cm diameter Uwitec gravity corer with a ball-based sediment catcher (coring positions were recorded using a HydroPro), and the South Basin cores were taken from the *S. S. Sear* rigid-inflatable boat (RIB) and positioned using a hand-held global positioning system (GPS). The sediment-water interface was sprinkled with silica gel in order to preserve the sediment surface features. The cores were taken to the University of Southampton for processing.

Core code	Co-ordinates (UTM 31N)	Co-ordinates (Decimal degrees)	Core length (cm)
+54-03/1 CS	501631, 6029288	54.41133 N, -2.97487 E	32
+54-03/2 CS	501642, 6029289	54.41134 N, -2.97470 E	41
+54-03/3 CS	502160, 6029594	54.41408 N, -2.96672 E	46
+54-03/4 CS	502167, 6029584	54.41399 N, -2.96661 E	43
+54-03/68 U1 CS	502913, 6029123	54.40984 N, -2.95512 E	42
+54-03/68 U2 CS	502902, 6029135	54.40995 N, -2.95529 E	45
+54-03/64 U1 CS	504170, 6024651	54.36964 N, -2.93581 E	37
+54-03/64 U2 CS	504184, 6024639	54.36953 N, -2.93560 E	28
CB1	503475, 6020833	54.33533 N, -2.94656 E	25
CB2	503488, 6020827	54.33528 N, -2.94636 E	20
67CS-1	503736, 6020840	54.33539 N, -2.94254 E	37
67CS-2	503764, 6020856	54.33553 N, -2.94211 E	35
57CS-1	503288, 6018757	54.31667 N, -2.94946 E	39
57CS-2	5032xx, 60187xx	54.32 N, -2.95 E	36

Table 2.2: Details of gravity cores taken in May 2014

2.1.3 Low Wray Bay

There has been a large amount of previous work on Windermere sediments, and much of it stems from cores taken from Low Wray Bay in the North Basin as a site easily accessible, sheltered, and containing a sequence from the deglaciation of the lake through the Holocene (Coope and Pennington, 1977; Pennington, 1947, 1943). However, much of this work is somewhat ambiguous (e.g. unclear coring locations, core lengths, and sometimes core descriptions) and thus difficult to tie to the findings from the long cores. Therefore, a suite of cores was obtained in August 2014 from Low Wray Bay in order to tie together the old information from the bay and the new information from the long cores, and characterise much of (for example) Pennington's work with colour photographs for future reference.

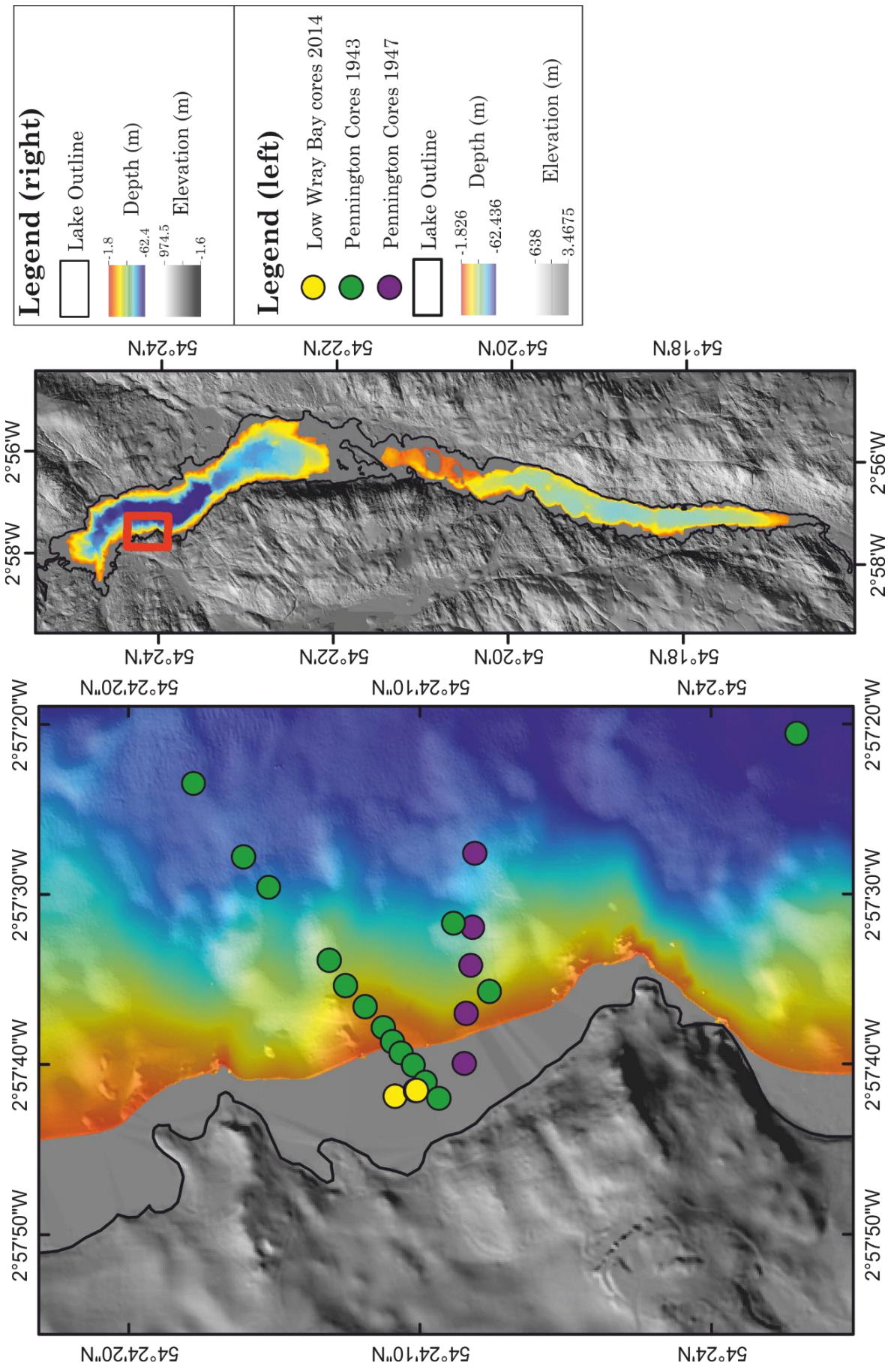
Legend (right)
Lake Outline
Depth (m)
-1.8
-62.4
Elevation (m)
-974.5
-1.6
Legend (left)
Low Wray Bay cores 2014
Pennington Cores 1943
Pennington Cores 1947
Lake Outline
Depth (m)
-1.826
-62.436
Elevation (m)
-638
3.4675
54°24'N
54°22'N
54°20'N
54°18'N
2°56'W
2°58'W
54°24'20"N
54°24'10"N
54°24'N
2°57'20"W
2°57'30"W
2°57'40"W
2°57'50"W

Figure 2.1: Left: Location of cores acquired in 2014 from Low Wray Bay (yellow), and approximate locations of some of Pennington's cores from Low Wray Bay (green and purple; (Pennington, 1947, 1943)). LIDAR topography (2 m resolution) is also shown (greyscale), along with multibeam bathymetry (rainbow). Right: Location of Low Wray Bay (red rectangle) within Windermere. Multibeam bathymetry (rainbow) and elevation (greyscale) are also shown.

Cores were taken from three sites in the bay (Figure 2.1). The coring locations were chosen based on Pennington's sediment cross-sections. The coring was performed in conjunction with a floating platform atop two ~2 m inflatable Zodiac craft. The craft were dragged into place with a RIB and anchored in place with four corner-anchors. The position of the platform was recorded using a hand-held GPS. A Livingstone corer was used with a 5 cm diameter, and cores were extruded into split gutter pipes and taped up for transport to the University of Southampton. Three cores were acquired: the first core, LWB1, comprised four non-consecutive sections designed to overlap by 6 cm. The second core (LWB2) comprised three sections, and the third core (LWB3) only one section. An additional gravity core was obtained using a 6 cm diameter Uwitec gravity corer from the site of LWB1 to acquire the sediment-water interface.

Core	**LWB 1 PC**			
Lat	54o 24.172'		**UTM E**	30 N 0502491
Long	02o 57.615'		**UTM N**	30 N 6028363
GPS Point	1		**Water Depth**	4.2 m
Section	**Length /m**	**Depth (upper)**	**Depth (lower)**	**Comments**
A	0.66	0	0.66	
B	0.86	0.6	1.46	
C	0.88	1.4	2.28	
D	0.53	2.2	2.73	Bottom of soft sediment and top of deglacial clay. Could not core further. Interstadial 23 cm, showed structure and internal colour changes.
Core	**LWB 1 CS**			

Lat	54o 24.172'		**UTM E**	30 N 0502491
Long	02o 57.615'		**UTM N**	30 N 6028363
GPS Point	1		**Water Depth**	4.2 m
Section	**Length /m**	**Depth (upper)**	**Depth (lower)**	**Comments**
A	~30	True 0	~0.3	Gravity core for full stratigraphic sequence

Core	**LWB 2 PC**			
Lat	54o 24.169'		**UTM E**	30 N 0502497
Long	02o 57.692 '		**UTM N**	30 N 6028342
GPS Point	4		**Water Depth**	5.2 m
Section	**Length /m**	**Depth (upper)**	**Depth (lower)**	**Comments**
A	0.82	0.5	1.32	
B	0.94	1.25	2.19	
C	0.21	2.1	2.31	Reached bottom of soft sediment and top of harder deglacial clay. Could not core further. Lost bottom 6 cm. Interstadial 21 cm in length.

Core	**LWB 3 PC**			
Lat	54o 24.168'		**UTM E**	30 N 0502497
Long	02o 57.692 '		**UTM N**	30 N 6028340
GPS Point	5		**Water Depth**	5.3
Section	**Length /m**	**Depth (upper)**	**Depth (lower)**	**Comments**
A	0.89	1.85	2.74	Only aimed to take replicate of Interstadial. Recovered all parts of sequence: Holocene-YD-Interstadial-deglacial.

Table 2.3: Details of Livingstone cores taken in August 2014 from Low Wray Bay

All four piston cores contain a sediment sequence from the initial deglaciation of the lake basin through to the latest Holocene, and all four cores were recovered from major sediment depocenters identified by the seismic and multibeam surveys to maximise sedimentation rates. The three cores collected in Low Wray Bay also contain this sediment sequence, although with a lower sedimentation rate and, between the different cores and sections, somewhat less continuity.

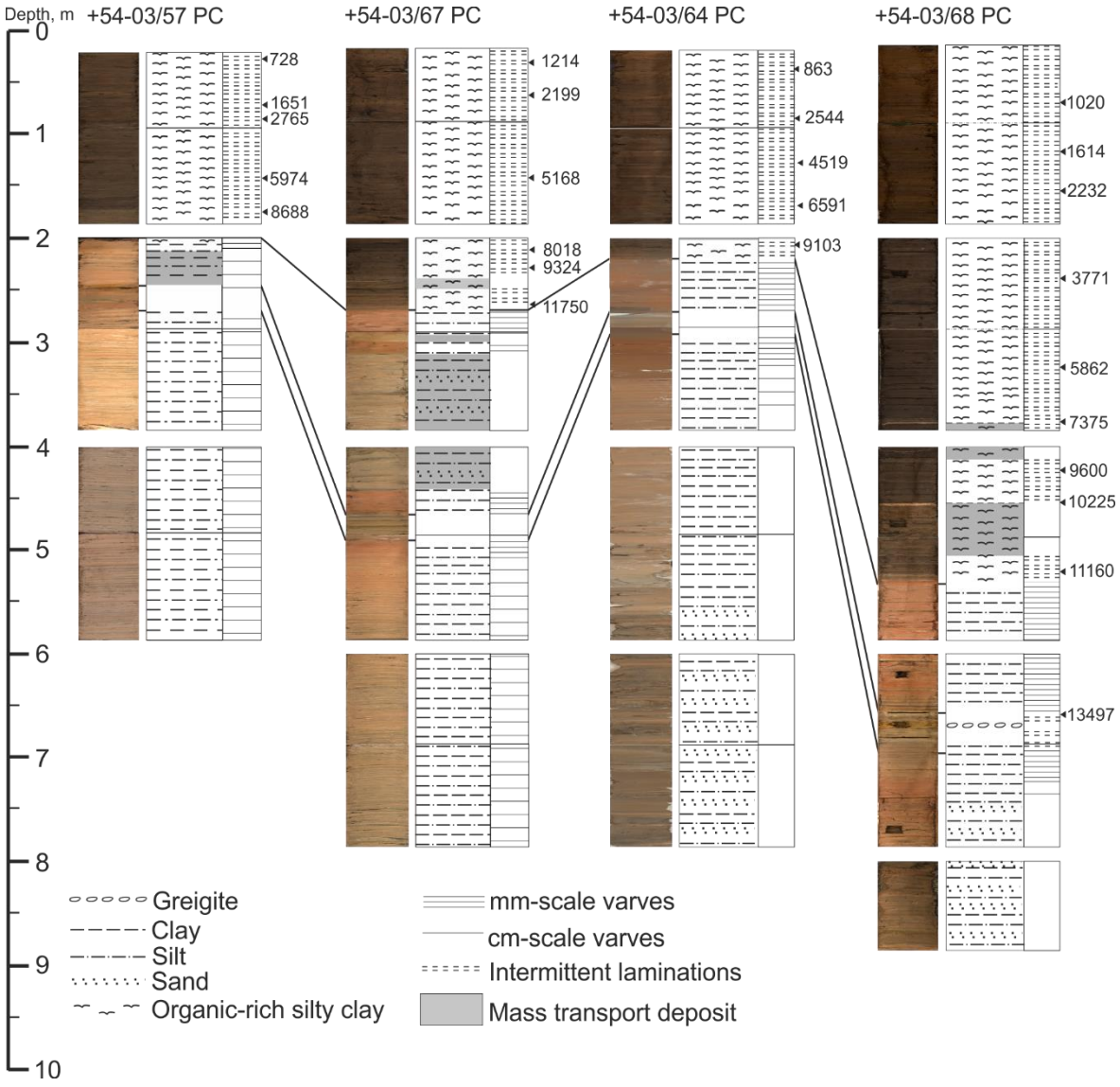

Figure 2.2: Core image (left) and lithostratigraphy (right) of Windermere Cores 57, 67, 64, and 68. Lithostratigraphic tie-points between the cores are included. Sediment ages given are median-probability radiocarbon dates in cal y BP calculated with Calib 7.1 (Stuiver and Reimer, 1993) using the Intcal13 calibration curve (Reimer et al., 2013). Full radiocarbon reporting can be found in Table 7.1.

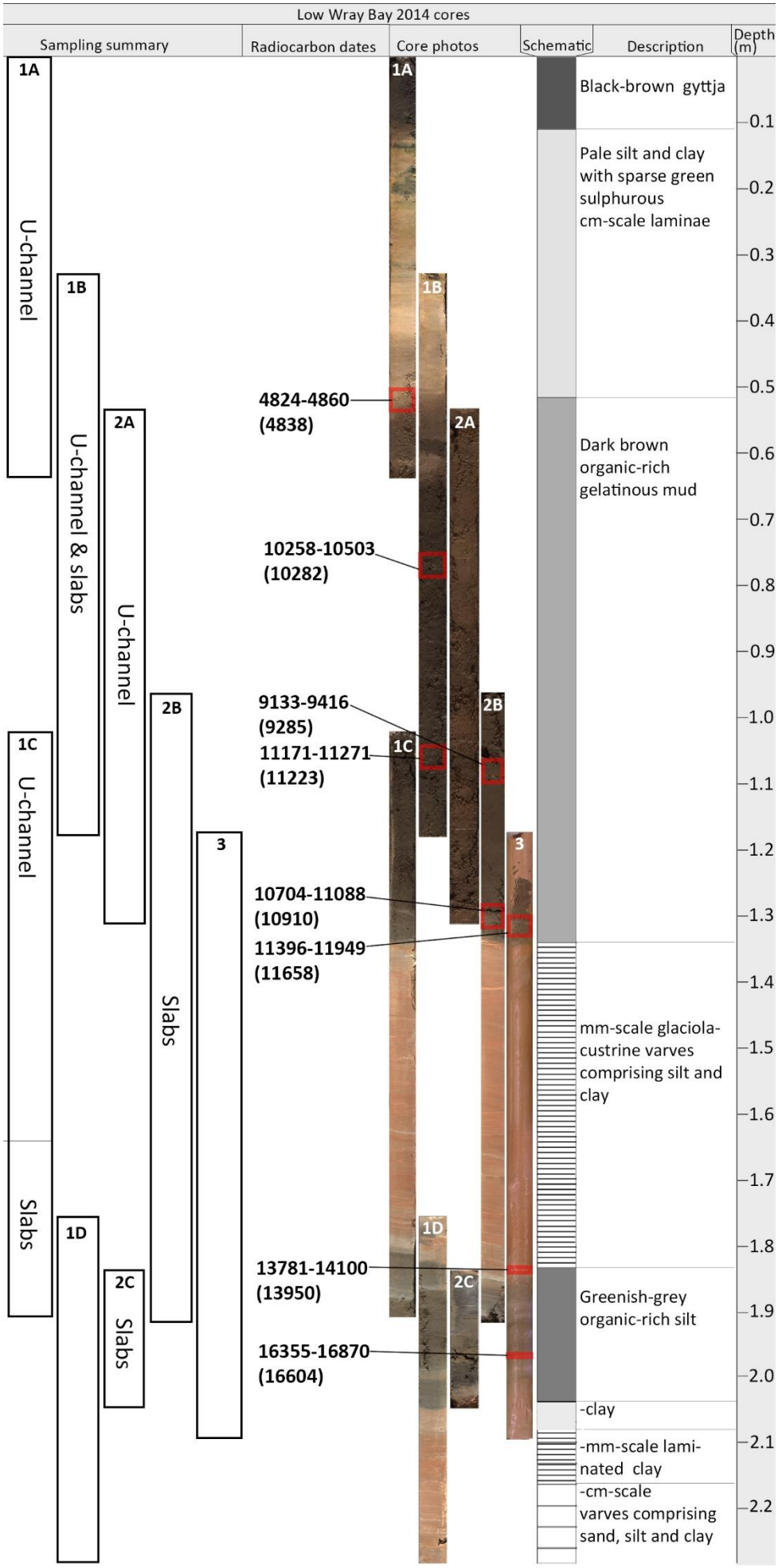
Low Wray Bay 2014 cores
Sampling summary
Radiocarbon dates
Core photos
Schematic
Description
Depth (m)
1A
U-channel
1B
U-channel & slabs
2A
U-channel
2B
Slabs
3
1C
U-channel
Slabs
1D
2C
Slabs
4824-4860 (4838)
10258-10503 (10282)
9133-9416 (9285)
11171-11271 (11223)
10704-11088 (10910)
11396-11949 (11658)
13781-14100 (13950)
16355-16870 (16604)
Black-brown gyttja
Pale silt and clay with sparse green sulphurous cm-scale laminae
Dark brown organic-rich gelatinous mud
mm-scale glaciola-custrine varves comprising silt and clay
Greenish-grey organic-rich silt
-clay
-mm-scale lami-nated clay
-cm-scale varves comprising sand, silt and clay
0.1
0.2
0.3
0.4
0.5
0.6
0.7
0.8
0.9
1.0
1.1
1.2
1.3
1.4
1.5
1.6
1.7
1.8
1.9
2.0
2.1
2.2

Figure 2.3: Low Wray Bay Cores 1-3 and a lithostratigraphic schematic. A schematic (far left) shows the sediment units in one of Pennington's cores, also from Low Wray Bay (Pennington, 1943). Right: sampling strategy for the LWB cores. Red bands: radiocarbon dates. Sediment ages given are median-probability radiocarbon dates in cal y BP calculated with Calib 7.1 (Stuiver and Reimer, 1993) using the Intcal13 calibration curve (Reimer et al., 2013). Full radiocarbon reporting can be found in Table 7.1.

2.2 Depth Scales

The piston-coring process was such that the sediment was likely to have been either slightly stretched or squeezed during recovery. Each 2 m core barrel contained 1.885 m space for sediment, with the remaining space taken by the core catcher. Therefore, we expect that in each 2 m core barrel, 11.5 cm of sediment is either compressed or missing due to the coring process.

The actual sediment depth of the top of each long core was ascertained using both ^{137}Cs and ^{210}Pb, and stratigraphic markers between the 2014 gravity cores and the 2012 piston cores. The sediment depth for the top core barrel for each core was shifted downward accordingly. In addition, the composite depths for each 2 m core barrel section were interpolated to fit 1.885 m, with the assumption that there had been a small amount of compaction or expansion for each barrel.

2.3 Overall Core Stratigraphy

For the following descriptions, please see Figure 2.2. Each of the four long (piston) cores in the suite (Cores 57, 67, 64, and 68) has an inorganic mineral-rich base and a brown organic-rich top with a sharp transition between the two major lithologies (Figure 2). Cores from the North Basin (Cores 64 and 68) have disturbed bases, with clay and silt, but also fine to medium sand present. The bases of the cores from the South Basin (Cores 57 and 67) have thick cm-scale laminations comprising medium silt and clay, a lithology which is also seen to a lesser extent in Cores 64 and 68 above the disturbed unit.

Overlying the basal sediment of all four cores are thinning mm-scale silt-clay couplets, with little organic material. These couplets are overlain by an organic-bearing non-varved silt unit with differing small-scale features in each core. Core 57 and 68 exhibit some degree of diagenetic iron inclusion, whilst Core 67 contains siliceous laminations.) The nature of these sediments is therefore likely controlled by depocenter-specific conditions.

This more organic unit is succeeded by a second unit of mm-scale clastic silt-clay laminations, overlain in turn by 2 – 5 m organic-rich intermittently laminated brown mud attributed to the Holocene. The transition between the minerogenic 'pink' sediment and the overlying organic-rich brown Holocene mud is extended, and exhibits a series of cm-scale organic-terrigenous laminations.

Mass-transport deposits (MTDs) are present in all cores, with the majority having thickness below 20 cm, although there are two ~1 m thick MTDS: one in the Lateglacial sediment of the South basin, and one in the early Holocene sediment of the North basin.

The Low Wray Bay (LWB) cores exhibit a similar macro-scale stratigraphy, with the base of the sequence characterised by an inorganic mineral-rich base, and the upper part of the sequence largely characterised by a dark brown, organic-rich mud. The main differences between the Piston sequence (Cores 57, 67, 64 and 68) and the Low Wray Bay sequence are in the top of the Holocene mud, where in the LWB sequence there is a section of very pale sediment that is not found in the piston cores and is of unknown origin. Additionally, the organic-bearing non-varved silt unit in the LWB cores is more organic than in the deep-water cores and shows some degree of internal structure based on silt colour and density.

The different sedimentary units are described in more detail in section Appendix C: and a detailed discussion of the silt-clay laminations is presented in Chapters 4 and 5.

2.4 Core Processing

The long (piston) cores were split into working and archive halves. The archive halves were imaged using photography and a Geotek Core Imaging System; some core sections were also X-radiographed using the ITRAX. The working halves were used for destructive sampling. A U-channel (2 x 2 x section length cm) and several 'slabs' (25 x 1 x 4 cm, or 5 x 1 x 4 cm for overlaps) were taken from each working half: the U-channel was used for ITRAX XRF and palaeomagnetic investigations, and the slabs were used for resin embedding for slide preparation and also for further subsampling. The slabs were also photographed and X-radiographed.

Further sampling included small 10 cm scrapes for tephra, samples for radiocarbon dating, cubes for magnetic fabric investigations, subsamples for Chironomid identification (detailed in Fielding 2017), subsamples for magnetic mineralogy experiments, and some subsamples for further Holocene investigations (see Fielding 2017).

In addition to data collected detailed in this chapter, this project made use of a GIS database compiled by Helen Miller (Miller 2017). Some core processing and analysis was carried out prior to the start of this PhD (Miller 2017), and the ensuing datasets were utilised.

2.4.1 Photography

The archive half of each long core was photographed with a NIKON D700 camera upon splitting. The images were later montaged to provide a continuous image of each core section. These images were of high resolution but suffered from some parallax.

Sections imaged: All

2.4.2 Core imaging system

Several archive halves were imaged at BOSCORF (the British Ocean Sediment Core Research Facility) Southampton on the Core Imaging System (CIS) at 300 dpi. The CIS images an entire core section in one continuous image using a slit. A digital ruler was added to each image to avoid the parallax problems associated with photography of real rulers.

Sections imaged: 57A-D, 67A-H, 64A-C, 68C-I, LWB1A-D, LWB2A-C, LWB3 (unsplit)

2.4.3 ITRAX X-radiographs

Some available archive halves were placed into the ITRAX micro-XRF machine to utilise the X-radiograph function. X-radiographs were taken to image the structure of the split cores prior to subsampling which would cause distortion.

Sections measured: 67C, 68C-I, LWB1A-D, LWB2A-C, LWB3

2.4.4 U-channels

Each working half had a U-channel taken from one side of its centre. A U-channel is a 2 x 2 cm (external edges) square-edged u-shaped plastic tube that can sample continuously down the length of a core section. Each U-channel had its plastic lid attached subsequent to sampling, and the ends were capped off with tape. The U-channels were used for ITRAX micro-XRF (X-ray fluorescence) and palaeomagnetic investigations.

Sections U-channelled: 57A-F, 67A-H, 64A-H, 68A-I, LWB1A-C, LWB2A

2.4.5 Slab Sampling

Each working half had 'slabs' taken from the other side of its centre. Each slab was a 1 x 4 x 25 cm block taken using a purpose-built sediment-cutter with extrusion block. Additionally, overlap slabs were taken from the edge of the slab sampling-line. These slabs were centred on the break between two adjacent slabs and were 1 x 4 x 5 cm in dimension. The slabs were used for preparation of microscope slides and for further subsampling for other methods.

In a typical core section, there would be four 25 cm slabs, marked 1 – 4 downcore, and three additional 5 cm overlap slabs, marked 1 – 2, 2 – 3, and 3 – 4 depending on which slabs were overlapped. For example, the third 25 cm slab down section F of Core 68 would be labelled '68F3'.

2.4.6 Slab photography

Each sediment slab (and slab overlap) was photographed upon sampling using a NIKON D700 camera. A ruler was placed next to the slab for scale, although there are some parallax effects associated with photography of rulers.

2.4.7 Slab X-radiography

Each sediment slab (and overlap) was X-radiographed. X-ray film 28 cm long was cut and sealed in the dark. Sediment slabs were placed on top of the film with metal identification and way-up markers. Soft, organic-rich sediment was X-radiographed at 35 kV for 200 s, whilst clay- and silt-rich sediment was X-radiographed at 56 kV for 120 s. Transition sediments were X-radiographed at both settings (on separate films) and at an intermediate setting, and the best image selected. The films were developed in a darkroom and dried whilst hanging from metal clips (hence the occasional clip marks on X-radiographs). The films were then digitised using a camera and a stencil-covered light-box. Although X-radiographs have centimetre scale bars, it should be noted that the X-radiographs became enlarged towards the tops and bottoms due to X-ray diffraction.

2.5 Slide preparation and imaging

Embedding methods are similar to those described in (Pike and Kemp, 1996) Paired slides were prepared from selected sediment slabs. Each sediment slab had a 1 x 1 x [slab length] cm piece cut off, which if necessary was cut into two ~12-13 cm lengths with a diagonal cut. Each length was placed inside a starched cotton mesh bent into a U-shape. Both ends of the cotton mesh were held in place with bent metal mesh. Each sediment section was placed in a plastic box, which were placed in groups into plastic tubs.

Each plastic box was inundated with acetone in a fume cupboard so that the sediment was covered, and the tub lids tightly secured to prevent evaporation. This process was repeated 10 times, spaced roughly three times a day, until all water had been driven off. Acetone in the boxes was removed with a syringe between inundations. After the acetone treatments, a four-part epoxy resin was prepared. The final acetone bath was removed and the resin was added to the boxes so that it covered the sediment. The resin was replaced using a syringe twice a day for 2.5 days until all acetone had been replaced. The resin-embedded sediment was then left to cure for 6 weeks.

Blocks of resin containing sediment were labelled with permanent marker then turned out of their boxes. Each block was marked up for sectioning with a unique slide number and way-up arrow on each slide-block, with all proposed cut-marks diagonal over 1 cm to ensure no mm-scale features were lost. The in-house sectioning lab then produced both a polished thin section (PTS) 200 - 300 microns thick and a covered thin section (CTS) 20 – 30 microns thick for each slide number. The covered thin sections were intended for optical sediment properties investigated with photography and optical microscopy, whilst the PTS were intended for Scanning Electron Microscope (SEM) investigations.

2.5.1 Covered thin section photography

All covered thin sections were photographed for posterity. Each covered thin section was placed on a light box and surrounded by lamps to ensure maximum light transmission. A technical camera was attached to a stand and straightened with a spirit level such that each image would be taken from directly above the slide. The camera was lowered towards the slide and focussed manually. Since it was difficult to see if the camera was perfectly focussed for such small and detailed subjects, each slide was photographed several times

with minutely-adjusted focussing. The images were later compared at 250 x magnification to select the image with the best focus.

2.5.2 Backscatter electron imaging

Polished thin sections were first carbon-coated using the Edwards carbon coater to stop the charging of specimens. Each PTS was imaged using the backscatter electron detector at 73 x magnification at optimum brightness and contrast using several fields overlapping by 25%, which were later mosaicked together using Adobe Photoshop CS5 and CS6. The brighter the pixel, the higher the atomic mass of the element hit by the electron beam. The brightness and darkness of each slide image was qualitative.

Subsequent to the acquisition of an energy-dispersive X-ray spectroscopy (EDS) unit and accompanying software AzTec, some later slides were imaged using the AzTec software, which has the advantage of forming an image of the whole slide much more quickly and mosaicking automatically. These slides were imaged at 100 x magnification.

Certain regions of interest (ROI) were also imaged at higher magnifications.

The EDS unit was used to identify constituent minerals in selected ROI, in the form of spot analyses and elemental maps.

2.6 ITRAX methods

Every U-channel underwent micro-XRF investigation. Each U-channel was placed in the ITRAX at BOSCORF (Croudace et al., 2006) and imaged. The U-channel was then covered in ultra-thin, X-ray-transmissive cling film. The measurement resolution was set at 200 microns. The ITRAX produced a digital X-radiograph for each U-channel, taking approximately 40 minutes for a 1 m section. The U-channel then returned to the start point and underwent XRF. Each element fluoresces at a different wavelength (or energy) when bombarded with X-rays, and the return values were measured in kilocounts per second (kcps) for each element.

The data were cleaned and processed in the following way:

1) Any rows with a validity of zero were deleted
2) Any rows with a root mean square error greater than 5 were deleted

3) Any rows with total kcps of under 10 000 were deleted
4) Rows from the ends of the U-channel which exhibited a sharp drop from the values of the rest of the U-channel were deleted
5) Columns (elements) in which kcps was consistently under 300 were marked as unreliable. They were not deleted but treated as either useless (in the case of very noisy columns) or auxiliary (in the case of elements where occasional spikes or increases were much greater than 300 kcps)
6) Element column kcps were normalised against total kcps to account for core density and surface topography changes (MacLachlan, pers. comm., 2016)
7) When interpreting data, spikes containing only 1-3 points were not considered significant
8) It was also worth keeping in mind that kcps values were surficial only

2.7 Low Wray Bay core processing

The Low Wray Bay cores were only 5 cm in diameter so could not be split into traditional working and archive halves. The cores were also not wide enough to accommodate both U-channel and slabbing equipment, so different core sections were designated for different processes. Sections 1A, 1B, the top 0.58 m of 1 C, and 2A were U-channelled for palaeomagnetic and ITRAX investigations. The bottom 0.3 m of section 1C as well as sections 1B, 1D, and 2B were slabbed for slide preparation. Radiocarbon samples were taken from sections 1A, 1B, 2B, and 3.LWB1C was sampled for tephra analysis. Unfortunately much of the data was not of sufficient quality to use in this thesis, but the cores are still in use for pollen work to be published in a future study.

2.8 Dating Methods and Macro-scale Chronology

2.8.1 Radiocarbon Dating

Carbon has three natural isotopes: ^{12}C, ^{13}C, and ^{14}C, which form ~99%, ~1%, and ~$1x10^{-10}$% of all C atoms (or ~1 atom ^{14}C per 10^{12} atoms of carbon respectively). Organisms, during their lives, take up carbon in all three forms to a level similar to that of atmospheric carbon concentrations at the time. ^{14}C is a radioactive isotope that decays with a half-life of 5730 $\pm$

40 years, and is constantly produced in the upper troposphere and the stratosphere from the interaction of cosmic rays with neutrons and nitrogen atoms. It is possible to date organic carbon based on the levels of ^{14}C left in the sample, back to 60 ka BP. The amount of ^{14}C in the atmosphere has changed over the last 60 kyr, and well-dateable archives (such as tree rings, speleothems, and continuous varve sequences) record these changes thus forming a calibration curve against which reported radiocarbon ages (in radiocarbon years) can be converted to calendar years on a probability distribution.

The Windermere cores contained some sediment suitable for radiocarbon dating, notably the organic-rich Holocene sediment and the sediment of the Windermere Interstadial, which was somewhat organic. The project was awarded two radiocarbon dating grants by the NERC Radiocarbon Facility, comprising a pilot study grant for 10 samples (allocation number 1736.1013) and a further grant for 30 samples (allocation number 1856.1014).

Each core section was first inspected for possible macrofossils within both the archive and working halves of the split cores and the sampled slabs. The top and bottom 10 cm of each core section was excluded from sampling to reduce the risk of carbon contamination. Macrofossils were sampled using clean metal implements and placed in either foil or glass containers to avoid carbon contamination (i.e. hydrocarbons in plastic). Each sample was weighed. Split cores were preferred over sampled slabs for contamination reasons, and when possible a laminar flow cabinet was used. Some cores did not contain enough macrofossils for the required number of radiocarbon samples, so bulk sediment had to be used. In this case, a 1 cm thick sample was taken using a metal spatula, weighed, and stored in carbon-free containers.

The samples were sent to the Natural Environment Research Council Radiocarbon Facility (NRCF) in East Kilbride. There they were turned to graphite and passed to the SUERC laboratory for accelerator mass spectrometry (AMS) 14C analysis (e.g. Linick, Damon, Donahue, & Jull, 1989).

2.8.2 Tephrochronology

2.8.2.1 Tephrochronology Motivation and Background

Volcanic eruptions often eject particles into the atmosphere, which remain airborne for days, weeks, or months depending on their weight. Tephra is the generic term for airborne

volcanic particles. Tephra layers near the volcanic source are often thick (mm to m scale) and visible containing larger particles, but much tephra is small enough (a few microns to a few hundred microns) to be caught up in atmospheric circulation and be deposited much more distally. Tephra from Icelandic volcanoes has been found in many parts of western to central Europe (Figure 7.2). Distal tephra layers are mostly invisible to the naked eye and are therefore termed 'cryptotephras'. Since transport time from eruption to deposition is a few months at most, tephra layers may provide stratigraphic markers present over an area of several thousand kilometres. Primary tephra layers are those that have been deposited straight from the air or within a few months of eruption and which have not been reworked. Primary layers found within a deposition area, which can be shown to be from the same eruption by geochemical fingerprinting, together form a regional isochron. Isochrones only form a regional stratigraphic marker, but when they are well-dated -usually a combination of high-quality radiocarbon dating and varve counting- dates may be transferred across the region. Tephrochronology is therefore a valuable climate-independent dating method, and lake sediments are a highly suitable medium for cryptotephra layer preservation.

The Windermere Lateglacial sediment was analysed in order to detect cryptotephra layers present, in particular that of the Icelandic Vedde Ash dated to 12 066 $\pm$ 42 cal y BP (Lohne et al., 2013; radiocarbon using IntCal09) and 12 121 $\pm$ 1 cal y BP (Rasmussen et al., 2006, using GIC1305 timescale), but also the Icelandic Penifiler (13 880 $\pm$ 100 cal y BP) and Borrobol (14 045 $\pm$ 95 cal y BP) tephras (Matthews et al., 2011).

2.8.2.2 Tephra methods

Sediment scrapes were sampled from 10-cm sections (overlapping by 1 cm) of the archive halves of 68F, 68G, 64C, 64D, and LWB1C from the Windermere Interstadial through the Younger Dryas to the beginning of the Holocene. The detailed methods used to search for tephra layers is given in Appendix A.

Each sample was placed in clean, pre-weighed foil in a crucible, and then re-weighed. The sediment was then dried in an oven overnight and placed in a furnace at 550^{o} for two hours to ash organic material. The samples were then re-weighed to calculate loss on ignition (LoI). The remaining sediment was placed in 10% hydrochloric acid (HCl) in centrifuge tubes overnight in order to remove calcium carbonate. The tubes were placed in a centrifuge at 2500 RPM (high acceleration, high brake) for five minutes then the HCl was replaced with de-ionised (DI) water and run again. Each sample was sieved up-core in order with a

100-micron sieve, funnel, beaker, and DI water. The > 100 micron particles were collected in a centrifuge tube and kept. The remaining sediment and water was passed through a 15-micron sieve into a second beaker. Anything smaller than 15 microns was discarded. The sieve meshes were discarded after every three samples. Sodium polytungstate (SPT) was made up at 2.00 specific gravity units, which is less dense than volcanic glass. Each 15-100 micron centrifuge tube was filled with 3 ml of 2.00 SPT, shaken, and run in the centrifuge at 2500 RPM (high acceleration, zero brake) for 15 minutes. The liquid was poured off into separate tubes. This process was repeated. SPT was then made up at 2.55 specific gravity units (denser than volcanic glass) and the centrifuge process was again run twice with the liquid being poured into another set of tubes. The grain-size fraction tubes were rinsed once using DI water in the centrifuge (high acceleration, high brake, 2500 RPM, 5 minutes) and the liquid poured off. The SPT-float tubes were rinsed seven times and the liquid poured into SPT recovery beakers. Glass slides were placed on an 80 ^{o}C hotplate then the sediment from the 2.55 SPT float samples was pipetted onto the glass slides. When the slides were dry, a small amount of Canada Balsam was placed over the sediment and a glass cover slip placed on top, expelling air bubbles where possible. Using a microscope at 20 x magnification, tephra detection took place. Silica appears somewhat purple under the microscope due to the Canada balsam, and the search was for glass shards which contained bubbles or vesicles and had a characteristic cuspid shape. In theory, 10 cm sections which contained high numbers of shards would then be re-sampled from the archive halves at 1 cm intervals to narrow down the tephra horizon location using the above method, and then the tephra horizon would be re-sampled and undergo geochemical fingerprinting.

2.8.3 Palaeomagnetic Chronostratigraphy

In addition to the above forms of dating, the sediments also underwent palaeomagnetic analysis in order to provide a further independent chronostratigraphic constraint. Full details of this method and ensuing results may be found in Chapter 3.

2.8.4 Lead and Caesium Dating

An additional date at each core sequence top was acquired from excess ^{210}Pb activity data by applying the constant flux: constant sedimentation model (Robbins, 1978). ^{137}Cs activity was also used to independently verify the estimate dates of peak atmospheric nuclear weapons testing (1963) and the Chernobyl nuclear reactor incident (1986) (Ritchie and McHenry, 1990). The short gravity cores were correlated to the long piston core tops

sedimentologically. The date from the ^{137}Cs-verified ^{210}Pb age model from each short gravity core was transferred to the top of each piston core at the point of overlap. For more details on the Lead and Caesium dating, see Fielding (2017). Please note, the age ^{210}Pb-decay based age models displayed in Appendix A were those used in the publication of (Avery et al., 2017), although since then the age models have been updated and may be seen in Fielding (2017).

2.9 Strontium methods

The high calcium levels in the lower sediment units of the cores were investigated in order to identify the provenance of the sediment containing these heightened element counts in the ITRAX data. Carbonates tend to include strontium (Sr), which has four isotopes. The ^{87}Sr/^{86}Sr ratio in different minerals is a form of geochemical fingerprint, such that the provenance of the Ca-rich sediment in the bases of the cores could be identified by matching the ^{87}Sr/^{86}Sr signature found in the core sediment with glacial till from a particular area of the catchment, and also a source rock in or near the Lake District.

Fieldwork was carried out in August 2015 to sample a selection of glacial tills from around the northern part of the Windermere catchment. In addition, five rock samples were taken from outcrops in and around the Lake District that were located in areas containing limestones or other carbonates. Finally, a small (~1 cm^3) cube of sediment from each of Cores 64, 67, and 68 was taken from a location that showed high Ca on the ITRAX data: section H4 for both Core 64 and 67, and section I4 for Core 68. Core 57 was not sampled because the difference in Ca levels in the ITRAX data between basal and mm-laminated sediment was possibly unreliable. The strongest difference in Ca levels was in Core 68.

Figure 2.4 Map showing fieldwork locations for till and calcareous bedrock samples. Till samples are

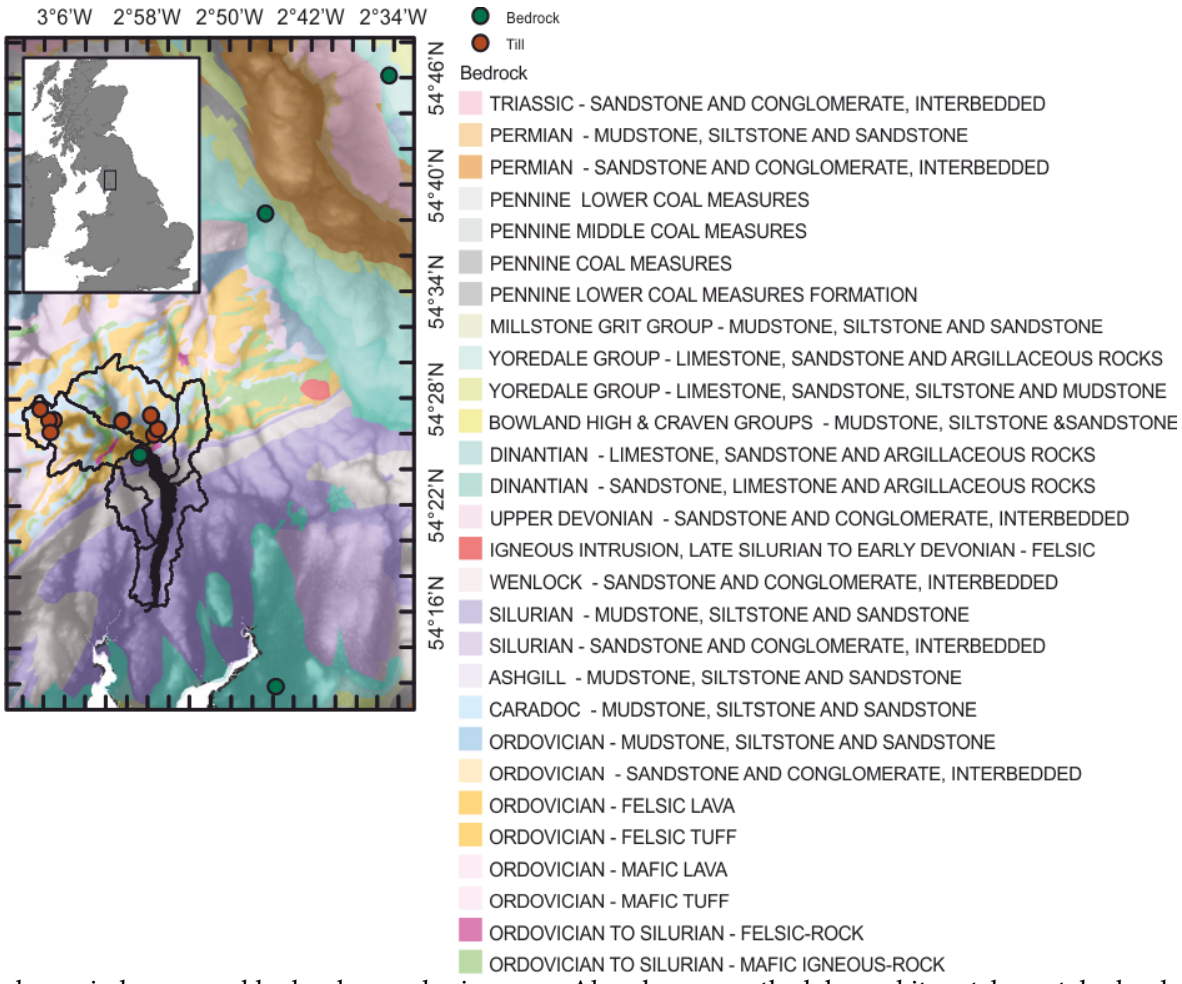

shown in brown and bedrock samples in green. Also shown are the lake and its catchment, bedrock geology at the 1:625 000 scale, terrain relief, and location in the UK.

A small amount of every sample (from all three types) was placed in contact with 10% nitric acid (HNO_3) in beakers. None of the till samples effervesced, but three rock samples did, as did all three sediment core samples. Based on these results, the three rock samples and sediment samples were selected for an acid leach, and the tills selected for total digest.

Small amounts of potential source rocks were crushed with a hammer then pestle and mortar to powder, and then placed in glass vials. The sediment samples were dried in a 50° C oven overnight then crushed to powder. In a clean lab, approximately 0.2 g of each sediment powder and 0.1 g of each rock sample were weighed out then placed in centrifuge tubes with 5 ml 5% acetic acid (CH_3COOH) and left overnight. Each tube was run in a centrifuge for five minutes to separate the leachate from the leftover sediment.

Using an acid-cleaned pipette, 20 µl sediment leachate was pipetted into clean bottles and diluted with 2 ml 3% HNO_3; 10 µl limestone leachate was also diluted with 5 ml 3% HNO_3. In addition, a blank was made up from 20 µl 5% CH_3COOH and 2 ml 3% HNO_3.

All diluted leachate samples and the blank were run on an inductively coupled plasma mass spectrometry instrument (ICP-MS) to ascertain Sr levels, where 0.5 µg is the lower end of measurable Sr. The results of this initial ICP-MS screen (Table 2.4) show that all six samples contained enough Sr to perform isotopic analysis on.

Standards screen	
Sample	**Sr (ppm, or µg/g)**
Blank	0
Sr 0.3 ppb	0
Sr 1 ppb	0.001
Sr 5 ppb	0.005
Sr 10 ppb	0.01
Sr 100 ppb	0.102
Samples screen	
Sample	**Sr (ppm, or µg/g)**
Blank	0
64H4	1.602
67H4	0.954
68I4	1.315
L1	11.39

Table 2.4 Pilot Sr screening levels from the ICP-MS. The top half of the table shows Sr standards being run, and the bottom half shows the results from the carbonate-rich Lake District samples.

L2	14.99
L5	2.188

An extract was taken from each diluted leachate in the volumes shown in Table 2.5 such that each extract contained 1 µg Sr. These extracts were then dried.

Table 2.5 Extracted leachate from each sample for one microgram of strontium.

Sample	**Extract amount (ml)**
64H4	0.6
67H4	1.0
68I4	0.8
L1	0.1
L2	0.1
L5	0.5

3. A new Holocene record of geomagnetic secular variation from Windermere, UK

In this chapter, the palaeomagnetic signal recorded in the sediments is investigated and compared with records from around the Northern Hemisphere. This chapter is a reproduction of an article published in Earth and Planetary Science Letters: "Avery, R. S., Xuan, C., Kemp, A. E. S., Bull, J. M., Cotterill, C. J., Fielding, J. J., Pearce, R. B., and Croudace, I. W. (2017), A new Holocene record of geomagnetic secular variation from Windermere, UK. Earth and Planetary Science Letters, 477C (2017) pp. 108-122, DOI 10.1016/j.epsl.2017.08.025". Supporting online-only information is included at the end of this chapter (Section 3.9).

3.1 Abstract

Palaeomagnetic secular variation (PSV) records serve as valuable independent stratigraphic correlation and dating tools for marine and terrestrial sediment sequences, and enhance knowledge of geomagnetic field dynamics. We present a new radiocarbon-dated record (WINPSV-12K) of Holocene geomagnetic secular variation from Windermere, updating the existing 1981 UK master PSV curve. Our analyses used continuous U-channel samples taken from the centre of four sediment cores retrieved from Windermere in 2012. The natural remanent magnetization (NRM) of each U-channel was measured before and after stepwise alternating field (AF) demagnetization on a superconducting rock magnetometer at intervals of 0.5-cm or 1-cm. The NRM data reveal a stable and well-defined primary magnetization.

Component declinations and inclinations estimated using Principal Component Analysis (PCA) of NRM data from the four Windermere cores correlate well on their independent radiocarbon age models. The four records were stacked using a sliding window bootstrap method, resulting in a composite Holocene PSV record (WINPSV-12K).

On millennial timescales, WINPSV-12K correlates well with other records from Western Europe and the northern North Atlantic to a resolution of ~1 kyr, given age uncertainties and spatial variability between records. WINPSV-12K also compares well to the CALS10k.2

and pfm9k.1a model predictions for Windermere. Key regionally-significant PSV inclination features of WINPSV-12K which correlate with other North Atlantic records include peaks at 5 – 6, 8.5, and 10 cal ka BP, and a trough at 7 cal ka BP. Key PSV declination features include the eastward swing from 5.5 – 2.3 cal ka BP followed by a major westward excursion at 2.3 cal ka BP, peaks at 1.1 and 7cal ka BP, and troughs at 5.4 and 8.2 cal ka BP, with the caveat that an estimated magnetic lock-in delay of at least 100 – 200 years is present. PSV variations on 1 – 3 kyr timescales are interpreted to represent strengthening and weakening of the North American versus the Siberian and European-Mediterranean high-latitude flux lobes, based on the close similarities between the North Atlantic regional records and the antiphase existing in the East Asian Stack record and the North East Pacific inclination stack. WINPSV-12K provides a regionally-important new PSV reference curve whose prominent features may serve as stratigraphic markers for North Atlantic palaeo-records.

3.2 Keywords

Palaeomagnetism, palaeoclimate, lake sediments, Holocene, Windermere, Palaeosecular Variation

3.3 Introduction

Palaeomagnetic secular variation (PSV) describes the variation in the Earth's geomagnetic field on timescales of a hundred years or longer in periods of stable magnetic polarity, and exhibits substantial variation throughout the Holocene (Turner et al., 2015; Turner and Thompson, 1981; Zheng et al., 2014). Fine magnetic particles in marine and lacustrine settings often preserve the direction and intensity information of the Earth's magnetic field during and shortly after deposition, forming a continuous PSV archive. Lake sediments are conducive to palaeo-record preservation due to relatively high sedimentation rates, good accessibility, and little influence from currents, waves, and macrofaunal bioturbation. PSV records reconstructed from marine and lacustrine sediments have become increasingly utilized over the last few decades (Mackereth, 1971; Ojala and Saarinen, 2002; Snowball et al., 2007; Stoner et al., 2013, 2007; Turner et al., 2015; Zheng et al., 2014). These records

provide continuous information on geomagnetic field dynamics beyond historical observations and archaeological measurements (Batt et al., 2017; Jackson et al., 2000), and provide data to inform and improve geomagnetic field models (Brown and Korte, 2016; Constable et al., 2016; Nilsson et al., 2014) while serving as a valuable stratigraphic correlation and dating tool that is independent of climate and ecological systems (Ólafsdóttir et al., 2013). In sediment cores exhibiting high sedimentation rates and little bioturbation, PSV records are particularly suitable for dating and improving the correlation of sedimentary records even over large regions (Zheng et al., 2014), and are thus valuable in developing understanding of rapid changes and diachroneity in the Earth System at high temporal resolution. There is a need across locations used in the study of late Quaternary climate variability to produce and utilize more PSV records using reliable dating methods, high measurement resolution (1 cm or better), and continuous sampling and measurement techniques. Having an independent dating and stratigraphic tool other than tephra layers enables the correlation of more spatially distributed records, especially between locations with no common tephra horizons.

The location of Windermere, UK, provides an opportunity to link continental Europe with Icelandic and Greenlandic records (Figure 3.1). Measurement of declination in the UK demonstrated the potential for the use of PSV as a dating method (Mackereth, 1971). The UK PSV master curve constructed in 1979-81 (Thompson and Turner, 1979; Turner and Thompson, 1981) has been used both to date other PSV records from around Europe (Saarinen, 1999; Vigliotti, 2006) and also in the construction of several palaeomagnetic field models, thus furthering understanding of the geomagnetic field (Constable et al., 2016). There has been little study of UK-based Holocene palaeomagnetic records since the development of the existing UK master curve, which was largely dated using 20 cm thick bulk radiocarbon samples using older radiocarbon processing methods (Thompson and Turner, 1979; Turner and Thompson, 1981). New piston cores from Windermere provide the opportunity to update the UK master curve (which was constructed partially from cores from Windermere, along with Llyn Geirionydd and Loch Lomond) using modern dating and palaeomagnetic analyses. The new cores span the length of Windermere, whereas the Windermere cores collected by Turner using a 'Mackereth' corer were all from a location similar to that of our Core 57 (Figure 3.1) (Turner and Thompson, 1981).

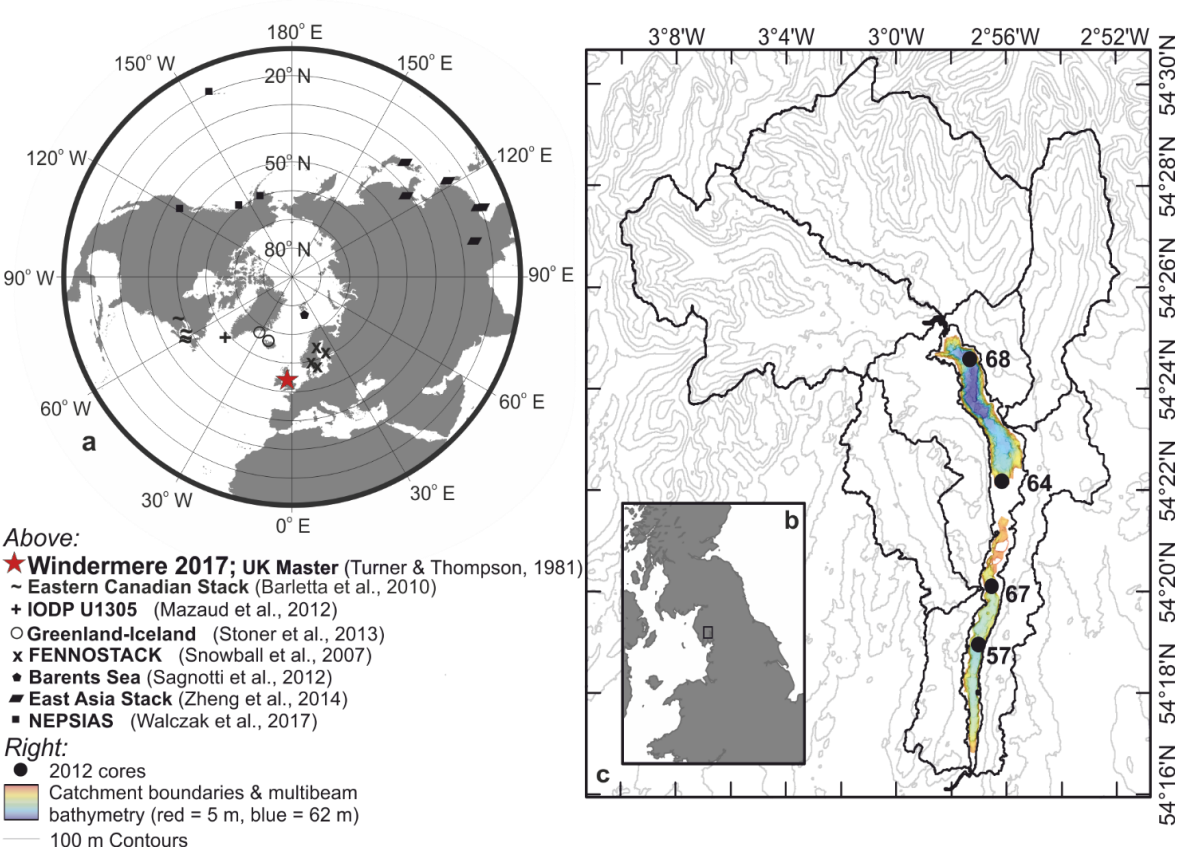

Figure 3.1. Above: Map of the 10 – 90° N latitudes, showing the locations of both Windermere (red star) and comparative records (other markers). Right: Map of the catchment of Windermere with 100 m contour lines, multibeam lake bathymetry, and core locations. Inset: Location of Windermere in the British Isles (black box).

In this study, we construct a composite Holocene PSV record (WINPSV-12K) using four sediment cores from Windermere, UK (Figure 3.1), with a view to updating the UK PSV master curve (Thompson and Turner, 1979; Turner and Thompson, 1981). The accelerator mass spectrometry (AMS) radiocarbon-dated record is high-resolution, with core sedimentation rates of 20 - 50 cm/kyr and palaeomagnetic measurements every 0.5 – 1 cm. WINPSV-12K is compared to well-dated records from the North Atlantic (Mazaud et al., 2012; Stoner et al., 2013), Scandinavia (Sagnotti et al., 2012; Snowball et al., 2007), the existing UK master PSV curve (Turner and Thompson, 1981), the UK archaeomagnetic curve (Batt et al., 2017), eastern Canada (Barletta et al., 2010), East Asia (Zheng et al., 2014), and the North East Pacific (Walczak et al., 2017). WINPSV-12K serves as a valuable new curve for synchronization of Holocene marine-terrestrial records across the northern North Atlantic (NNA) geomagnetic region.

3.4 Materials and Methods

3.4.1 Geological setting of Windermere

Windermere, situated in the southeast of the English Lake District near the West coast of England (54.04° N, 2.95° W), is a north-south trending glacial ribbon lake in a steep-sided pre-glacial river valley overdeepened by successive glaciations (Pennington and Pearsall, 1973; Pinson et al., 2013). The lake is 17 km long with a maximum width of 1.5 km, an elevation of 39 m above Ordnance Datum Newlyn, and a present maximum water depth of 62 m (Lowag et al., 2012; Miller et al., 2013). Windermere drains a catchment of 242 km^2 (Miller et al., 2013) with Ordovician Borrowdale Volcanic Group bedrock in the north and Windermere Supergroup (Silurian mudstones and siltstones) in the south. A bedrock high separates Windermere into a north and South Basin, and a sill dams the lake in the south forcing drainage to the west into the River Leven (Wilson, 1987). Windermere in its present form has been accumulating sediment since exposure following the retreat of the British-Irish Ice Sheet c. 17 ka BP (Ballantyne et al., 2009; Coope and Pennington, 1977).

3.4.2 Coring and core stratigraphy

A multibeam bathymetry site survey coupled with chirp, parametric, and multi-channel boomer seismic reflection surveys were used to identify sediment depocentres which had not been significantly disturbed by meter-scale mass transport deposits (Lowag et al., 2012; Miller et al., 2013; Vardy et al., 2010). Several sediment cores were collected using both a Uwitec piston corer and Uwitec gravity corer in 2012 as part of a coring campaign by the British Geological Survey (BGS) and the University of Southampton. Piston cores were acquired in 2 m sequential sections with 9 cm diameter core barrels. The piston core sections were then cut into 1 m sections and split lengthways into working and archive halves. Four 6 - 10 m long cores with the highest deposition rates and longest timespans of the core suite were selected for this study (Figure 3.2).

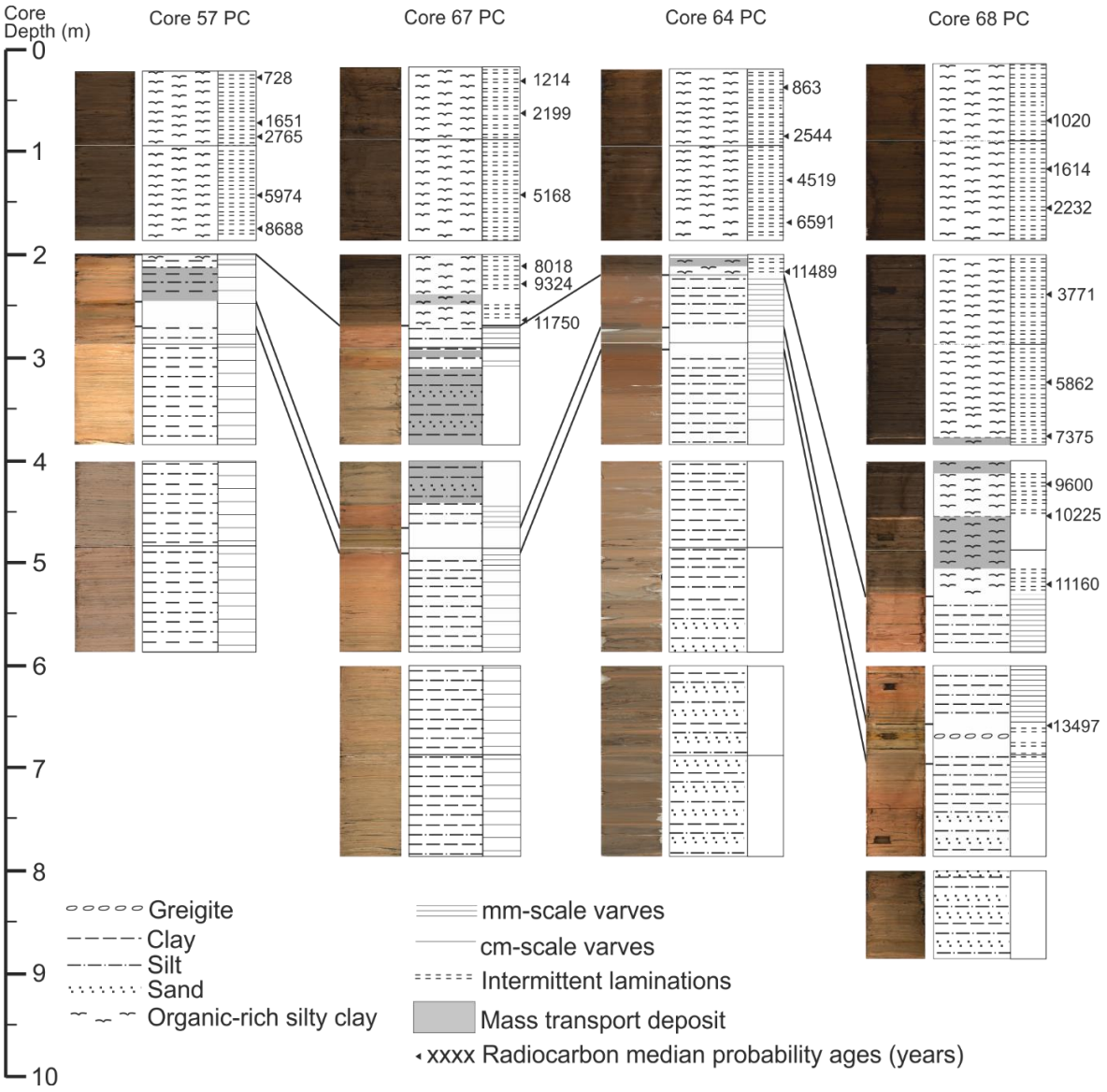

Figure 3.2. Core image (left) and lithostratigraphy (right) of Windermere Cores 57, 67, 64, and 68. The Holocene PSV record is based on the dark brown organic sections of the four cores. Lithostratigraphic tie-points between the cores are included. Sediment ages given are median-probability radiocarbon dates in cal y BP calculated with Calib 7.1 (Stuiver and Reimer, 1993) using the Intcal13 calibration curve (Reimer et al., 2013).

Each of the four cores has an inorganic mineral-rich base and a brown organic-rich top with a sharp transition between the two major lithologies (Figure 3.2). Cores from the North Basin (Cores 64 and 68) have disturbed bases attributed to oscillating proximal glaciers in the North Basin catchment, whilst the bases of the cores from the South Basin (Cores 57 and 67) have thick cm-scale varves comprising silt and clay. Overlying the basal sediment of all four cores are mm-scale clastic silt and clay varves. These are overlain by an organic-bearing non-varved silty clay unit with differing small-scale features in each core (e.g. diatoms, iron

inclusions, presence/absence of laminations) controlled by depocentre-specific conditions. This is succeeded by a unit of mm-scale clastic varves, overlain in turn by a relatively uniform, organic-rich, intermittently-laminated brown pelletized mud of Holocene age. Mass-transport deposits (MTDs) are present in all cores, mostly of a thickness less than 20 cm, although there are two thicker MTDs: one in the Lateglacial sediment of the South Basin (1.5 m), and the other in the early Holocene sediment of the North Basin (0.53 m) (Figure 3.2). Inspection of the microstructure of the sediment using a scanning electron microscope and transmitted light microscope indicate that MTDs are not present in the Holocene sediment of the piston cores except at the base.

3.4.3 Palaeomagnetic samples and measurements

The four cores were continuously sampled using U-channels (~1.8 × 1.9 cm^2 cross-section and the length of the core section) from the centre of the working half of each core section. The natural remanent magnetization (NRM) of each U-channel was measured at the University of Southampton on a 2G Enterprises superconducting rock magnetometer (SRM) designed for U-channel samples. Measurements for each U-channel were made at 0.5-cm (Core 68) or 1-cm (Cores 57, 64, and 67, since the results were equally good but quicker to produce) intervals with an additional 10 cm measured beyond both ends of the sample. NRM of the U-channels were measured before and after stepwise alternating field (AF) demagnetization with peak fields up to 100 mT (see Table 3.1 (Supplementary Table 1) for details). After completion of NRM measurements for each U-channel, an anhysteretic remanent magnetization (ARM) was imparted in a 100-mT peak AF and a 50-μT direct current (DC) bias field along the long-axis of the U-channel. The acquired ARM was measured prior to demagnetization and after stepwise AF demagnetization at the same peak fields used for NRM. Subsequently, the U-channels were used for progressive ARM acquisition, during which each U-channel acquired increasing ARM as the peak AF (along the long axis of the U-channel) was increased using the same peak fields used for NRM with a constant 50-μT DC bias field. For each ARM acquisition step, the acquired (partial) ARM was measured at the same intervals as for NRM.

Bulk sediment samples from representative lithologies of the four cores were taken for room temperature hysteresis loops, backfield, and isothermal remanent magnetization (IRM) acquisition experiments on a Princeton Measurements Corp. Model 3900 Vibrating

Sample Magnetometer (VSM) at the University of Southampton. IRM of the samples were acquired and measured at fifty field steps on a logarithmic scale ranging from ~0.4 μT to 1 T. Hysteresis loops of the samples were measured at 5-mT field steps, with the applied field ranging between -1 T and +1 T. For the backfield experiment, a 1-T field was first applied, followed by repeated remanence measurements after increasing the applied field (with a 2-mT increment) in the opposite direction until zero remanence was reached. Hysteresis loop data were drift-corrected following the procedures suggested by Jackson and Solheid (2010), and normalized against sample mass. Selected bulk samples were also freeze-dried and ground, then magnetic susceptibility of the samples was monitored on heating from room temperature to 700 °C and subsequent cooling to room temperature, in an argon gas environment, using an AGICO KLY-4S Susceptibility Bridge.

3.4.4 Age model construction

Age models for Cores 57, 67, 64 and 68 (Figure 3.3) were constructed using 4, 6, 4, and 9 accelerator mass spectrometry (AMS) radiocarbon dates respectively. Dates were ascertained from both macrofossils such as terrestrial leaves and twigs, and from 1 cm thickness bulk sediment samples. Radiocarbon sample depths are indicated in Figure 3.2. Radiocarbon dates were provided by the NERC Radiocarbon Facility in East Kilbride, Scotland, and dates were calibrated using Calib 7.1 (Stuiver and Reimer, 1993) and the Intcal13 calibration curve (Reimer et al., 2013). An additional date at each core top was acquired using ^{137}Cs and ^{210}Pb radiochronology. Dating sample details are summarized in Table 3.2 (Supplementary Table 2). [Thesis-only edit: An outline of construction of the ^{137}Cs and ^{210}Pb chronology is given in Section 2.8.4 and Appendix A, and further details may be found in (Fielding, 2017).]

Sections of sediment containing MTDs were removed from the depth records prior to construction of a 'normal sedimentation' age model (Figure 3.3). The start of the Holocene has been dated to ~11.7 cal ka BP (Walker et al., 2009), and the radiocarbon dates from the Windermere cores show that an abrupt lithological transition from inorganic-dominant silt and clay varves to organic-rich intermittently laminated mud occurred around this time. We therefore take this transition to mark the start of the Holocene in Windermere.

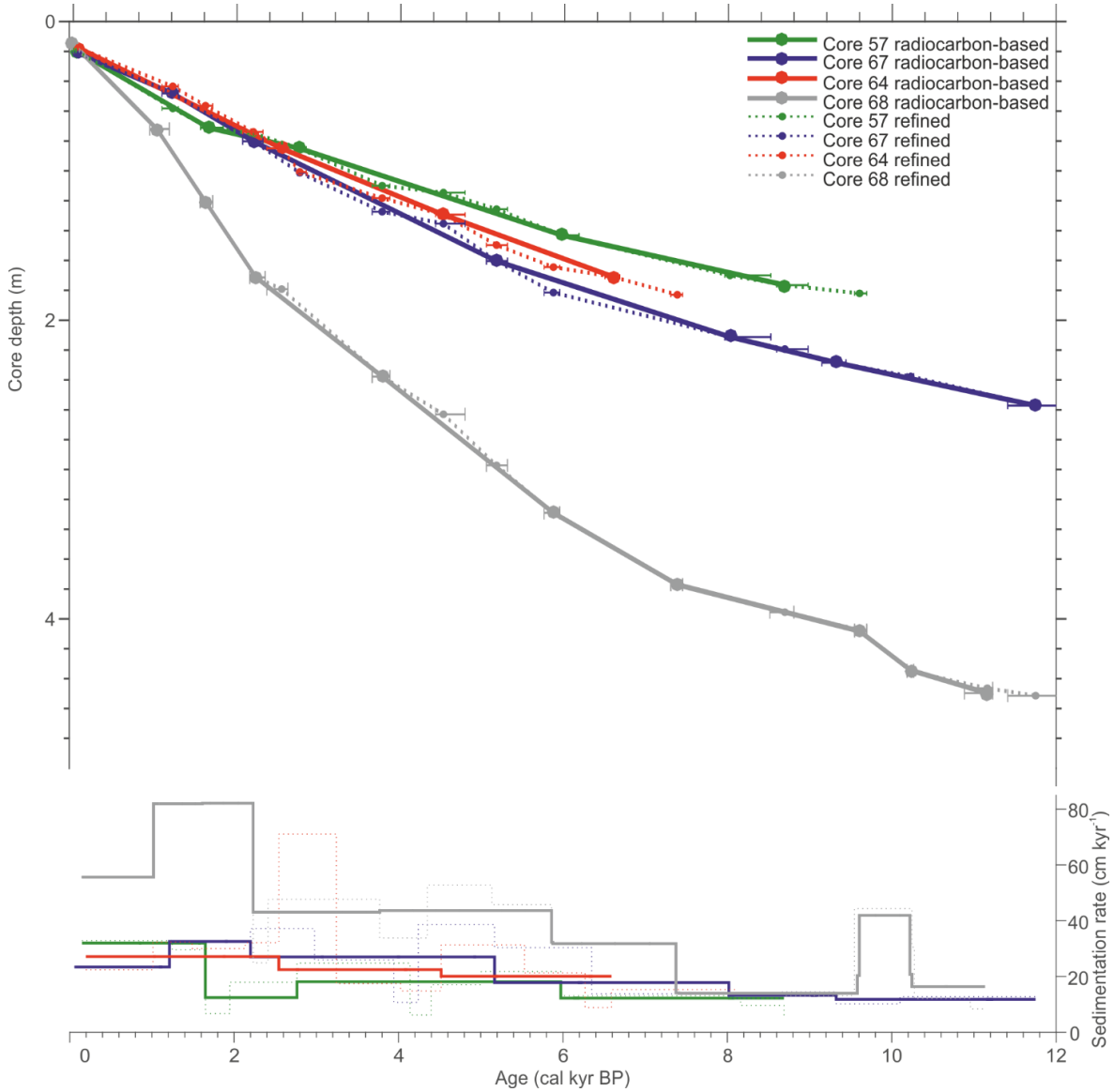

Figure 3.3. Age-depth profiles (upper panel) and sedimentation rates (lower panel) for Windermere Cores 57 (green), 67 (blue), 64 (red), and 68 (grey). Ages are based on calibrated (Calib7.1; Stuiver and Reimer, 1993) radiocarbon dates (NRCF 1736.1013; NRCF 1856.1014) calibrated with the IntCal13 calibration curve (Reimer et al., 2013). Markers indicate median probability calibrated radiocarbon dates, and error bars indicate the upper and lower 2σ age calibrations. Points are fitted using a linear interpolation. Smaller markers and dotted lines indicate transferred radiocarbon tie-points from other cores and thus the refined age model used when building the WINPSV-12K stack. Sedimentation rates are shown below on both original and refined age models.

3.5 Results

3.5.1 Magnetic minerology

Median destruction field (MDF) of the NRM across the four cores (Figure 3.11 (Supplementary Figure 1a – d)) ranges from 44-58 mT (comparable to 43-45 mT reported by Turner and Thompson (1981) for Windermere cores). NRM of the Holocene sediment in all four cores was completely demagnetized after AF demagnetization with a 100 mT peak field (see Figure 3.4), suggesting a low-coercivity Holocene NRM carrier such as magnetite. Magnetic susceptibility of Holocene samples from the cores show a possible Hopkinson peak at ~520 °C upon heating (Figure 3.5a) and abrupt decrease or increase at temperatures of ~580-585 °C during heating (Figure 3.5a) and cooling (Figure 3.5b) respectively, further suggesting magnetite as the primary magnetization carrier in the Holocene sediment. Additionally, gradients of the IRM acquisition curves for Holocene sediments follow normal distributions (on logarithmic field scales) with mean coercivity of ~50-70 mT (Figure 3.5e) show that the Holocene sediment samples typically reach saturation at an applied field of <100 mT, and contain a significant amount of paramagnetic materials. Coercivity of remanence for the samples is mostly around 45 mT (inset in Figure 3.5e). Hysteresis parameter ratios (i.e. Mr/Ms and Hcr/Hc, where Mr, Ms, Hcr, and Hc are saturation remanence, saturation magnetization, coercivity of remanence, and coercivity, respectively) of all Holocene samples are shown on a Day et al. (1977) plot in Figure 3.5f. Holocene sediments from all four cores fall into the pseudo-single domain (PSD) category, in the area associated with fine magnetite particles.

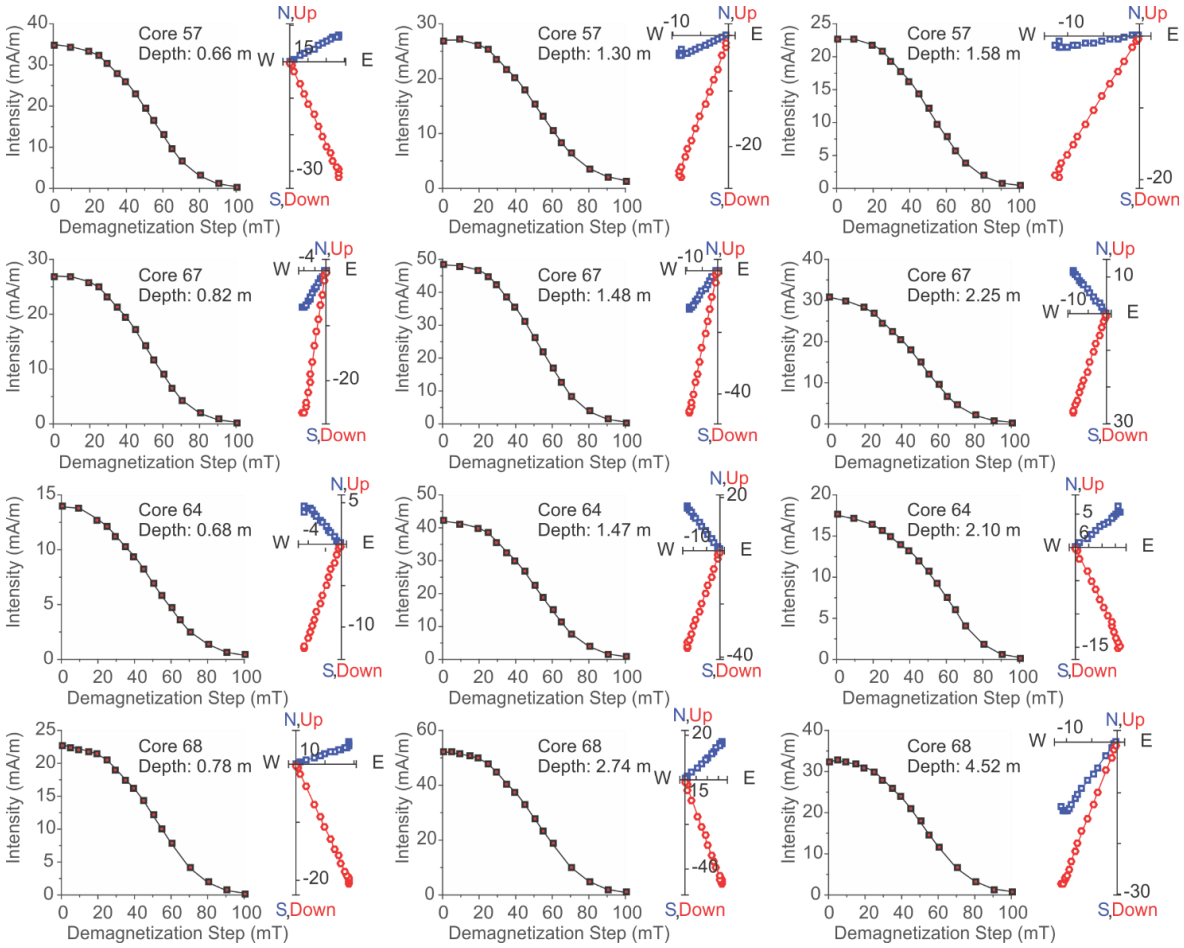

Figure 3.4**.** Representative NRM AF demagnetization behaviours of Holocene sediments of Cores 57, 67, 64, and 68. For each selected 1-cm interval from the four cores, the NRM intensity versus AF demagnetization step plot are shown on the left and the orthogonal projection plot of NRM is shown on the right (blue squares = horizontal projections, red circles = vertical projections). Three examples are shown from each core.

AF demagnetization on NRM of pre-Holocene (Lateglacial) sediments in the cores clearly show the presence of a high coercivity component (e.g. Figure 3.12 (Supplementary Figure 2)). Further magnetic mineralogy experiments including hysteresis loops and IRM acquisition also indicate the existence of a high coercivity magnetic mineral. This high coercivity magnetic component clearly has a large influence on NRM of the sediments, for example large inclination deviations of tens of degrees from the Holocene interval and from the expected geocentric axial dipole (GAD) inclination for the core locations. It is possible that magnetite in the Holocene Windermere sediments is soil-derived through soil magnetite enrichment (Mullins, 1977), while Lateglacial Windermere sediments are mainly derived from erosion of the up-catchment weathered volcanic bedrock that could contain hematite (Stone et al., 2010). The pre-Holocene Windermere sediments are not considered

suitable for PSV studies due to large lithology-induced inclination fluctuations. This PSV study therefore focuses on Windermere's Holocene sediments, with magnetite as the single primary magnetization carrier. The Holocene sediments of Windermere appear similar between cores, and relatively uniform within-core (with the exception of the very early Holocene, where terrigenous material is more abundant). The base sediment matrix comprises pelletized mud containing organic fragments and numerous microfossils (e.g. diatoms and chironomids), with no detectable carbonate. Each core exhibits intermittent millimetre-scale laminations which differ in detrital versus organic material, and therefore density. Some iron variations correspond with these laminations, which can vary over several laminae. The bands are much thinner than the SRM response function and upon inspection of the sediment do not appear to affect the downcore magnetic parameters. The mineralogy experiments also confirm that fine-grained magnetite is dominant throughout the Holocene. Total organic content for the majority of the Holocene is typically 9-15% [Thesis-only: See additional Figure 3.15]. Downcore values of ARM/κ (where κ is magnetic susceptibility) for Cores 67, 64, and 68 largely follow the general pattern of ARM, whilst ARM/κ for Core 57 is in antiphase with NRM MDF (Figure 3.11 (Supplementary Figure 1)).

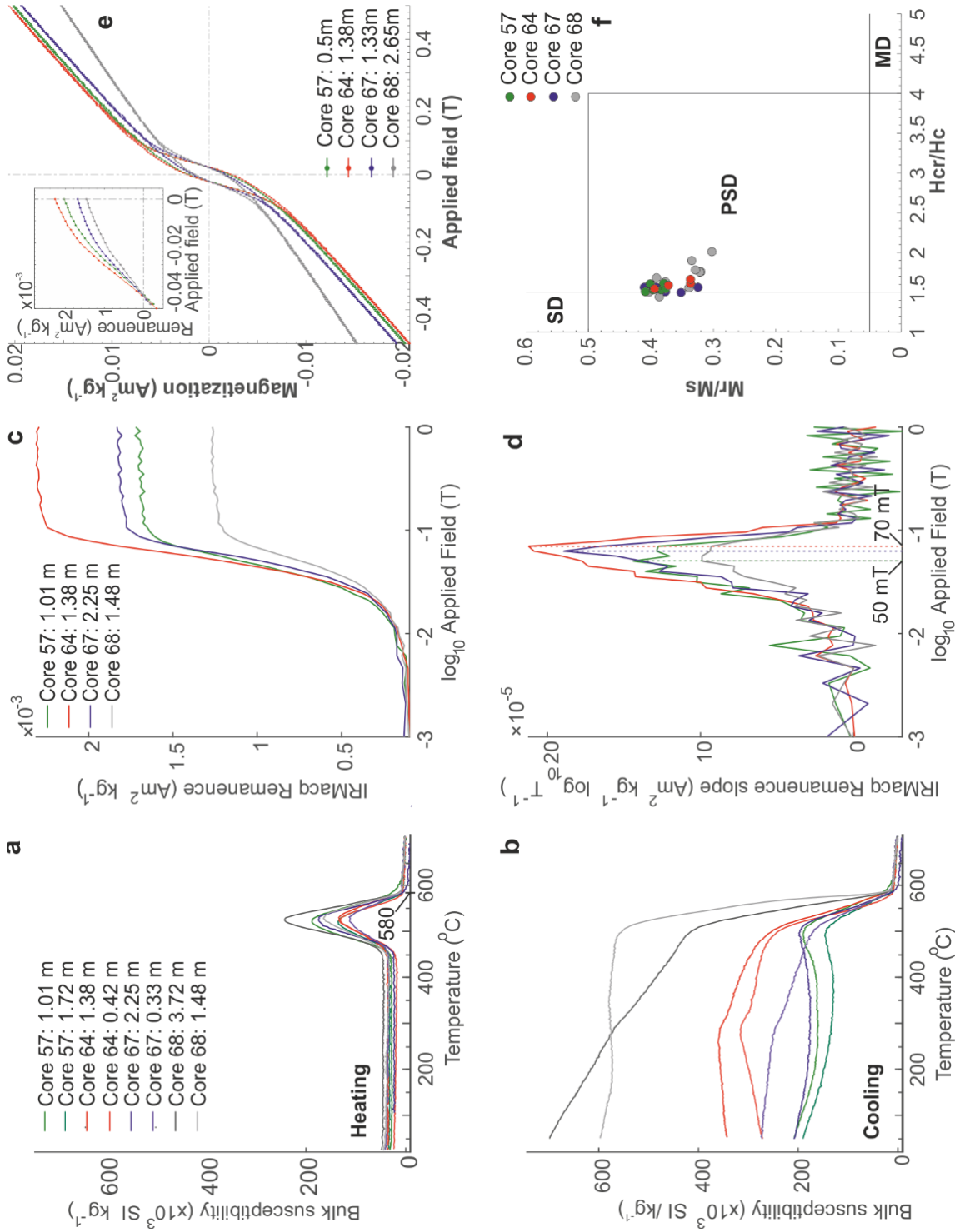

Figure 3.5 Magnetic susceptibility of Holocene bulk sediments from the four cores monitored while (a) heating the samples from room temperature to 700°C, and (b) cooling the samples from 700°C to room temperature. (c) IRM acquisition curves for selected bulk samples from the four cores, (d) gradient of the IRM acquisition curves, (e) hysteresis loops and backfield data of representative Holocene samples from the four cores, and (f) hysteresis parameter ratios of all measured Holocene samples shown on a Day et al. (1977) plot. The thermomagnetic curves show abrupt changes at ~580°C, and the gradient of IRM acquisition curves show single magnetic components with mean coercivity of ~50-70 mT.

3.5.2 Palaeomagnetic directional records

For each U-channel measurement interval, component magnetization directions were calculated using principal component analysis (PCA, Kirschvink, 1980) and UPmag software (Xuan and Channell, 2009). PCA calculations used NRM data acquired during the 20-60 mT demagnetization interval (without anchoring directions to the origin of orthogonal projections), and are associated with maximum angular deviation (MAD) values that monitor the quality of fitting for the PCA. MAD values associated with the PCA estimates for all four cores are generally <1°, indicating the component directions are very well defined (see Figure 3.11(Supplementary Figure 1a – d)). Results were removed from intervals with voids, apparent disturbance (including the core tops), and MTDs. Results from the top and bottom 4 cm of the U-channels were also removed to avoid edge effects due to convolution of the magnetometer sensor response function.

The studied cores had not been azimuthally oriented during coring and splitting, so declination values for each core-section are arbitrary. The approximate time duration covered by individual 1 m core sections ranges from approximately 1 – 4 kyr according to the radiocarbon based age models. Correction of declination values of each core by a simple subtraction of the mean was considered unsuitable because significant secular variation occurs on this millennial timescale. Component declinations of each core were placed on their independent radiocarbon age models and compared to the well-dated Greenland-Iceland composite declination record (Stoner et al., 2013, 2007). Declination correction for each core section was performed by subtracting the mean difference between prominent declination features on the Greenland-Iceland composite curve and those of each Windermere core section where they overlap in time. Cores used to construct the Greenland-Iceland composite curve had been split on a constant plane (Stoner et al., 2007) and declination of the cores had been corrected to have zero mean, which is reasonable considering that over ten thousand years of geomagnetic behaviour is being averaged (Merrill and McFadden, 2003).

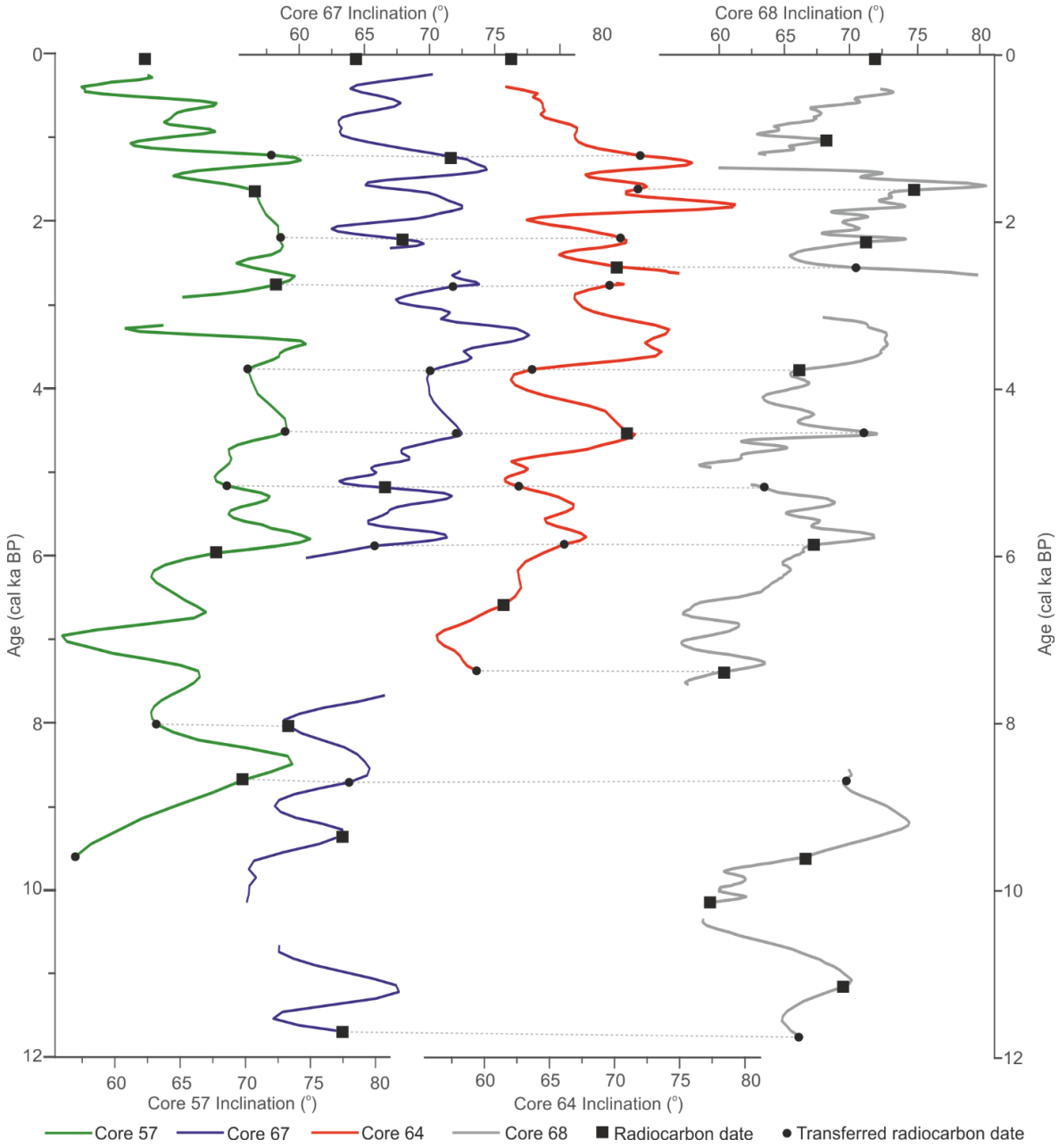

Figure 3.6: Holocene inclination curves for the Windermere suite (Core 57: green, Core 67: blue, Core 64: red, Core 68: grey) on refined age models, showing the locations of radiocarbon dates for each core (black squares) and radiocarbon dates transferred from other Windermere cores based on inclination features (black circles). Grey dashed lines indicate tiepoints between curves. Declination and RPI curves were subsequently placed on this age model (see Figure 3.7).

Component inclinations from the four cores vary between 54° to 83° with similar mean values of ~65 - 70°. On the radiocarbon chronology, component inclinations of the cores show correlations. The age model for each core was refined by transferring selected

radiocarbon dates (closed square; Figure 3.6) from the other three cores through correlating appropriate inclination features. The refined age models (dashed lines; Figure 3.3) were then used for other down-core records. On a millennial timescale, component inclinations from the four cores show a similar pattern including steeper inclinations between 1 - 7 cal ka BP and shallower inclinations between 6 - 9 cal ka BP (Figure 3.6, Figure 3.7a). Common sub-millennial inclination features include the four peaks between ~3.5 - 6 cal ka BP and similar variabilities between ~8.5 - 11.5 cal ka BP. Corrected declinations from the four cores also show common features such as high-amplitude variabilities since 4 cal ka BP and relatively low amplitude changes prior to 4 cal ka BP (Figure 3.7b). There are also differences in both inclination and declination records between the four cores, especially on centennial timescales. [Thesis only: for example, the Core 68 peak at ~9.2 cal ka BP is older than Cores 57 and 67 due to radiocarbon constraints; the Core 57 trough at ~3.2 cal ka BP is older than the troughs of the other cores due to core-section gap constraints.] These differences could be caused by changes in sedimentation rates not accounted for by the radiocarbon dates from each core (Ólafsdóttir et al., 2013), the differing smoothing effects of the sediment magnetization process (due to lock-in) from each sedimentation rate, and age model uncertainties. The cores may also have subtly-differing lithologies, since they are situated in separate sediment depocentres (Figure 3.1). Differences between the palaeomagnetic directions of the four cores do not appear to relate to higher MAD values. ARM/k and NRM MDF both show similar overall trends: ARM/ κ in all four cores indicates magnetic grain size slightly fining upward from the base of the Holocene to about 6 cal ka BP, then slightly coarsening throughout the remainder of the Holocene (and the Day Plot also shows little difference in grain size within and between cores), so magnetic grain size does not appear to underlie the between-core differences.

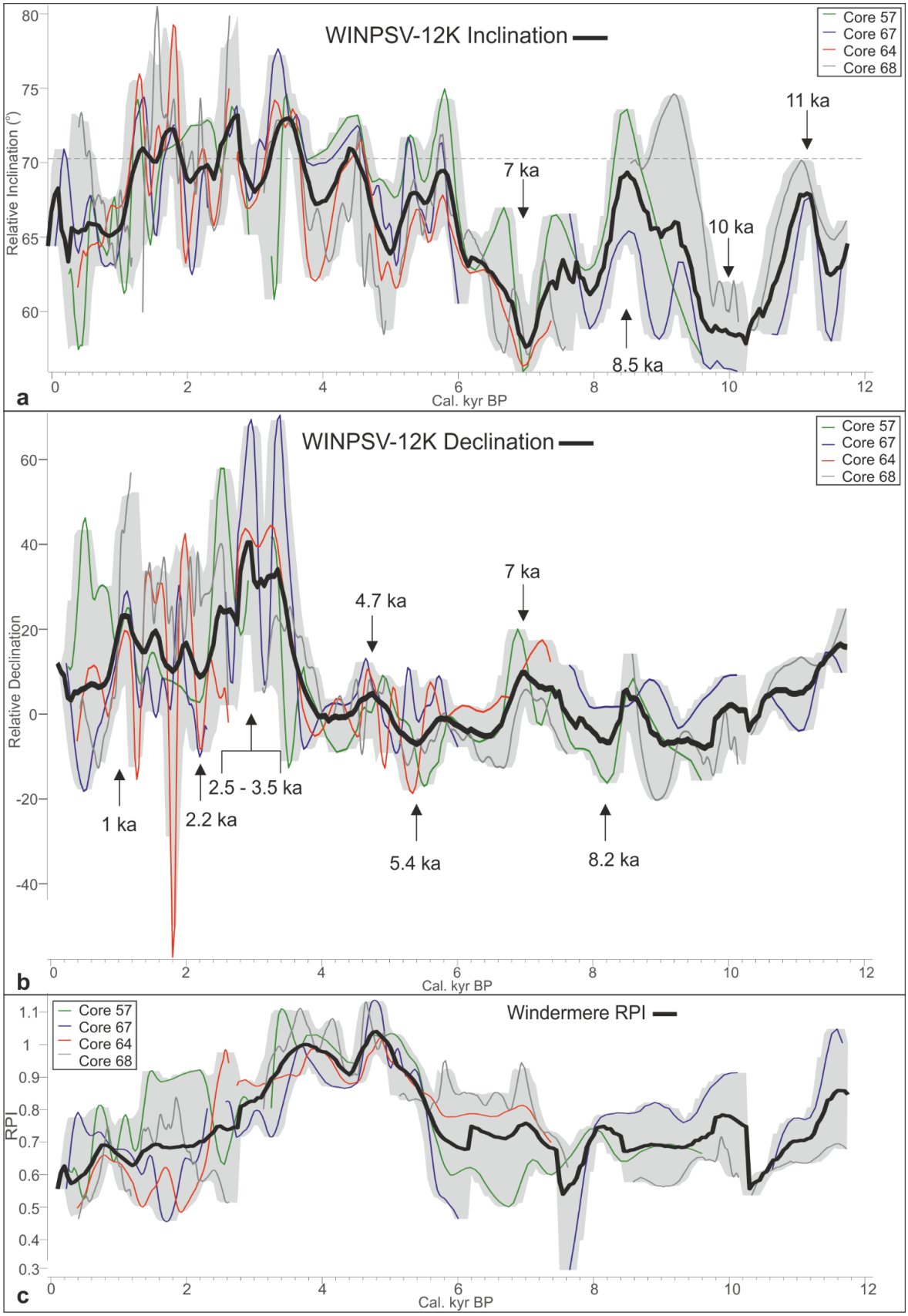

Figure 3.7: Stacked Windermere palaeomagnetic records for (a) inclination; (b) declination; and (c) RPI. Each panel individual records from Cores 68 (grey), 64 (red), 67 (blue), and 57 (green) overlain with the WINPSV-12K stack (black) with 90% confidence interval estimate

from 10,000 bootstrapped populations (grey envelope). Dipole inclination value for the latitude of Windermere is shown as dashed black line in Figure 3.7(a). Key features of WINPSV-12K are marked with vertical arrows.

To average out noise and highlight common palaeomagnetic directional changes, the direction and intensity records of the Windermere cores were stacked over the last ~12 kyr to form WINPSV-12K. Construction of the stack records followed a similar method to Xuan et al. (2016) for a North Atlantic palaeointensity stack (HINAPIS) record. The four Holocene records were normalized to have common means and standard deviations for each variable. The stacking was performed at 50-year intervals between -50 and 11750 cal y BP, with an interval half-window size of 150 years (comparable to the mean uncertainty of the calibrated ages). At each interval centre and for each variable, 2500 values were randomly taken from each core record within the interval window. A square interval window was used, giving all age possibilities within the window an equal weight. Each subsequent window overlapped with the previous one by 250 y. For each time interval, the stack was formed from the mean of the total randomly taken values (10,000 where no core records had gaps), and the top and bottom 5% of values were identified to estimate the 90% confidence intervals (Figure 3.7).

3.5.3 Relative palaeointensity estimates

Normalized records of sedimentary NRM are often used as a proxy for relative palaeointensity (RPI) of the geomagnetic field (Levi and Banerjee, 1976; Tauxe, 1993). Normalization is generally carried out using laboratory-induced magnetization such as anhysteretic remanent magnetization (ARM), isothermal remanent magnetization (IRM), or magnetic susceptibility, to compensate for changes in magnetic concentration of remanence carrying grains. For each 0.5-cm (Core 68) or 1-cm (Cores 57, 67, and 64) measurement interval of the Windermere cores, RPI proxies (Figure 3.11 (Supplementary Figure 1)) were calculated using the slopes of best-fit lines between NRM lost vs. ARM lost as well as NRM lost vs. ARM acquired during 20-60 mT treatment steps (where the slopes of best-fit lines between NRM lost and ARM acquired are multiplied by -1). RPI estimates were determined using the UPmag software (Xuan and Channell, 2009), and each slope calculation was accompanied by a linear correlation coefficient (R-value) that monitors the quality of the line fit (mean R-values sat around 0.981 – 0.996).

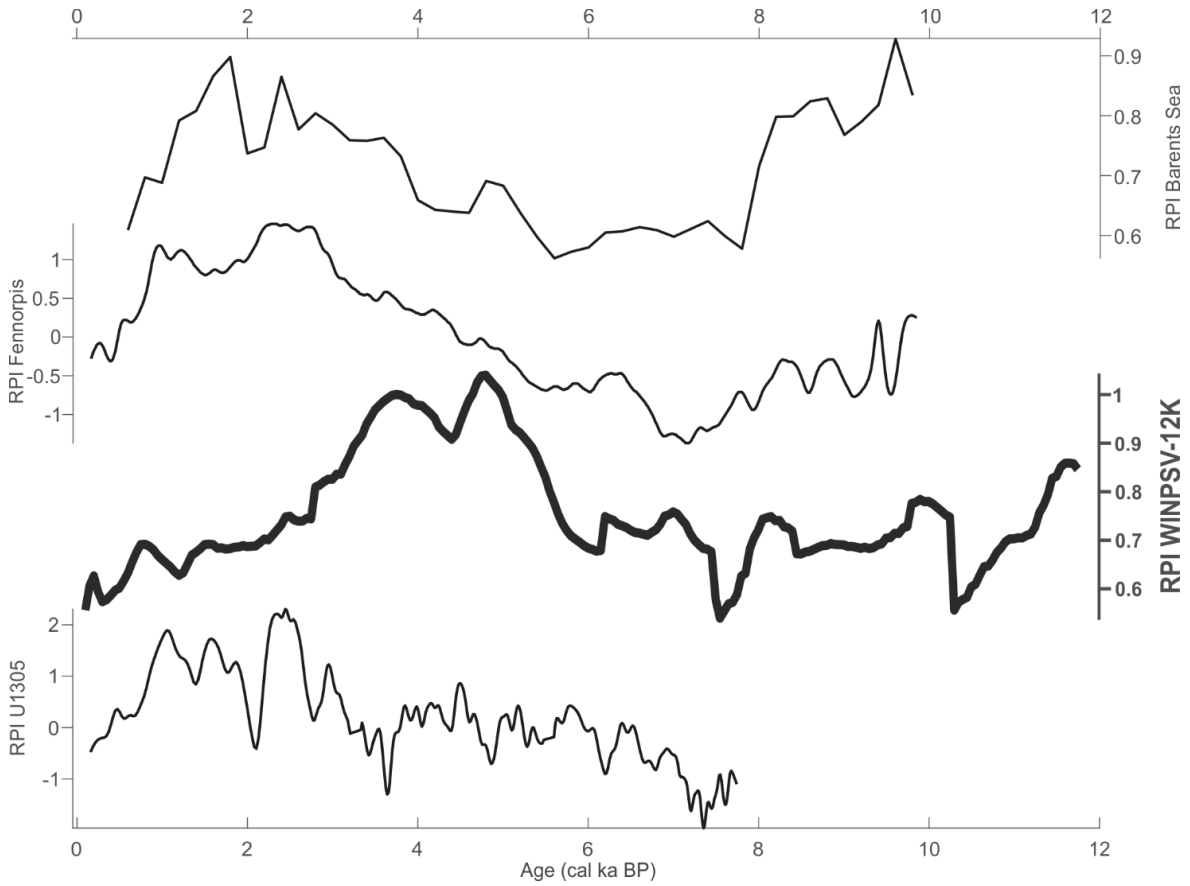

Figure 3.8: WINPSV-12K RPI record compared with RPI records from nearby regions. From top to bottom: the Barents Sea (Sagnotti et al., 2012), FENNORPIS (Snowball et al., 2007), WINPSV-12K, and IODP U1305 (Mazaud et al., 2012).

3.6 Discussion

3.6.1 Holocene PSV at Windermere

The WINPSV-12K inclination stack (Figure 3.7a) exhibits centennial-scale variation with peak-to-trough boundaries of 55° - 75° and a mean of ~65°, close to (and slightly shallower than) the expected geocentric dipole inclination of ~70° at Windermere. The whole Holocene inclination stack shows a quasi-regular inclination variability on a ~1-kyr timescale, with each swing (peak to trough) being ~6°. WINPSV-12K inclinations are generally shallower between 6 - 12 cal ka BP (mean of ~63°) and steeper since 6 cal ka BP (mean of ~69°). Notable inclination stack features include characteristic peaks at ~8.5 and ~11 cal ka BP, and troughs at ~7 and ~10 cal ka BP.

The WINPSV-12K declination stack exhibits peak-to-trough variation within a range of 55° (Figure 3.7b). The individual declination curves follow similar trends on a multi-kyr

timescale but are less similar on short timescale than the inclination curves, possibly related to uncertainties on core section declination corrections. An eastward declination feature from ~2.5 - 3.5 cal ka BP dominates the record, accompanied by other prominent eastward declinations at ~1, ~4.7, and ~7 cal ka BP. WINPSV-12K declination also exhibits marked troughs (i.e. westward declinations) at ~2.2, ~5.4, and ~8.2 cal ka BP.

The four RPI records generally agree with each other on millennial timescales, showing high RPI between ~3 - 5 cal ka BP, and low RPI between ~6 - 11 cal ka BP and after ~2.5 cal ka BP (Figure 3.7c). On sub-millennial timescales, the four records correlate less well. A reliable RPI record would not correlate with the normalizer, since a high correlation implies inappropriate normalization and undue influence of grain size or lithology on the RPI signal. RPI estimates from Cores 57, 67, and 68 show low correlations with their corresponding normalizer records (Figure 3.11, Figure 3.13 (Supplementary Figures. 1 and 3 respectively)), suggesting the RPI records from these cores are generally not influenced by lithology. The strong correlation between RPI and ARM for Core 64 is mostly caused by the sediment younger than 2.5 cal ka BP (~0.8 m depth) (Figure 3.11c, Figure 3.13c (Supplementary Figures. 1c and 3c respectively)).

The RPI stack exhibits a broadly similar trend on a multi-millennial timescale to other published records from nearby regions, including FENNORPIS (Snowball et al., 2007), the stacked EGLACOM and SVAIS records from the Barents Sea (Sagnotti et al., 2012), and IODP Site U1305 (Stoner et al., 2013) (Figure 3.8) [Thesis only: with the exception of the last ~3.8 kyr]. The Barents Sea, FENNORPIS, and Windermere records all show generally decreasing RPI from early Holocene to ~7 cal ka BP. After ~7 cal ka BP, the Barents Sea, FENNORPIS, and IODP Site U1305 records show increasing RPI until ~1-3 cal ka BP, followed by decreasing RPI. The Windermere RPI, however, starts to decline after ~3.8 cal ka BP in all four cores (Figure 3.7c). No apparent changes in lithology or magnetic remanence carrier were observed over the last ~4 kyr, compared with the earlier Holocene sediment. The disparity of the Windermere RPI compared with other records during the last 3.8 kyr is likely related to inappropriate normalization (probably over-normalization) of the NRM in the upper sediments. For example, subtle changes in floc size due to changes in lake-wide water chemistry (e.g. salinity) around 3.8 cal ka BP could have led to changes in NRM acquisition efficiency (e.g. Tauxe et al., 2006) that are not accounted for by the ARM record. However, we currently cannot rule out that the drop-off in RPI starting ~3.8 cal ka BP could represent a genuine difference in field behaviour at Windermere compared with

the other locations (Figure 3.1). [Thesis only: The drop-off in RPI at ~3.8 cal ka BP is not chronology-related. Inclination, declination, and RPI form a vector, thus their chronologies are by definition the same. Since the inclination and in particular declination curves in the later Holocene display a good likeness to other published records (Figure 3.9, Figure 3.10), it is doubtful that the disparity in RPI records is chronology-related.]

3.6.2 Comparison with records from other locations

In Figure 3.9 and Figure 3.10, the WINPSV-12K inclination and declination stack records are compared with other well-dated records from nearby locations and from farther afield (Figure 3.1). Comparison curves include the North-East Pacific Inclination Anomaly Stack (NEPSIAS; Walczak et al., 2017), the East Asia Stack (Zheng et al., 2014), the Barents Sea record (Sagnotti et al., 2012), FENNOSTACK (Snowball et al., 2007), the existing UK master curve (Turner and Thompson, 1981) and the archaeomagnetic curve from the British Isles (Batt et al., 2017), the Iceland-Greenland composite record (Stoner et al., 2013, 2007), the IODP Site U1305 record (Stoner et al., 2013), and the Eastern Canadian Stack (Barletta et al., 2010).

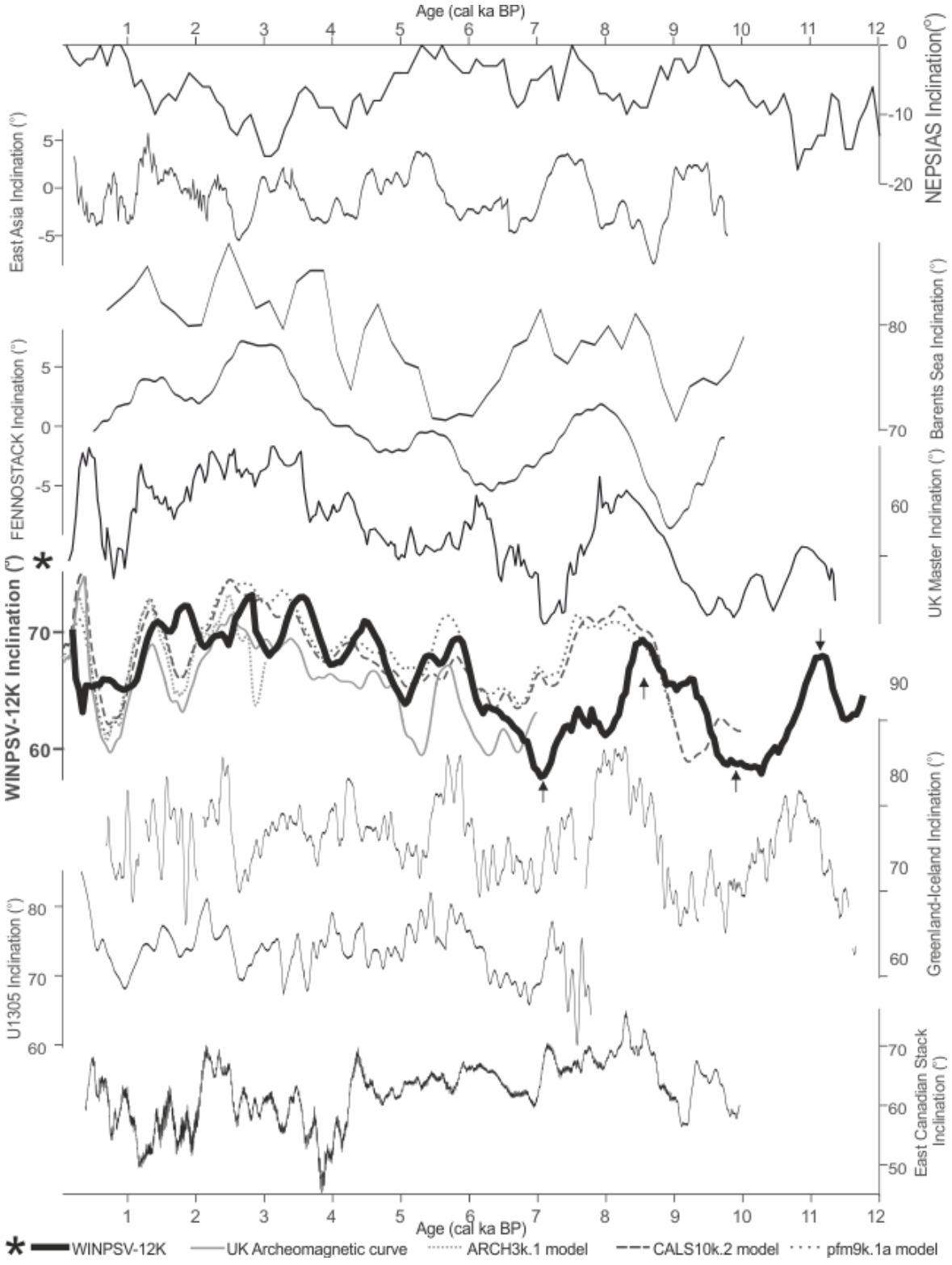

Figure 3.9: Comparison of WINPSV-12K inclination record with published records from the North Atlantic, Northern Europe, and East Asia. In order from the top: NEPSIAS (Walczak et al., 2017), East Asian Stack (Zheng et al., 2014), the Barents Sea (Sagnotti et al., 2012), FENNOSTACK (Snowball et al., 2007), the UK master curve (Turner and Thompson, 1981), WINPSV-12K, the Greenland-Iceland shallow marine composite (Stoner et al., 2013), IODP U1305 (Mazaud et al., 2012), and the Eastern Canadian Stack (Barletta et al., 2010). WINPSV-12K is shown overlain on the UK archaeomagnetic curve (Batt et al., 2017; pale grey solid

line), the ARCH3k.1 model (Korte et al., 2009; pale grey dotted line), the CALS10k.2 model (Constable et al., 2016; dark grey dashed line), and the pfm9k.1a model (Nilsson et al., 2014; dark grey dotted line). Key inclination features of WINPSV-12K are shown with vertical black arrows.

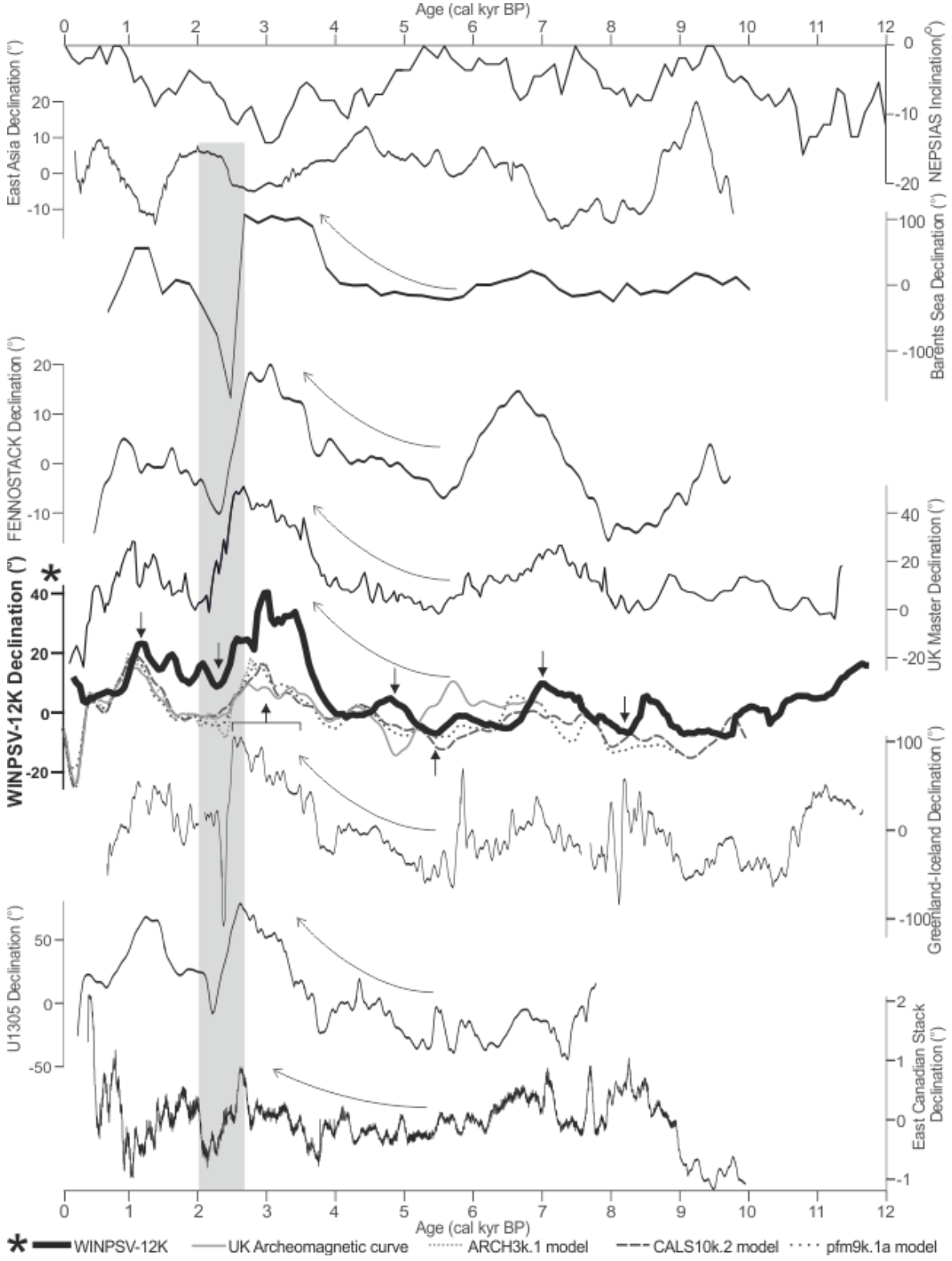

Figure 3.10: Comparison of WINPSV-12K declination record with published records from the North Atlantic, Northern Europe, and East Asia. In order from the top: NEPSIAS

(Walczak et al ., 2017), East Asian Stack (Zheng et al., 2014), the Barents Sea (Sagnotti et al., 2012), FENNOSTACK (Snowball et al., 2007), the UK master curve (Turner and Thompson, 1981), WINPSV-12K, the Greenland-Iceland shallow marine composite (Stoner et al., 2013), IODP U1305 (Mazaud et al., 2012), and the Eastern Canadian Stack (Barletta et al., 2010). WINPSV-12K is shown overlain on the UK archaeomagnetic curve (Batt et al., 2017; pale grey solid line), the ARCH3k.1 model (Korte et al., 2009; pale grey dotted line), the CALS10k.2 model (Constable et al., 2016; dark grey dashed line), and the pfm9k.1a model (Nilsson et al., 2014; dark grey dotted line). Key inclination features of WINPSV-12K are shown with vertical black arrows.

WINPSV-12K shares most of its inclination and declination features with the existing UK master curve (Figure 3.9 and Figure 3.10), which incorporates data from Loch Lomond, Lake Geirionydd, and Windermere. WINPSV-12K has an inclination peak between 5.3 – 6 cal ka BP not present in the UK master but prominent in the IODP Site U1305, Greenland-Iceland, and FENNOSTACK records. Similarly, WINPSV-12K has a small double-peak in declination at ~4.7 and ~5.9 cal ka BP which is present in the Greenland-Iceland stack and IODP Site U1305 but not present in the UK master. The 50-year time increment and 150-year averaging half-window used during the stacking produces a smoother record than the existing UK master curve, with reduced noise associated with centennial inclination features.

Over the whole Holocene, WINPSV-12K shows similar inclination behaviour to other regional (i.e. North Atlantic margin) records, i.e. a gradual steepening in inclination through the Holocene, and particularly since 7 cal ka BP. The opposite trend is apparent in the Eastern Canadian stack, possibly implying weakening in the North American flux lobe and strengthening in the European flux lobe (Stoner et al., 2013). On multimillennial timescales (i.e. 2 – 3 kyr), WINPSV-12K shows similar features to other regional records. For the inclination records, this includes the inclination peaks centred at 8.5 and 11 cal ka BP, a trough centred at 7 cal ka BP, and a peak at 5.3 – 5.9 cal ka BP. These features may be used as key regional stratigraphic markers. In the declination records, the main regional feature is the apparent gradual eastward swing starting from ~5.4 cal ka BP, followed by a major westward excursion at ~2 – 2.3 cal ka BP. This feature is so prominent it can be correlated over a long distance: the same feature is seen in the East Asia stack but in antiphase. There exist other similarly well-correlated declination features, notably characteristic peaks at ~7 and 1.1 cal ka BP, and troughs at 9.3 and 5.4 cal ka BP.

On a centennial scale, the WINPSV-12K directional features appear slightly older (0 – 3 centuries) than those of IODP Site U1305, Iceland-Greenland composite records, and FENNOSTACK. When the age uncertainty envelope (Figure 3.7) is considered, the only one of these records which differs significantly from Windermere (i.e. age differences consistently greater than the averaging window) is FENNOSTACK.

There are several possible reasons for the observed age differences of declination and inclination (and RPI prior to ~4 cal ka BP) features among the records. Snowball et al. (2007) note that the existing UK master curve is consistently older than FENNOSTACK by a few centuries and attribute this to dating problems in the UK master curve, where almost every date was ascertained using bulk sediment samples ~20 cm thick. The dating used in the current study, however, is higher quality than that of the existing UK master curve, with the use of ^{210}Pb and ^{37}Cs radiochronology for the core tops, AMS radiocarbon dating, a higher proportion of radiocarbon samples being macrofossils, and any bulk samples being only 1 cm thick rather than ~20 cm. Most of the macrofossils used are terrestrial (e.g. leaves and twigs), precluding radiocarbon hard-water error in at least these samples; furthermore Windermere is not a hard-water catchment. It is therefore unlikely that excessive dating uncertainty is the cause for the observed age differences. Bioturbation has also been suggested as a cause for greater ages for PSV records of the UK master curve (Snowball et al., 2007), but microscopic analysis of the sediment shows little evidence for the bioturbation mixed layer being greater than 1cm (~20 – 50 yr) .

There is likely a delay in magnetization "lock-in" in the Windermere sediments. The depth at which the Windermere sediment becomes cohesive enough to piston-core is ~19-25 cm, which corresponds to an age of ~90 - 140 years (based on ^{210}Pb and ^{37}Cs dates in the gravity and piston cores). This possible lock-in time is comparable to those reported for other European lake sediments (Haltia-Hovi et al., 2010; Saarinen, 1999; Snowball and Sandgren, 2002; Zolitschka et al., 2000), and may partly explain the observed age differences (up to 300 yr for FENNOSTACK, and up to 150 yr for other records). When compared with the archaeomagnetic record (Batt et al., 2017) and the ARCH3K.1 model predictions (Korte et al., 2009), the WINPSV-12K declination matches well, and appears around 80 years older than the archaeomagnetic curves. The inclination records match less well between 2.5 – 1.5 cal ka BP and after 0.8 cal ka BP. Where the records match, the apparent age difference is somewhat greater, around 150 years. Compaction in the tops of the cores during coring may have influenced inclination values in the last thousand years. Overall it is likely that

the time lag caused by lock-in for the upper part of the Windermere record is between 100 - 200 years. Downcore, the sedimentation rate decreases such that in the period between 7.4 – 9.6 cal ka BP, the sedimentation rate of all four cores drops to below 20 cm/kyr. Lock-in caused time delay increases with decreasing sedimentation rate, explaining why certain features of WINPSV-12K, especially between 7.4 – 9.6 cal ka BP, have a greater age offset than those up-core. It should be noted that for the existing UK master curve, Llyn Geirionydd and Loch Lomond are both reported to have higher sedimentation rates than Windermere (Turner and Thompson, 1981) partially explaining why it appears a little younger than WINPSV-12K in places (although the difference is likely mostly due to differing dating methods).

The observed age differences in directional features on WINPSV-12K (and possibly the UK master) and FENNOSTACK could also be caused by geomagnetic field spatial variability. Higher between-record variability is expected between spatially-distributed records where geomagnetic structure is more prevalent. Windermere's inclination and declination curves appear to share more similarity with those of the Iceland-Greenland composite record and IODP Site U1305 than FENNOSTACK or the Barents Sea (Figure 3.9 and Figure 3.10), despite U1305 being twice the distance from Windermere longitudinally than the FENNOSTACK records' location (Figure 3.1).

3.6.3 Comparison with model predictions

WINPSV-12K was compared against the CALS10k.2 and the pfm9k.1a model predictions for Windermere (Constable et al., 2016; Nilsson et al., 2014). CALS10k.2 is a time varying spherical harmonic model of the geomagnetic field over the last 10 kyr, based on both archaeomagnetic and sediment-based geomagnetic data. The pfm9k.1a model is also a spherical harmonic model and uses the same data as CALS10k.2, but treats the data differently (e.g. changing the weight distribution of sedimentary archives and adding more weight to archaeological sources). The pfm9k.1a model prediction was acquired from the GEOMAGIA database (Brown et al., 2015).

Both models incorporate data from the original UK master curve. The two model predictions of PSV at Windermere are very similar to one another, the main difference being the amplitude of the inclination peak at 5.3 – 5.9 cal ka BP (pfm9k.1a has the higher amplitude). The model predictions are rather similar to the Greenland-Iceland inclination

curve before 5 cal ka BP, meaning the pattern in WINPSV-12K between 5 - 7 cal ka BP is replicated in the models but that the inclination peak at 8.5 cal ka BP appears older than the model predictions (the data contributing to the Greenland-Iceland stack are included in the models (Korte et al., 2011; Stoner et al., 2007). After 5 cal ka BP, both models show more similarity to the UK master curve, meaning some centennial-scale features do not quite correlate with WINPSV-12K, likely because of dating differences. However, the millennial-scale features are shared between data and models (e.g. the inclination peaks at ~1.5, ~2.5, and 4.4 cal ka BP). The declination model curves have reduced amplitude compared with the WINPSV-12K data (and also the UK master curve data). The timing of features in the models is close to that of the Greenland-Iceland declination data, so the WINPSV-12K declination curve can lag the model by 100 – 400 yr in places (e.g. ~7, ~4.5, and 1 cal ka BP). This difference is likely related to magnetization lock-in (especially around 7 cal ka BP), which is minimal in the Greenland-Iceland stack due to its very high sedimentation rate (Stoner et al., 2013), but is estimated to be 100-200 years in the latter-Holocene Windermere sediment and possibly longer in the earlier Holocene (section 4.2). The only major difference between WINPSV-12K and the models is in the inclination record between 7 and 9.7 cal ka BP. The main peak of the inclination feature lags the model by ~300 yr, but also the steepness of the inclination drops before that of the models and some other records. In addition to lag caused by lock-in, the fact that two of the individual Windermere cores (i.e. Cores 64 and 67) have core section breaks around this interval have likely contributed to the lower inclination values of WINPSV-12K (Figure 3.7a).

3.6.4 Implications on geomagnetic field behaviour

Historical geomagnetic field measurements clearly show persistent regions of concentrated geomagnetic flux (i.e. flux lobes) at the core-mantle boundary, which may reflect long-term regulation of heat flux from the core to the mantle (e.g. Bloxham and Gubbins, 1985; Jackson et al., 2000). Through comparisons of well-dated high-resolution Holocene PSV records from the northern North Atlantic (NNA) and Eastern Canada (North America), Stoner et al. (2013) hypothesized that Holocene PSV is largely driven by oscillations of flux concentrations at a few recurrent high-latitude locations (e.g. below Canada, Siberia, and the Europe/Mediterranean region). The authors recognized two distinct modes controlling the PSV records: a "North American mode" characterised by high North American intensities, western North Atlantic declination, and GAD-like virtual geomagnetic poles

(VGPs); and a "European mode" characterised by relatively low North American intensities, eastward North Atlantic declination, and lower latitude VGPs. Walczak et al. (2017) recently constructed a NE Pacific sedimentary inclination anomaly stack (NEPSIAS) capturing the common signal over an area spanning over 30° longitude and latitude from Alaska through Oregon to Hawaii (Figure 3.1a). NEPSIAS inclinations largely co-vary with NNA declinations during the Holocene (i.e. steeper NE Pacific inclinations are associated with westward NNA declinations), suggesting that the Pacific is sensitive to temporal variability in the relative strength of distal flux-lobe features in quasi-persistent locations under North America and Europe (Walczak et al., 2017).

Similar to PSV records from the NNA, WINPSV-12K declinations and inclinations are more consistent with European than North American records (Figure 3.9 and Figure 3.10). The East Asia inclination stack shows a broadly in-phase relationship to NEPSIAS and an apparently anti-phase relationship to the NNA and European records on 1-3 kyr timescales. The fact that a relationship exists among these PSV records spanning such a large area (20-70° in latitudes and almost all longitudes; Figure 3.1a), suggests that PSV from these regions are responding to a common forcing at this timescale. The East Asian Stack and NEPSIAS (perhaps also East Canadian Stack for some time intervals) are in antiphase with the NNA and European records for most of the Holocene, implying that the activity of the competing flux lobes is occurring between the sites of the East Asia stack/NEPSIAS and the NNA and European regional records. For example, the eastward swing in declination between 5.4 and 2.3 cal ka BP in the NNA and European records, and the westward swing in the East Asia Stack along with the shallowing of inclination in the NEPSIAS and Eastern Canadian Stack suggest a steady weakening of the North American flux lobe while the Siberian and European/Mediterranean region flux lobes strengthen. The VGP positions estimated from the WINPSV-12K, the East Asia, and the Barents Sea PSV records all show an apparent trend approximately along the 45°E-135°W longitude line (Figure 3.14 (Supplementary Figure 4)). The offset between the different VGP position estimates could be related to declination correction and resolution of the individual records. The ~45°E-135°W longitude line may represent the main axis between the competing flux lobes, linking the "North American mode" and "European/Mediterranean mode".

3.7 Conclusions

Palaeomagnetic inclination and declination records from the Windermere cores show similar features on millennial timescale and were stacked to create a new PSV reference curve for the UK, WINPSV-12K. WINPSV-12K inclination and declination compare well with the CALS10k.2 and pfm9k.1a model predictions for Windermere on millennial timescales. Comparison of WINPSV-12K directional records with other PSV curves from the NNA- Europe region demonstrates that there are inclination and declination features on the millennial scale which may be confidently correlated and could act as partial isochrones, especially when inclination or declination features are well-constrained by tephra dating or reliable radiocarbon dates across multiple records. Dating uncertainties and noise in both the Windermere and the other presented records make correlation on timescales shorter than a few centuries difficult. Over the whole Holocene, WINPSV-12K shows similar behaviour to other regional records, especially on timescales of 2 – 3 kyr. For inclination, this includes the wide peaks at 8.5 cal ka BP and 10 cal ka BP, a trough at 7 cal ka BP, and a peak at 5-6 cal ka BP. The most prominent declination feature is the apparent eastward motion starting from ~5.5 cal ka BP, followed by a major westward excursion at ~2 – 2.3 cal ka BP. These regionally-significant features may be used as key stratigraphic markers, with the caveat that in the latter half of the Holocene a magnetic lock-in delay of 100 – 200 years is estimated, and that due to reduced sedimentation rates in the early Holocene (prior to 7.4 cal ka BP), the lock-in delay here is likely to be greater.

The antiphase relationship between the NNA regional records and NEPSIAS and the East Asia Stack on 1 – 3 kyr timescales indicates that competition between high-latitude flux lobes is a common driver for PSV variations throughout the Northern Hemisphere on these timescales, and that the main axis for competition between flux lobes could be the ~45°E - 135°W longitude line.

WINPSV-12K represents an update to the existing UK master curve. Given the location of the UK between continental European archives and records from Iceland and Greenland, a fully-updated UK PSV master curve for the Holocene is of great importance to correlations between these regions.

3.8 Acknowledgements

We are grateful to Richard and Daniel Niederreiter, Helen Miller, John Davis, and Stuart Jarvis for their support during sediment coring, and to the BGS marine operations crew and hydrographic surveyors of the R/V White Ribbon. We thank Martin Dodgson and the Windermere Lake Wardens for their assistance, as well as the Freshwater Biological Association.

We are very grateful to Martin Frank and two anonymous reviewers for their helpful comments, which greatly improved this manuscript.

Charlotte Bryant advised on radiocarbon dating. This work was supported by the NERC Radiocarbon Facility NRCF010001 (allocation numbers 1746.1013 and 1856.1014), the BGS University Funding Initiative (Reference S243), and the University of Southampton.

Carol J Cotterill publishes with the permission of the Executive Director of the British Geological Survey, Natural Environment Research Council.

3.9 SUPPLEMENTARY MATERIAL FOR ONLINE PUBLICATION ONLY

3.9.1 Supplementary Tables

Measurement interval, cm	Alternating field demagnetization step peak field, , mT	No. steps
0.5	0, 5, 10, 15, 20, 25, 30, 35, 40, 45, 50, 55, 60, 70, 80, 90, 100	17
1	0, 10, 20, 25, 30, 35, 40, 45, 50, 55, 60, 65, 70, 80, 90, 100	16
1	0, 10, 20, 25, 30, 35, 40, 45, 50, 55, 60, 65, 70, 80, 90, 100	16
1	0, 10, 20, 25, 30, 35, 40, 45, 50, 55, 60, 65, 70, 80, 90, 100	16

Table 3.1: Supplementary Table 1. NRM and ARM demagnetization treatment steps and measurement resolution for U-channel samples from Cores 57, 67, 64 and 68.

Core	Depth, cm	Sample number	Material dated	Weight, mg	Reported age, 14C y BP	Median Probability, cal y BP	Min. 2σ	Max. 2σ
57[a]	19.4	-	Bulk	-	33	-	-	-
57	72.3	SUERC-64862	Wood	-	1739	1651	1554	1732
57	86.0	SUERC-62199	Leaf	90	2646	2765	2737	2844
57	143.6	SUERC-62194	Bulk	11000	5227	5974	5912	6175
57	176.6	SUERC-62208	Bulk	5120	7885	8688	8588	8972
67[a]	21.1	-	Bulk	-	58	-	-	-
67	48.1	SUERC-62198	Twig	20	1260	1214	1083	1282
67	80.2	SUERC-52714	Leaf	-	2181	2199	2068	2315
67	160.4	SUERC-55686	Leaf	-	4505	5168	5044	5301
67	211.2	SUERC-55684	Leaf	-	7209	8018	7955	8157
67	228.5	SUERC-55685	Seed	-	8302	9324	9140	9434
67	257.2	SUERC-62213	Bulk	10360	10119	11750	11409	12003
64[a]	17.6	-	Bulk	-	60	-	-	-
64	85.0	SUERC-62194	Leaf	230	2456	2544	2363	2705
64	129.4	SUERC-62203	Leaf	70	4046	4519	4423	4784
64	170.1	SUERC-62204	Bulk	10300	5790	6591	6491	6673
64	219.2	SUERC-62209	Bulk	13100	10008	11489	11280	11709
68[a]	14.5	-	Bulk	-	-13	-	-	-
68	72.0	SUERC-64854	Bulk	-	1114	1020	934	1172
68	120.7	SUERC-64859	Bulk	-	1708	1614	1548	1702
68	171.4	SUERC-52708	Leaf	-	2242	2232	2153	2342
68	237.7	SUERC-52709	Leaf	-	3499	3771	3649	3866
68	329	SUERC-52710	Leaf	-	5124	5862	5748	5939
68	377.1	SUERC-62207	Bulk	10600	6468	7375	7295	7439
68	428.2	SUERC-52711	Leaf	-	8653	9600	9539	9688
68	454.4	SUERC-62206	Bulk	11900	9061	10225	10180	10260
68	521.7	SUERC-52713	Twig	-	9708	11160	10881	11225

Table 3.2: Supplementary Table 2. Accelerator Mass Spectrometry Radiocarbon measurements and subsequent calibrated radiocarbon ages in calendar years BP for Cores 57, 67, 64 and 68.

[a] Calendar age ascertained using ^{137}Cs and ^{210}Pb radiochronology

3.9.2 Supplementary Figures

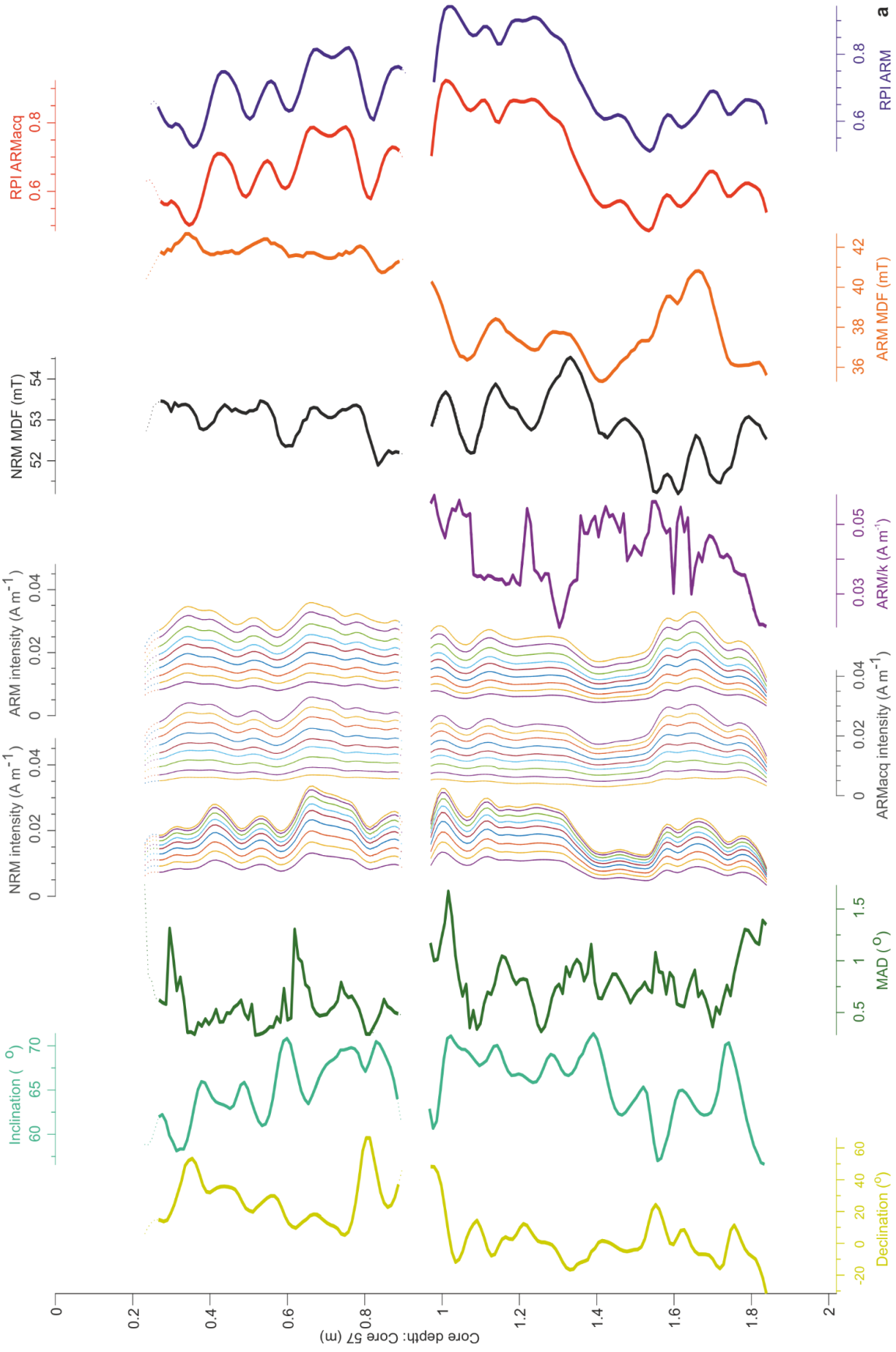
a
RPI ARM
0.6
0.8
ARM MDF (mT)
36
38
40
42
ARM/k (A m-1)
0.03
0.05
ARMacq intensity (A m-1)
0
0.02
0.04
MAD (°)
0.5
1
1.5
Declination (°)
-20
0
20
40
60
RPI ARMacq
0.6
0.8
NRM MDF (mT)
52
53
54
ARM intensity (A m-1)
0
0.02
0.04
NRM intensity (A m-1)
0
0.02
0.04
Inclination (°)
60
65
70
0
0.2
0.4
0.6
0.8
1
1.2
1.4
1.6
1.8
2
Core depth: Core 57 (m)

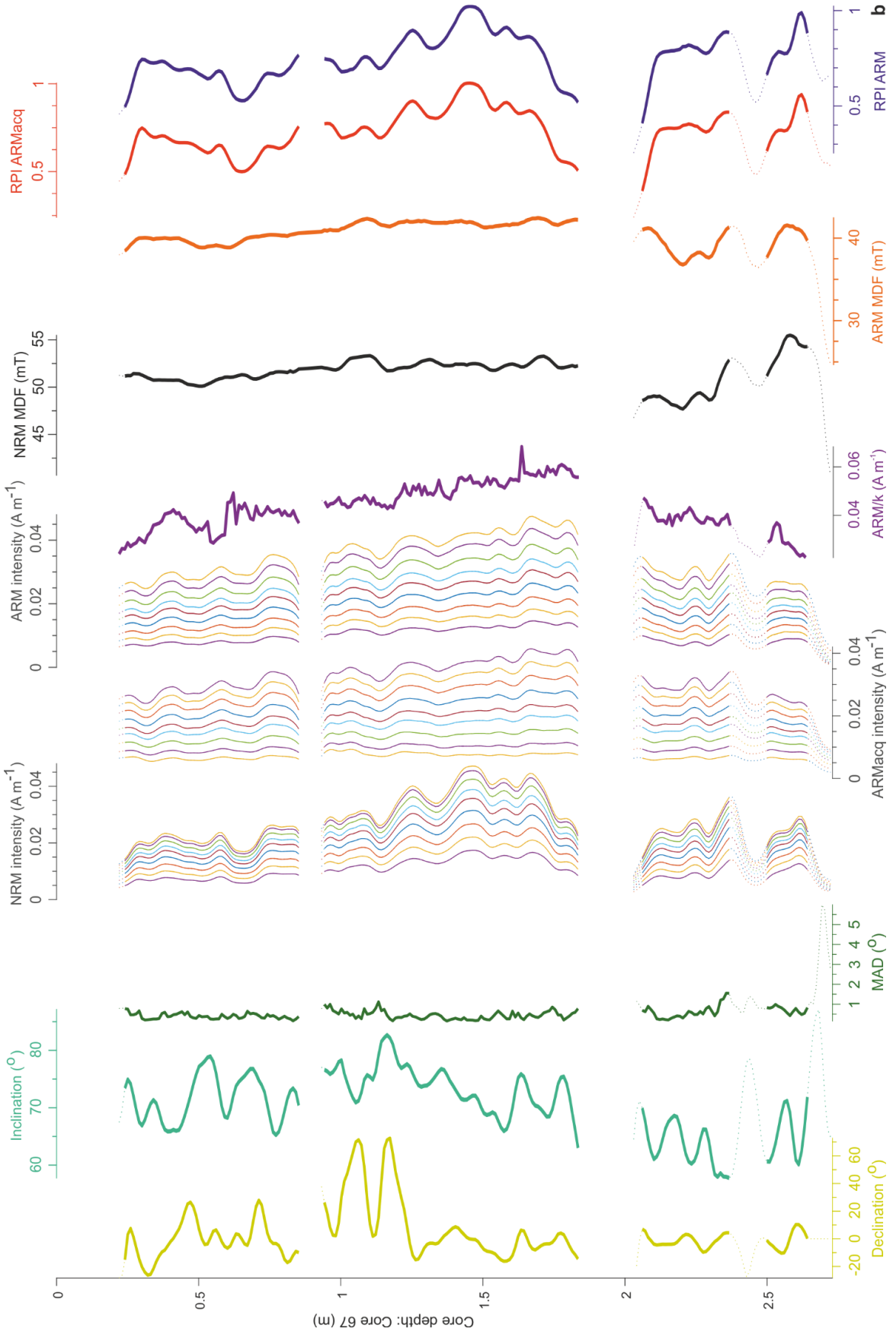
RPI ARMacq
0.5
1
NRM MDF (mT)
45
50
55
ARM intensity (A m-1)
0
0.02
0.04
NRM intensity (A m-1)
0
0.02
0.04
Inclination (°)
60
70
80
0
0.5
1
1.5
2
2.5
Core depth: Core 67 (m)
-20
0
20
40
60
Declination (°)
1
2
3
4
5
MAD (°)
ARMacq intensity (A m-1)
0
0.02
0.04
ARM/k (A m-1)
0.04
0.06
ARM MDF (mT)
30
40
0.5
1
RPI ARM
b

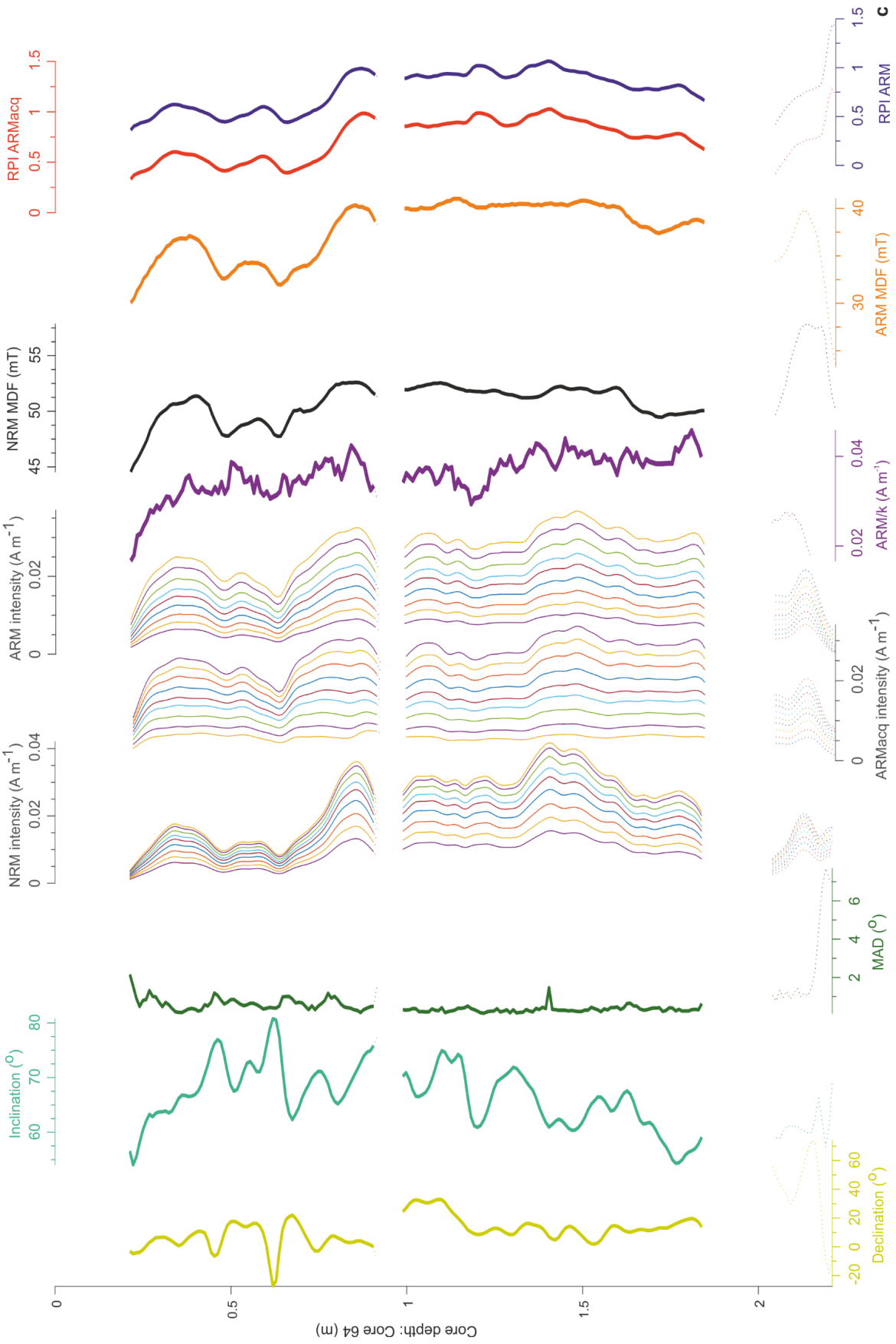
RPI ARMacq
NRM MDF (mT)
ARM intensity (A m-1)
NRM intensity (A m-1)
Inclination (o)
Core depth: Core 64 (m)
c
RPI ARM
ARM MDF (mT)
ARM/k (A m-1)
ARMacq intensity (A m-1)
MAD (o)
Declination (o)

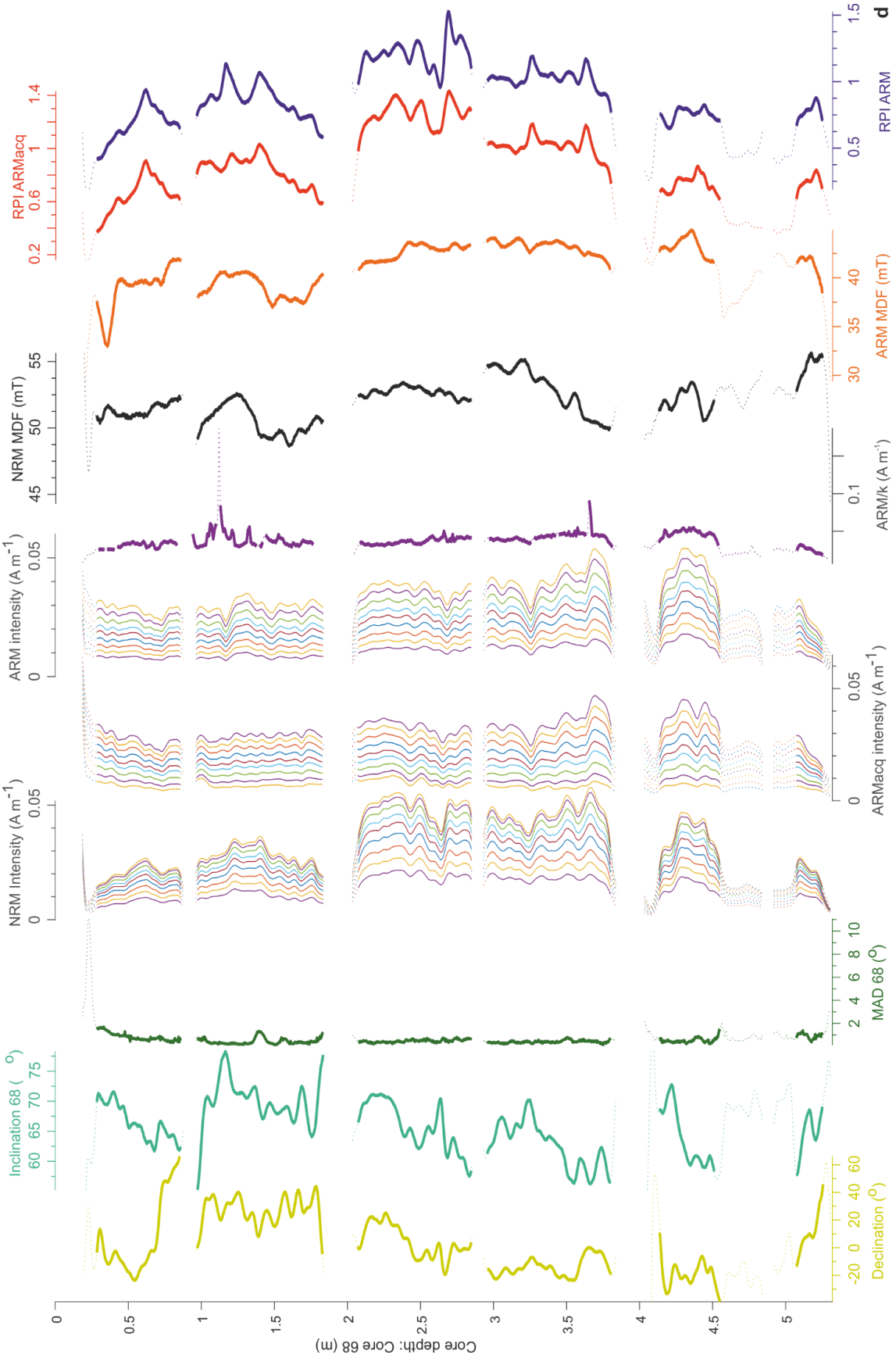
RPI ARMacq
NRM MDF (mT)
ARM intensity (A m-1)
NRM Intensity (A m-1)
Inclination 68 (o)
ARM MDF (mT)
ARM/k (A m-1)
ARMacq intensity (A m-1)
MAD 68 (o)
Declination (o)
RPI ARM
d
Core depth: Core 68 (m)

Figure 3.11: Supplementary Figure 1 (above). Downcore palaeomagnetic records for cores (a) 57, (b) 67, (c) 64, and (d) 68. From left to right, records show: Declination, inclination, maximum angular deviation (MAD), NRM intensity, intensity of progressively acquired anhysteretic remanent magnetization (ARMacq), intensity of progressively demagnetized ARM, ARM/magnetic susceptibility, median destruction field (MDF) of NRM, MDF of ARM, RPI derived from slopes of NRM vs ARMacq, and NRM vs ARM best-fit lines.

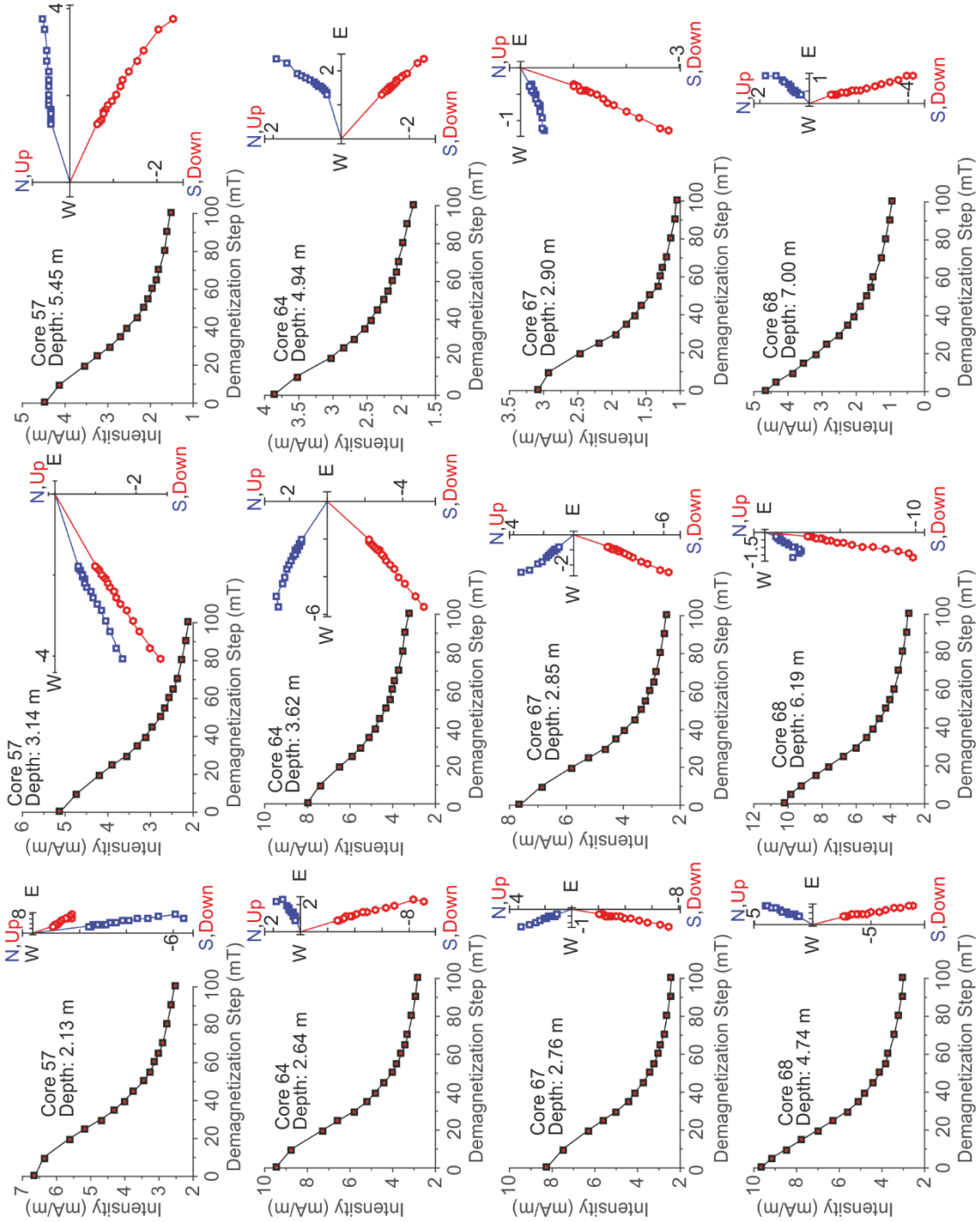

Figure 3.12: Supplementary Figure 2. Representative NRM AF demagnetization behaviours of pre-Holocene sediment from Cores 57, 67, 64, and 68. For each selected 1-cm interval from the four cores, the NRM intensity versus AF demagnetization step plot are shown on the left and the orthogonal projection plot of NRM is shown on the right (blue squares = horizontal projections, red circles = vertical projections). Three examples are shown from each core.

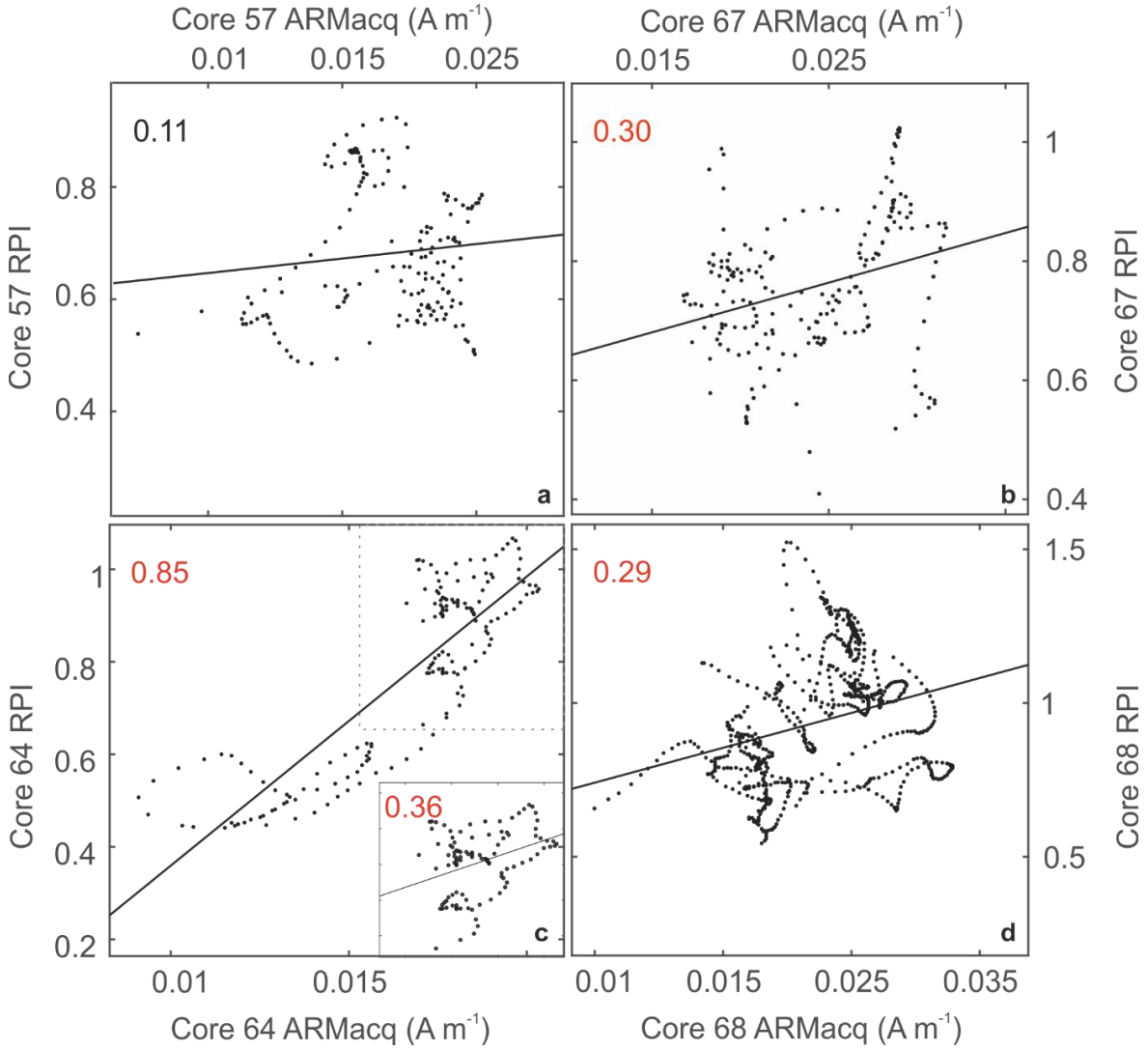

Figure 3.13: Supplementary Figure 3. RPI plotted against RPI normalizer (ARMacq) for (a) Core 57, (b) Core 67, (c) Core 64, and (d) Core 68. Numbers indicate R-values of correlation, and the colour of the number indicates reliability (red = P-value < 0.05; black = P-value ≥ 0.05). The inset in panel (c) indicates the correlation between RPI and ARMacq for Core 64 prior to 2 cal ka BP.

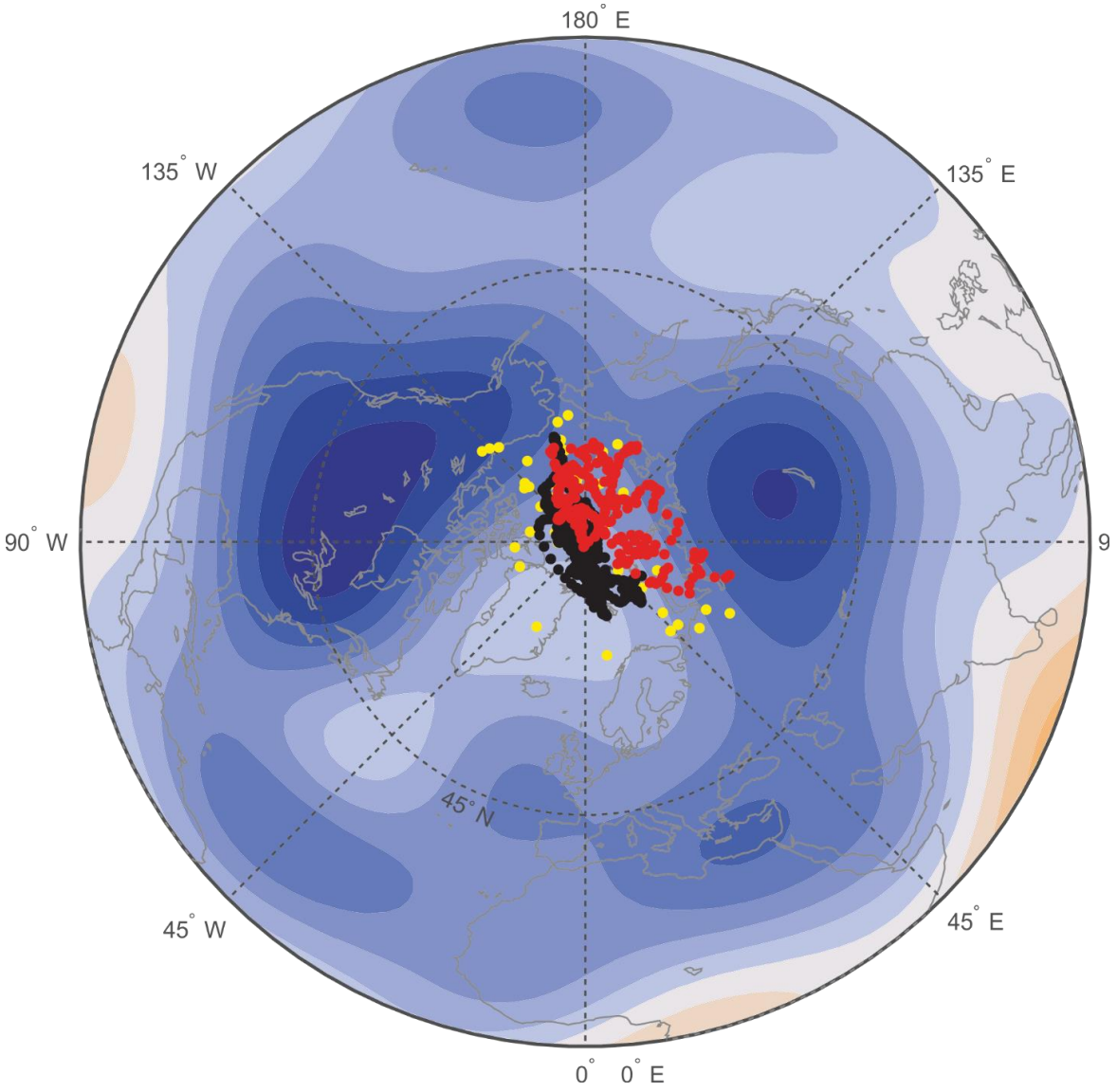

Figure 3.14 Supplementary Figure 4: Virtual geomagnetic pole (VGP) positions estimated from WINPSV-12K (red circles), East Asia PSV stack (Zheng et al., 2014) (black circles), and Barents Sea PSV record (Sagnotti et al., 2012) (yellow circles). See Figure 1a for record locations. Overlaid contour map shows the vertical component of magnetic field at the core-mantle boundary averaged over the 1590-1840 time interval (after Gubbins et al., 2006; Stoner et al., 2013)

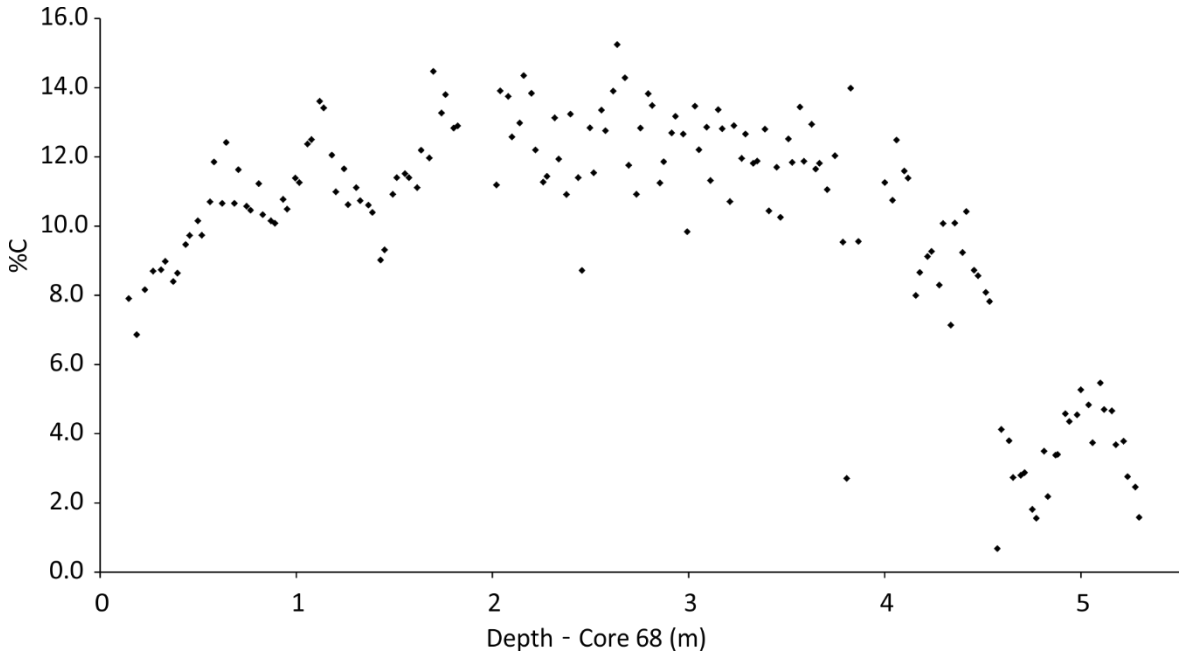

Figure 3.15: Total organic carbon percentages throughout the Holocene sediment of Core 68.

4. Varve Sequences from Windermere, UK: New Insights into the Deglaciation of the Lake District

In this chapter, the varves that were deposited in Windermere prior to the Lateglacial Interstadial are investigated, and used to build a more complete picture of the deglaciation of the Lake District. This chapter is a manuscript in preparation for submission to Quaternary Science Reviews.

4.1 Abstract

The interval from the end of the Last Glacial Maximum around 19 ka to the start of the Holocene at 11.7 ka was marked by rapid climate oscillations that ultimately led to the complete demise of the British and Irish and Fennoscandian Ice Sheets. Understanding the dynamics of earth system behaviour through this period relies on the development records of sufficiently high resolution to capture the relative timing of change. Annually laminated sediments or varves provide an appropriate temporal resolution but are rare in the early part of the deglaciation. Here we present the first glaciolacustrine varve record from the area of the Eurasian Ice Sheets from the interval prior to the rapid warming of the Lateglacial Interstadial (GI-1), from Windermere in the Lake District of Northwest England.

Evidence from varved sequences from four cores in the Windermere North and South Basins are integrated with seismic stratigraphic records to reconstruct the regional deglaciation. The final phase of ice retreat commenced abruptly within 250 years of the main Interstadial transition and led to a change from cm-scale glaciolacustrine varves to nival varves within 36-40 years in the South Basin, and a change in mineralogy as the main ice sheet was lost and fragmenting valley glaciers receded. Rapid ice retreat up the North Basin was recorded by a series of De Geer moraines and chaotic outwash sediments. The new cores, combined with the seismic evidence, show the potential for a centuries-long varve chronology and climate history through Heinrich Stadial 1.

4.2 Introduction

The termination of the last glaciation was marked by a series of warm and cool episodes that were separated by abrupt changes in temperature (C. D. Clark et al., 2012). The annually resolved chronology from the Greenland ice-core records has demonstrated that several of these major climate shifts occurred on timescales of decades (Rasmussen et al., 2006). Understanding the operation of the Earth system through these rapid changes is a priority for the climate science community and a key objective to underpin this has been the development of chronologies to identify the synchroneity or otherwise of global changes through this interval (Lowe et al., 2008). Varved or annually laminated lake sediments possess a resolution directly comparable to the ice-core records and may be used to quantify the duration of climatic intervals and also to establish the rate of change between them (Ojala et al., 2012; Zolitschka et al., 2015). Varved sediments have been extensively used in Holocene and Lateglacial sediments, but only rarely to document the earlier part of the deglaciation and the transition to the first major warming, the Bølling-Allerød interstadial or Lateglacial Interstadial (GI-1). Development of the North American Varve Chronology has enabled direct matching of sub-centennial scale climatic transitions between North America and the Greenland ice-core records through this interval (Ridge et al., 2012). While the North American Varve Chronology extends from 18.2 – 12.5 cal ka BP (Ridge et al., 2012), no deglacial varve records prior to the Bølling-Allerød (GI-1) are known from the Eurasian Ice Sheets. Here we present the first analysis of such a deglacial varve sequence in cores taken from the lake basin of Windermere in the Lake District of northwest England.

The formation of varves is relatively uncommon, requiring both strong seasonality of one or more depositional processes, and preservation of lakebed microstructure with little to no bioturbation (Zolitschka, 2007). Varves in glacial climates are usually of the clastic type, comprising a 'summer' (i.e. melt season) coarse graded layer derived from glacial or nival meltwater, usually silt, and a fine 'winter' layer of clay that settles through the water column when the lake is frozen over. Varves are a composite record of seasonal variations in sedimentation, and thus the controls on the sedimentary environment and the climatic conditions. In a proglacial environment, varve thickness is controlled by the level of meltwater production from catchment ice masses, such that thicker varves indicate more melting degree-days during a given year (Ridge et al., 2012). Early attempts to correlate

varve sequences on a global scale to infer teleconnections were not successful (e.g. De Geer, 1937), to the extent that varve science as a whole was somewhat discredited (Francus et al., 2013; Ridge et al., 2012). A resurgence in varve studies from the 1970s was underpinned by more reliable dating methods including radiocarbon and the use of tephra layers to verify well-dated varved sediment chronologies as a framework for detailed climatic and environmental studies across wider regions (Zolitschka et al., 2015). Varves are of particular value for the Lateglacial since subfossil trees are absent for this period in most high-latitude settings.

The Cumbria-Irish Sea area is thought to have started to deglaciate around 17 cal ka BP (Ballantyne et al., 2009), and was entirely or almost entirely ice-free at 14.7 cal ka BP (Wilson and Lord, 2014). In this study we present new deglacial varve sequences from Windermere, UK, which document the retreat of valley glaciers as the regional climate warmed in the ~300 yr immediately prior to the abrupt transition to the Lateglacial Interstadial at 14.7 ca ka BP. Working on new, radiocarbon-dated, cores from Windermere, we have applied a suite of techniques including image-based (optical and SEM), geochemical, and grain size measurement, to reconstruct the sedimentary history prior to the Lateglacial Interstadial (GI-1). Several varve sequences have been identified and used to better constrain the pattern and timing of the retreat of the British and Irish Ice Sheet from the Windermere Valley and NW England. Varves are also developed the Younger Dryas –age sediments, and these are discussed in Chapter 5.

4.3 Stratigraphy of pre-Interstadial Sediments

4.3.1 Study Location

Windermere is a north-south trending glacial ribbon lake in the southeast of the English Lake District (Figure 4.1), lying in a steep-sided pre-glacial river valley that has been overdeepened by successive glaciations (Pennington and Pearsall, 1973; Pinson et al., 2013). The lake has a present maximum water depth of 62 m and an elevation of 39 m above Ordnance Datum Newlyn. It has maximum dimensions of 17 km x 1.5 km and drains a catchment of 242 km^2 (Lowag et al., 2012; Miller et al., 2013). The catchment bedrock comprises the Ordovician Borrowdale Volcanic Group in the north and the Windermere Supergroup (Silurian mudstones and siltstones) in the south.

The lake is separated into a north and South Basin by a bedrock high, with the South Basin draining westward into the River Leven (Wilson, 1987). Windermere has accumulated sediment since being exposed during retreat of the British-Irish Ice Sheet c. 17 ka (Ballantyne et al., 2009; Coope and Pennington, 1977).

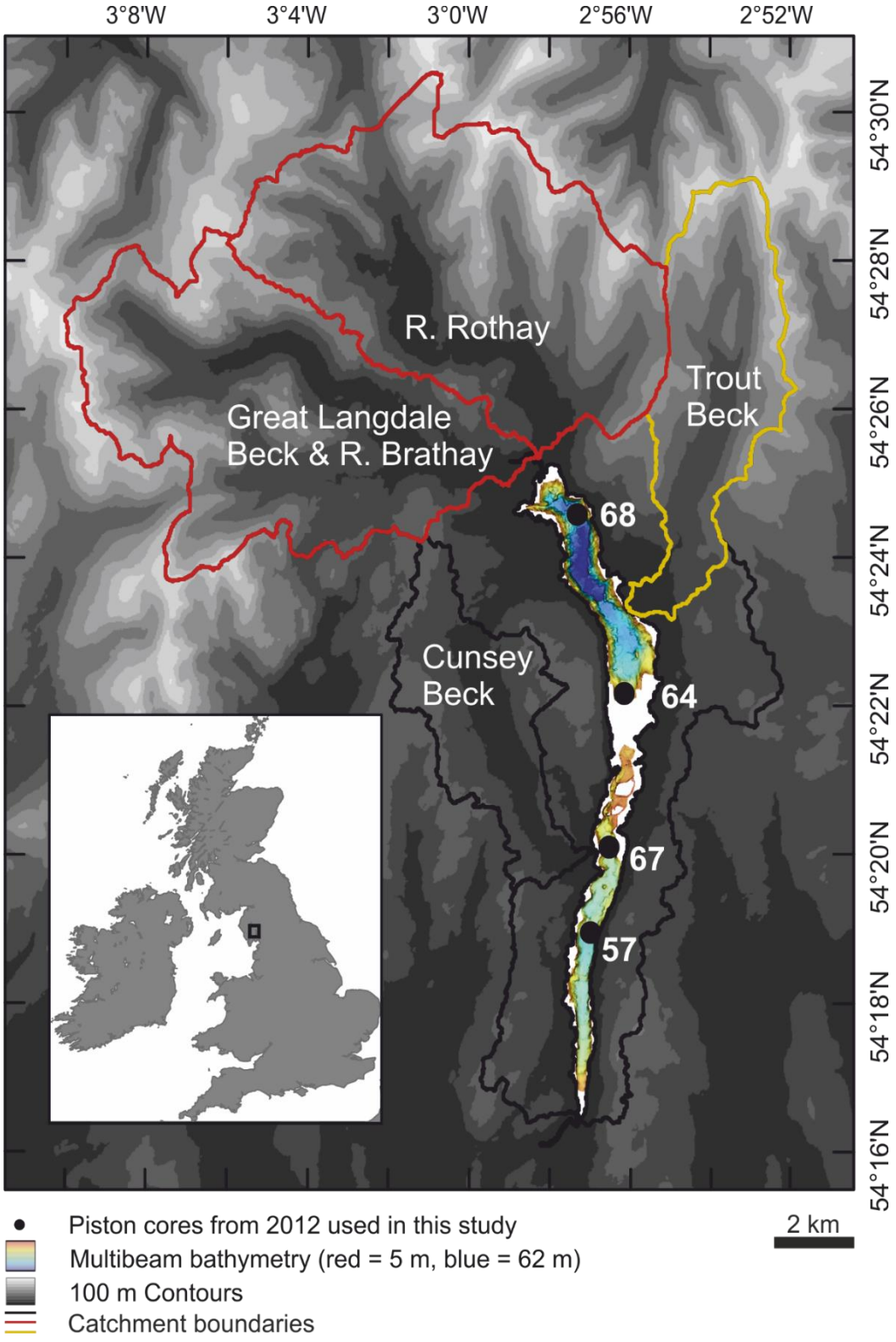

Figure 4.1: Map of the study area. The lake catchment of Windermere is shown in bold outlines (significant sub-catchments are shown in red and yellow). Significant fluvial inputs to the lake are named in the catchments. One hundred metre contours are shown as a greyscale colourmap. The locations of Cores 57, 67, 64, and 68 are shown as filled black circles. Multibeam lake bathymetry is shown as a rainbow colour palette, where dark blue is deepest and red is shallowest. Inset: The location of the study site (black rectangle) in the British Isles (grey).

4.3.2 Seismic stratigraphy

Two-dimensional multichannel boomer seismic reflection surveys of Windermere reveal several distinct lakebed units (Table 1) above the bedrock (Pinson et al., 2013). The seismic reflection sections were prestack migrated to give depth rather than time sections and four major seismic units were identified. Seismic Facies I (SF I) is interpreted to be over-consolidated till and morainic material, SF II is glaciolacustrine and lacustrine sedimentation prior to the Holocene, SF III represents Younger Dryas –age mass movement complexes, and SF IV is the organic Holocene drape. Some units (SFI and SFII) are further subdivided (Figure 4.2, Figure 4.3).

Pinson et al (2013) interpreted SF I as representing 9 recessional moraines and 28 De Geer moraines within the catchment. Recessional moraines are interpreted to represent localised still-stands or readvances, whilst de Geer moraines can sometimes represent annual retreat formations (Bouvier et al., 2015). Seven out of nine recessional moraines are located in the South Basin, which suggests that ice retreated in a series of phases in the narrow valley. Only two recessional moraines are in the North Basin, implying a much faster retreat (supported by the wider valley structure and presence of De Geer moraines). The overall seismic and morphological interpretation of the deglaciation of Windermere is that of complex and active glacial retreat up-valley (with some localised isolated downwasting), with the northern sub-catchments deglaciation after those of Cunsey Beck and Trout Beck.

Seismic unit (after Pinson et al., 2013)	**Seismic characterisation (from Pinson et al., 2013)**	**Sediment type as seen in cores (see section 4.5.1)**
SF IV	A 2- to 5-m-thick draped deposit, with several low-amplitude but continuous layered internal reflection. [~1490 m s^{-1}]	Organic-rich Holocene mud
SF III	Disturbed, erosive deposit with weak, chaotic internal reflections or discrete, transparent deposits with high-amplitude bounding reflection. [~1500 m s^{-1}]	Younger Dryas mass movement deposits (an example is seen in Core 67)
SF IIb	Unit with weak, closely spaced (<0.5m) internal reflections, grades into SF IIa and is only observed in the South Basin. [1500 m s^{-1} + 6 m s^{-1} per metre]	Glaciolacustrine infill, relating to cm-scale laminations that may thicken downwards through the unit. This unit is only present in the South Basin.
SF IIa	Up to 35-m-thick deposit infilling the SF I topography with strong, layered internal reflections that widen with depth [1500 m s^{-1} + 6 m s^{-1} per metre]	Glaciolacustrine infill, relating to cm- and mm-scale clay and silt laminations and Interstadial sediment. Sandier deposits towards the bases of Cores 64 and 68 may be transitional to SF I.
SF I	Complex unit with several sub-units and internal structure, bounded by strong top and bottom internal reflections. [2300 $\pm$ 300 – 3500 $\pm$ 500 m s^{-1}]	A complex sequence of tills and moraines with localised flowed till and ice-front fan deposits, as well as an upper unit of supraglacial and melt-out till. No cores penetrated into this unit.

Table 4.1: Seismic stratigraphy of the sub-bottom Windermere sediments, following Pinson et al., 2013.

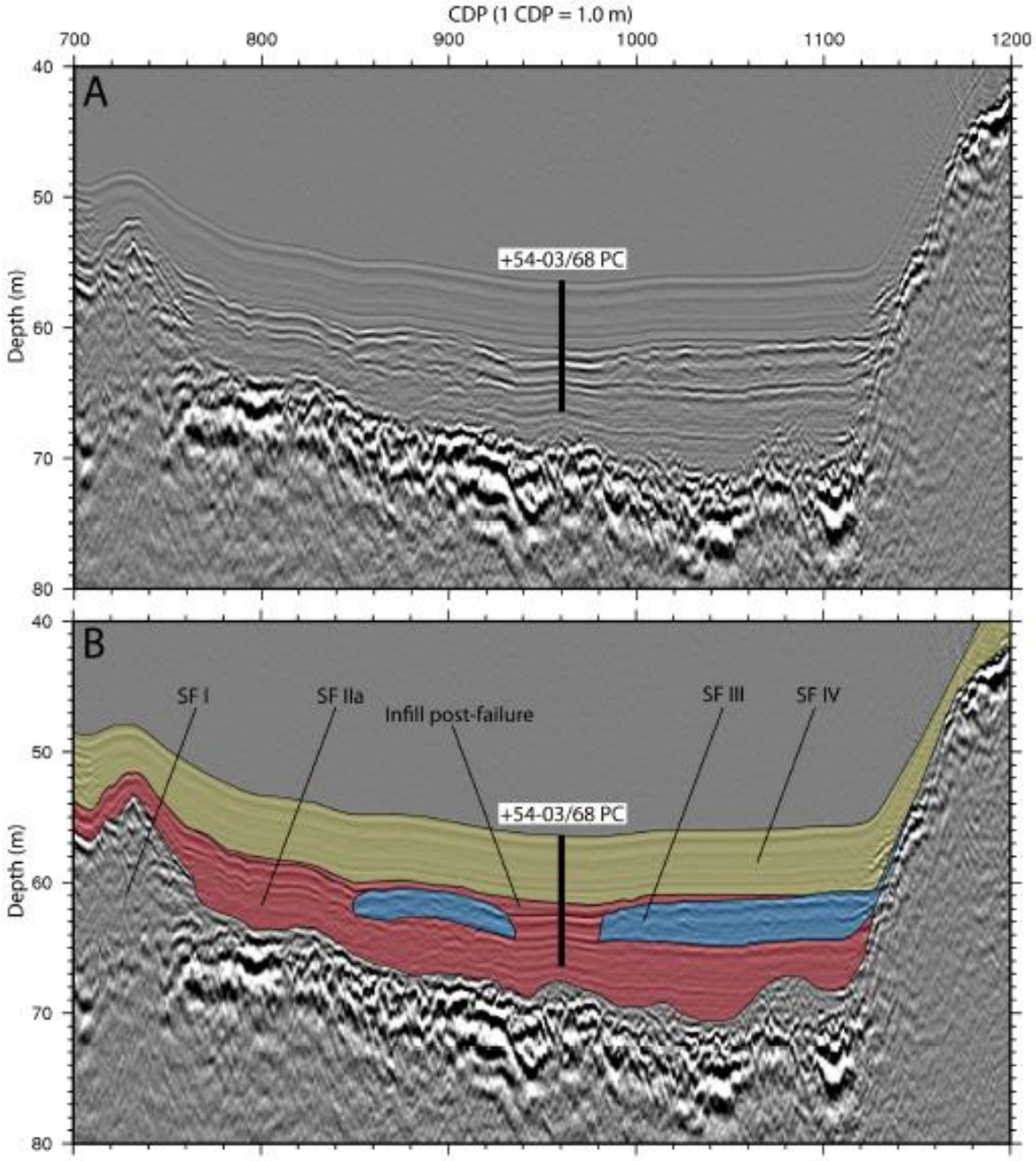

Figure 4.2: Multi-channel seismic stratigraphy of the location of Core 68 (vertical black line). Top: Uninterpreted depth-migrated seismic reflection profile; Bottom: Interpreted seismic reflection profile. After Miller, 2014.

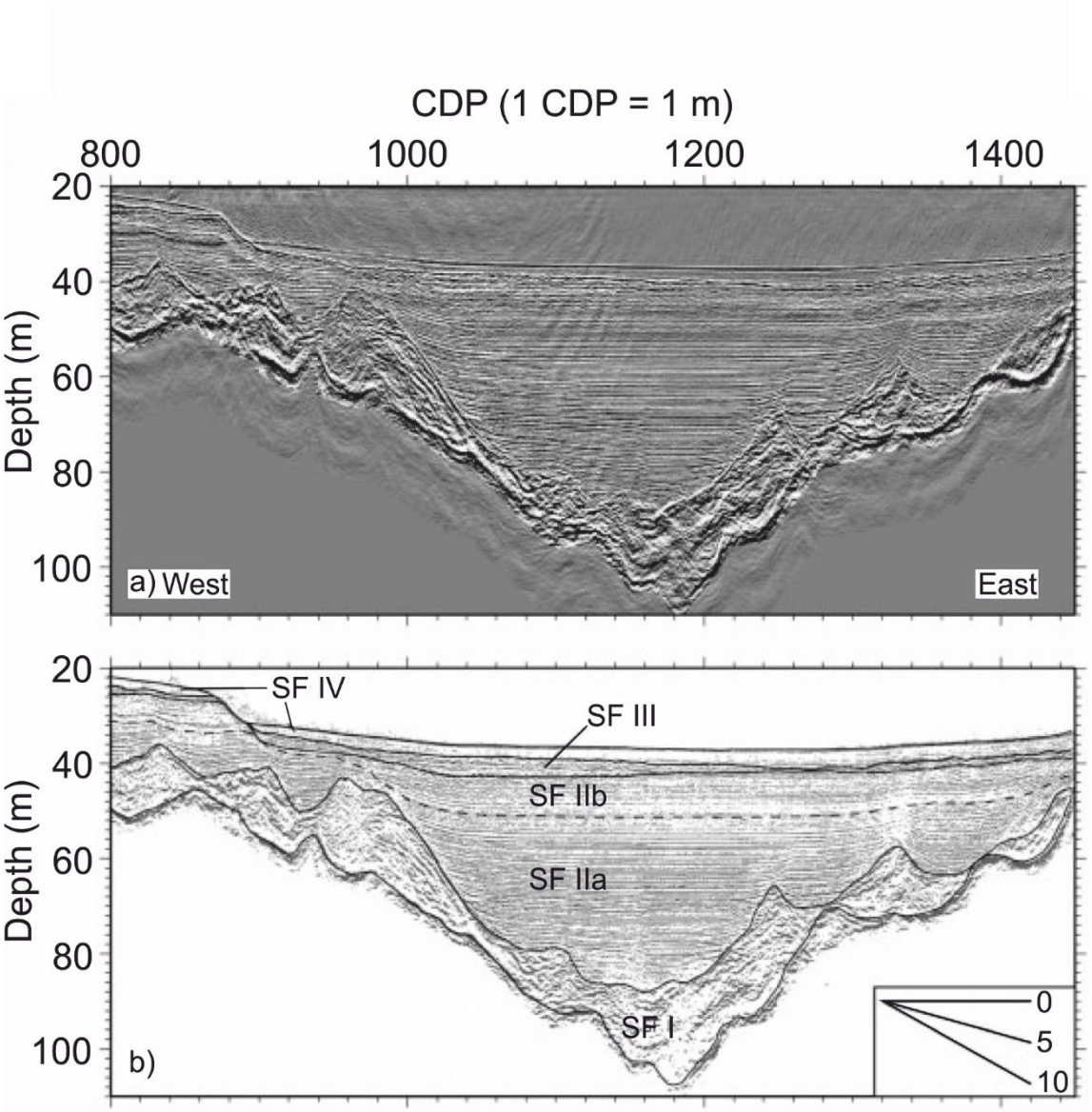

Figure 4.3: Uninterpreted (top) and interpreted (bottom) depth-migrated seismic reflection profiles of very near the location of Core 57. Core 57 is 6 m long, and it can be seen that the glaciolacustrine sedimentation (SF IIa, IIb) in the depocentre continues for a further ~50 m. *Reprinted from Journal of Quaternary Science, 28 (1), Pinson, L. J. W., Vardy, M. E., Dix, J. K., Henstock, T.J., Bull, J. M., Maclachlan, S.E., Deglacial history of glacial lake Windermere, UK: implications for the central British and Irish Ice Sheet, p. 83-94., © (2013), with permission from Wiley.*

4.4 Methods

4.4.1 Sediment coring and stratigraphy

The multibeam bathymetry, chirp, parametric, and multi-channel boomer seismic reflection surveys were used to select a series of locations in sediment depocentres for piston coring. (Lowag et al., 2012; Miller et al., 2013; Pinson et al., 2013; Vardy et al., 2010). A coring

campaign in 2012 by the British Geological Survey (BGS) and the University of Southampton facilitated the collection of several sediment cores using both a Uwitec piston corer and Uwitec gravity corer (Miller, 2014). Piston cores were recovered in consecutive 2 m sections in 9 cm diameter liners. These sections were subsequently sectioned into 1 m units and split lengthways to produce working and archive core halves. The four cores which had the highest deposition rates, which covered the longest time intervals, and which were recovered from depocentres identified by the geophysical surveys as mostly unaffected by mass transport deposits (MTDs) were selected for this detailed study.

The four cores (+54-03/57 PC, +54-03/67 PC, +54-03/64 PC, and +54-03/68 PC; hereafter 'Core 57', 'Core 67, 'Core 64, and 'Core 68' respectively) all exhibit similar major lithological units: an inorganic mineral-rich base overlain by a dark organic rich unit. Radiocarbon dating shows that the dark brown organic unit is of Holocene age, whilst the underlying sediment is pre-Holocene (Figure 4.4).

The base of the pre-Holocene unit in cores from the North Basin exhibits a disturbed base containing irregular laminations, deformation, and massive sand beds overlain by several cm-scale alternating silt and clay laminations. The base unit in cores from the South Basin contains only the cm-scale alternating silt and clay laminations, thinning into mm-scale silt and clay laminations. The overlying unit is silty clay and contains diatoms and other organic matter, as well as ferric growths. A reliable radiocarbon date from near the top of this silty clay unit indicates that it is of Lateglacial Interstadial age. In all cores, the organic silty clay unit is succeeded by a unit of mm-scale laminated silt and clay of Younger Dryas age. The cores of the South Basin also bear mass transport deposits (MTDs) in this unit up to 1.5 m thick. This study focuses on the sediment of pre-Interstadial and early Interstadial age.

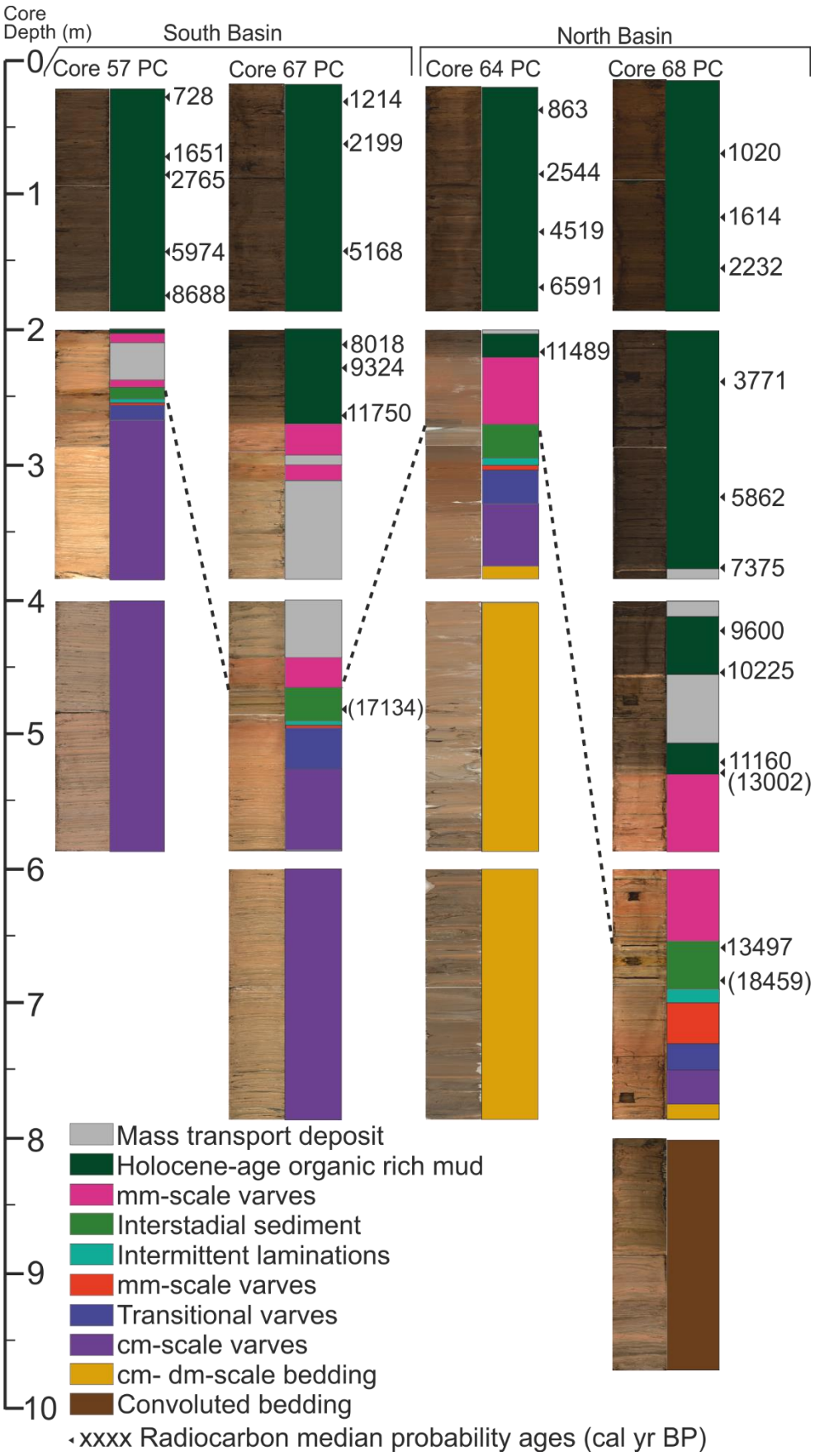

Figure 4.4: Stratigraphy of the four studied cores in Windermere. For each core, a split-core photograph is shown (left), along with a colour-coded log showing the locations of the sediment types. Median-probability radiocarbon dates are shown to the right of each core in cal yr BP, and unreliable dates are shown in brackets. Sediments studied in this chapter are below the dotted line.

4.4.2 Age model

Several radiocarbon dates were obtained from the Windermere cores. From the Holocene sediments, age models for Cores 57, 67, 64 and 68 (Figure 4.4) were constructed using 4, 6, 4, and 9 accelerator mass spectrometry (AMS) radiocarbon dates respectively (Avery et al., 2017). In addition to the Holocene, radiocarbon dates were obtained from the organic silty clay unit, which stratigraphically corresponded to the Lateglacial Interstadial. The dates were obtained from both macrofossils such as terrestrial leaves and twigs, and from 1 cm thick bulk sediment samples. Radiocarbon dates were provided by the NERC Radiocarbon Facility in East Kilbride, Scotland, and dates were calibrated using Calib 7.1 (Stuiver and Reimer, 1993) and the Intcal13 calibration curve (Reimer et al., 2013). An additional date at each core top was acquired using a ^{137}Cs-validated ^{210}Pb-decay age model (2.8.4). A detailed radiocarbon dating table can be found in Appendix A.

The date obtained from the upper part of the Lateglacial Interstadial (median probability age 13,497 cal yr BP from Core 68) appears close to what would be expected. However, the dates sourced from the earliest part of the interstadial (18,459 cal yr BP from Core 68; 17,134 cal yr BP from Core 67) are too old and are consistent with the "old" age of 17.8 ka obtained from a similar position by Coope and Pennington, (1977). Due to the absence of terrestrial microfossils in the basal interstadial sediments, our dates were obtained from bulk sediment and so were likely subject to a number of processes typical in deglacial environments that lead to anomalously old dates. These may include the washing in of old carbon from the recently exposed ice-free terrain, and also reservoir effects including the influence of old groundwater: such discrepancies are typical in Northern European late glacial lake sediments (Blystad and Selsing, 1989; Wohlfarth, 1996) and in deglaciated environments in general (Hutchinson et al., 2004). Taking the onset of GI-1 as 14.7 cal ka BP gives excess ages of between 2,000 and 4,000 years which seem large, but reservoir age corrections of up to 3260 yr have been documented in Tibetan lakes (Wu et al., 2010). Although a soft-water lake throughout the Holocene, the early-Interstadial Windermere may also have been subject to a 'hardwater effect', since there was significant carbonate present in the glacial outwash and thicker cm-scale laminations deposited in the lake (see section 4.5.2 below) that likely contributed to an anomalously old age for the lake's dissolved inorganic carbon reservoir (Philippsen, 2013).

The pre-Interstadial sediment did not contain enough carbon to perform radiocarbon dating (and it would have been subject to old-carbon inwash in any case). Additionally, no

tephra layers were found. Therefore, the varve chronology produced in this study should be considered floating, but immediately before the onset of the Lateglacial Interstadial.

4.4.3 Sampling and imaging

Split cores were sampled at the British Ocean Sediment Core Facility (BOSCORF), producing U-channels and 1 x 5 cm sediment slabs from the centre of the core. The U-channels were used for Itrax ED-XRF core scanning. For presentation purposes, data were 20-point smoothed to filter out the 'noise' of individual grain variations and focus on the signal of the millimetre- to centimetre-scale sediment variations.

The slab samples were taken using a metal 'Cookie Cutter', following methods of (Dean et al., 1999). The sediment slabs were subsampled to produce 1 x 1 x [slab length] cm sediment blocks. which were embedded in a fluid-displacing four-part epoxy resin (Kemp et al., 1998; Pike and Kemp, 1996), before being sectioned into overlapping thin sections 3 – 4 cm long. For each sediment depth, both a covered thin section (CTS) and a polished thin section (PTS) were produced. All split cores and slab subsamples were imaged using a combination of photography and X-radiography, and thin sections produced from the slabs were imaged using photography (covered thin sections) and backscatter electron microscopy (polished thin sections).

In order to ascertain certain mineral compositions of parts of the sediment, energy-dispersive X-ray spectroscopy (EDS) maps were produced using the EDS detector on the SEM and AzTec Energy software at 2500 x magnification. Mineral phases were identified for each map. Itrax data showed that the silt and sand fractions of the sediment at the bases of all four cores contained heightened levels of calcium, but that the calcium signal almost disappears at the top of the cm-scale laminations. EDS maps of selected regions were therefore produced in order to identify the mineralogy and provenance of the calcium. An additional X-ray diffraction method was employed on one sample from the bottom of Core 68 to identify constituent minerals.

Detailed versions of these methods may be found in Sections 2.4, 2.5, and 2.6.

4.4.4 Strontium Isotope Measurement

Fifteen tills were collected from the Langdale/Rydal catchments, in addition to three limestone samples from the carbonate limestone surrounding the Lake District. A sample

was taken from a high-calcium area from each core. A small amount of each sample was placed in 10% nitric acid, whereupon the limestone samples and the core samples effervesced, but the till samples did not. The sediment and rock samples were selected for acid leach and the tills used for XRD analysis. The limestones were crushed, dried, and crushed again. In the clean lab, 0.2 g sediment or 0.1 g limestone was acid digested using acetic acid. Leachate was diluted with 10% nitric acid, and a blank sample was prepared from acetic acid and nitric acid. All samples were run on an indictively coupled plasma mass spectrometer to ascertain Sr levels, and all six samples contained enough Sr for isotopic analysis. An extract from each sample containing 1 μg Sr was dried and run again on the mass spectrometer. A detailed version of these methods may be found in Section 2.9.

4.4.5 Varve Thickness Measurement

A clastic varve is generally defined as having a coarse base with a sharp lower contact (usually silt or fine sand) which grades into a distinctive clay cap (Zolitschka et al., 2015).

Varves thinner than ~20 mm were measured using the SEM from backscatter images of polished thin sections and from optical microscopy of covered thin sections, whilst thicker laminations were measured from CIS images of the split core, alongside auxiliary X-radiographs. In some cases, several of the methods were used in parallel for cross-checking (Figure 4.5). For all measurement methods, three vertical lines were drawn on the image, and horizontal lines were drawn at each lamina boundary. The thickness of the laminations was measured using the semi-automated method of Francus et al. (2002). Each sequence was counted twice, each time by a different researcher. The discrepancy between the counts is given as a + or – uncertainty, and the error is calculated as the total absolute uncertainty as a percentage of the final count (count 1).

For the sequences in cores 57 and 67, counts were made between 16 well-correlated reference layers, allowing varve-by-varve correlations between said layers (See Supplementary Section 4.10.2). This method allowed for greater certainty on individual laminations that were clear (or definably varves) in one core but not the other, as each core's count was re-appraised by comparison with equivalent sections of the other core (Larsen et al., 2011; Rein et al., 2007; Tomkins et al., 2008). From this method, a composite varve chronology between the South Basin cores was constructed. Cores 64 and 68 did not contain the same reference layers, and the varves present in these cores were counted without

between-core cross-referencing (with the exception of the first varve in all four cores defined as the 'organic-rich indistinct' type; 4.6, 4.7).

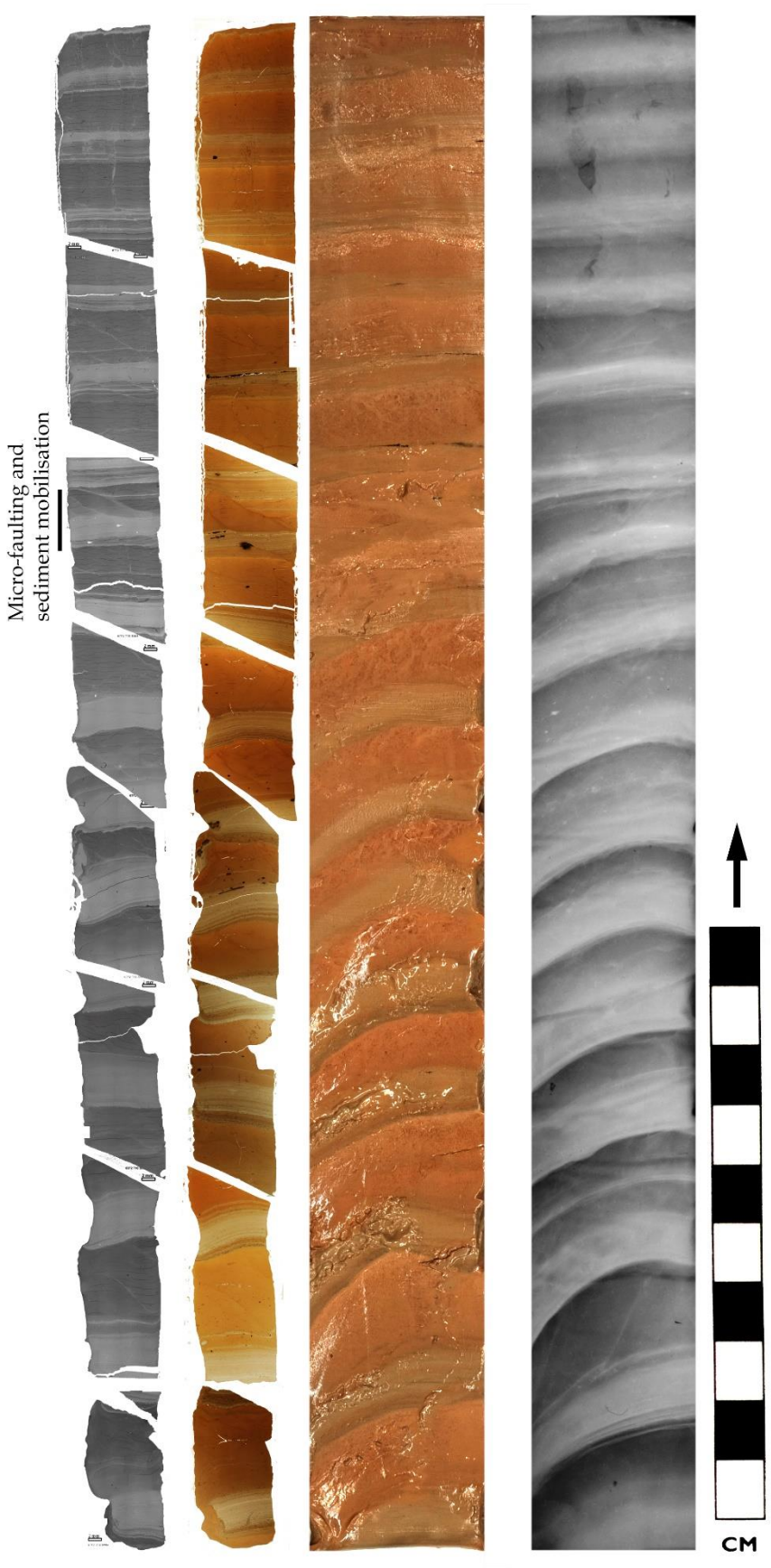

Figure 4.5: Centimetre-scale lamination macro-scale visualisation from Core 67, showing examples of the methods used in varve identification and cross-checking. From left: BSEI of polished thin sections; Covered thin section photographs; Slab photograph; Slab X-radiograph.

4.4.6 Grain Size Measurement

Representative sediment samples were taken from each sediment facies for grain size analysis. Each sample was dried at 50° before being de-flocculated in 5% pH-neutralised sodium hexametaphosphate. Suspended particles from extracted sub-samples were analysed on a Beckman Coulter LS 130 Laser Diffraction Particle Size Analyser, and grain size distributions obtained. This procedure complemented SEM-based grain size work.

4.5 Results

4.5.1 Sediment Facies

The seven major sediment types present in the studied cores (Figure 4.4) are, from core bottom to top, as follows: Disturbed basal sediment (Core 68 only), centimetre to decimetre-scale beds (Cores 64 and 68 only), centimetre-scale beds, thinning transitional laminations, millimetre-scale laminations, indistinct and intermittent laminae, and Interstadial sediment. A summary of the different sediment facies found in the Interstadial and pre-Interstadial sediments is given in Figure 4.6, a stratigraphic log of the pre-Interstadial facies is given in Figure 4.12, and each facies is described in Sections 4.5.1.1 to 4.5.1.7 below. The seismic facies as given by Pinson et al., (2013) which corresponds to each sediment type is given in Table 4.2.

Sediment type	Seismic facies from Pinson et al., (2013)
Basal disturbed sediments	IIa (possibly transitioning to I)
Centimetre to decimetre-scale layered silt and clay	IIa (possibly transitioning to I)
Centimetre-scale laminations	IIa in North Basin, IIb in South Basin
Multi-phase thinning laminations	IIa in North Basin, IIb in South Basin
Simple millimetre-scale laminations	IIa in North Basin, IIb in South Basin
Intermittent indistinct laminae	IIa in North Basin, IIb in South Basin
Interstadial Sediment	IIa in North Basin, IIb in South Basin

Table 4.2 Summary of sediment types found in the cores and their corresponding seismic facies.

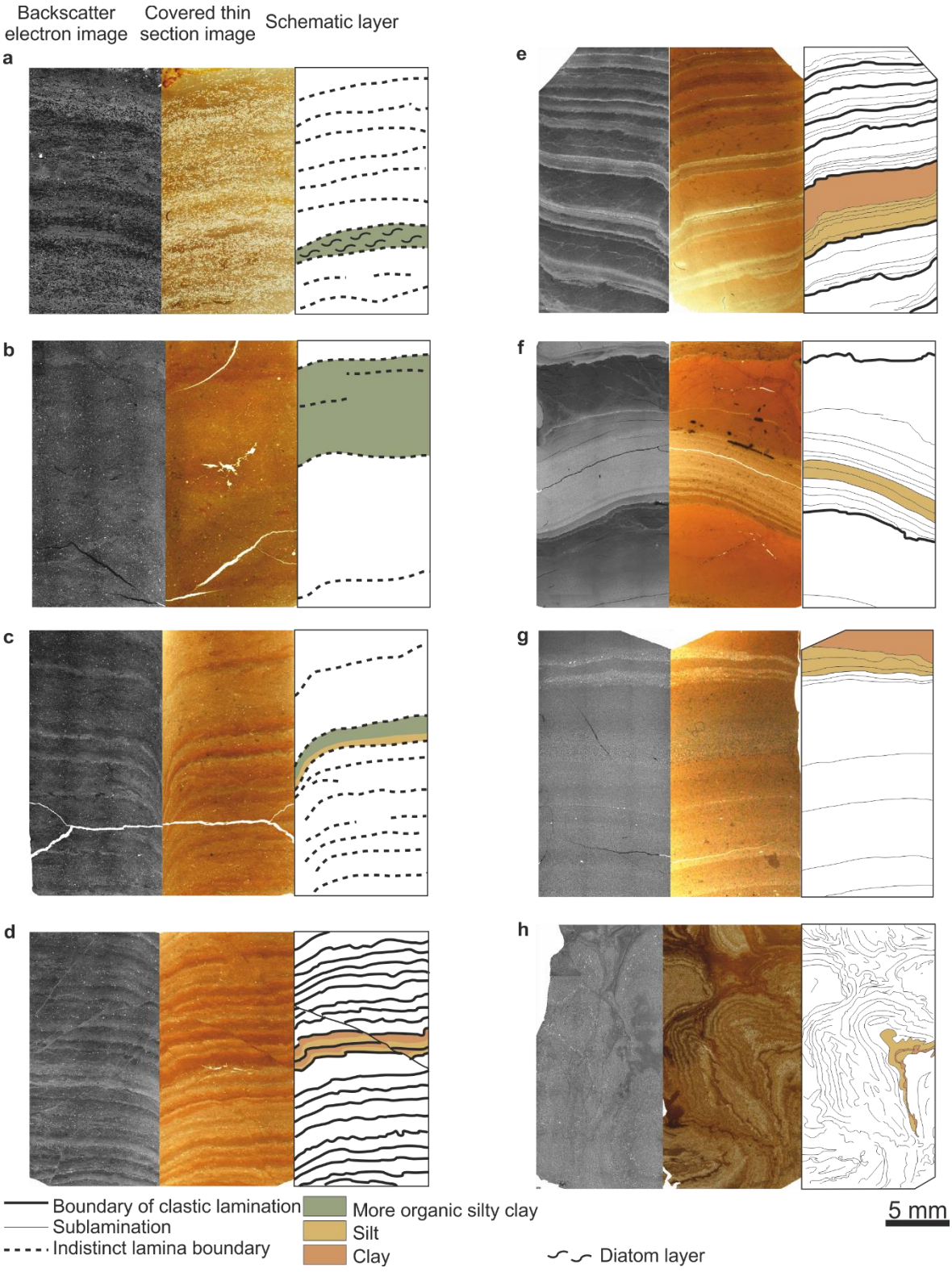

Figure 4.6: Summary of major sediment types present in the studied sections of sediment. Left: BSEI of polished thin section. Centre: optical photomicrograph of covered thin section of counterpart. Right: Schematic overlay of sediment type. a) Interstadial sediment containing *Ellerbeckia* sp.; b) Interstadial sediment; c) Intermittent indistinct laminae; d) mm-scale laminations; e) Transitional multi-phase beds; f) cm-scale beds; g) cm-dm-scale beds; h) Disturbed basal sediment.

4.5.1.1 Basal disturbed sediments

The basal sediments were recovered only at the base of Core 68, between ~9 - 10 m (Figure 4.4), although the facies overlaps with the overlying cm-dm scale bed facies. The grain size ranges from clay to medium sand (only seen at >9.5 m depth and not in embedded sediment), often in well-sorted bands, although some bands which contain the largest grains are poorly sorted. Bedding that is locally present is often convoluted, folded, or faulted (Figure 4.6h). The overall character of this facies is that of disturbed, bedded sediment, some of which exhibits fluid escape structures. Some laminations are present but are distorted to varying degrees.

4.5.1.2 Centimetre to decimetre-scale beds

Centimetre to decimetre-scale beds are found directly overlying (and slightly interfingering with) the basal disturbed sediments of Core 68, and the unit is also the lowest of Core 64, between 4 – 8 m (Figure 4.4). The beds largely comprise multiple bands of well-sorted silts varying between medium to very coarse, with a clay cap (Figure 4.6g, Figure 4.16). The silt sublaminations range in thickness between ~0.1 mm to ~1 cm. The bed thickness ranges from ~35 cm at the base of Core 64 (~7 - 8 m) to only ~2 cm at ~4 m depth. In Core 68, the layers are only a maximum of ~13 cm thick. Occasional fine sand clasts are present in this unit between 8 – 9 m in Core 68, whilst in the section below (9 – 10 m) there exist some ~0.5 - 3 cm thick sand beds that contain medium sand as a significant component.

4.5.1.3 Centimetre-scale beds

Centimetre-scale beds are present in all four cores. All beds of this facies are characterised by a well-defined layer of fine to very fine silt overlain by a well-defined layer of clay, and typically range in thickness between ~0.8 cm to ~6 cm in the recovered sediment (Figure 4.7). In Cores 64 and 68, they overlie the cm- dm-scale beds, and in Cores 57 and 67 they are present from the core bases (Figure 4.4, Figure 4.6f, Figure 4.7).

The silt component is commonly composite and may comprise several discrete silt sublaminations of 0.5 mm to 2 mm, some of which are graded. Some sublaminations contain very coarse silt or very fine sand grains (e.g. Figure 4.17d). The lowermost silt sublamination may be finer or more clay-rich than the silt lamination overlying it (Figure 4.17d), and in several cases the topmost sublamination is somewhat coarser or siltier than most others (Figure 4.17b). The clay cap is thick, usually at least as thick as the silt layer,

and often exhibits vein structures similar to those attributed to palaeoseismicity (Brothers et al., 1996).

The upper boundary of the basal silt layer is often abrupt rather than gradational, whilst the clay-silt contact at the base of the overlying bed is very sharp (especially in Core 57) even if the initial overlying silt sublamina is very fine silt. Micro- load casts are common, in keeping with the higher density of the silt layers seen in X-radiographs of the beds (Figure 4.17a). Occasionally there may be a very thin (single-grain) silt layer or train of silt grains interrupting the clay cap (not shown).

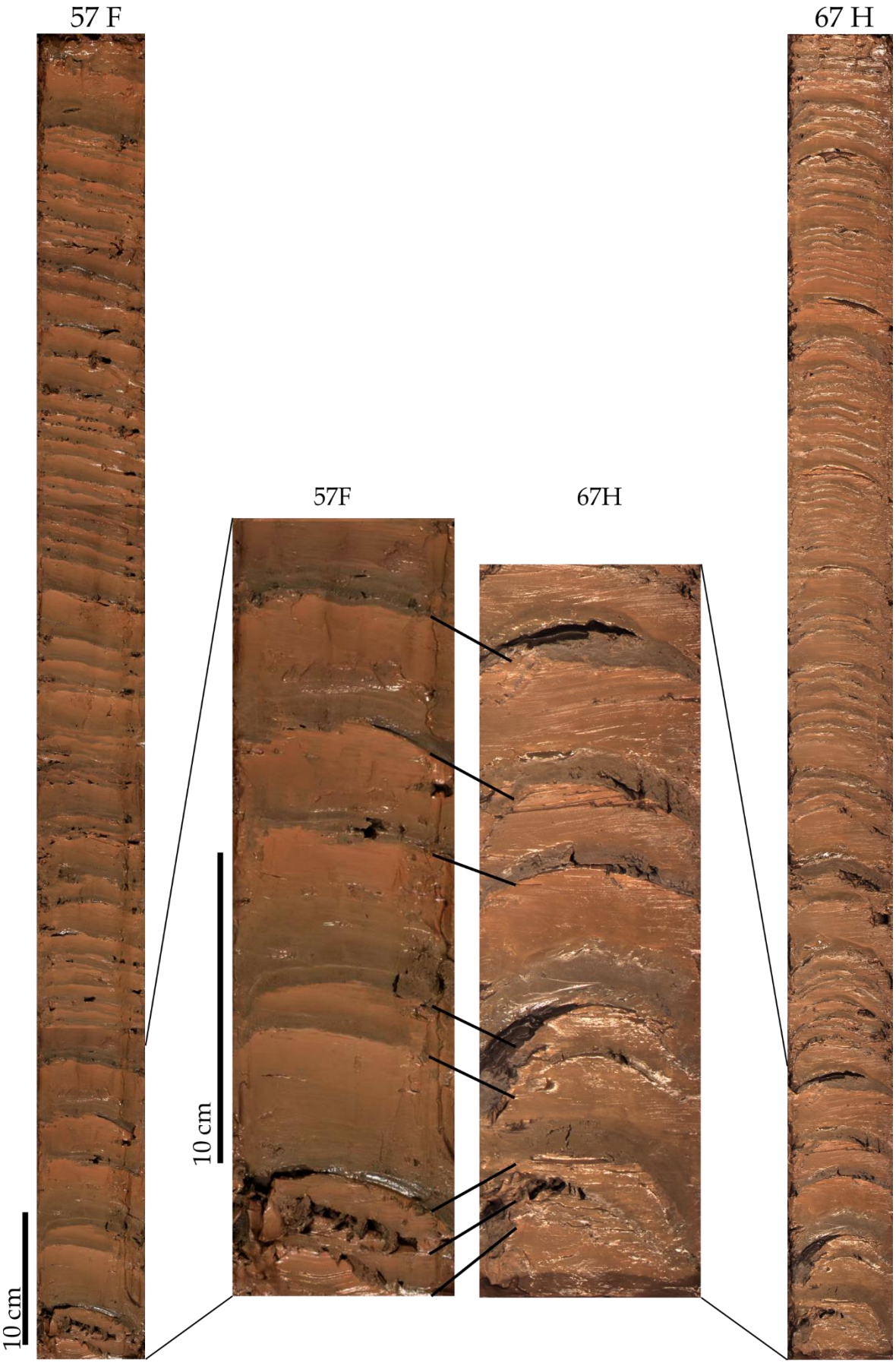

Figure 4.7: Split-core photographs showing the centimetre-scale beds present in Cores 57 (~5-6 m) and 67 (~7-8 m). An example of tiepoints between equivalent beds in Cores 57 and 67is shown in the centre.

4.5.1.4 Transitional thinning (cm to mm) beds

A transitional sequence of thinning couplets occurs above the cm-scale couplets prior to regular mm-scale couplets in all four cores (Figure 4.4). As with the cm-scale beds, the grain size is very fine silt in the South Basin but the North Basin also contains a coarser fraction (in this case medium to very coarse silt). These beds, which progressively become thinner up-core, are distinguished by the presence of multiple internal silt sublaminations and more clay-rich sub-laminations (Figure 4.6e). This bed type ranges in thickness from ~1 cm at the unit base to ~1 mm at the unit top.

The basal components of these beds are made up of several fine silt sublaminae, ~0.1 – 1 mm-thick, each grading to clay or silty clay, often resembling the clay cap of the cm-scale beds. The middle and top parts of the bed are very similar to a cm-scale bed (Figure 4.18). The thinnest (uppermost) examples of the transitional beds are around 1 – 2 mm in thickness, with the clay cap being typically thinner than the silt unit (Figure 4.19).

4.5.1.5 Simple millimetre-scale laminae

Millimetre-scale laminae are found in all four cores, overlying the thinning transitional beds (Figure 4.4). The bases of millimetre-scale laminae typically comprise medium silt grading to fine silt that may contain trains of medium silt and isolated coarse silt grains. This is then overlain by a thinner clay cap (Figure 4.6d, Figure 4.20). The clay cap exhibits small fluid-escape or bioturbative structures at the top of the silt layer, which may make the upper and lower boundaries of the clay cap harder to distinguish.

We take the first mm-scale varve which exhibits significant evidence of catchment biota (coarse clasts homogeneously throughout, microfossils, bioturbation, vague boundaries) to mark the nominal onset of the Lateglacial Interstadial.

4.5.1.6 Intermittent Indistinct laminae

Thin transitional units of intermittent, indistinct laminae 2 – 5 mm thick are present in all four cores overlying the mm-scale laminae (Figure 4.6, Figure 4.20). The laminations comprise very fine to medium silt as with the mm-scale laminae, although coarse and very coarse silt grains are dispersed homogenously throughout (Figure 4.6c, Figure 4.21). The basal part of each lamina is around ~0.5 - 1 mm thick, similar in nature to a mm-scale lamina, but instead of a pure clay cap the sediment is more a silty clay and has a more 'organic' nature, containing several microfossils including testate amoebae, Chironomid

and diatom fragments, lithic larva cases, or moulds left by decayed organisms. Total organic carbon is between 0.1% for the mm-scale laminae and 0.8 % for the Interstadial sediment, where each estimate is based on one measurement- likely around 0.5% based on linear interpolation (see Figure 4.24 for TOC values). Some intermittent laminae are potentially distinguishable as proto-varve sequences due to there being a regular pattern, whilst others are isolated amongst non-laminated sediment (Figure 4.21a). Up-core, these laminae become more intermittent (i.e. from every ~1 mm to every ~2 – 5 mm), until only the full-Interstadial-type sediment is present.

4.5.1.7 Full-Interstadial sediment

The Interstadial unit is present in each core, and overlies the intermittent lamina unit (Figure 4.4). In all cases, the base sediment comprises a relatively homogenous silty clay with an organic carbon content of ~0.8%. Present in the matrix are fairly homogenously-distributed coarse to very coarse silt clasts and numerous microfossils, some plant fragments, and indeterminate organic particles (Figure 4.6b, Figure 4.22). The interstadial sediments in Cores 57 and 64 are both made up entirely of this sediment type, with only a faint indications of mm – cm-scale variation in silt content (although part of this unit in Core 57 is absent through erosion). Core 68 also contains cm-scale beds of varying colour and density and in the central part of the Interstadial sediments of Core 68 there are also diagenetic iron-rich growths present, which are shown to contain sulphur and are tentatively defined as Greigite (Fe_3S_4).

In Core 67, the matrix is relatively homogenous but there are several ~1 – 2 mm thick laminations present, which are made up of layers of the diatom genus *Ellerbeckia* sp. The diatom layers are also associated with higher concentrations of coarse detrital grains (Figure 4.6a, Figure 4.22).

4.5.2 Grain Size

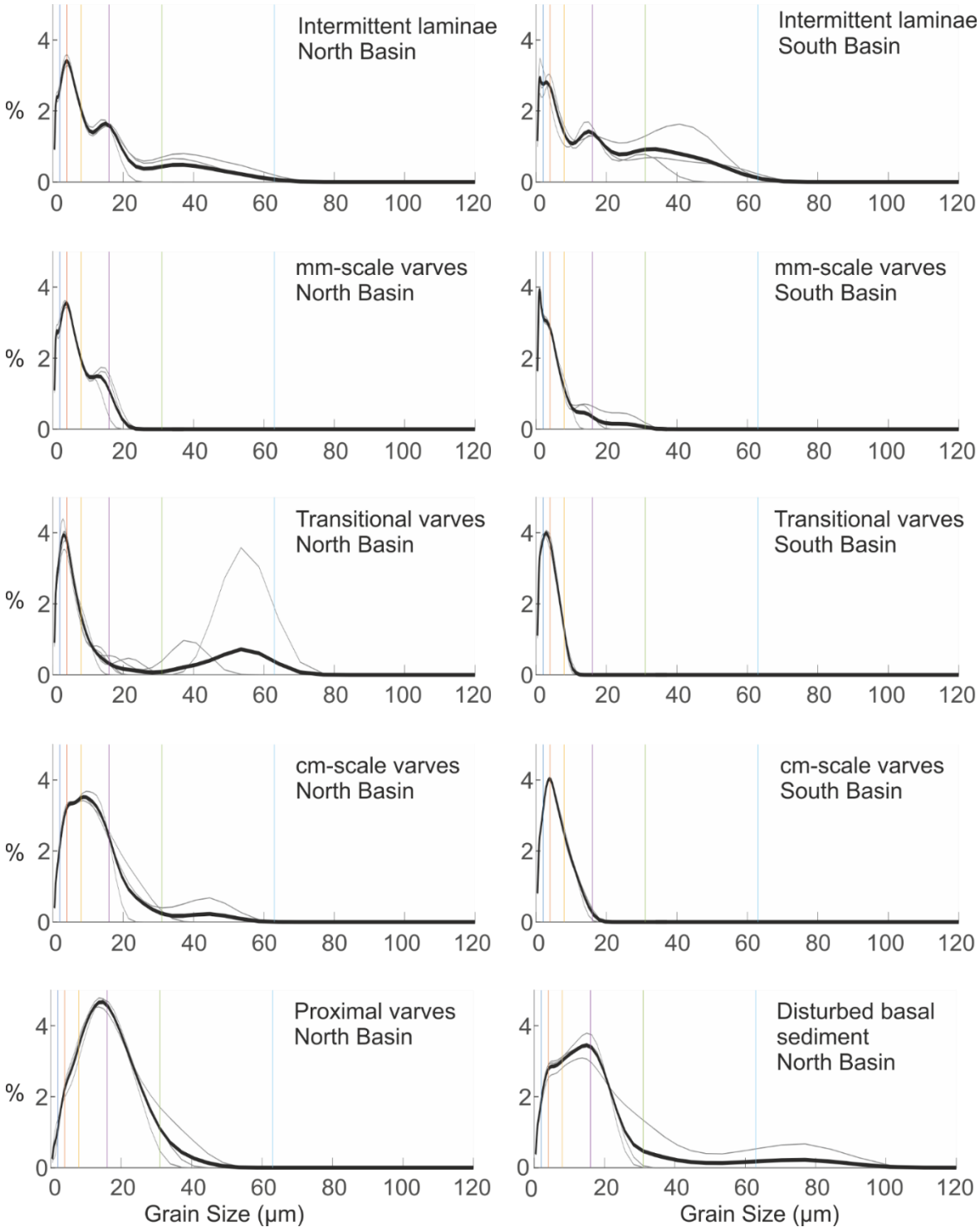

Figure 4.8: Grain size distributions for samples of each sediment type. Thin grey lines are the individual measurement runs, and the thicker black line shows the mean for the runs. Vertical lines are the lower grain size boundaries as follows: Blue- Very fine silt (2 – 4 µm); Orange- Fine silt (4 – 8 µm); Yellow- Medium silt (8 – 16 µm); Purple- Coarse silt (16 – 31 µm); Green- Very coarse silt (31-63 µm); Blue2- Very fine sand (63 – 125 µm).

Grain size results for each sediment type and for each basin (Figure 4.8) are summarised in Table 4.3. Note that from estimates of grain size in BSEI there are modes in the different facies that are not always found in the modes given by the Laser diffraction analysis, however, the general characteristics may be observed.

Sediment type	Core	Median grain size(s) (μm) for each run	Mode(s) (μm) of mean of runs
Intermittent Laminae, N Basin	Core 68	3.144, 3.439, 3.621	3.816 (Very fine (VF) silt), 14.95 (Medium (M) silt), 37.17 (Very coarse (VC) silt)
Intermittent Laminae, S Basin	Core 67	2.178, 2.831, 3.496	1.066 (Clay), 2.904 (VF silt), 14.95 (M silt), 33.94 (VC silt)
mm-scale laminae N Basin	Core 68	2.626, 2.931, 2.982	1.168 (Clay), 3.816 (VC silt), 13.65 (M silt)
mm-scale laminae S Basin	Core 67	1.753, 1.788, 1.9	1.066 (Clay), 2.904 (VF silt), 13.65 (M silt)
Transitional beds N Basin	Core 64	2.538, 2.843, 3.117, 2.771, 2.548	*3.181 (VF silt), 12.46 (M silt), 16.38 (Coarse (C) silt), 21.52 (C silt), 37.17 (VC silt), 53.5 (VC silt)
Transitional beds S Basin	Core 67	2.147, 2.229, 2.264	2.651 (VF silt)
cm-scale beds N Basin	Core 68	4.885, 5.541, 5.66	5.015 (Fine (F) silt), 8.661 (M silt), 44.6 (VC silt)
cm-scale beds S Basin	Core 57	2.959, 3.069, 3.205	3.816 (VF silt)
dm-scale beds N Basin	Core 64	9.317, 9.754, 10.48	14.95 (M silt)
Basal sediment N Basin	Core 68	6.038, 6.109, 7.419	5.015 (F silt), 14.95 (M silt), 77.01 (VF sand)

Table 4.3 Basic grain size distribution statistics for the different sediment types.

* For this sediment type, modes from each run were given, as there was enough disagreement between the runs in the coarse fractions that modes from individual runs did not resolve in the mean of the runs.

Grain size	Sediment delivery style (after Gammon et al., 2017)
Clay	Suspended load (low-density flocs)
Fine and very fine silt	Suspended load (suspended via turbulence)
Medium silt	Suspended bedload sortable silt (suspended via turbulence)
Coarse silt	Suspended bedload or bedload (turbulent suspension vs saltation boundary)
Very coarse silt	Bedload (likely saltation)
Very fine sand	Bedload via traction (perhaps rolling)
Fine sand	Bedload via traction (perhaps sliding)

Table 4.4: Depositional processes for different grain sizes, after Gammon et al., (2017).

4.5.3 Geochemistry and Mineralogy

EDS maps were produced to identify major constituent minerals in the cores, complemented by XRD analysis. The main silt and sand minerals yielded in the XRD study of the base of Core 68 I (~8.8 m) are quartz, plagioclase feldspar, orthoclase feldspar, and calcite (Table 4.5). Further EDS mapping of this sediment also yields a single grain of Fe_2O_3, as well as some dolomite, apatite, and rutile (Figure 4.9).

Plagioclase Feldspar %	Calcite %	Chlorite (clay) %	Orthoclase (K) Feldspar %	Quartz %	Illite (clay) %	Total Clay %	TOTAL %
18.1	3.8	6	3.9	48.3	20	26	100

Table 4.5: X-ray diffraction results from a sediment sample from the base of Core 68I, situated ~2 m above the contact for SFI.

EDS mapping of selected sediment from the cm-scale beds of Cores 57 and 67 also indicate the presence of quartz, dolomite, rutile, apatite, and ferric oxide (Figure 4.9). Much of the

sediment is made up of indistinguishable oxides of Si, Al, Mg Na, K, and Fe in varying proportions, indicating possibly clinochlore and feldspars. Occasional Cu-rich grains are present.

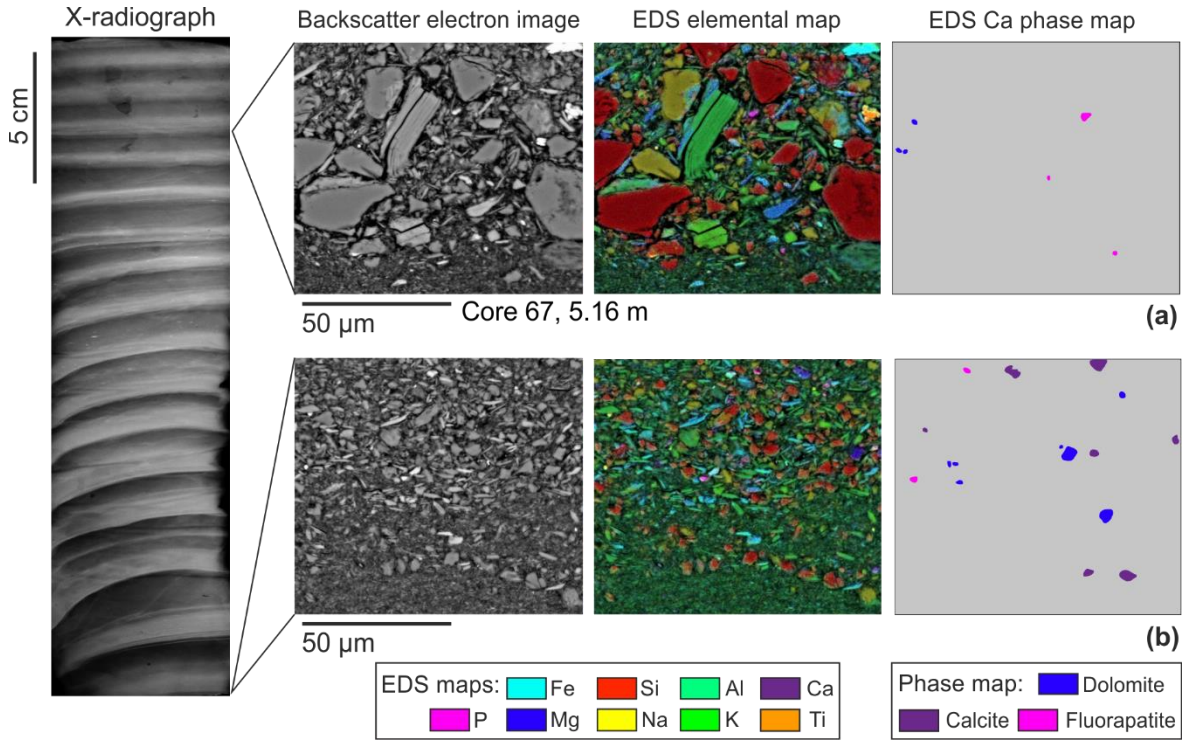

Figure 4.9 Energy-dispersive X-ray spectroscopy (EDS) maps demonstrating the differing calcium content upcore. Far left: Descriptions of sediment type and calcium signal. Left: X-radiograph (top three panels) or BSEI (bottom panel) showing the sediment overview. Middle: BSEI of sediment. Right: EDS elemental map showing the elements present. Far right: EDS mineral phase map showing which calcium-bearing minerals are present.

A major compositional change is shown with calcium (Ca) in both Itrax XRF curves (Figure 4.10) and in EDS phase maps (Figure 4.9). In the cm-scale beds and outwash sediments, calcium levels are high, and EDS phase maps show that the constituent Ca-bearing minerals are calcite, dolomite, and fluorapatite. As the beds thin to mm-scale couplets, the amplitude of the Itrax calcium signal decreases and the EDS phase maps show that the calcite and dolomite are lost. Ca content then remains minimal for the remainder of the core sequence and only a small amount of fluorapatite contributes any calcium to the silt layers. (Figure 4.10).

Strontium isotopes ($^{87}Sr/^{86}Sr$) from ~8.8 m in Core 68 match those from the carboniferous limestones that extensively surround the Lake District, suggesting glacial transport of calcium-bearing minerals from outside the catchment, likely the calcite and dolomite from carboniferous limestone bedrock by the BIIS. The isotopes of the samples from the bottoms of Cores 67 and 64 are more different, possibly due to the Trout Beck catchment crossing the Coniston Limestone formation (Supplementary Figure 1).

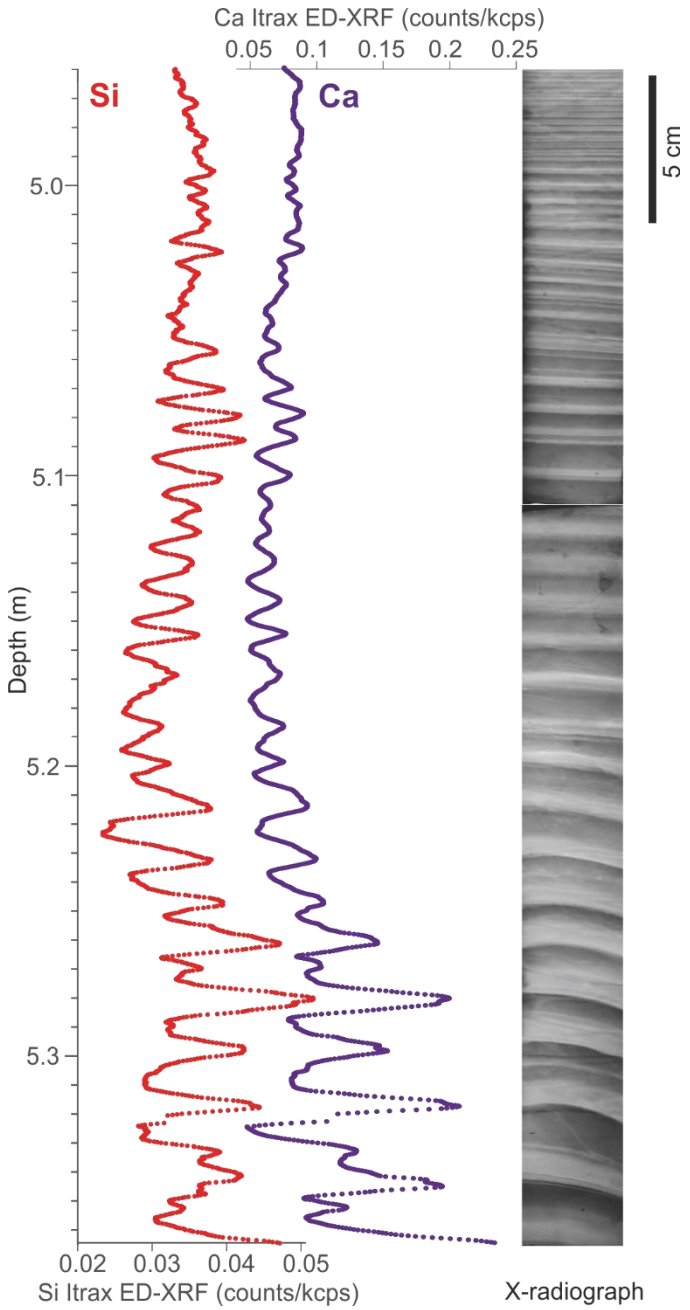

Figure 4.10: The transition from centimetre-scale to millimetre-scale beds, and the accompanying decrease in the Itrax ED-XRF calcium signal. Left: 20-point smoothed Itrax silica signal. Middle: 20-point smoothed Itrax calcium signal. Right. X-radiograph (negative: dark = less dense) of Core 67 (section F, slab 2).

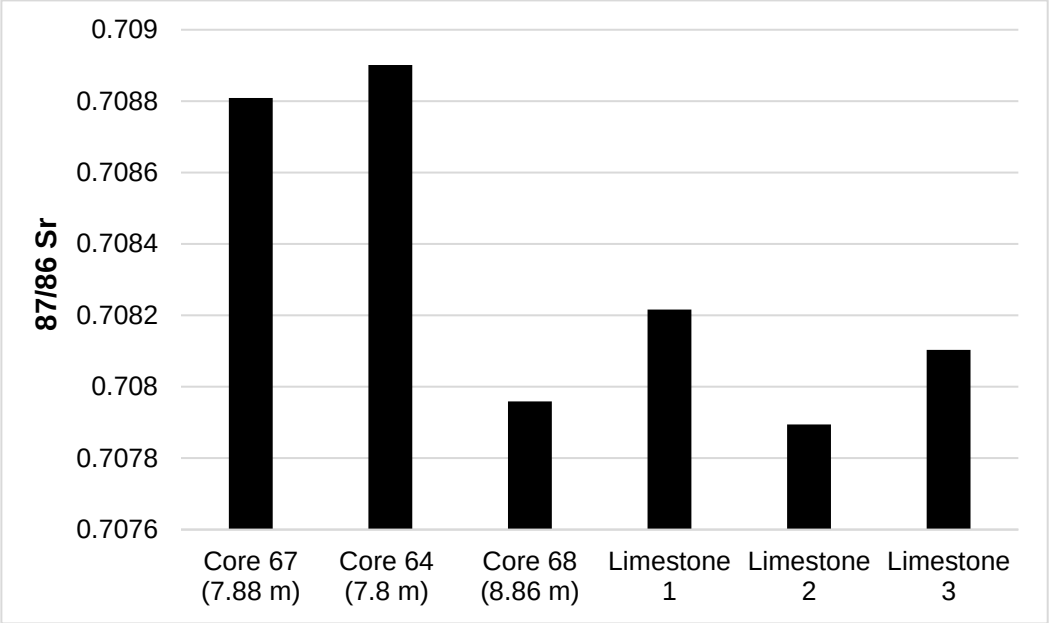

Figure 4.11: 87/86 Sr levels for selected sediment samples from the Ca-rich parts of Cores 64, 67, and 68; and for three Carboniferous Limestone samples from localities adjacent to the Lake District.

4.6 Interpretation of facies

4.6.1 Varve argumentation

The millimetre-scale and centimetre-scale laminations were defined as varves based on their sedimentary characteristics. For the most part, laminations defined as varves had a component interpreted as a melt-season layer, characterised by a unit of coarser material (typically silt), which sometimes contained sublaminations within the unit. The coarser unit was capped with clay, taken to be the non-melt season component formed by the slow settling of fines. Some varves were laid down in a somewhat more porous matrix which contained isolated coarse silt clasts (and sometimes microfossils) throughout, but the basic structure of the varve was still present despite bioturbation and isolated coarse silt clasts. Other examples of varves from alpine, High Arctic and montane Canadian settings also display these features (e.g. Amann et al., 2014; Chutko and Lamoureux, 2008; Kaufman et al., 2011; Menounos and Clague, 2008; Appendix D).

A second basis for the definition of varve was the regularity of the alternating coarse-fine laminations in all four cores, particularly the very close match in thickness between Cores 57 and 67 (4.4.5, 4.7). The sequence of changes up-core from glacially-sourced sediment to nivally-sourced sediment (4.6), occurs within a number of laminations appropriate to

varves in line with the rapid climate amelioration seen in the region (P. U. Clark et al., 2012; Hoek, 2008; Lowe et al., 2008; Rasmussen et al., 2006).

4.6.2 Basal sediments and cm – dm bed facies

The basal sediments in Core 68 are interpreted to represent ice-proximal deposits influenced by a complex catchment with a chaotic ice-marginal deposition regime. This is supported by the thickness of well-sorted bands; presence of massive sand beds including some beds of medium sand grade in the basal 50 cm of Core 68, likely transported by underflows or density currents (Table 4.4) (Francus et al., 2008; Gammon et al., 2017); and evidence of soft-sediment deformation, including convolution and generally poor sorting. The median grain size for the sample from ~8.8 m depth in Core 68 is the second highest (at 6 – 7.5 μm as opposed to 9 – 10.5 μm in the base of Core 64), and the modes include very fine sand. The core base has even larger grain sizes (medium sand beds and some coarse sand grains), leading us to interpret the basal 2 m of Core 68 as being the highest-energy sedimentary environment of the core suite. The main inflow to the north of the location of Core 68 is sourced from six valleys, the interplay of which would be expected to produce a complex sedimentary signal. The cm- dm-scale beds present in Cores 64 and 68 are interpreted to be ice-proximal (having a median grain size of 9 – 10.5 μm in Core 64), but less chaotic. These beds may be varves, based on their quasi-regularity and on the existence of similar varves up to ~20 cm thick found in North America, and if so were likely deposited within a few decades of ice recession (Ridge et al., 2012).

4.6.3 Centimetre-scale beds

The regular centimetre-scale couplets are interpreted to be centimetre-scale varves. The silt bases of the centimetre-scale varves in the South Basin are typically very fine to fine silt grade (median grain size ~2.9 – 3.2 μm, mode 3.82 μm), consistent with deposition from suspension (Table 4.4) (Gammon et al., 2017), and are interpreted as being ice-distal, with the absent coarser fraction having been deposited more proximally to the ice margin (Smith et al., 2004; Zolitschka, 1996). The structure of the melt season layer is dominated by the main melt season sediments, containing several micrograded silt sublaminations (cf. Chutko and Lamoureux, 2008; Cockburn and Lamoureux, 2007; Menounos and Clague, 2008). Distinct graded silt sublaminations at varve bases likely represent early-season melt and run-off. Some of the tops of the melt season layers have the second strongest (thickest or densest) melt pulse after the initial main melt season pulse, interpreted as a late-season

runoff event. Other varves have much weaker late-season sedimentation, likely from years with less intense late melt events.

4.6.4 Thinning transitional beds

The thin, faint sublaminations at the bases of the early transitional varves suggest small regular nival or glacial melt events (e.g. every melting degree-day or group of days) before the air temperature reached the ice mass melt threshold (e.g. Chutko and Lamoureux, 2008; Ridge et al., 2012). The later transitional varves resemble the millimetre-scale varves, but with more sub-laminations. They likely formed in a more snowmelt-controlled environment, but with vestiges of summer glacier melt, possibly from cirque glaciers. The upper, or late-season, melt layers have more coarse grains which could be associated with autumn rainstorms (Gilbert et al., 2006; Hughen et al., 2000; Smith et al., 2004), or a greater aeolian influence on the catchment and thus coarse grains being blown onto the lake surface (Francus et al., 2008).

4.6.5 Millimetre-scale couplets

The millimetre-scale couplets are interpreted to be varves formed in a periglacial environment with clastic input primarily by snowmelt (e.g. Francus et al., 2008; Hambley and Lamoureux, 2006; Kaufman et al., 2011). Grain sizes for both basins decrease from the core bases to the mm-scale varves (Figure 4.8, Table 4.3), in keeping with increased distance from the sediment sources and decreased energy from meltwater (Smith et al., 2004; Zolitschka, 1996). The loss of carbonate with the transition to mm-varves is also consistent with the cessation of outflow from the main ice cap that likely contained the exotic carboniferous limestone carbonate detritus. The evidence of bioturbation is indicative of the onset of organic production in the lake and associated activity of benthic organisms.

4.6.6 Indistinct laminae and transition to interstadial sediments

The increased porosity in BSEI and the presence of microfossils including testate amoebae contributes evidence that the catchment was vegetated with developing soils. Since in the South Basin the silt grain size in the varves is mostly fine and medium (due to ponding of coarser grains up-catchment), the presence of coarse silt grains throughout the intermittent lamina matrix and the presence of grain populations around 40 μm in both basins (Table 4.3, Figure 4.8) indicates a sediment source other than dwindling nival melt. It is possible

that these coarse grains entered the lake through floods and runoff from a deglaciated landscape resulting in a higher runoff intensity and traction deposition (Gammon et al., 2017). The increased intermittency of the laminae reflects decreased recurrence of years with enough snow to produce significant runoff, together with increased benthic activity. In the Interstadial sediments of Core 67, the *Ellerbeckia* sp. layers are also accompanied by a higher concentration of coarse silt clasts, such that each *Ellerbeckia* layer may represent a runoff event.

4.7 Varve sequences and varve correlation between cores

The total number of varves in each sequence, along with uncertainties, is given in Table 4.6 and Figure 4.12 below.

Core	57	67	64	68
Number of Varves	264	273	107	226
Uncertainty	+1	+3-2	+2-4	+3-6
Error (%)	0.38	1.83	5.61	4.91

Table 4.6: Summary of pre-Interstadial varve counts

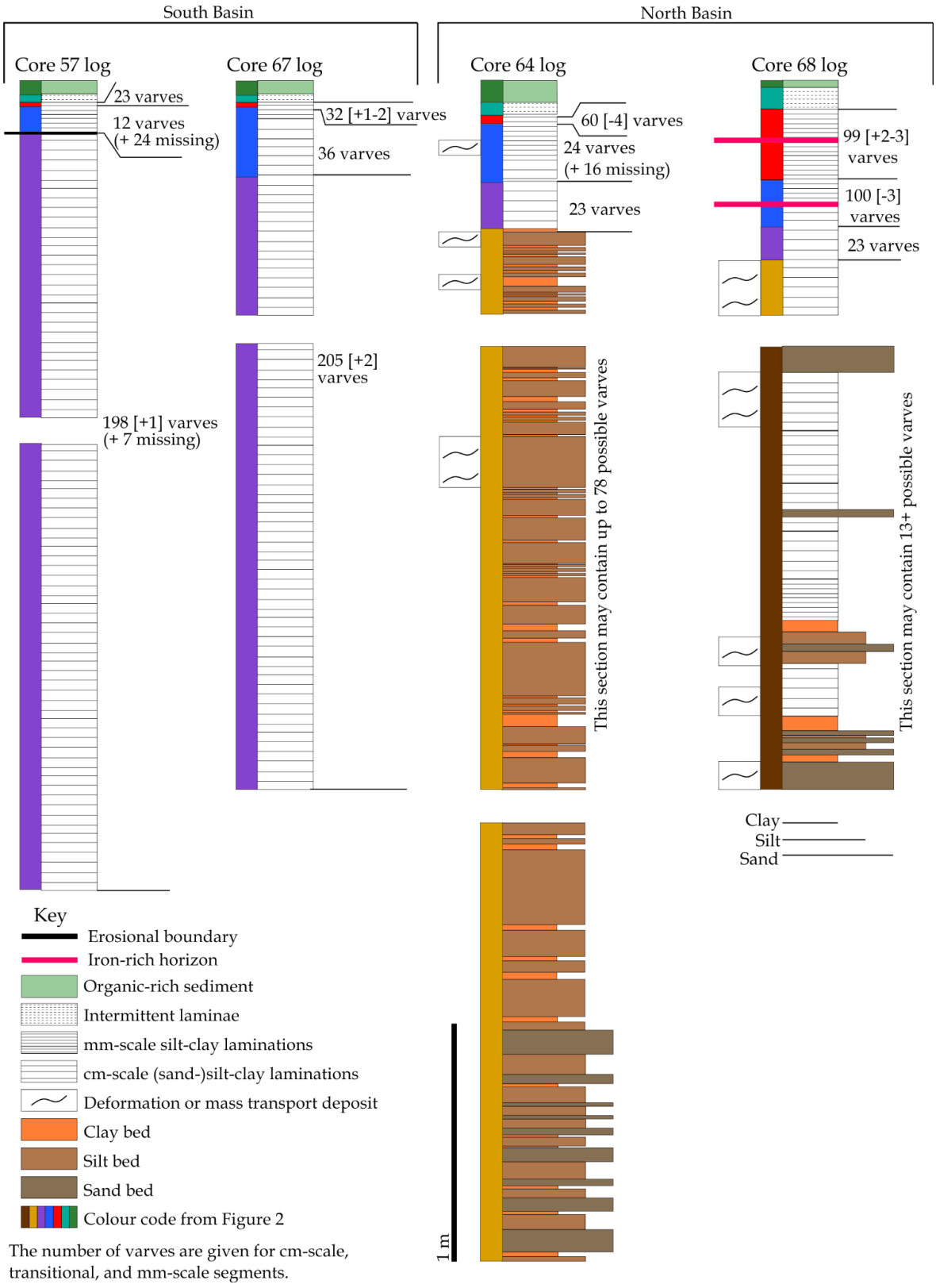

Figure 4.12: Stratigraphic logs of the pre-Interstadial sediments of the four cores. Left: Sedimentary features, e.g. deformation or erosion. Centre: Colour code used in Figure 4 for reference. Right: Sedimentary log. Where practical, beds have been denoted as sand, silt, or clay; where the beds become too thin they have been represented as sequences of laminations.

The principal tie point for all four cores was the onset of organic-rich indistinct varves (Figure 4.13), taken to represent the abrupt and synchronous warming and vegetation of the catchment.

The thicknesses of the cm-scale varves in Core 64 correlate well with Cores 57 and 67 at the multi-annual level when tied at the first 'organic'- type varve, although the individual lamina-by lamina variations are not identical. The bed thicknesses prior to the record in Figure 4.13 are significantly greater, ranging up to 335 mm. The thicker beds are not included in the final varve sequence as there is too little known about their nature, but **Error! Reference source not found.** shows the thickness patterns of these cm-dm-scale beds in Cores 64 and 68 as if they were varves. It can be seen that the overall thickness trends of Cores 64 and 68 are decreasing from the starts of the records (varve numbers 109 and 106), whereas the Core 57 and 67 records only retreat at a similar rate from varve number 122. Similarly, the cessation of Ca-rich sediments occurs in Cores 67 and 64 at varves 204 and 198 respectively, and in Core 57, the change occurs in the erosional gap.

The thickness measurements for Core 68 appear very different from those of the other cores. The cessation of the Ca Itrax signal occurs 64 – 70 vyr before the equivalent event in Cores 64 and 67 respectively, as does the final rapid drop in varve thickness. At the same time, there exist 99 [+2-3] mm-scale varves in Core 68 as opposed to 60 [-4], 32 [+1 -2], and 23 in cores 64, 67, and 57 respectively.

Looking at the four varve thickness records plotted logarithmically (Figure 4.13a), it is evident that from varve 225 onwards the four records co-vary on a multi-annual scale. Similarly, it can be seen that the thickness patterns between Core 68 and Cores 67 and 57 maintain some similarity prior to Varve 173, but that the Core 68 record does not relate to the others between these points.

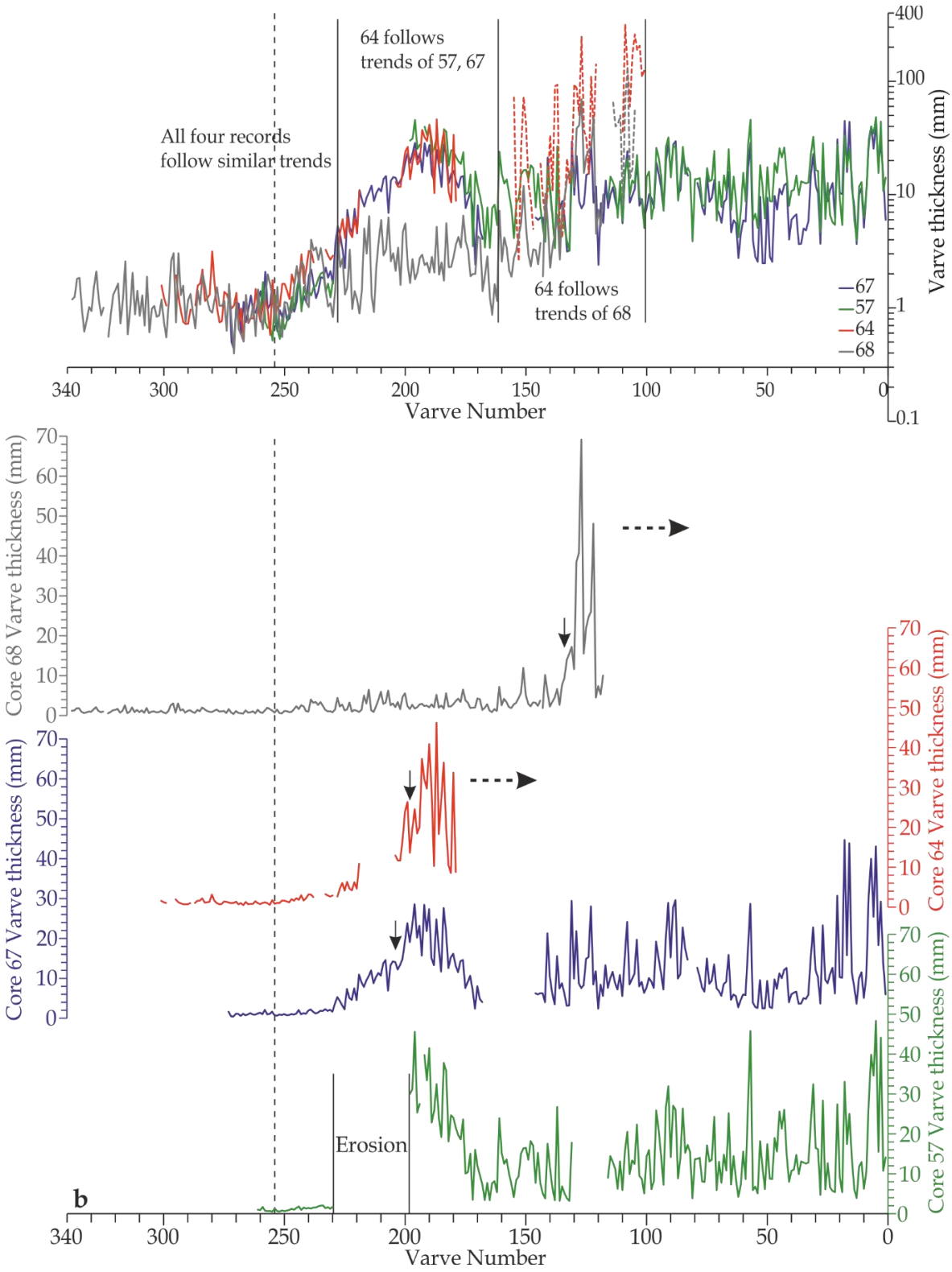

Figure 4.13: Pre- Interstadial varve thickness sequences in millimetres. a) All four cores plotted on a $\log_{10}$ scale to show maximum variability at different scales. Possible-varves from Cores 64 and 68, which may in fact be non-varve glacial outwash, are shown as dashed lines. b) Each individual varve thickness record on a linear scale. From the top: Core 68 (grey), Core 64 (red), Core 67 (blue), and Core 57 (green). Vertical arrows indicate the where the Ca signal diminishes in the Itrax data, representing the cessation of carbonate erosion and transport. The thickness records are all tied at the first major transition to a more organic-rich indistinct varve (vertical dashed line), on the assumption that the whole lake catchment would vegetate simultaneously. Horizontal dashed arrows indicate that the cores continue, but that varve measurements are no longer reliable because

they may in fact be be non-varve glacial outwash, or are heavily deformed. A version of the logarithmic figure, which includes an attempt at recording the cm-dm-scale possible varves in Cores 64 and 68, is shown in **Error! Reference source not found.**.

4.8 Deglacial history

4.8.1 Regional retreat of the British and Irish Ice Sheet (BIIS)

The retreat of the British-Irish Ice Sheet (BIIS) following the end of the Last Glacial Maximum at around 19 ka (Chiverrell and Thomas, 2010; P. U. Clark et al., 2012), involved progressive ice surface lowering that led to separation and retreat of ice to multiple ice centres occupying high ground (Hughes et al., 2014). The Tyne Gap (northeast of the Lake District, between the North Pennines and Scottish Southern Uplands) became ice-free before 16.4 – 15.7 ka (Livingstone et al., 2015) signalling isolation of the Lake District ice from the remaining BIIS, which was thereafter confined to Scotland and the north of Ireland. Evidence for progressive thinning of the remaining ice is provided by exposure ages. Taken together, a cosmogenic isotope age of 17.3 ± 1.1 kyr from a 750 m col of Scafell Pike, the Lake District's highest peak (Ballantyne et al., 2009) and a mean age of 17.35 ± 0.5 kyr from erratic boulders of Shap granite from eastern Cumbria at heights of 275-325 m (Wilson et al., 2013), suggest progressive emergence from ice cover. However, further exposure ages in the Lake District from erratic boulders and a roche moutonnée are interpreted to indicate the persistence of valley glaciers until around 15 ka (Wilson and Lord, 2014). The ice-free date of 17.7 cal ka BP from inside the Windermere catchment (Coope and Pennington, 1977) is considered anomalous – see discussion in Section 3.2, and Wilson and Lord (2014). The succession of sediment types in the Windermere suite shows a transition from a glaciated catchment with proximal ice in the North Basin (4.6.2 - 4.6.4), to an unglaciated vegetated catchment (4.6.5 - 4.6.6) (cf. Bendle et al., 2017; Palmer et al., 2008). The varve sequences may be used to better understand the nature and timing of the retreat of the ice in the catchment and the implications for the retreat of the British-Irish Ice Sheet.

4.8.2 Ice retreat in the South Basin

Seven recessional moraines identified in the sub-bottom topography indicate that ice actively retreated up the South Basin of the steep-sided Windermere Valley from south to north with several still-stands or small readvances, although no ages can be specified

(Pinson et al., 2013). The series of tills and moraines that evidence the ice retreat (Seismic Facies (SF) I in Table 4.1) are overlain by the parallel laminated SF IIa and SF IIb, which constitutes the cm-scale varve facies penetrated by Cores 57 and 67. The seismic reflection sections show that in a depocenter near the location of Core 57, SF IIb extends ~8 m deeper than the penetration of the cores, and the underlying SF IIa constitutes a further ~35 m . Taking the mean thickness of the bottom 20 varves (the best compromise between representing a greater range of existing varve thicknesses, while taking into account a possible thickening trend towards the core bottoms) at the bottoms of Cores 57 and 67 (1.95 cm), and extrapolating through the depocentre, this gives a potential further 384 yr of sedimentation in SF IIb and 1790 yr in SF IIa. In fact the seismic sections do not have the resolution to determine between varves and general glaciolacustrine sedimentation, so it is unlikely that the sediment in the 45 m depocentre is varved to the bottom, but we anticipate that SF IIb is likely varved.

The fine grain size of the South Basin cm-scale varves (Table 4.3, Figure 4.8), associated with settling from suspension (Gammon et al., 2017), and the close correlation of varves between Cores 57 and 67 (some 2.25 km apart) are consistent with deposition from meltwater plumes of suspended very fine silt sourced from a glacier whose edge lay north of the bedrock high between the basins (now represented by a series of islands including Belle Isle (Figure 4.1)). We infer that the ice retreating up the Windermere Valley was situated to the north of Belle Isle near to the mouth of the Trout Beck valley up to (but likely fewer than) 384 years prior to the onset of recovered South Basin varves, and that this represented a southern margin of the Lake District Ice Cap. The presence of SF IIa (larger grain size) in the South Basin depocentres represents sedimentation, possibly varved, from this ice margin when it was pinned on, or south of, Belle Isle; from the Cunsey Beck valley; or from both (see lakebed moraines described in Pinson et al., (2013)).

4.8.3 Initiation of final retreat up the North Basin and separation of the Trout Beck Glacier

The rapid retreat of the ice up the North Basin prior to onset of North Basin sedimentation is evidenced by the occurrence of 28 De Geer moraines identified in sub-bottom profiles (Pinson et al., 2013), and these may represent potentially annual steps in ice retreat (Bouvier et al., 2015). The seismic section for the location of Core 68 shows that the corer penetrated down to ~1 m above the SF I unit (over-consolidated till), such that the disturbed basal sediments at the bottom of the core were likely deposited only a few years after the ice

retreated past the core location.). We therefore suggest that the retreating ice mass had not reached the location of Core 68 by the time of Varve number 1, but that by varve 130 the site had been receiving sediment for several years (if the cm-dm-scale beds in Cores 64 and 68 are taken to be varves). **Error! Reference source not found.** shows that the Core 64 thickness patterns prior to Varve ~130 are similar to those of Core 68. Until this point, the location of Core 64 was therefore likely to be in receipt of significant amounts of sediment from the Northern catchments (outlined in red in Figure 4.1), even before the location of Core 68 was exposed.

Ice-distal sedimentation was relatively short-lived in the location of Core 64, evidenced by the relatively small number of centimetre-scale varves in Core 64 which correlate well in thickness with Cores 57 and 67 (Figure 4.13), overlying ~4 m recovered thick, ice-proximal, possibly-varved sedimentation. The good (but not exact) correlation of these cm-scale varves with those of the South Basin, however, suggests a common sediment source at this time- the Trout Beck Valley (outlined in red in Figure 4.1). Therefore by varve 179, Northern Catchments meltwater did not have the energy to be a dominant control on sedimentation at Core 64.

Despite possible seismic evidence from the placement of De Geer moraines suggesting that the Trout Beck valley deglaciated before the Northern catchments (Pinson et al., 2013), the sedimentary evidence suggests that ice in the Trout Beck valley remained more proximal to the location of Core 64 up to 61 years after ice had become distal from the location of Core 68 (transition to cm-scale varves = 37-61 vyr). However, the presence of 100 (-3) thinning transitional varves in Core 68 and only 36-40 in the other cores, and the persistence of mm-scale varves in Cores 64 and 68 after varve 273, indicates that although initial glacier recession in the Northern catchments occurred before that of Trout Beck, the Trout Beck valley became ice-free first as a result of a more rapid retreat. Similarly, the Ca Itrax signal (calcite and dolomite, Figure 4.9) ceases in Core 68 66-72 vyr earlier than the other cores. The limestone presence in the sediment likely represents transport by the ice from the Carboniferous Limestone terrain adjacent to the Lake District, and this may indicate that the Northern catchments separated from the main Lake District Ice cap earlier than the Trout Beck valley, possibly due to earlier exposure of the higher watershed rocks in the Northern catchments.

4.8.4 Deglaciation of the northern valleys of Windermere

There are 234 (+2 -6) continuous varves in the pre-Interstadial sequence in Core 68 (in addition to proximal glacial outwash), including the cm-dm ice-proximal possible varves. In contrast with the sedimentation of the South Basin, which is long-lived, the time between exposure of the Core 68 site and the cessation of varves is likely under ~250 years (100 (-3) of which are classified as thinning transitional varves, which are interpreted to represent active ice retreat up-valley

Within the 222 (+2-6) ice-distal varves in Core 68, thicker (up to 1 cm) varves are interspersed with mm-scale and thinning transitional type. This is likely a result of the six valleys potentially contributing snow and ice melt in the more complex Northern catchments (Figure 4.1), as well as ponding up-catchment. The large size of the double catchment and high relief of the surrounding watershed may have also contributed glacial melt sedimentation despite heightened sediment bioturbation, indicative of a lake catchment hospitable to vegetation and microfauna. The persistence of the intermittent laminae in Core 68 is likely to relate to its location in the deep basin and being in reception of more terrestrial sediment from the uplands of the Northern catchments at the start of the Interstadial.

In a proglacial environment, a thicker varve corresponds with greater glacial melt, itself a function of melting degree-days in the melt season (Ridge et al., 2012). The catchments supplying Core 68 are more complex and have a higher-altitude watershed, meaning that the 'glacier-dynamic' signal from each individual ice mass in the varve record is damped and the multi-annual trend may represent interannual climate variability. The relative simplicity of the Trout Beck glacier means that the varve thickness variations in the South Basin may reflect multidecadal glacier dynamics as well as overarching climate. It also appears that glacial melt from the Northern catchments persisted into the early Lateglacial Interstadial for ~100 years.

In general, the small number of mm-scale varves in all four records prior to the organic-rich varve tiepoint (12 in Cores 57, 67, and 64, and 14 in Core 68) indicates that there was a very rapid switch between a glaciated and hospitable (possibly vegetated) environment at the onset of the Lateglacial Interstadial. This may point to ice-dynamic hysteresis whereby the climate had warmed to an average of above 0^{o} C before the last ice finally melted.

4.8.5 Relation to the North Atlantic and the 'Mystery Interval'

The period directly before the onset of the Lateglacial Interstadial, from which the varve sequences in this study originate, is known as the 'Mystery Interval'. It refers to the ~3000 yr interval starting at ~17.5 ka, directly after the LGM, which was characterised by a major ice-rafting event (Heinrich Event 1) leading to particularly cold winters in North-western Europe and Greenland and a colder northern Atlantic Ocean (within the main IRD belt) and Mediterranean (Denton et al., 2006). Prior to the HS1 ice rafting event, the northern Atlantic may have been freshened instead by melting Eurasian ice sheets post-LGM (Hodell et al., 2017). At the same time, rising CO_2 underpinned warming that drove terrestrial glacier retreat (e.g. the European Alps, New Zealand, and the Andes) (Denton et al., 2006 and references therein). The Mystery Interval may be split into two separate phases: one from 18 – 16.1 ka (Figure 4.14c) corresponding in Greenland ice cores to less negative $\delta^{18}O$ (warmer) values, succeeded by a colder Greenland phase from 16.1 – 14.6 ka (Broecker and Putnam, 2012; Hodell et al., 2017).

In a broader study of earlier Dansgaard-Oeschger cycles 3 – 17 in a core from the heart of the IRD belt (at 59° N), the transitions to interstadials show a gradual surface warming that lasted, on average, for around 800 years compared with the ca. 40 year shifts in NGRIP (Rasmussen et al., 2016). This has been used to suggest a direct southern (Antarctic) influence on North Atlantic variability, with most of the North Atlantic being in phase with the south and out of phase with the abrupt warmings in the Greenland ice cores, the Nordic Seas and otherwise in areas of the North Atlantic impacted by large meltwater inputs during stadials (Rasmussen et al., 2016).

The varve sequences presented here extend back to ~255 yr prior to the onset of the Lateglacial Interstadial, and would have formed as sea surface temperature was increasing, towards the end of the second phase of the Mystery Interval and very soon after a discharge from the Laurentide Ice Sheet. The potential extended varve sequence in the South Basin could shed light on the behaviour of relatively maritime glaciers well into this interval, in relation to the Greenland-Atlantic phase question (Figure 4.14).

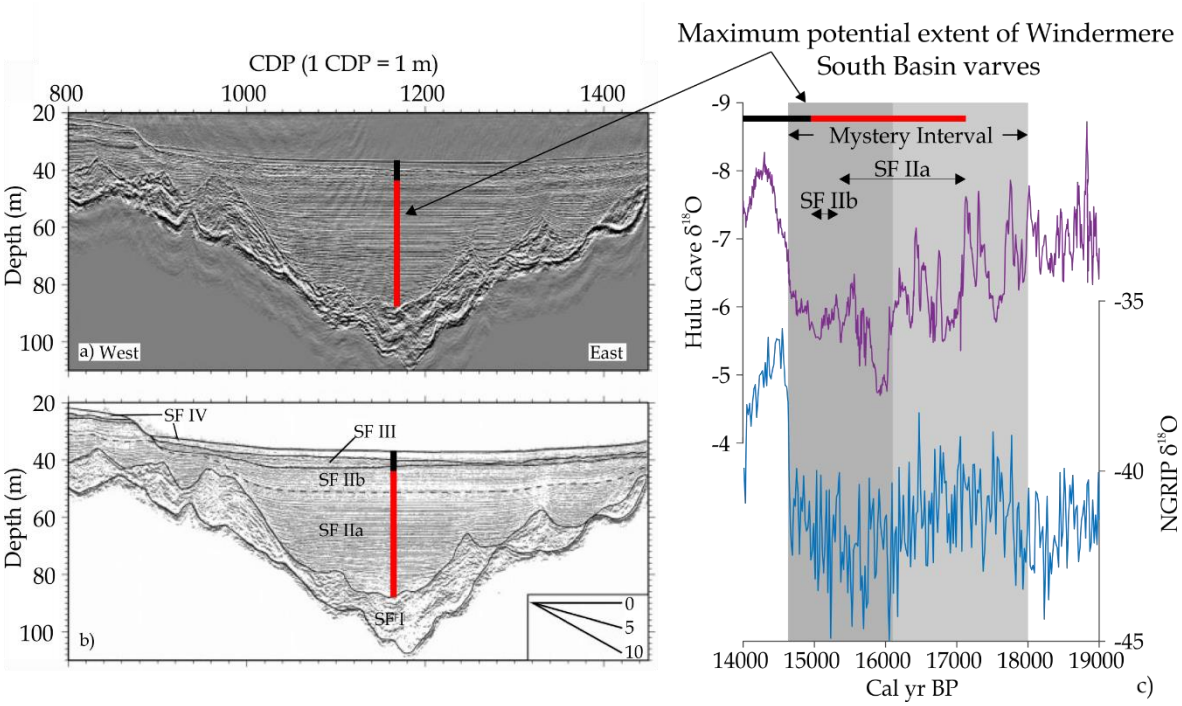

Figure 4.14: The potential extent of the Core 57 varve suite through the Mystery Interval. Uninterpreted (a) and interpreted (b) depth-migrated seismic reflection section through a location near to Core 57. Vertical bar indicates extent of Core 57, where the red section represents pre-Interstadial varves and potential varves. c) $\delta^{18}O$ record from NGRIP (blue) on the GICC05 timescale (Rasmussen et al., 2006), and a $\delta^{18}O$ record from Hulu Cave, China (purple), using data from (Wang, 2001; Wu et al., 2009), and the timescale of (Southon et al., 2012).

4.9 Conclusions

In this study, a sediment sequence present in the four cores of Windermere was investigated in order to understand better the retreat dynamics of the Lake District ice cap in the Windermere valley. We demonstrate that Windermere is host to a ~255 yr pre-Interstadial proglacial and periglacial varve sequence (plus some ~54 possible cm-dm-scale varves), the first of its kind from a pre-Interstadial Eurasian Ice Sheet setting. Previous work in this area identified several recessional and de Geer moraines in the Windermere lakebed which were interpreted as a stepped retreat of ice up the Windermere valley, but no timings could be pinned to the moraines (Pinson et al., 2013).

The varve sequences, combined with seismic reflection sections, show that the southern ice front of the Lake District Ice Cap was situated between Belle Isle and Trout Beck up to ~380 vyr prior to recovered varves. The ice front subsequently retreated up the North Basin and the location of Core 68 was exposed between Varves 1 and 130. Records of carboniferous limestone presence and varve thickness indicate that the Trout Beck valley glacier remained attached to the ice cap for longer than the ice of the Northern catchments, such that the Northern ice started to retreat first (no longer influencing Core 64 sedimentation significantly by Varve 155, possibly earlier). However, the length and nature of the mm-scale varve records show that the complex Northern catchments remained partially glaciated (at least in some of the six valleys) for 100 vyr whilst in the cores fed by the Trout Beck glacier, there are only 36 - 40 varve years between the 'glacial-melt' cm-scale varves and the 'snowmelt' mm-scale varves. The switch from the first snowmelt-controlled varve to the first varve with evidence of catchment biota was only 12-14 vyr. Further coring in the South Basin could recover a potential extended varve sequence laid down through the Mystery Interval.

4.10 Supplementary Material

4.10.1 Detailed figures of sediment facies

4.10.1.1 Basal sediments

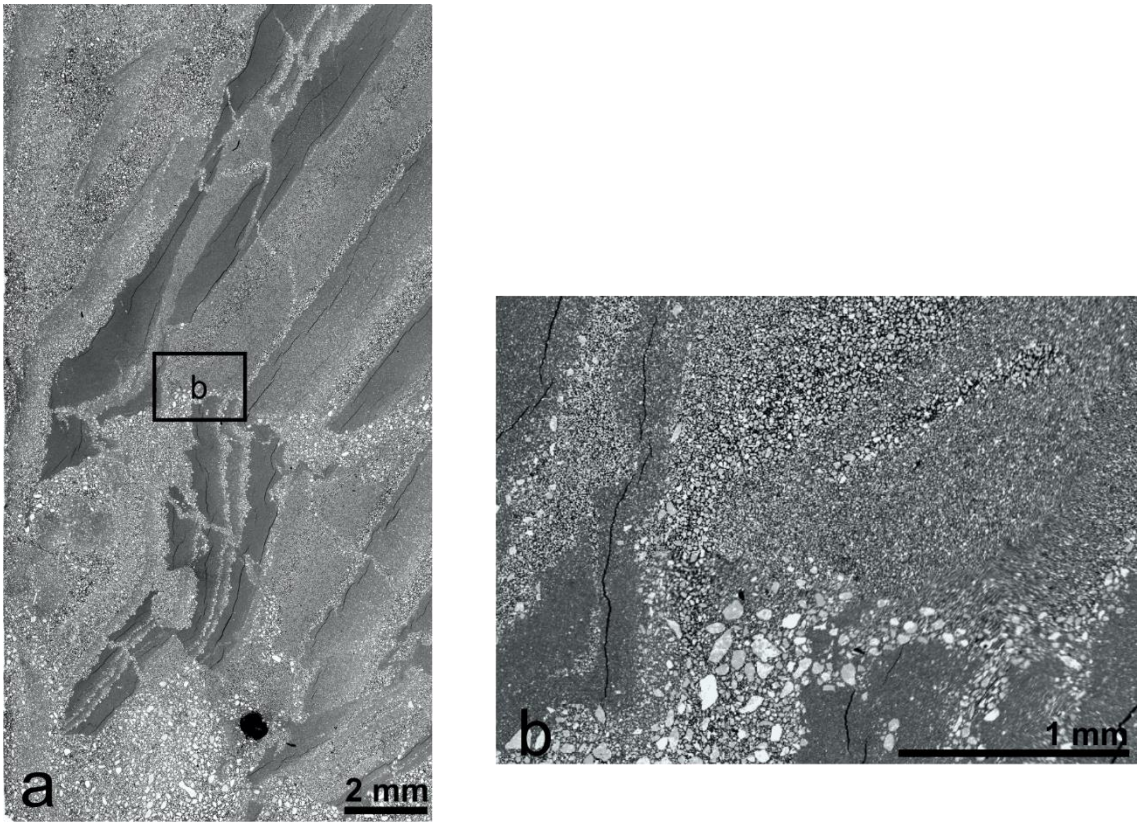

Figure 4.15: BSEI showing of the disturbed nature of the basal sediment. Laminations are present (a), but they are faulted and disjointed. The close-up image on the right (b) shows the range of grain sizes present (clay to very fine sand).

4.10.1.2 Dm-scale beds

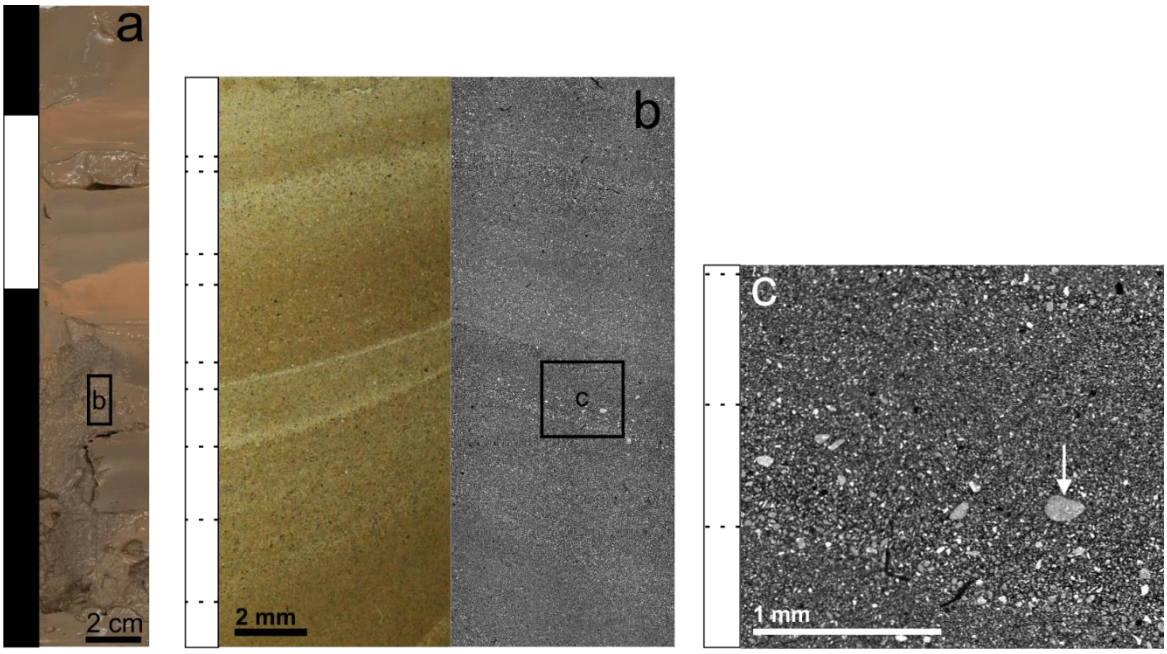

Figure 4.16: An example of part of a centimetre- to decimetre-scale bed from Core 64. a) A sediment slab photograph of ~25 cm sediment. Beds are denoted as black and white alternating bars. b) Optical photomicrograph (left) and BSEI (right) showing the nature of the silt laminae within the bed's coarse component. c) BSEI showing the variation in grain size of a silt sublamina. Note the band of medium – coarse silt (shown by the lowermost dotted line to the left of (c) with isolated fine sand grain (arrowed). The bed displayed here is 17.9 cm thick, with the silt laminations being deposited later in the melt season.

4.10.1.3 Cm-scale beds

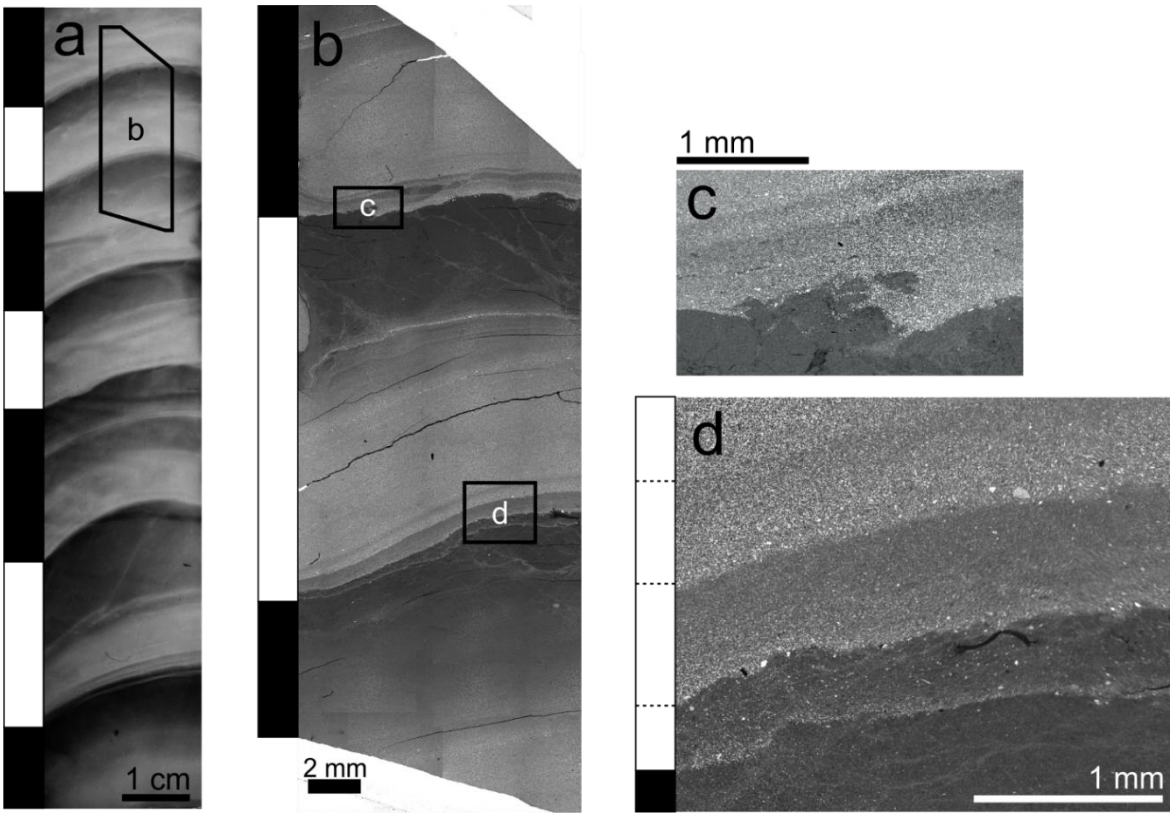

Figure 4.17: Centimetre-scale beds. Black and white sidebars denote bed boundaries, and dotted lines denote bed sublaminations. a) X-radiograph showing cm-scale beds. b) Polished thin section BSEI showing the structure of the beds. c) BSEI detail of load casting on the bed base; d) BSEI detail of the sublaminations at the base of the bed.

4.10.1.4 Thinning transitional beds

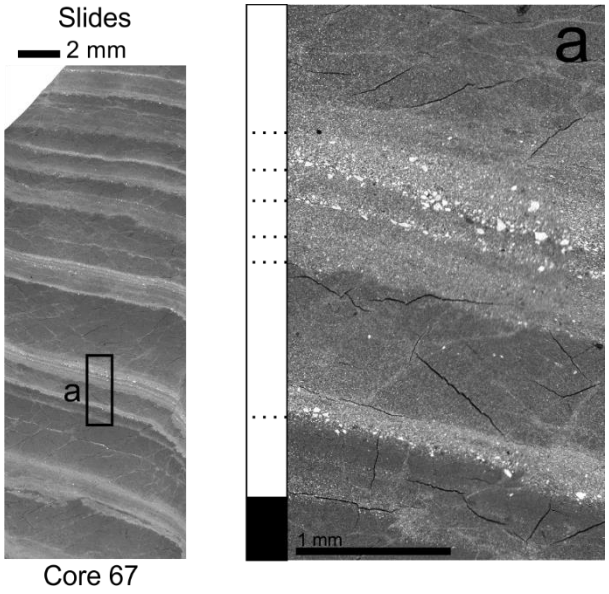

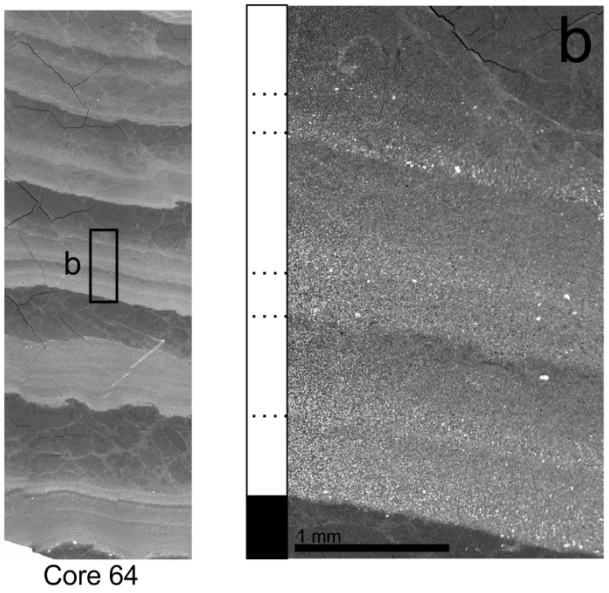

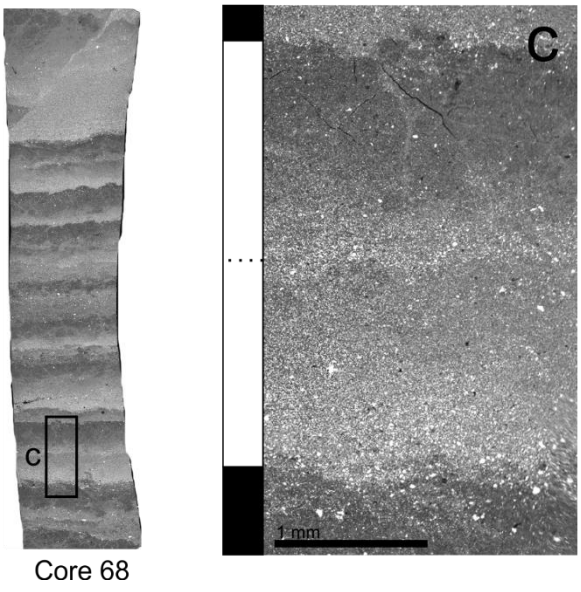

Figure 4.18: BSEI showing examples of mid-unit thinning transitional beds from Cores 67 (a), 64 (b), and 68 (c). Black and white sidebars denote bed boundaries, and dotted lines denote bed sublaminations.

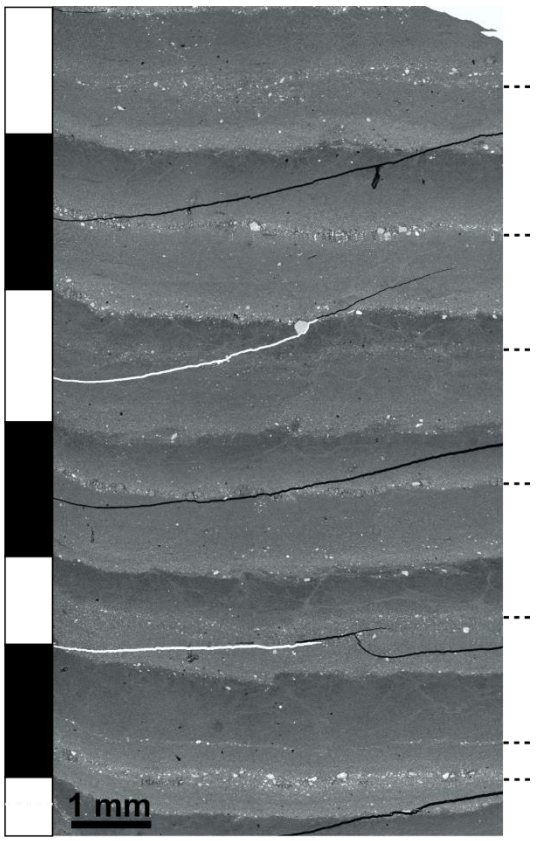

Figure 4.19: BSEI of upper-unit transitional-to-mm beds, from Core 57. The black and white side bar denotes bed boundaries, and dotted lines denote bed sublaminations.

4.10.1.5 *Mm-scale laminations*

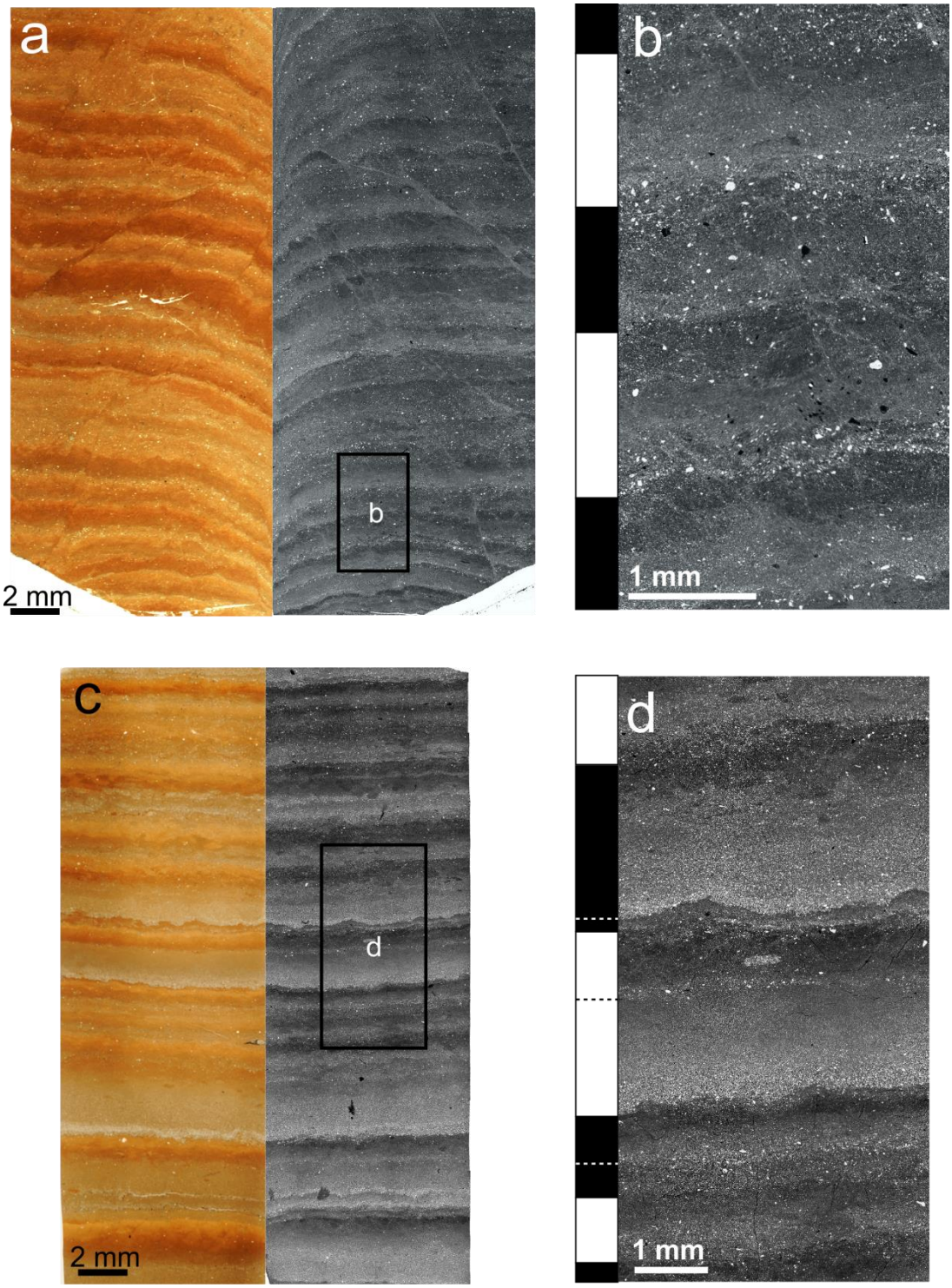

Figure 4.20: Examples of millimetre-scale laminations from Core 67 (top: a, b) and Core 68 (bottom: c, d). a, c) Optical photomicrographs (left) and BSEI (right) showing lamina sequences. b, d) close-up images of mm-scale laminae, showing lamina structure. Alternating black and white bars denote lamina boundaries, and dotted lines show sublaminations. Note that the laminae of Core 68 have more microstructure, and that the ~1 mm thick laminae are interspersed with thicker examples.

4.10.1.6 Intermittent laminations

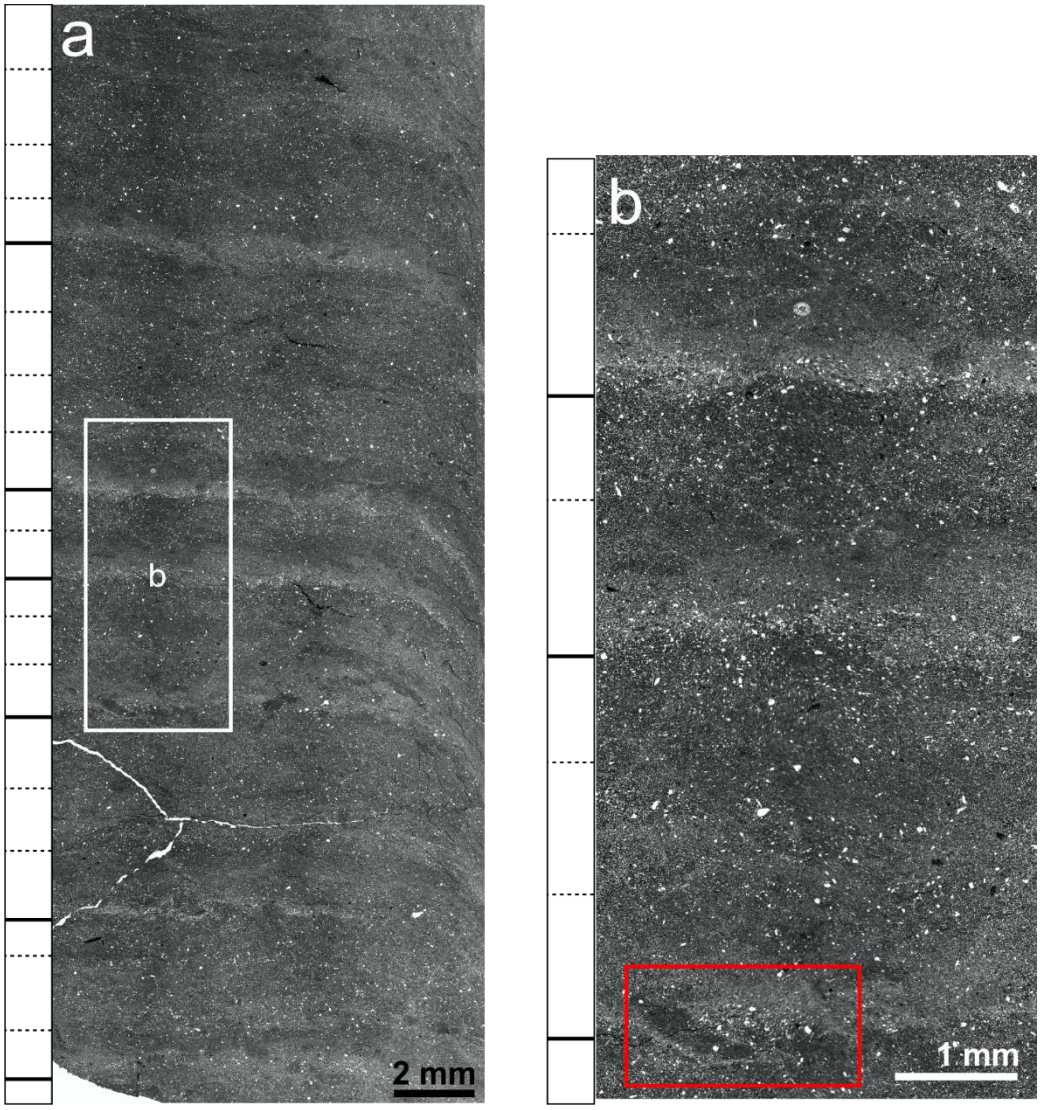

Figure 4.21: BSEI showing intermittent indistinct laminae at the lower boundary of the Lateglacial Interstadial. The dotted lines on the sidebar indicate possible laminations, and the solid lines show clearer laminations. Detail in red rectangle of (b) shows redistribution of dark and pale sediment likely by burrowing activity of micro-biota.

4.10.1.7 Interstadial Sediment

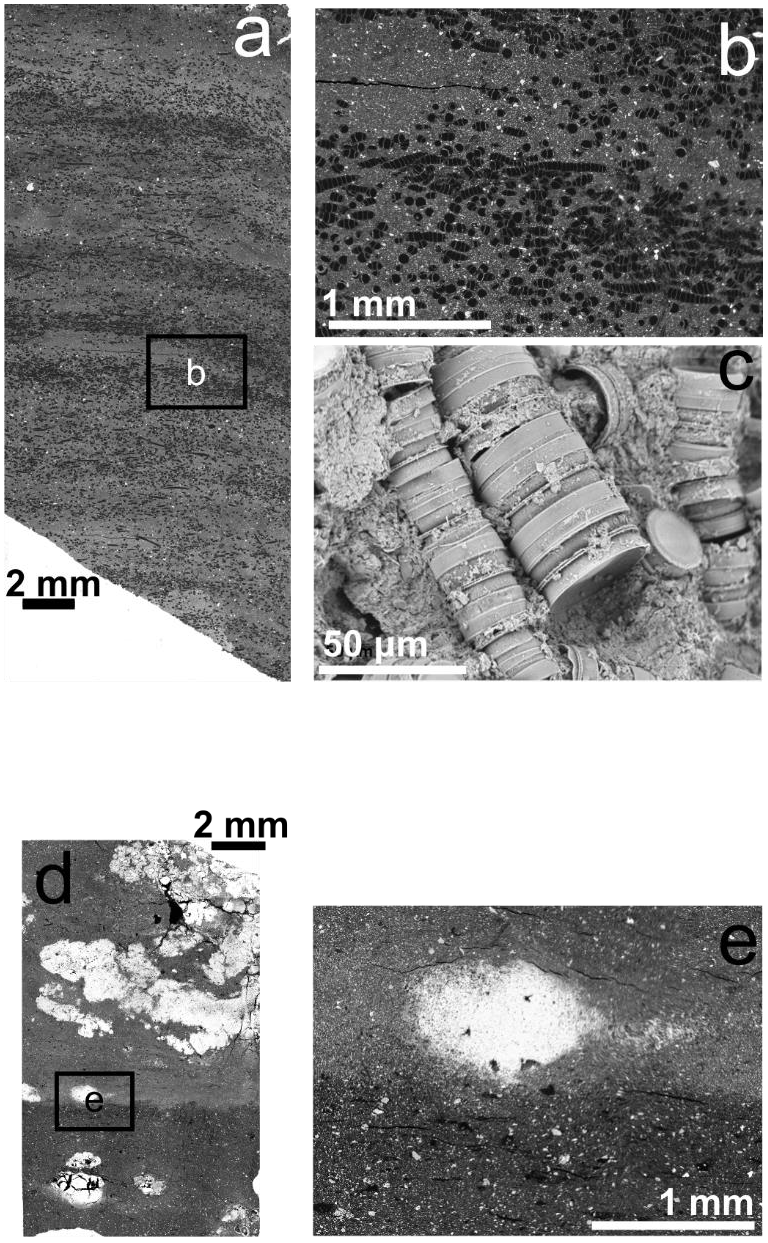

Figure 4.22: BSEI of Interstadial sediment. a) Interstadial sediment of Core 67, with *Ellerbeckia* sp. laminae, with details in b) and c) (topographic image showing *Ellerbeckia* chains). d) An example of the iron-rich growths found in the Interstadial sediments of Core 68, with detail in e.

4.10.2 Details on varve counts

The tables below give details on the varve counts between tiepoints and uncertainties.

Before comparing discrepancies with 57 Core 67			Uncertainty	
Tie	Count 1	Count 2	+ve	-ve
0-T3	19	18	1	-2
T3-T2	12	13	1	0
T2-T1	36	36	0	0
T1-A	14	14	0	0
A-B	8	8	0	0
B-C	13	13	0	0
C-D	30	30	0	0
D-E	4	4	0	0
E-F	21	21	0	0
F-G	12	12	0	0
G-H	19	19	0	0
H-I	11	11	0	0
I-J	16	16	0	0
J-K	26	24	2	0
K-L	16	16	0	0
L-M	15	15	0	0
TOT	272	270	4	-2
% Error	2.21			

After comparing discrepancies with 57			Uncertainty	
Tie	Count 1	Count 2	+ve	-ve
0-T3	20	18	0	-2
T3-T2	12	13	1	0
T2-T1	36	36	0	0
T1-A	14	14	0	0
A-B	8	8	0	0
B-C	13	13	0	0
C-D	30	30	0	0
D-E	4	4	0	0
E-F	21	21	0	0
F-G	12	12	0	0
G-H	19	19	0	0
H-I	11	11	0	0
I-J	16	16	0	0
J-K	26	24	2	0
K-L	16	16	0	0
L-M	15	15	0	0
TOT	273	270	3	-2
% Error	1.83			

Table 4.7: The tiepoints used in the Core 67 pre-Interstadial varve sequence. Counts by two different researchers between each tiepoint are given, and the total uncertainty is given, calculated as the absolute number of disputed varves as a percentage of the total count (count 1).

Before comparing discrepancies with 67				
Core 57			Uncertainty	
Tie	Count 1	Count 2	+ve	-ve
0-T3	11	11	0	0
T3-T2	12	12	0	0
T2-T1	36	36	0	0
T1-A	14	14	0	0
A-B	8	8	0	0
B-C	13	13	0	0
C-D	30	30	0	0
D-E	4	4	0	0
E-F	21	21	0	0
F-G	12	12	0	0
G-H	19	20	1	0
H-I	11	12	1	0
I-J	16	16	0	0
J-K	26	26	0	0
K-L	16	15	0	-1
L-M	15	15	0	0
TOT	264	265	2	-1
% Error	1.14			

After comparing discrepancies with 67				
			Uncertainty	
Tie	Count 1	Count 2	+ve	-ve
0-T3	11	11	0	0
T3-T2	12	12	0	0
T2-T1	36	36	0	0
T1-A	14	14	0	0
A-B	8	8	0	0
B-C	13	13	0	0
C-D	30	30	0	0
D-E	4	4	0	0
E-F	21	21	0	0
F-G	12	12	0	0
G-H	19	20	1	0
H-I	12	12	0	0
I-J	16	16	0	0
J-K	26	26	0	0
K-L	15	15	0	0
L-M	15	15	0	0
TOT	264	265	1	0
% Error	0.38			

Table 4.8: The tiepoints used in the Core 57 pre-Interstadial varve sequence. Counts by two different researchers between each tiepoint are given, and the total uncertainty is given, calculated as the absolute number of disputed varves as a percentage of the total count (count 1).

Core 64			Uncertainty	
Tie	Count 1	Count 2	+ve	-ve
0-T3	48	46	0	-2
T3-N	16	14	0	-2
O-P	16	16	0	0
Q-R	27	29	2	0
TOT	107	105	2	-4
% Error	5.61			

Table 4.9: The tiepoints used in the Core 64 pre-Interstadial varve sequence. Counts by two different researchers between each tiepoint are given, and the total uncertainty is given, calculated as the absolute number of disputed varves as a percentage of the total count (count 1).

Core 68			Uncertainty	
Tie	Count 1	Count 2	+ve	-ve
0-T3	85	85	2	-3
T3-S	16	16	0	0
S-T	24	24	0	0
T-U	21	23	2	0
U-V	24	23	0	-1
V-W	20	19	0	-1
W-X	8	7	0	-1
X-Y	16	17	1	0
Y-Z	10	10	0	0
TOT	224	224	5	-6
% Error	4.91			

Table 4.10: The tiepoints used in the Core 68 pre-Interstadial varve sequence. Counts by two different researchers between each tiepoint are given, and the total uncertainty is given, calculated as the absolute number of disputed varves as a percentage of the total count (count 1).

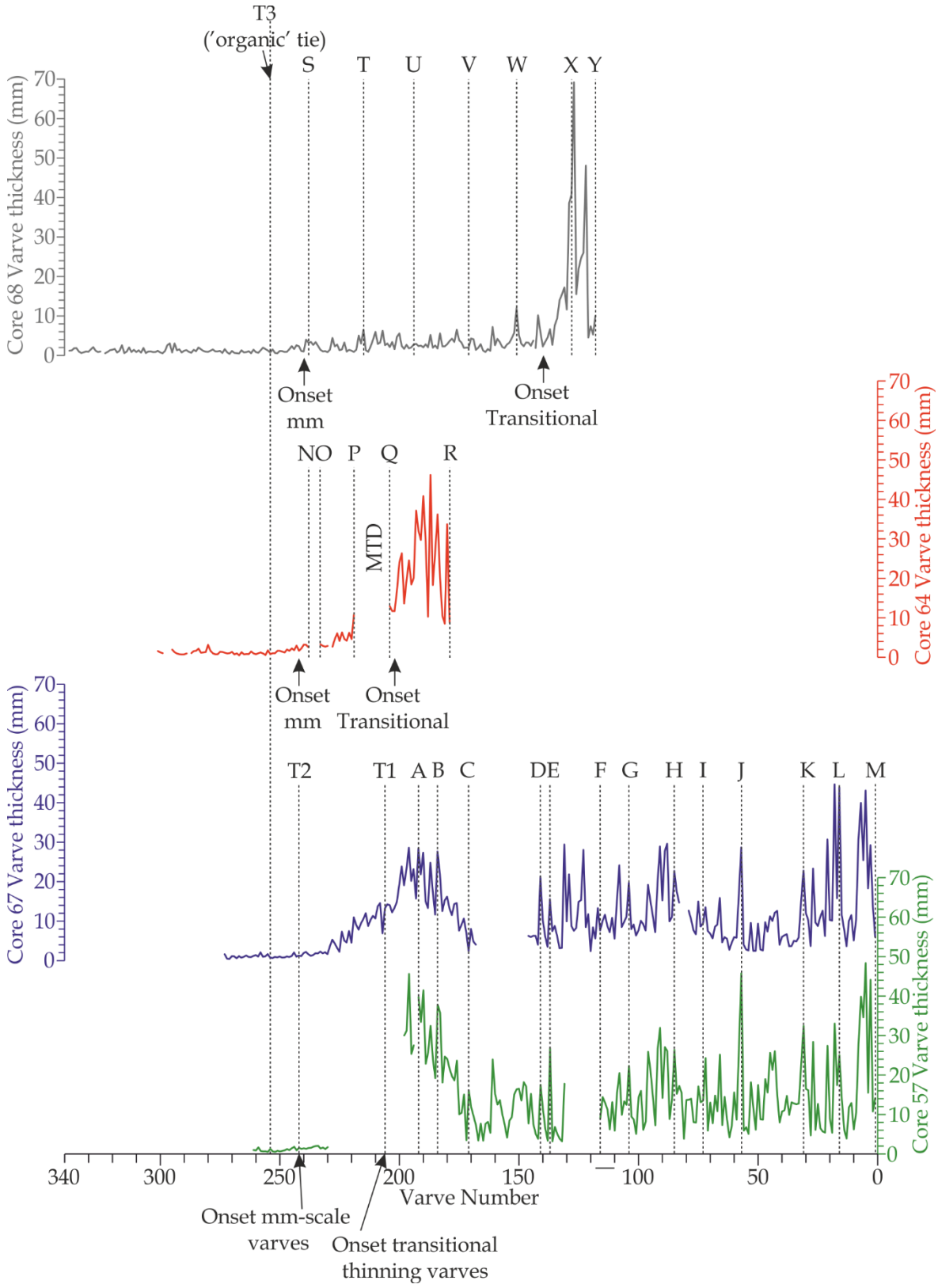

Figure 4.23: Varve thickness sequences with the counting tiepoints shown. Cores 57 (green) and 67 (blue) share tiepoints since the sequences were so similar. For all sequences, the transition between cm-scale and 'transitional-type varves ('onset transitional') and the transition between transitional-type and mm-scale varves ('onset mm') is shown. 'T3' refers to the first varve with more 'organic-type' features (e.g. bioturbation, coarse soil-derived clasts) and is the only tiepoint shared between all four cores.

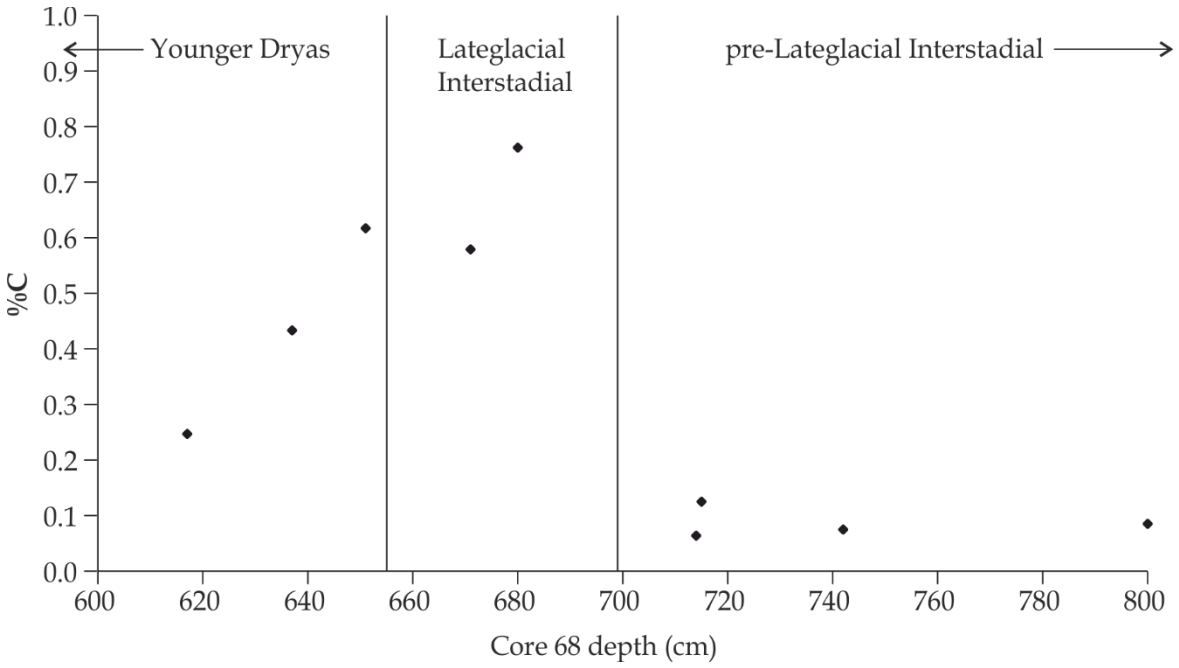

Figure 4.24: Percent carbon for Core 68 sediments between 6 and 8 m, which incorporates pre-Interstadial sediment, Lateglacial Interstadial sediment, and early Younger Dryas sediment.

5. Younger Dryas-age varve sequences from Windermere, UK

In this chapter, the Younger Dryas- age mm-scale varves are investigated and placed in the wider climatic context.

5.1 Abstract

The acquisition of high-resolution palaeoclimate archives through abrupt climate transitions is critical to developing an understanding of earth system behaviour sufficient to predict future change. Of particular interest is the ~ 1200 yr Younger Dryas (YD) cold interval (~12.9 – 11.7 ka BP), the most recent abrupt change that interrupted warming during the last deglaciation. The rapidity of change in this climate upheaval is recorded in the annually resolved Greenland Ice Cores, and while annually-laminated sediments or varves provide comparable resolution, the only lake record from western Europe, to date, to provide a continuous annually laminated sequence through the entire YD is the sequence of Lake Meerfelder Maar in Germany. Here we present the first varved sediment records from a currently active British or Irish lake, from Windermere in the Lake District of Northwest England that also contain continuously varved sediment throughout the YD. We find that the YD-age sediments from the Windermere North Basin are typified by mm-scale varves derived predominantly form snowmelt. The varves of the first ~ 680 varve years of the YD contain evidence of strong winds and stormy conditions, being more bioturbated and containing coarse silt grains of aeolian origin. During the mid-Younger Dryas, there is a shift towards a less bioturbated varve style, indicative of less wind-driven mixing and consistent with existing evidence for a northwards shift in storm tracks following a retreating sea-ice front at this time. An increase in varve thickness also evidences warmer, moister conditions, which promoted greater snowfall and melt. Rapidly thickening varves near the top of the YD-age unit (in the top 13 varves) indicate abrupt warming prior to the onset of the non-varved Holocene sediment. The smoothed composite Windermere varve thicknesses appear to co-vary with the NGRIP $\delta^{18}O$ data for GS-1 after 12200 yr BP on timescales of 50 – 100 yr suggesting a shift to more modern temperature and precipitation regime, although Windermere age model uncertainty makes robust comparison impossible. Our floating varve chronology shows the potential for the

development of a precise, annually resolved chronology through the YD interval from a UK site.

5.2 Introduction

The last deglaciation was punctuated by a series of rapid alternations between warm and cold climate intervals, and the quest to understand the causality of these continues to challenge the scientific community. The most recent of the shifts to colder climate states was the onset of the Younger Dryas Stadial, which returned the circum-North Atlantic regions to near-glacial temperatures within decades and persisted for around 1200 years between 12.9 and 11.7 ka prior to the final Holocene warming. Critical to the understanding of such Earth system behaviour is the requirement for palaeo-records at a sufficiently high temporal resolution to reveal the causal interplay between ocean, atmosphere, and ice in generating and transmitting change. The annually resolved Greenland Ice Cores highlight the rapidity of change through this interval, and engender a need for similarly resolved palaeoclimate archives. Annually laminated sediments, or varves, provide comparable resolution but, to date, the sequence of Lake Meerfelder Maar in Germany is the only lake record from Western Europe to provide a continuous annually laminated sequence through the entirety of the Younger Dryas interval (Brauer et al., 2008; Lane et al., 2013). Here we present new records obtained from a series of sediment cores from Windermere in the Lake District of Northwest England that demonstrate the potential of a continuously varved sediment throughout the Younger Dryas. The Windermere cores yield a sediment sequence from prior to the Lateglacial Interstadial until the present day, including varve sequences from the 'Mystery Interval' (~GS2) and Younger Dryas (GS1). During the Younger Dryas, the Windermere catchment contained ice masses at some of the valley heads in the form of plateau icefields and cirque glaciers, but the catchment did not contain a significant amount of ice (Brown, 2009; McDougall, 2001; Sissons, 1980; Wilson, 2004; Wilson and Clark, 1998). Here, we investigate the YD-age sediments and in particular the sedimentology of the varve sequences. We discuss the varve counts and sedimentary nature in the context of other studies of the period.

5.3 Study location

Windermere is a north-south trending glacial ribbon lake in the southeast of the English Lake District (54.4° N, 2.9° W) (Figure 5.1), lying in a steep-sided pre-glacial river valley that has been overdeepened by successive glaciations (Pennington and Pearsall, 1973; Pinson et al., 2013). The lake has a present maximum water depth of 62 m and an elevation of 39 m above Ordnance Datum Newlyn. It has maximum dimensions of 17 km x 1.5 km and drains a catchment of 242 km^2 (Lowag et al., 2012; Miller et al., 2013). The catchment bedrock comprises the Ordovician Borrowdale Volcanic Group in the north and the Windermere Supergroup (Silurian mudstones and siltstones) in the south.

Windermere is separated into a north and South Basin by a bedrock high, with the South Basin draining westward into the River Leven (Wilson, 1987). Windermere has accumulated sediment since the retreat of the British-Irish Ice Sheet c. 17 ka (Ballantyne et al., 2009; Coope and Pennington, 1977).

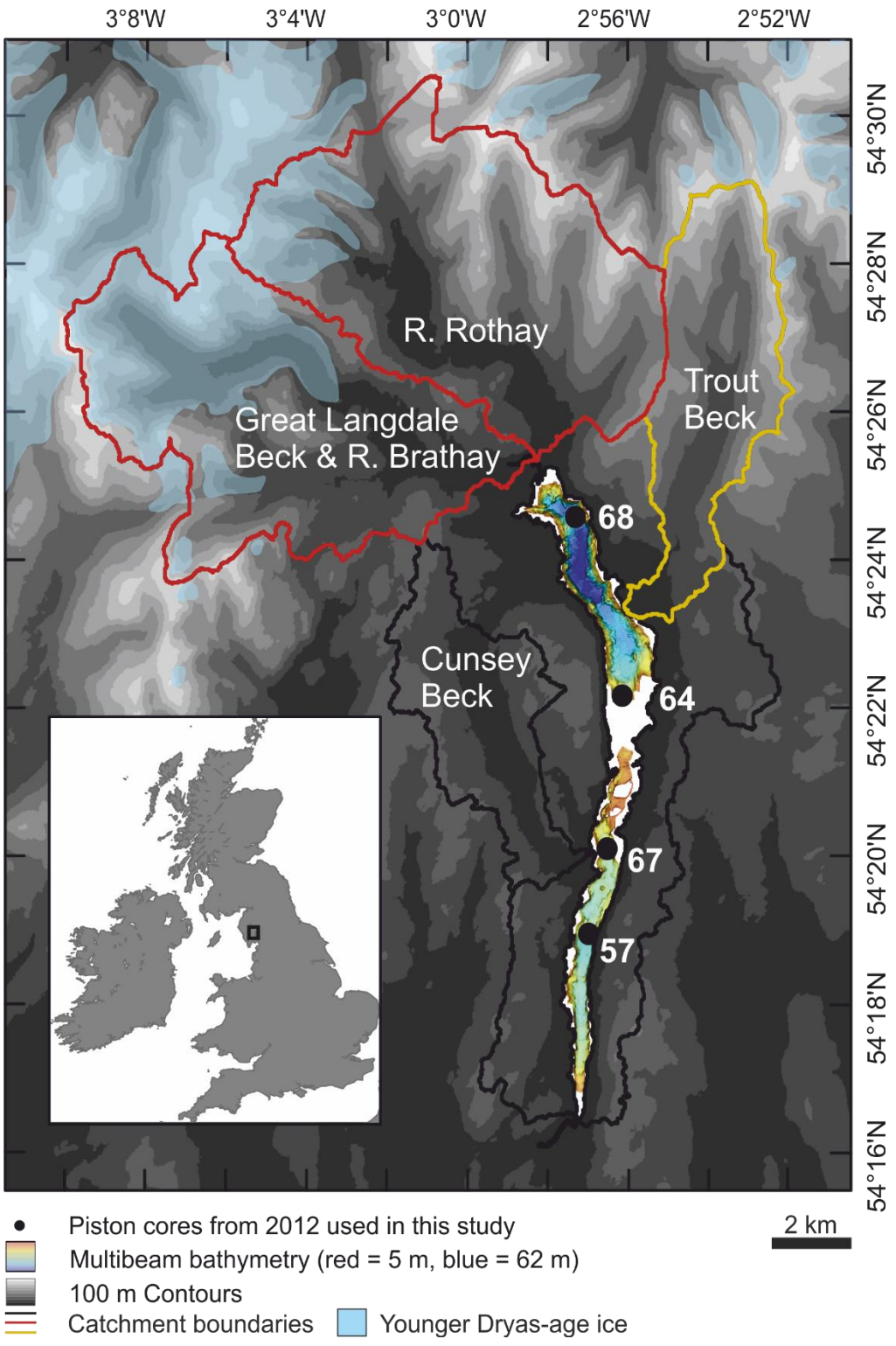

Figure 5.1: Map of the study area. The lake catchment of Windermere is shown in bold outlines (significant sub-catchments are shown in red and yellow). Significant fluvial inputs to the lake are named in the catchments. One hundred metre contours are shown as a greyscale colourmap. The locations of Cores 57, 67, 64, and 68 are shown as filled black circles. Multibeam lake bathymetry is shown as a rainbow colour palette, where dark blue is deepest and red is shallowest. Ice presence during the Younger Dryas is shown in semi-transparent pale blue, after (Brown, 2009; McDougall, 2001; Sissons, 1980; Wilson, 2004; Wilson and Clark, 1998) Inset: The location of the study site (black rectangle) in the British Isles (grey).

5.4 Methods

5.4.1 Sediment coring

Sediment depocentres in Windermere suitable for piston coring were identified using a suite of multibeam bathymetry, chirp, parametric, and multi-channel boomer seismic reflection surveys (Lowag et al., 2012; Miller et al., 2013; Vardy et al., 2010). A subsequent coring campaign in 2012 by the British Geological Survey (BGS) and the University of Southampton facilitated the collection of several sediment cores using both a Uwitec piston corer and Uwitec gravity corer (Miller, 2014). Piston cores were recovered in consecutive 2 m sections in 9 cm diameter liners. These sections were then cut into 1 m units and split lengthways to form working and archive halves. The four cores which had the highest deposition rates and which covered the longest time intervals were selected for this detailed study. The core lengths and water depths for the four cores is given in Table 5.4, and basic core description is given in the supplementary information (5.12).

5.4.2 Core sampling

The centre of each working half was subsampled using both u-channels (a ~1.8 × 1.9 cm^2 cross-section down the length of the core section) and slab-cutters (1 x 1 x 25 cm for main slabs, and 1 x 1 x 5 cm for overlaps). The U-channels were used for palaeomagnetic and Itrax ED-XRF analysis. The slabs were photographed and X-radiographed, then further subsampled. Two sets of thin sections were produced from the slabs by sectioning 1 x 1 x [slab length] cm sediment blocks embedded in a 4-part epoxy resin (Kemp et al., 1998; Pike and Kemp, 1996): covered thin sections (CTS) for optical microscopy, and polished thin sections (PTS) for scanning electron microscopy.

5.4.3 Core Imaging

The archive halves of the split cores were imaged using a GeotekTM MSCL-CIS (CIS) in BOSCORF. Sampled sediment slabs and CTS were photographed Nikon D700 DSLR camera, then X-radiographed using a Hewlett Packard Faxitron X-radiography cabinet at 56 kV for 120 s. Polished thin sections were imaged using a LEO 1450VP Scanning Electron Microscope (SEM) at 100 x magnification, where in greyscale lighter colours correspond with higher atomic numbers. In order to ascertain certain mineral compositions of parts of the sediment, energy-dispersive X-ray spectroscopy (EDS) maps were produced

using the EDS detector on the SEM and AzTec Energy software at the University of Southampton at 2500 x magnification. Mineral phases were identified for each map. An additional X-ray diffraction analysis was performed on a sample of mm-scale laminated sediments from Core 68 to identify mineral components.

5.4.4 Varve counts and thickness

Certain sections of the sediment (see Figure 5.4) contained mm-scale laminated couplets defined as varves.

5.4.4.1 Measurement

Optical micrographs were stacked alongside backscatter images and X-radiographs in order to identify continuously varved core sections. Varves were identified by the presence of a clay cap overlying a coarser component in a regular sequence of clastic laminated couplets (e.g. Francus et al., 2008; Larsen et al., 2011; Menounos and Clague, 2008). Within the coarser component of the varves, parallel silt bands were defined as sublaminae. The algorithm of Francus et al. (2002) was used to semi-automatically measure the mean thickness of each varve along three parallel vertical lines for each slide in the study, and from this a varve thickness time series was created. Any varves which were tilted from horizontal were measured in the same way, and then the true thickness calculated trigonometrically. Varves were counted by two independent researchers, and the uncertainty given as the discrepancy between the two counts. Error is given as the absolute uncertainty as a percentage of the final count (count 1).

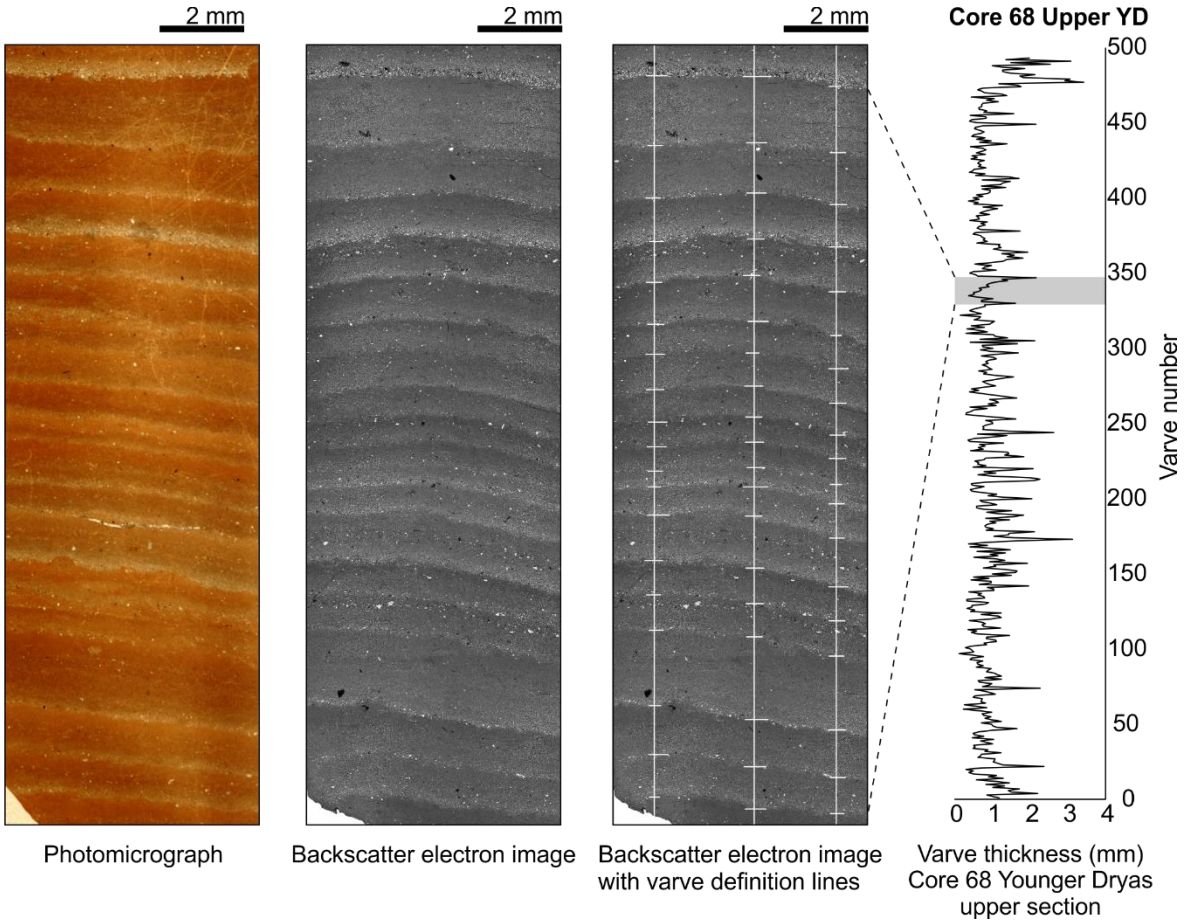

Figure 5.2: From left: Photomicrograph and BSEI showing an example of varved sediment; BSEI of varved sediment showing varve definition lines; varve thickness time series where sediment shown is indicated by a grey bar.

5.4.4.2 Bioturbation indices

Although there is no large-scale bioturbation or lakebed disturbance, it is common for laminae to be bioturbated on the micro-scale. In order to try and quantify the bioturbation levels in the varve sequences, bioturbation indices were created, with varves being assigned numbers from 1 (least bioturbated) to 4 (most bioturbated). The lowest level of bioturbation (1) is characterised by very small irregularities in the varve's lower contact. The second level of bioturbation (2) is characterised by some pelletisation and/or greater irregularity in the lower varve contact. The third bioturbation level (3) has higher levels of pelletisation, and/or heavily undulating varve bases, and/or is faint and discontinuous. In addition, the differentiation between the clay and silt components of the varve may be less clear. The fourth level of bioturbation (4) is characterised by complete or almost complete homogenisation of the varve or group of varves. Even with the highest level of bioturbation, very faint or discontinuous laminae may be visible but not necessarily definable as a varve.

In Core 64, bioturbation was measured as varve presence/absence. Both indices are shown smoothed in Figure 5.4, and the unsmoothed index for Core 68 is shown in Figure 5.7d.

5.5 Overall Core Stratigraphy and Age Model

5.5.1 Primary Sediment Sequence

The four cores all exhibit similar major lithological units: an inorganic mineral-rich base overlain by a dark organic rich unit. The radiocarbon-derived age model (see Chapters 2 and 3) indicates that the dark organic-rich unit is of Holocene age. The underlying unit is interpreted as sedimentation since the British and Irish Ice Sheet (BIIS) retreated up the Windermere lake valley after the Last Glacial Maximum (LGM) (see Chapter 4).

The bases of the cores are from before the Lateglacial Interstadial and are described in Chapter 4. In all cores, the organic silty clay unit representing the Lateglacial Interstadial (as discussed in Chapter 4) is succeeded by a unit of mm-scale laminated silt and clay couplets, which is the unit in this study.

In Core 68, the mm-scale laminations occur directly above the organic-rich, Interstadial-type non-laminated sediment and occur throughout the whole unit until a gradational transition into the intermittently laminated Holocene unit above. In Core 64, the mm-scale couplets begin to occur as intermittent laminations that transition into regular couplets. The mm-scale laminated unit is truncated at the top by erosion and small (< 10 cm) mass transport deposits (MTDs) of Holocene- age sediment. The lowest radiocarbon date in Core 64 has a median probability age of ~11500 cal yr BP, and the lowest Holocene sediment is also similar to that of the very early Holocene as seen in Cores 67 and 68, indicating that the erosion of the latter Younger Dryas-age sediments must have occurred in the very earliest Holocene.

SEM EDS analysis of the mm-scale laminated unit shows the primary silt mineralogy to be quartz and volcanic rock fragments, with small amounts of fluorapatite, rutile, and other oxides (e.g. MgO, Al_2O_3, Fe_2O_3), all likely sourced from the Borrowdale Volcanic Group (Figure 5.3). XRD analysis indicates the presence of both illite and chlorite in the clay layers. Supplementary Figure 5.9 and Supplementary Figure 5.10 show elemental variations Downcore using Itrax WD-XRF.

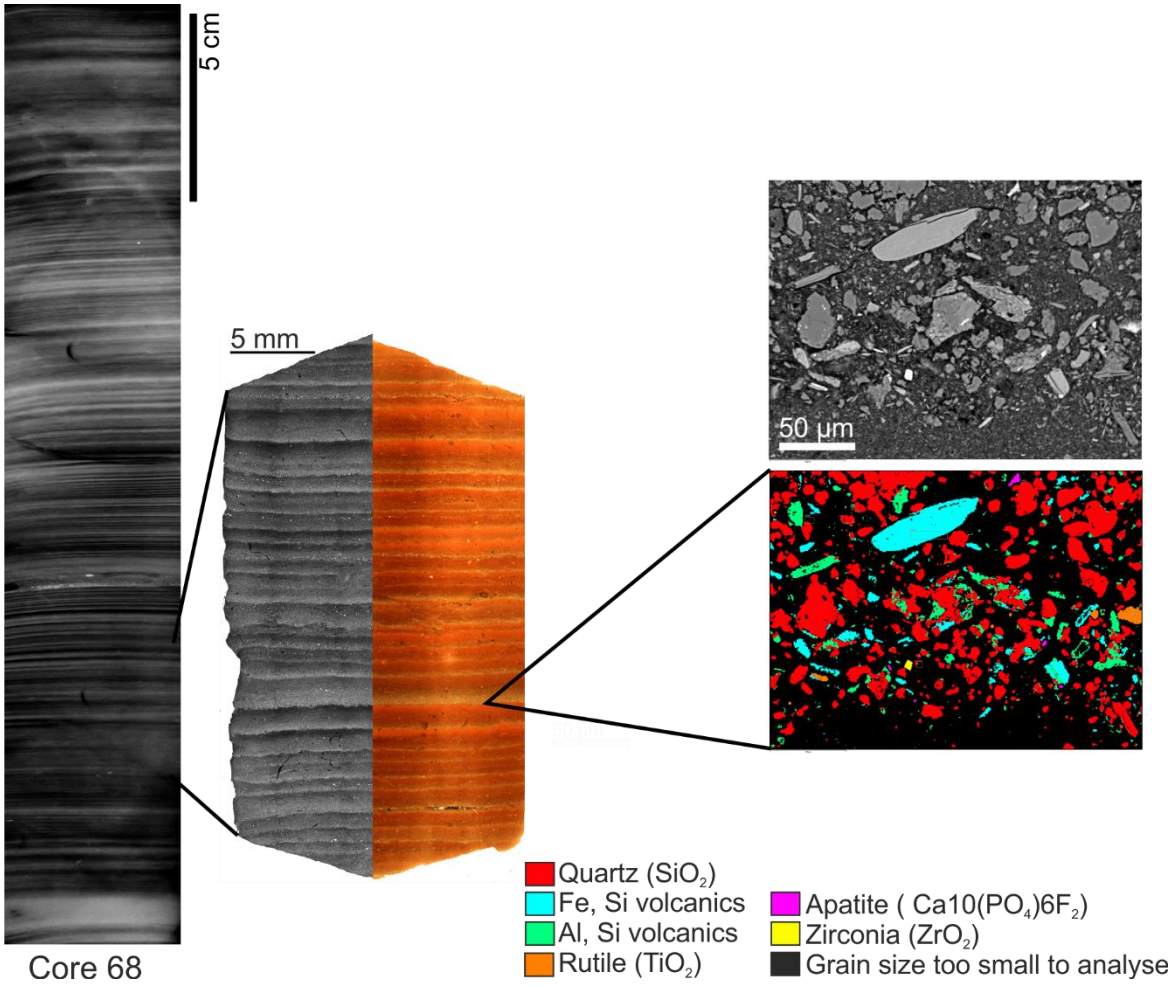

Figure 5.3: Mineral phases in the coarse layer of a mm-scale lamina in Core 68. Left: X-radiograph. Centre: Backscatter electron image and covered thin section image of the source slides. Right: Backscatter electron image (top) and EDS phase map (bottom) showing constituent minerals in the sediment at the base of a couplet.

5.5.2 Age model of sediment sequence

An age model for the organic-rich dark brown sediments was created through the use of a ^{137}Cs-validated ^{210}Pb-decay-based age model at the core tops, and through radiocarbon dating for the remainder of the unit (Avery et al., 2017; Fielding, 2017). The base of this dark brown unit was ascertained to be of earliest Holocene age, and thus the mm-laminated silt and clay unit directly below was inferred to be of Younger Dryas (~ Loch Lomond Stadial, Greenland Stadial 1) age. This inference was supported by further radiocarbon dates from the more organic unit directly below, which confirmed it to be of Lateglacial Interstadial (~Windermere Interstadial, Greenland Interstadial 1, Bølling-Allerød) age. A tephra search, intended to strengthen the inference of the mm-scale laminated unit being of YD age did not yield any results. However, the nature of the sediment did strengthen the inference: the Lateglacial Interstadial and Holocene are both known to have been warmer, wetter, and

more hospitable than the Younger Dryas. Furthermore, pollen searches in the current project and in previous studies have yielded herbaceous and arboreal pollens in these stratigraphic units but little to no pollen in the YD unit (Coope and Pennington, 1977; Fielding, 2017; Pennington, 1947; Scaife, R, pers. comm. 2018).

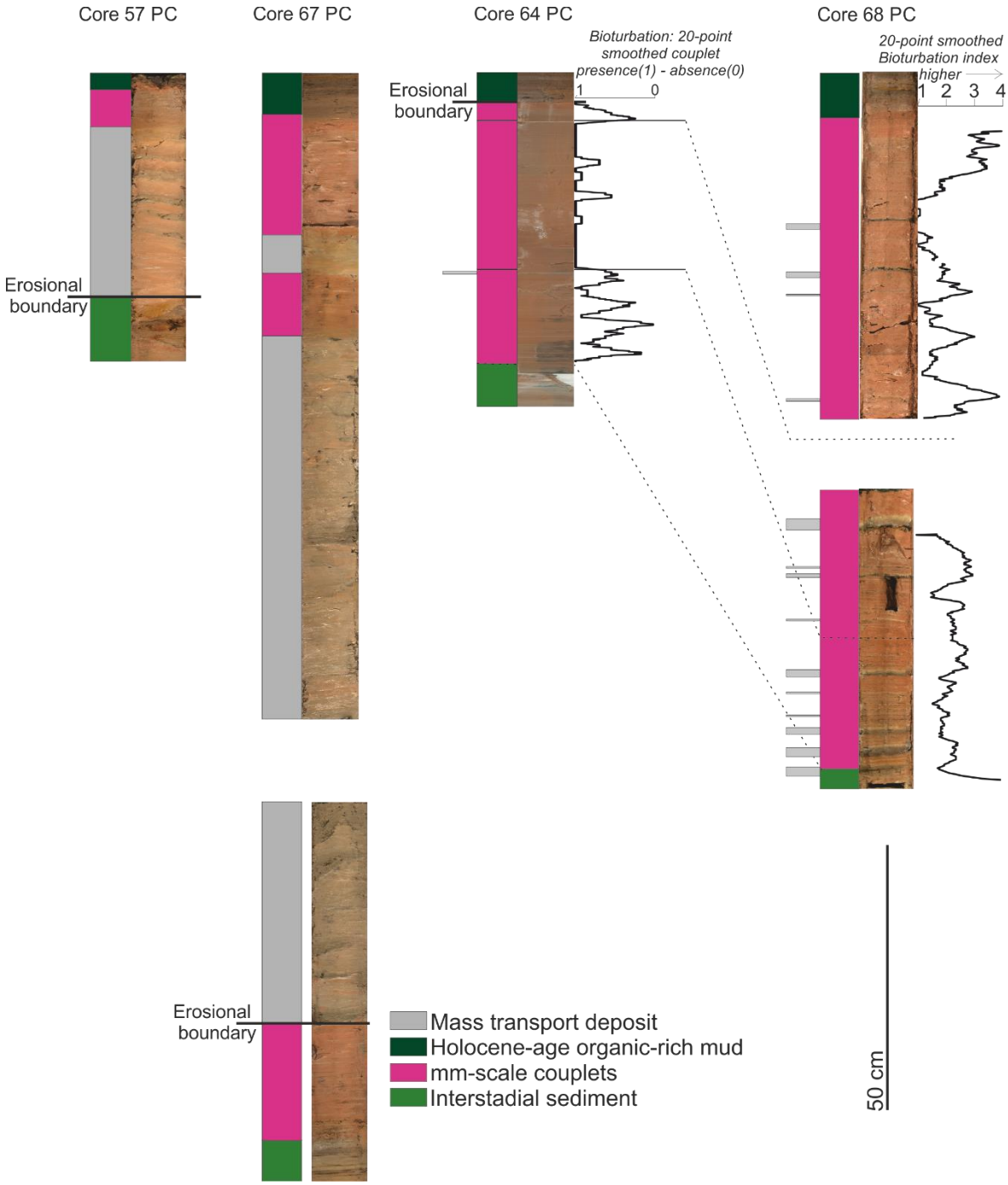

Figure 5.4: Logs of YD-age sediment for the four cores (for stratigraphic figures of the entire core sequences, see Figure 2.2). For each core, the colour code and split-score photograph from Figure 2 is shown. Major erosional boundaries are marked as horizontal black lines. Multi-mm – cm-scale graded beds are shown as grey boxes on the left. For Cores 64 and 68, bioturbation levels are shown. For Core 68 there is a 20-point smoothed bioturbation index with four levels, where left is minimal bioturbation and right is heavy bioturbation, and for Core 64, the index has two levels (mm-lamina presence/absence).

5.5.3 Interruptions to sediment sequence

5.5.3.1 Mass Transport Deposits

In Core 67, most of the YD-age interval comprises a 1.43 m-thick MTD, the base of which occurs in a suite of intermittent pre-varve laminae in the Interstadial-Younger Dryas transition. Only 10 cm of mm-scale laminae are present directly beneath the Holocene. The lower half (44 cm) of the MTD, found below 4 m, shows some quasi-horizontal structure on the decimetre scale (as seen in X-radiograph, Supplementary Figure 5.13a). The upper half, above the core gap, is more complex, containing a whorl and large (up to 2.5 mm) disaggregated mud clasts. Overlying this segment is a series of mm-scale varves (~8 cm) which appear to sit conformably above the MTD sediment. However, the varved unit is overlain by <10 cm of MTD material, above which normal sedimentation resumes. It is not clear whether the ~8 cm of mm-scale varves represents normal sedimentation which is then overlain by a second <10 cm MTD, or whether the varve unit actually represents a small cohesive block within a single MTD.

In Core 57, the Interstadial sediment is interrupted by an MTD comprising cohesive cm-scale beds, and is overlain by <10 cm mm-scale laminations before being erosively truncated by Holocene sediment. In BSEI, it can be seen that the sediment fabric of the cm-scale beds is pervasively disturbed by microfaulting and the clay caps are heavily veined (Supplementary Figure 5.12c, d).

With the occurrence of large MTDs in the South Basin cores, the focus of this study is on the North Basin cores (Cores 64 and 68).

5.5.3.2 Graded Beds

The mm-scale laminated sequences of silt-clay couplets (in particular Core 68) contain several graded beds, distinguished from the 'normal sedimentation' couplets by their greater thickness (typically 0.4 – 2 cm) and generally coarser basal grain size (coarse silt to fine sand) (See Figure 5.4 for stratigraphic locations, and Supplementary Figure 5.11 for detailed images). Several of these graded beds also contain internal structure, with laminations of finer and coarser grains present. The bases of the graded beds are largely very fine sand and very coarse silt, interspersed with some coarse and medium silt, and many appear possibly erosive. The graded bed bases often contain some organic fragments similar in size to the clastic grains.

5.5.3.3 *Soft Sediment Deformation*

A section of mm-scale laminated sediment in Core 68 is also deformed, preventing inclusion of these laminations into the recorded sequence. The base of the deformation consists of a series of detachments where the laminae become increasingly folded up-core with the axis of the fold migrating (to the right, in the frame of the X-radiograph). The fold is overlain by another detachment then a graded bed. Above the graded bed there are more mm-scale varves including a fully sheared fold, and several more folds and detachments. Detailed figures of MTDs, graded beds, and deformation may be found in the Supplementary Information (5.12.3).

5.6 Sediment facies

The Windermere laminated sediment sequences have been broken down into several microfacies, which are characterised in the section below. In addition to the regularly-laminated sediment, the characteristics of intermittently laminated sediments transitional to the Holocene are also described.

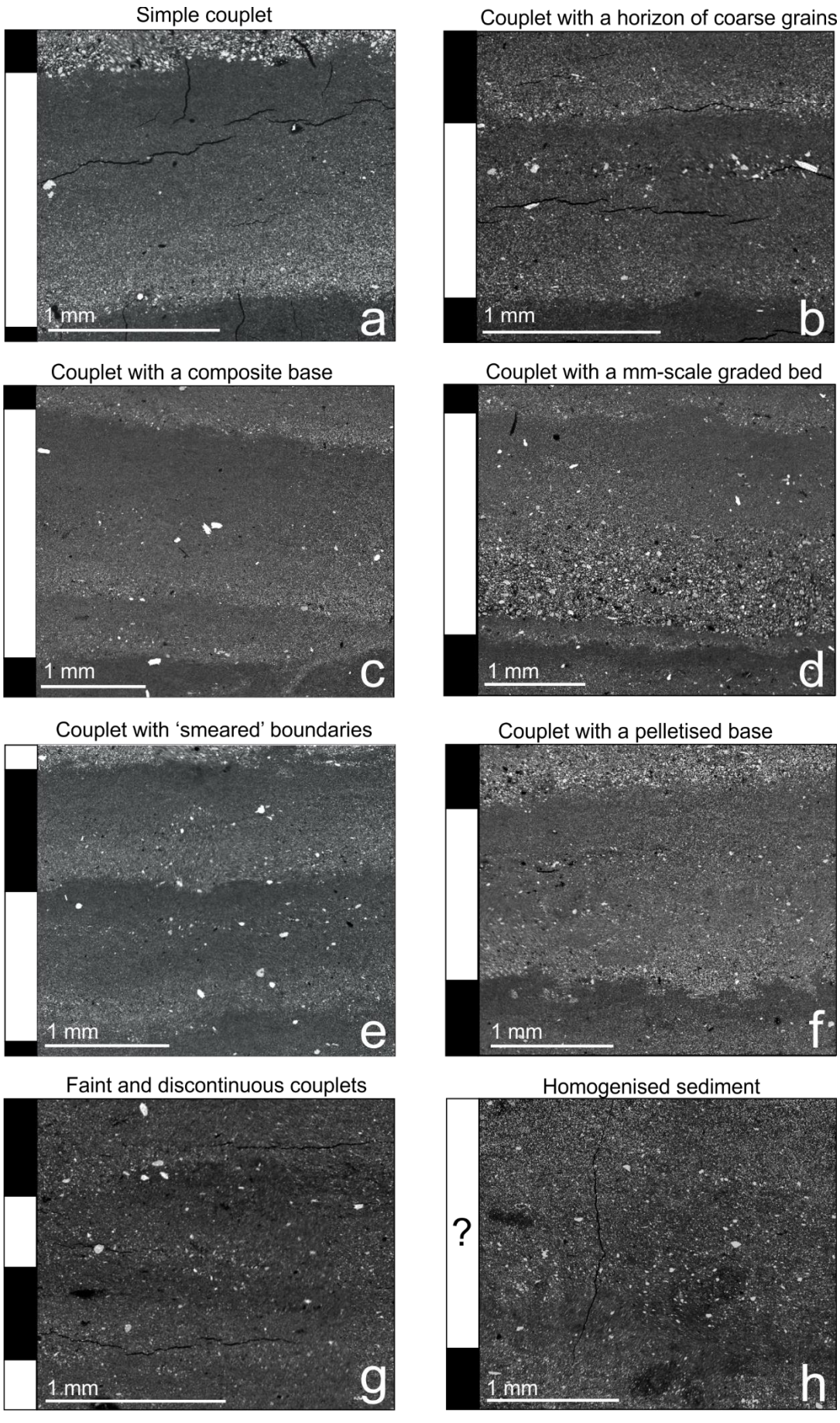
Simple couplet
1 mm
a
Couplet with a horizon of coarse grains
1 mm
b
Couplet with a composite base
1 mm
c
Couplet with a mm-scale graded bed
1 mm
d
Couplet with 'smeared' boundaries
1 mm
e
Couplet with a pelletised base
1 mm
f
Faint and discontinuous couplets
1 mm
g
Homogenised sediment
?
1 mm
h

Figure 5.5: Examples of different lamina types found in the sediments. The 'simple' alternating lamina in the top left is the basic facies upon which variations are imposed by differing sedimentation conditions and/or bioturbation.

5.6.1 Simple clay-silt couplets

Simple clay-silt couplets are typically clearly defined, with a medium or coarse silt base overlain by, or fining into, a distinct clay cap (Figure 5.5a; further examples in Supplementary Figure 5.15d-3 and Supplementary Figure 5.16d-5). Disturbance to the horizontal laminar structure of the couplet is minimal, the couplet bases having generally sharp lower contacts that may display a slight undulation. Small (max. coarse silt-sized) organic fragments or single isolated coarse silt clasts may be present within the sediment.

In Core 68 this facies occurs primarily in the middle and upper part of the laminated sequence, above 6 m core depth. In Core 64, this facies is uncommon and only really occurs between 2.47 and 2.5 m.

5.6.2 Complex clay-silt couplets

Many couplets exhibit the presence of isolated or discrete coarse and very coarse silt grains at the top of the silt component or within the clay, often forming a single-grain horizon (Figure 5.5b; further examples in Supplementary Figure 5.15c-3 and c-7, and Supplementary Figure 5.16c-2).

Less commonly, the coarse couplet component may be made up of more than one distinct sublamina, with each sublamina defined by a coarser base and finer top (Figure 5.5c; a further example is in Supplementary Figure 5.15d-4). Some couplets exhibit a sublamina that is distinctly coarser and often thicker than the couplet base and may incorporate more organic fragments than a usual couplet (Figure 5.5d). The base of this sublamina may be found in the silt or the clay component of the couplet.

5.6.3 Disturbed clay-silt couplets

Many silt-clay couplets exhibit some disturbance to their horizontal laminar structure. There is significant variation in the level of disturbance and hence lamina definition within the facies. The boundary between the silt component and the clay cap is often undulating and smeared (Figure 5.5e). The laminae in this facies have generally distinct lower contacts, but they may be irregular, showing some pelletisation and sediment entrainment into the

clay layer directly below (Figure 5.5f). Some of this irregularity to the base of the silt layer has the appearance of small loading features. Further examples of disturbed couplets may be found in Supplementary Figure 5.16d-2 and Supplementary Figure 5.17.

This facies is found in Core 68 throughout the mm-laminated sequence, but especially below 6 m depth and towards the top of the YD sediments some 9 cm before the transition to the Holocene. In Core 64 this facies is also found throughout the sequence, often in packages of 5 – 7 couplets.

5.6.4 Indistinct and homogenised clay-silt couplets

The level of disturbance in some couplets is great enough that the contacts between the silt and clay are discontinuous and the couplets appear faint in either or both of backscatter and micrograph images (Figure 5.5g; further examples in Supplementary Figure 5.18). There is considerable evidence for redistribution of sediment across boundaries. This level of disturbance makes couplet definition more difficult, but a combination of BSEI and optical microscopy, and use of varying image contrast, was generally successful.

Laminae of this type are found throughout the Core 64 YD sediments, usually in packages alternating with couplets that are more distinct. In Core 68 the facies is also found throughout the sequence, but more commonly below 6 m core depth and in the top 9 cm of the laminated sequence.

Found almost entirely in Core 64, some couplets are disturbed to the extent that laminae cannot be reliably identified (Figure 5.5h; further examples in Supplementary Figure 5.19). Although some remnants of lamina boundaries may be observed, there is insufficient lateral or vertical continuity for confident lamina definition. The thickness of these units are similar to the thicknesses of the other types of lamina packages, being around 5-7- couplet thickness equivalents (~2 – 10 mm).

5.6.5 Intermittent fossil-bearing laminae

At the very end of the YD, directly after the cessation of mm-scale laminated sediment, there occur intermittent fossil-bearing laminae (present in Cores 68 and 67 only, as the end-Holocene is truncated in the other cores). The sediments contain many different microfossils, including small numbers of the diatom *Ellerbeckia* sp, testate amoebae, coleoptera, and chironomids (Fielding, 2017). An example may be found in Supplementary

Figure 5.20, esp. a) and e). Similar sediments also occur directly below the YD sediment, and are particularly prevalent in Core 68.

5.7 Interpretation of sediment facies

5.7.1 Simple clay-silt couplets

The simple silt-clay couplets are interpreted to be millimetre-scale varves derived from a snowmelt-controlled regime. The interpretation of varves is supported by the structure of the couplets- a medium or coarse silt base overlain by, or fining into, a distinct clay cap- which is a widely-documented form of annual lamination known as a clastic varve, formed from weathered minerogenic sediment (see Zolitschka, 2007; Zolitschka et al., 2015; Section 1.2 for summary; see Appendix D for examples). The regularity of occurrence of the mm-scale silt-clay couplets also supports the interpretation of varves, as does the overall number, which is approximately consistent with the number of years in the Younger Dryas (when conditions would have promoted clastic varve formation).

The interpretation of a snowmelt-controlled sedimentation regime for these varves is given despite the presence of a small amount of upland ice in the catchment (Figure 5.1) (Brown et al., 2013; McDougall, 2013, 2001). The thickness (i.e. mm-scale) of the varves is in keeping with those in other snowmelt-dominated lake regimes (Francus et al., 2008; Hambley and Lamoureux, 2006; Kaufman et al., 2011; Zolitschka, 1996). The interpretation of nival origin is also supported by the simplicity of the varves, with the lack of a thick compound secondary layer (with sublaminae) which is characteristic of proglacial varves (e.g. Chutko and Lamoureux, 2008; Menounos and Clague, 2008; Ridge et al., 2012)

Grain size samples exhibit a wide range of silt grades (Figure 5.6; Table 5.1). The consistent presence of coarse silt (evidencing traction) suggests sediment lake entry by underflows (Gammon et al., 2017; Hodder et al., 2007; Lewis et al., 2005), followed by settling of clay by flocculation (Hodder, 2009; Hodder and Gilbert, 2007). In many cases a large proportion of the sediment is discharged within the early part of the melt season over a period of several days during peak snowmelt (Cockburn and Lamoureux, 2008; Cuven et al., 2011; Hardy, 1996; Lewis et al., 2005; Menounos and Clague, 2008). Spring floods (high-intensity water discharges) sometimes contribute almost all of the year's sediment input (Hardy, 1996; Leemann and Niessen, 1994; Lewis et al., 2012; Zolitschka, 1996). The presence of coarse

and very coarse silt in the Core 67 sample indicates that the South Basin was receiving sediment from a proximal source rather than from the North Basin only.

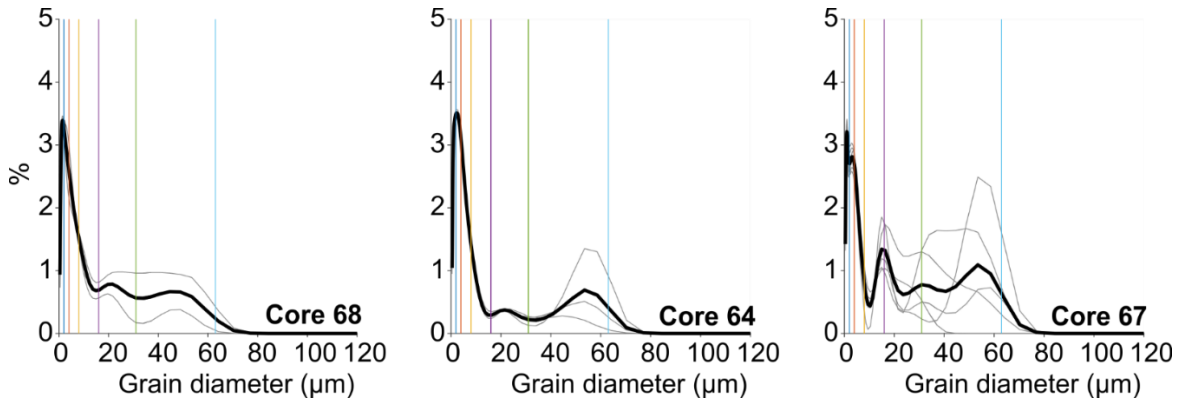

Figure 5.6: Grain size for YD-age samples from (left) Core 68, (centre) Core 64, and (right) Core 67. Thin grey lines are the individual measurement runs, and the thicker black line shows the mean for the runs. Vertical lines are the lower grain size boundaries as follows: Blue- Very fine silt (2 – 4 μm); Orange- Fine silt (4 – 8 μm); Yellow- Medium silt (8 – 16 μm); Purple- Coarse silt (16 – 31 μm); Green- Very coarse silt (31-63 μm); Blue2- Very fine sand (63 – 125 μm).

Core	Median grain size(s) (μm) for each run	Mode(s) (μm) of mean of runs
Core 68	2.326, 2.603	1.535 (Clay), 21.52 (Coarse (C) silt), 44.6 (Very coarse (VC) silt)
Core 64	2.454, 2.377, 2.268	2.21 (VF silt), 21.52 (C silt), 53.5 (VC silt)
Core 67	2.558, 2.23, 2.199, 2.639, 2.485	0.974 (Clay), 3.181 (Very fine (VF) silt), 14.95 (Medium (M) silt, 32 (C silt), 53.5 (VC silt)

Table 5.1: Basic grain size distribution statistics for the different sediment types.

Grain size	Sediment delivery style (after Gammon et al., 2017)
Clay	Suspended load (low-density flocs)
Fine and very fine silt	Suspended load (suspended via turbulence)

Medium silt	Suspended bedload sortable silt (suspended via turbulence)
Coarse silt	Suspended bedload or bedload (turbulent suspension vs saltation boundary)
Very coarse silt	Bedload (likely saltation)
Very fine sand	Bedload via traction (perhaps rolling)
Fine sand	Bedload via traction (perhaps sliding)

Table 5.2: Depositional processes for different grain sizes, after Gammon et al., (2017)

5.7.2 Compound clay-silt couplets

The discrete grains in the coarse clast horizons are usually between 40 and 80 μm. The size and context of these grains are similar to those described by Francus et al., (2008), which were interpreted to have been transported onto the frozen lake surface via aeolian means, and which have settled to the lake bed later in the ice-free months. Varves which have these coarse clast horizons may be indicative of reduced snow cover over the sediment source area, promoting increased erosion.

The coarse varve bases which contain more than one sublamina, which occur occasionally in the YD varves, we interpret as multiple discrete snowmelt events (Chutko and Lamoureux, 2008; Hambley and Lamoureux, 2006; Kaufman et al., 2011; Zolitschka, 1996) or possibly a nival melt component and a secondary glacial melt component.

The sublaminae which are significantly coarser and sometimes thicker than the varve base are thought to be micro-graded beds, formed either from late-season pluvial events causing sedimentation from high-energy meltwater or slope instability, or possibly from small-scale or distal subaqueous slumping.

5.7.3 Disturbed, indistinct, and homogenised clay-silt couplets

The disturbances in varve structure present in both the Core 68 and Core 64 sequences, are interpreted to have arisen from bioturbation, i.e. from activity of lake- or sediment-dwelling organisms. The pelletisation of small sediment packages, and the entrainment of such packages into adjacent laminae, is thought to be the result of burrowing organisms or copepods depositing faecal pellets in the sediment (Smith and Syvitski, 1982).

The level of bioturbation ranges from minor disturbance to complete varve homogenisation. Low bioturbation could be indicative of colder conditions less hospitable to micro-organisms, or a less oxygenated lakebed environment due to increased stratification. The lower bioturbation levels in Core 68 are mostly due to the greater water depth of the core site, and thus lower oxygenation levels. In Core 64, the earlier and latest parts of the sequence are more bioturbated and homogenised, to the point that many sections exist where varves are undefinable (Figure 5.7a). This is likely due to the shallower water depth of the location of Core 64, which would have been more sensitive to lake level fluctuations but also would have had a better ventilated lakebed environment and greater light penetration (Cook et al., 2009; Zolitschka, 2007, 1996).

5.7.4 Graded beds

The grading and internal structure with parallel lamination and the coarser grain sizes than the varve silt components are all consistent with a turbidity current origin. Turbidity currents in lakes are typically generated by extreme river discharge as a hyperpycnal flow, or slope failures through direct slope destabilisation through loading (Lewis et al., 2010; Zolitschka, 1996). The texture and thickness of the Windermere graded beds closely resemble lake turbidites originating from extreme flood events documented in Lillooet Lake, British Columbia (Figure 5 in Gilbert et al., 2006). Such layers may form from late-season rainfall events causing increased runoff in autumn, (Desloges and Gilbert, 1994; Menounos and Clague, 2008). Most graded beds appear in Core 68 with only one present in Core 64, consistent with the location of Core 68 being closer to the larger, more complex catchment (Figure 5.1)

5.7.5 Intermittent fossil-bearing laminae

The sediments directly above and below the YD-aged sediment unit are determined (both stratigraphically and using radiocarbon dating) to be from the earliest Holocene and the late Lateglacial Interstadial respectively. These climatic periods are associated with a warmer and wetter climate than the YD, and also with increased vegetation levels (Coope and Pennington, 1977; Fielding, 2017; Pennington, 1947). The lack of varve structure is likely a consequence of less sediment availability due to vegetation, increased lake biota precluding varve formation and preservation conditions, and more temperature-related water column effects (e.g higher oxygen levels, more lake overturn events).

5.8 Varve sequences and correlation

The YD varves of Core 68 are split into two sections separated by an 11.5 cm core gap (due to the core catcher). The deformed varves at the top ~11 cm of section G are also not counted due to the presence of sediment detachments and faults, such that the varves cannot be guaranteed to be in situ (see section 5.12.3.3). The exact number of varves in this gap is unknown, but an estimate using the mean of the thicknesses of the ten measurable varves either side of the gap (1.01 mm) gives a potential varve gap of 227 varves. When correlated with the Core 64 record using two tiepoints, the varve gap in 68 consists of 231 varves. This appears consistent, given that the number of measurable YD varves in Core 68 is currently 887 (+7), and the length of the Younger Dryas is ~1100 - 1200 yr. The resulting sequence is shown in Figure 5.7c. The tie-points were chosen by wiggle-match, with the knowledge that the beginning of the Core 64sequence transitions continuously from the Interstadial but the end is truncated by an erosive contact. This indicates that approximately 480 varves have been removed by erosion in the Younger Dryas-age sediments of Core 64.

The total number of defined varves in the Core 64 YD sequence is 688 (+3-11). The varve thickness sequences are shown in Figure 5.7. Counting details are given in Supplementary Section 5.12.5.

Core	Core 64	Core 68
Count	688	887 (not including gap of 231)
Uncertainty	+3-11	+7
% Error	2.03	0.79

Table 5.3: Varve counts and uncertainties for Cores 64 and 68.

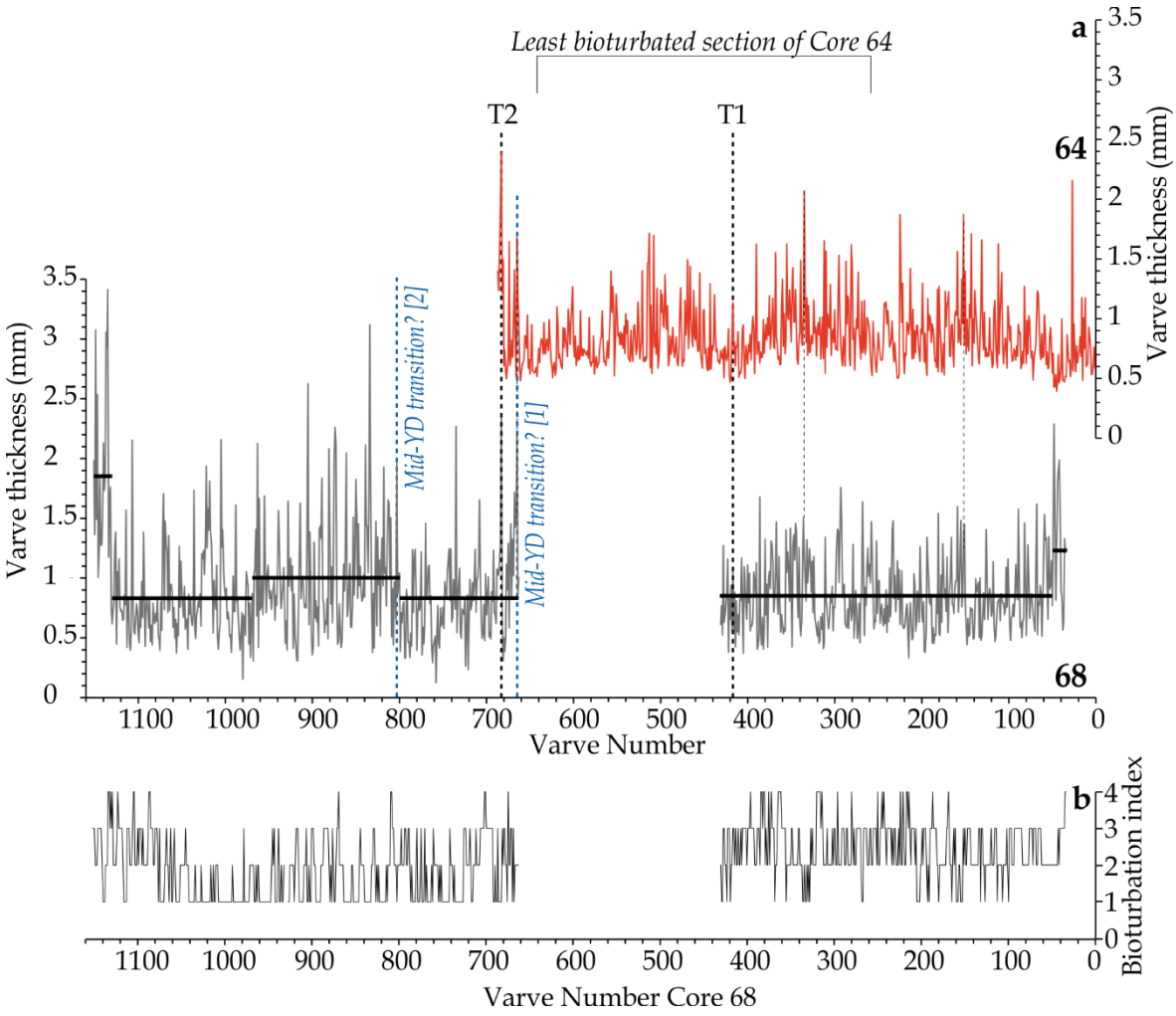

Figure 5.7: a) Varve thickness for the mm-scale Younger Dryas-age varves. Higher varve numbers are more recent and stratigraphically higher. Core 64 = red, Core 68 = black. Two tiepoints between the records, T1 and T2, are shown, and faint dashed lines indicate examples of resultant ties. Mean thicknesses for selected sections of Core 68 are shown as thick black horizontal lines. Possible locations for the mid-Younger Dryas Transition is shown as a dashed blue line. b) Bioturbation (or varve clarity) index for Core 68, where 4 is the most bioturbated, and 1 is the least.

5.9 Environment of Windermere in the Younger Dryas in a North Atlantic regional context

The varve chronology that results from this correlation is floating, since no tephra was found. However, we are still able to demonstrate the potential of Windermere to produce a varve chronology, and we also endeavour to interpret the changes in the nature of the varves in the context of regional climate change during the YD. Our varve thickness record cannot be directly compared with that of the Lochaber Master Varve Chronology (the

existing Younger Dryas-age UK varve chronology; (Palmer et al., 2010)), since the mechanisms controlling varve thickness are different (Windermere: snowmelt, precipitation; LMVC: ice dynamics, lake level).

5.9.1 Early Younger Dryas

The onset of the Younger Dryas was accompanied by a rapid sea-ice expansion southwards, to 52° north (Brauer et al., 2008; Isarin et al., 1998). This caused the Atlantic winter storm track (which in the modern day skirts round the northern edge of the British Isles (Bader et al., 2011) to move south, such that it crossed the body of the British Isles and continental Europe (Renssen et al., 1996). Unlike in the modern day, where westerlies carry warm, moist air, the storms of the Younger Dryas transported cold (-30 - -35 °C) dry air sourced from above the sea ice which was inhibiting marine evaporation. This resulted in regionally increased aridity and continentality, as well as temperatures 6 – 10 °C lower in summer and up to 30 °C lower in winter than present (Isarin et al., 1998). At the same time, the upland areas of Britain reglaciated most extensively in the Highlands of Scotland where an ice cap developed in the "Loch Lomond Readvance" (Golledge, 2010). Smaller ice masses formed in other upland areas (Barr et al., 2017; Carr, 2001; Hughes, 2009; Mitchell, 1996), and in the Lake District, cirque glaciers were accompanied by plateau icefields up to 55 km^2 (McDougall, 2013, 2001). There was likely some ice present in the Windermere catchment (Figure 5.1), but relatively thin in relation to the pre-Interstadial Lake District ice cap (Brown, 2009; McDougall, 2013, 2001; Sissons, 1980; Wilson, 2004; Wilson and Clark, 1998). Strong winds coupled with sparse vegetation in the British Isles (open ground and tundra in Northwest England) likely precluded formation of thick snowpack (Isarin et al., 1998; Jones et al., 2002).

In Meerfelder Maar varves, the early YD diatom laminae are interpreted to have formed in response to strong wind-driven upwelling, while increased autumn/winter storminess is indicated by the onset of detrital organic matter, siliciclastics, and reworked shallow water material in the "winter" lamina (Brauer et al., 2008; Lane et al., 2013). Elevated storminess is consistent with the relatively high levels of bioturbation in Windermere as wind-mixing in the lake would have disrupted stratification, increased ventilation and inhibited lamina preservation especially in the shallower Core 64 (25.6 m water depth), where there are several non-varved intervals. The rapid decrease in varve thickness at the beginning of the YD in Core 68 may have been caused by a swift decrease in precipitation across Europe as sea ice rapidly expanded (Brauer et al., 2008). Other aspects of the Windermere record are

also consistent with increased storminess. The regular presence of turbidites in the lower half of Core 68 is evidence of repeated occurrence of extreme rainfall events.

The many varves that contain isolated coarse and very coarse silt grains with a likely aeolian source (Cuven et al., 2010; Francus et al., 2008) further attest to strong wind activity.

5.9.2 Mid-YD transition

Warming summer temperatures around 12.5 ka brought on the onset of ice retreat from, for example, the Western Highlands ice cap (Ballantyne, 2012). By 12,262 ± 85 cal yr BP the ice cap had fully retreated (Bromley et al., 2014). Glaciers in the Mourne Mountains, Northern Ireland, also retreated well before the end of the YD. Also at 12, 240 $\pm$ 40 varve yr BP in Meerfelder Maar (100 yr prior to the deposition of the Vedde Ash), the varve style changed from 'stormy' to simple clastic snowmelt varves, interpreted to represent a northwards shift of the westerly wind systems (Lane et al., 2013). In the sediments of Kråkenes, coastal Norway, a similar transition (in this case to increased glacial melt flux representing a less stable environment inferred from Ti content) was observed 20 yr after the deposition of the Vedde Ash (Bakke et al., 2009), as storm tracks moved north to Scandinavia (Lane et al., 2013).

The Windermere varves do record a shift from more to less bioturbated overall, but it is far from clear or definitive. One shift may occur immediately at the end of the varve gap in Core 68 (in the last 6 varves of Core 64; see Figure 5.7a, Mid YD transition 1, Varve 683), accompanied by an increase in the number of isolated thicker varves (> 1.5 mm). There is additionally a step-thickening of the varves in Core 68 (after the Core 64 record is lost) at varve 803 (Figure 5.7a, Mid YD Transition 2). The somewhat-reduced bioturbation may be evidence of more permanently-decreased wind speeds and thus less lake mixing, and the increased thickness may be due to increased precipitation as warmer moister air reached the British Isles and the dry, cold storms moved north due to receding sea ice latitudes.

A search for YD-age tephra in the Windermere sediments (such as the Vedde Ash) did not yield results, possibly as a result of the Lake District being towards the southern edge of the Icelandic tephra deposition envelope (Figure 7.2), and/or due to the dispersion of tephra throughout a large and complex catchment. However, the earliest reliable Holocene radiocarbon date from this project has a median probability age of 11750 cal yr BP (for date distributions, see Table 7.1). Counting backwards using varves, we would expect the Vedde Ash to be found ~390 yr prior to the Holocene transition (with the caveats of uncertainty in

the radiocarbon dates and also the lack of radiocarbon dates within the varve sequence). Mid YD Transition 1 occurs at varve 683, approximately 468 varve years before the start of the Holocene sediment, whilst Mid YD Transition 2 occurs at varve 803, approximately 350 varve years before the start of the Holocene sediment (Figure 5.7). Given the 2σ uncertainties of the earliest radiocarbon date (from Core 67: 11750 +253 -341 cal yr BP) however, along with the unknown time between the last varve and the first radiocarbon date, it is not possible to determine which Mid-YD Transition candidate is the correct one, or when this transition was in relation to MFM and Kråkenes. Further work involving the full recovery of a continuously varved sequence from Core 68 site will aid in building the time-transgressive picture of the mid-Younger Dryas.

5.9.3 Late Younger Dryas

The topmost varves in Core 68 return to the bioturbated style, and there is a marked increase in varve thickness (Figure 5.7). The large-scale MTD in Core 67 also occurred in the late YD (since there are few YD-age varves above it), and the same may be true for Core 57 (Figure 5.4). The increased varve thickness in Core 68 may have been caused by either increased (nival) precipitation, melting of any long-term snowpack, or both, as a result of rapidly increasing temperatures towards the onset of the Holocene. The increased bioturbation was probably not wind-driven at this point, but the lake may have warmed to the point that spring and/or autumn overturning occurred. The presence of the large scale MTD occurring in the late YD (as well as possibly the MTD in Core 57, a large-scale MTD in the early Holocene in Core 68 (Avery et al., 2017), and the early Holocene erosive event in Core 64) shows that the catchment at this time was unstable, possibly as a result of changing precipitation and vegetation regimes, and melting of permafrost.

5.10 Comparison with Greenland

The varve thickness record was compared with the NGRIP δ18O record, on the assumption that increased air temperature on Greenland (Masson-Delmotte, 2005; Steffensen et al., 2008) would be associated with a more northerly northern limit of warmer, moister air masses and therefore precipitation in the UK and thicker varves. To do this, a composite thickness record was produced by splicing the time series from Cores 64 and 68. Because the Core 64 sedimentation rate is lower, the varve thicknesses for Core 64 were transformed to have the same mean as the parts of the Core 68 record with which it overlapped. The

composite record was then smoothed using 20 points, since the NGRIP GICC05 record has 20-year resolution.

The results show that on a broad scale (~50 – 100 yr), the two records appear to co-vary after c. varve 650, but not before (Figure 5.8). Other varve data from Scotland also finds some degree of phase locking with Greenland (Palmer et al., 2012). An explanation is that in the modern-day system, surface temperature and winter precipitation in both Greenland and the UK tend to correlate on a large scale(Trenberth and Shea, 2005), but that the vastly increased sea-ice extent in the earlier part of the Younger Dryas decoupled these variables. In the later part of the Younger Dryas, the sea ice extent reduced and a more 'modern-day' atmospheric regime came into being. Due to the uncertainty of the Windermere age model, this comparison is considered speculative and would require the production of a full tephra-validated chronology in order to be properly tested, although if true the 'MID YD Transition 1' is likely to be the correct one.

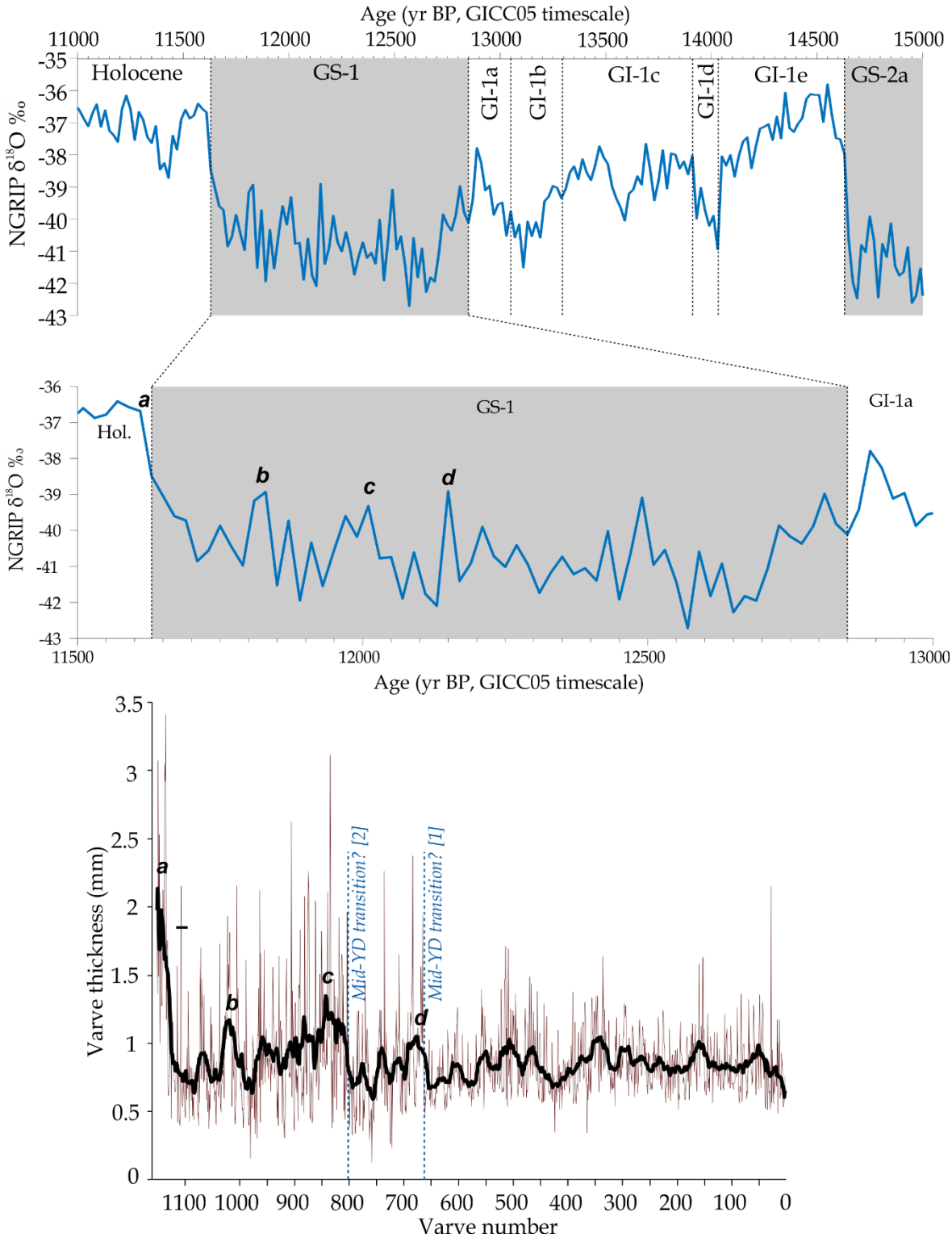

Figure 5.8: Top: NGRIP δ18O data between 11 – 15 ka BP. Data are on the GICC05 timescale, transformed from b2k to BP. Greenland stadials (grey) and Interstadials (white) are shown. Middle: Expanded NGRIP δ18O data for the GS-1 (~Younger Dryas age) interval. Bottom: Varve thickness composite for Cores 68 and 64. The Core 64 thickness data has been transformed to have the same mean as the overlapping section in Core 68. A 20-point smoothed composite record is shown as a thick black line. Possible tie-points between the Windermere cores and the Greenland data are given with letters a-d. Possible locations for the Mid-Younger Dryas Transition are shown as blue dashed lines.

5.11 Conclusions

The Younger Dryas- age sediments of Windermere are typified by mm-scale nival-style varves in Cores 64 and 68, and large-scale mass transport deposits in Cores 57 and 67. The varves of the early Younger Dryas are more bioturbated and contain many coarse grains, indicative of stormy conditions. The increased frequency of graded beds in the early Younger Dryas sediments also attests to increased storminess and is in accordance with the interpretation of the varved lake sequence from Meerfelder Maar in Germany (Brauer et al., 2008; Lane et al., 2013). A step-increase in varve thickness at varve 803 indicates an influx of warmer, precipitation-bearing air into the Windermere region as the cold, dry storm tracks shifted northwards. A similar possible shift occurs at varve 683. A slight decrease in bioturbation index values towards the late Younger Dryas also indicates less wind-driven mixing. Similar transitions are seen in Meerfelder Maar and Kråkenes, coastal Norway (Bakke et al., 2009; Lane et al., 2013), although the floating Windermere varve chronology cannot be used to compare timings. In the latest Younger Dryas sediments, an increase in bioturbation and a pronounced increase in varve thickness heralds the onset of much warmer, wetter conditions and the resumption of lake overturning. When compared, the smoothed composite Windermere varve thicknesses appear to co-vary with the NGRIP $\delta^{18}O$ data for GS-1 after 12200 yr BP. This indicates that after this point North Atlantic winter precipitation and temperature were coupled as the sea ice extent moved to more modern day conditions and supports the position of 'Mid Younger Dryas Transition [1]', although our chronology is not sufficiently precise to move beyond speculation. We have produced a floating varve chronology, and our results show the potential for construction of precise annually resolved varve record throughout the Younger Dryas interval.

5.12 Supplementary Material

5.12.1 Coring information

Core	Core length (m)	Water depth (m)
Core 68	10	53.7
Core 64	8	25.6
Core 67	8	26.9
Core 57	6	37.3

Table 5.4: Core lengths and water depths of the four cores.

5.12.2Downcore elemental variation from Itrax WD-XRF

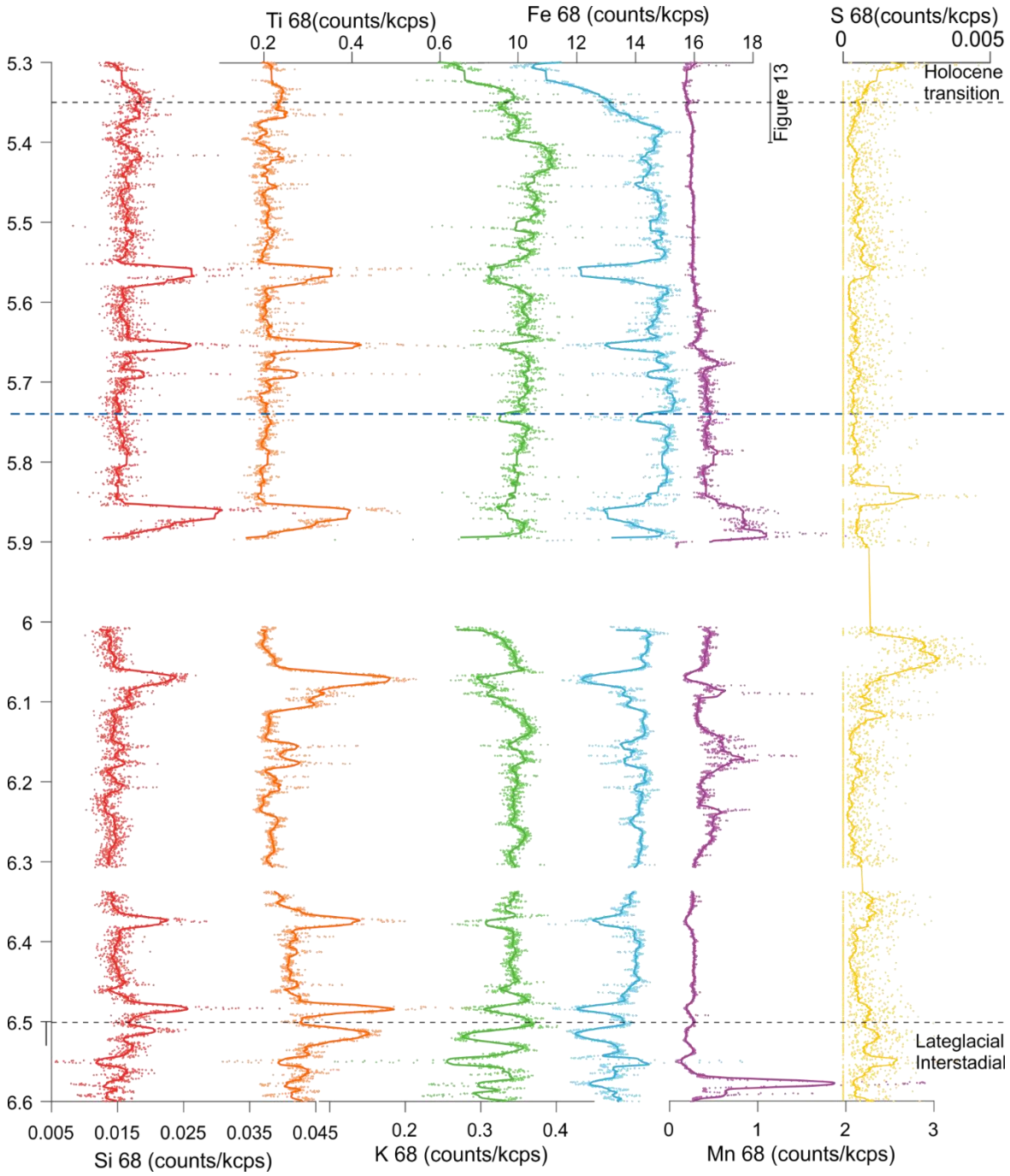

Figure 5.9: Itrax ED-XRF curves for selected elements in Core 68 through the YD-age sediments. From left to right: Silica (red), Titanium (orange), Potassium (green), Iron (blue), Manganese (purple), and Sulphur (yellow). Blue horizontal dashed line indicates where laminations thicken.

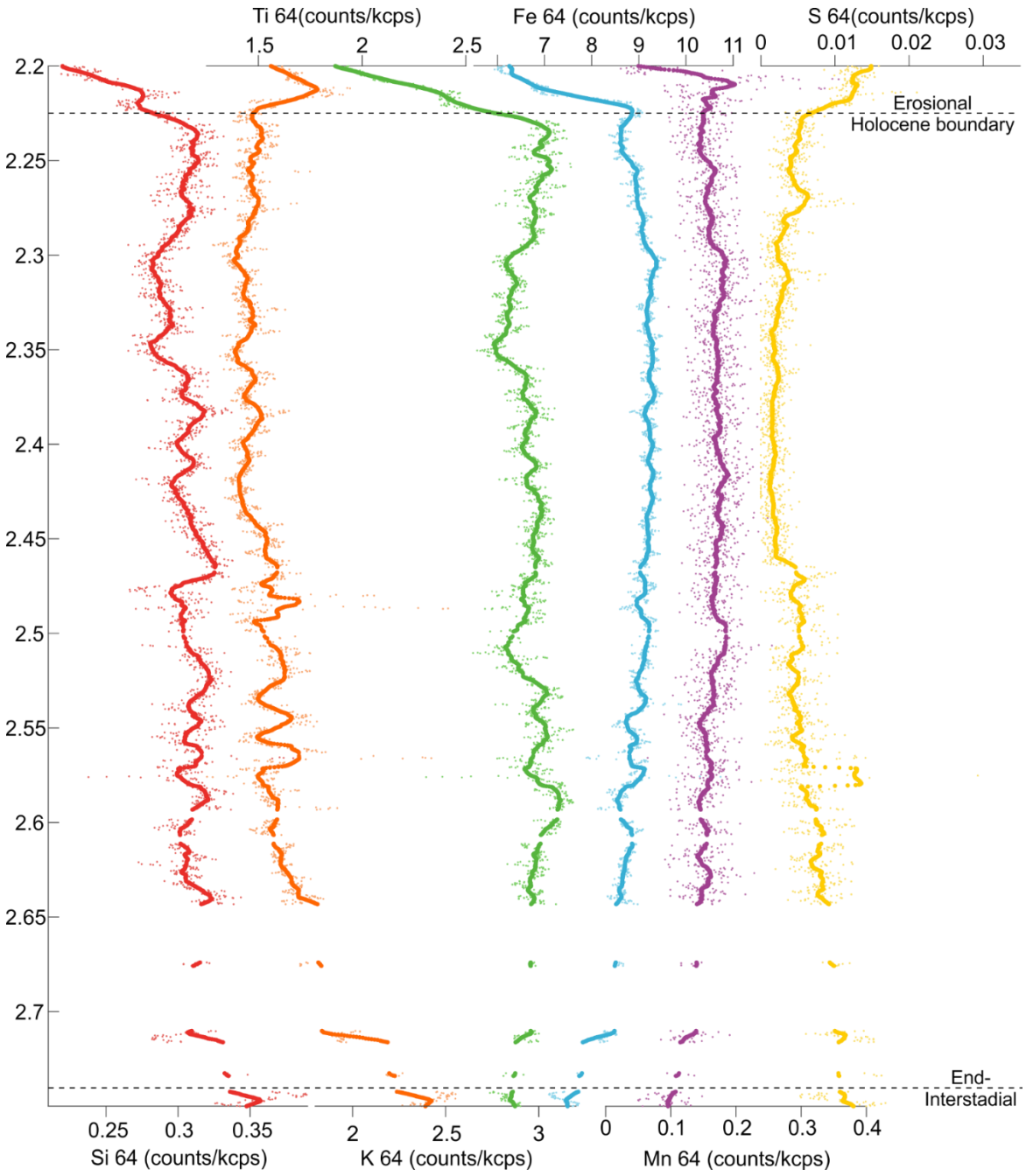

Figure 5.10: Itrax ED-XRF curves for selected elements in Core 64 through the available YD-age sediments. From left to right: Silica (red), Titanium (orange), Potassium (green), Iron (blue), Manganese (purple), and Sulphur (yellow). The gaps can be due either sediment voids or deleted bad data.

5.12.3Laminated sequence interruptions

5.12.3.1 Graded beds

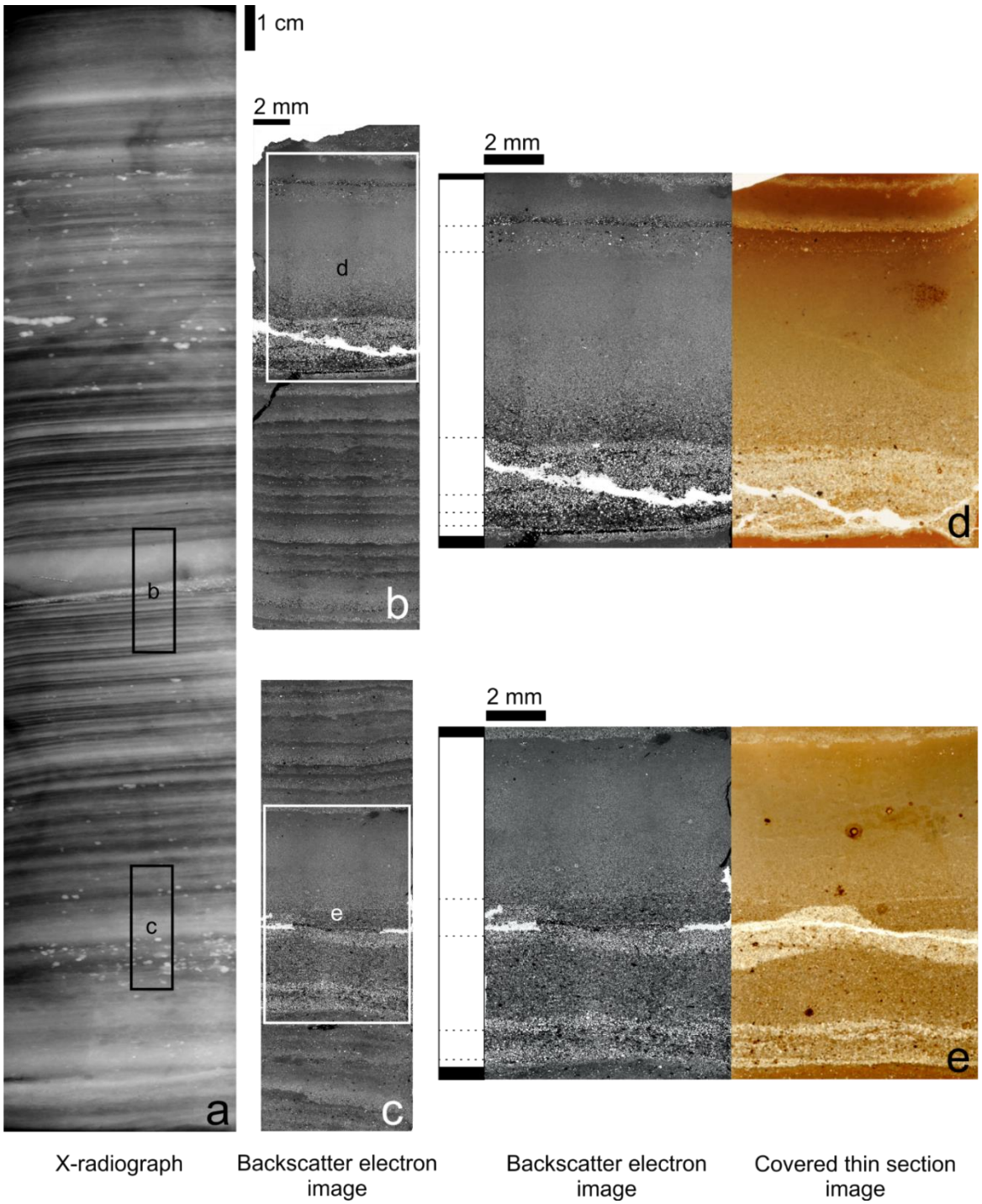

Figure 5.11: Graded beds found in Core 68. a) X-radiograph showing 25 cm of sediment; b) and c): Backscatter electron images of polished thin sections; d) and e): A backscatter electron image and covered thin section image showing the detail of the sediment. The alternating black and white bar to the left indicates different 'normal sedimentation' couplets (where present), and dotted black lines show graded bed internal structure.

5.12.3.2 Mass Transport Deposits

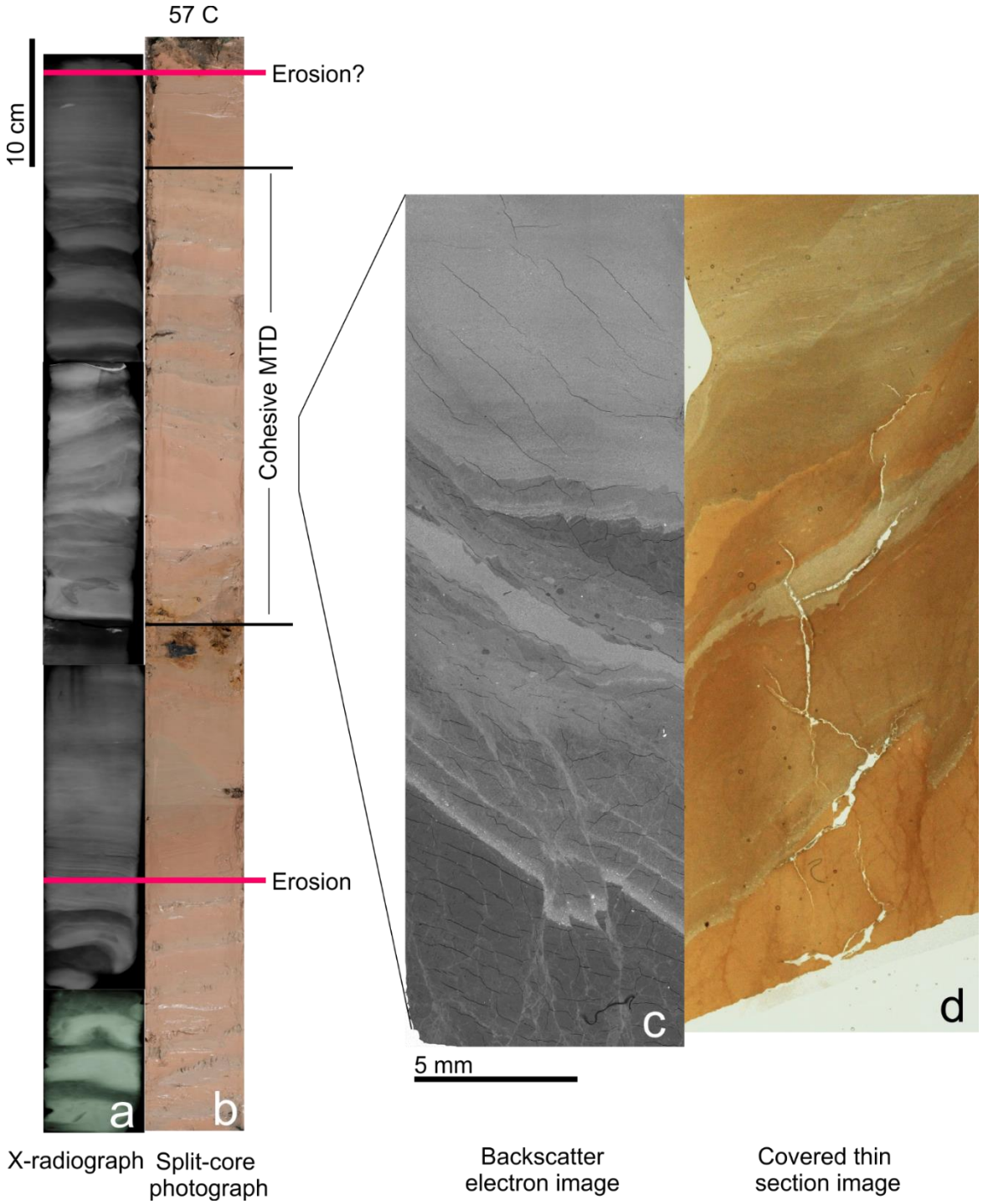

Figure 5.12: Cohesive mass transport deposit in Core 57. Left: X-radiographs (a) and split-score image (b) of the third core section in Core 57 (2 – 2.87 m), with black horizontal lines showing the bounds of the cohesive MTD which truncates the Lateglacial Interstadial sediment, and pink horizontal lines showing erosive boundaries. Right: backscatter electron image (c) and covered thin section image (d) showing detail of two cm-scale varves present in the MTD.

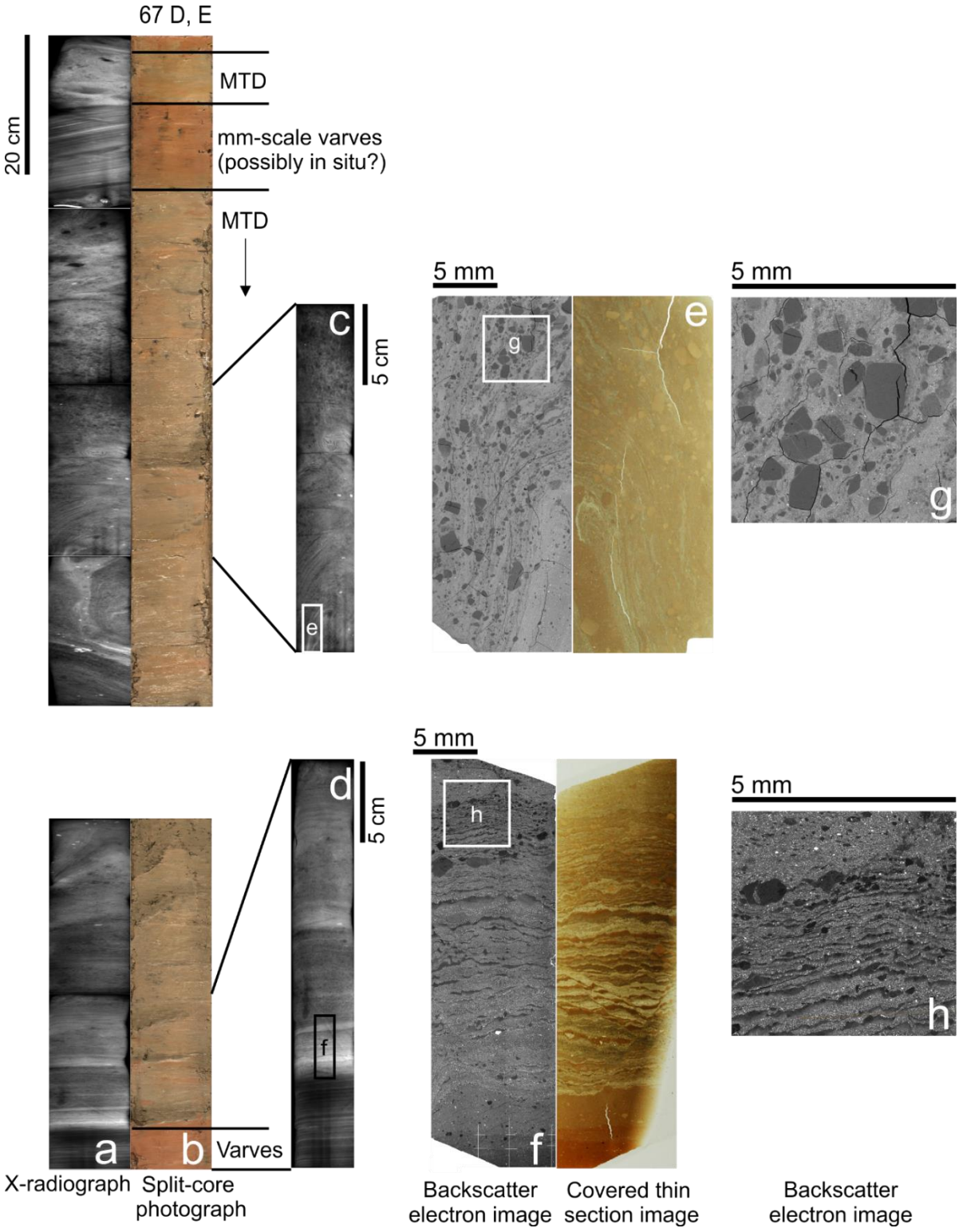

Figure 5.13: Mass transport deposit in Core 67. X-radiographs (a) and split-score image (b) of sections D and E in Core 67 (3.84 – 4.75 m), with black horizontal lines showing the bounds of the MTD. Individual slab X-radiographs of two sections of the MTD (c, d). Backscatter electron images and covered thin section images of selected slides within the MTD (e, f). Backscatter electron images of sediment detail from the MTD (g, h).

5.12.3.3 Soft Sediment Deformation

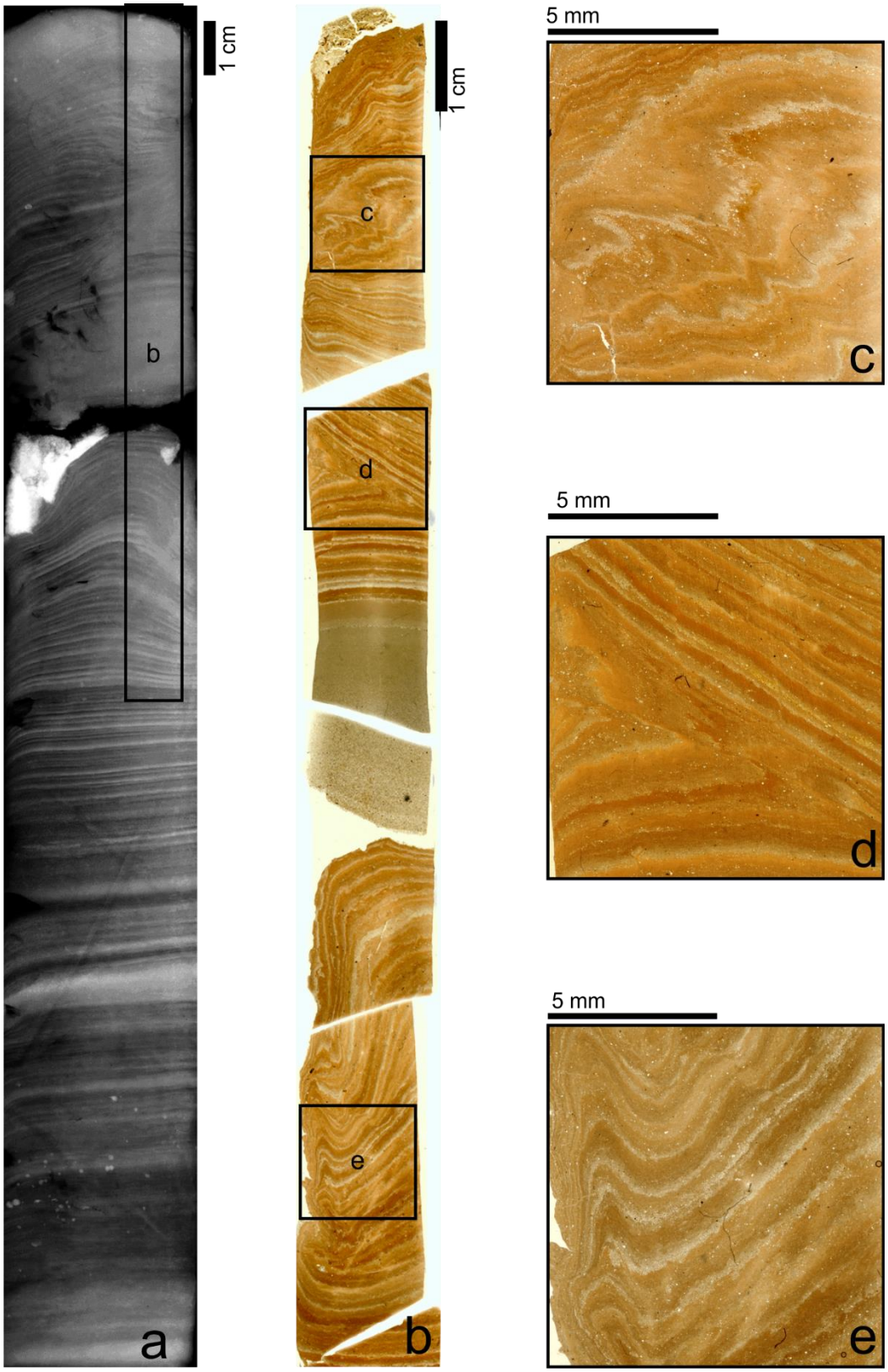

Figure 5.14: Micro-scale deformation in Core 68 between 6 m and 6.15 m. Left: X-radiograph. Centre: Photomicrographs showing the general features of the micro-scale deformation. Right: Photomicrographs showing the detail of the deformation through the section.

5.12.4 Examples of described sediment facies

5.12.4.1 Simple and compound couplets from Core 68

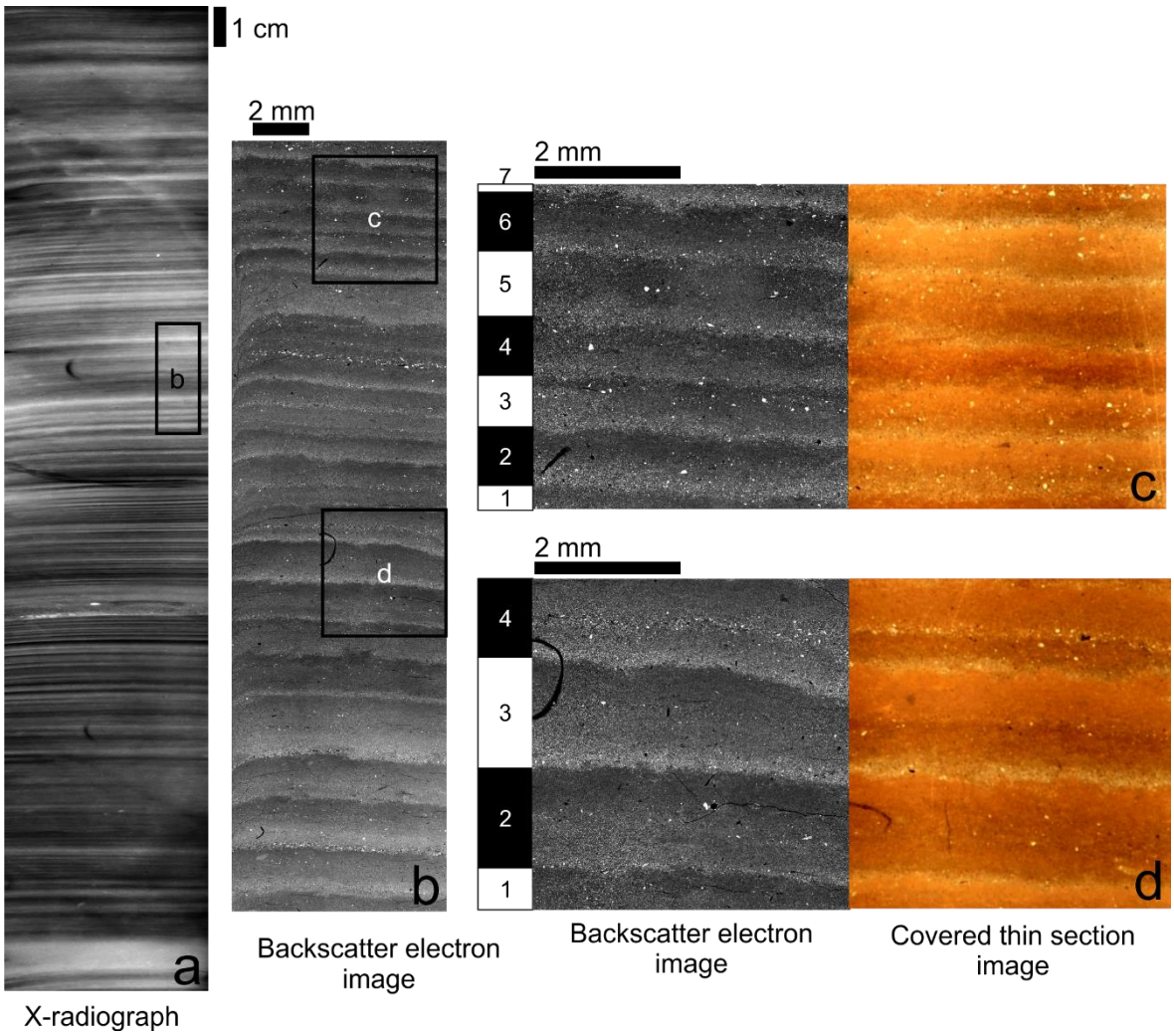

Figure 5.15: Example of distinct mm-scale laminae showing minimal bioturbation from Core 68. a) X-radiograph showing 25 cm of sediment; b) A backscatter electron image of a polished thin section showing ~25 laminae; c) and d) A backscatter electron image and covered thin section image showing the detail of a few laminae. The alternating black and white bar to the left indicates different laminae.

5.12.4.2 Simple and compound couplets from Core 64

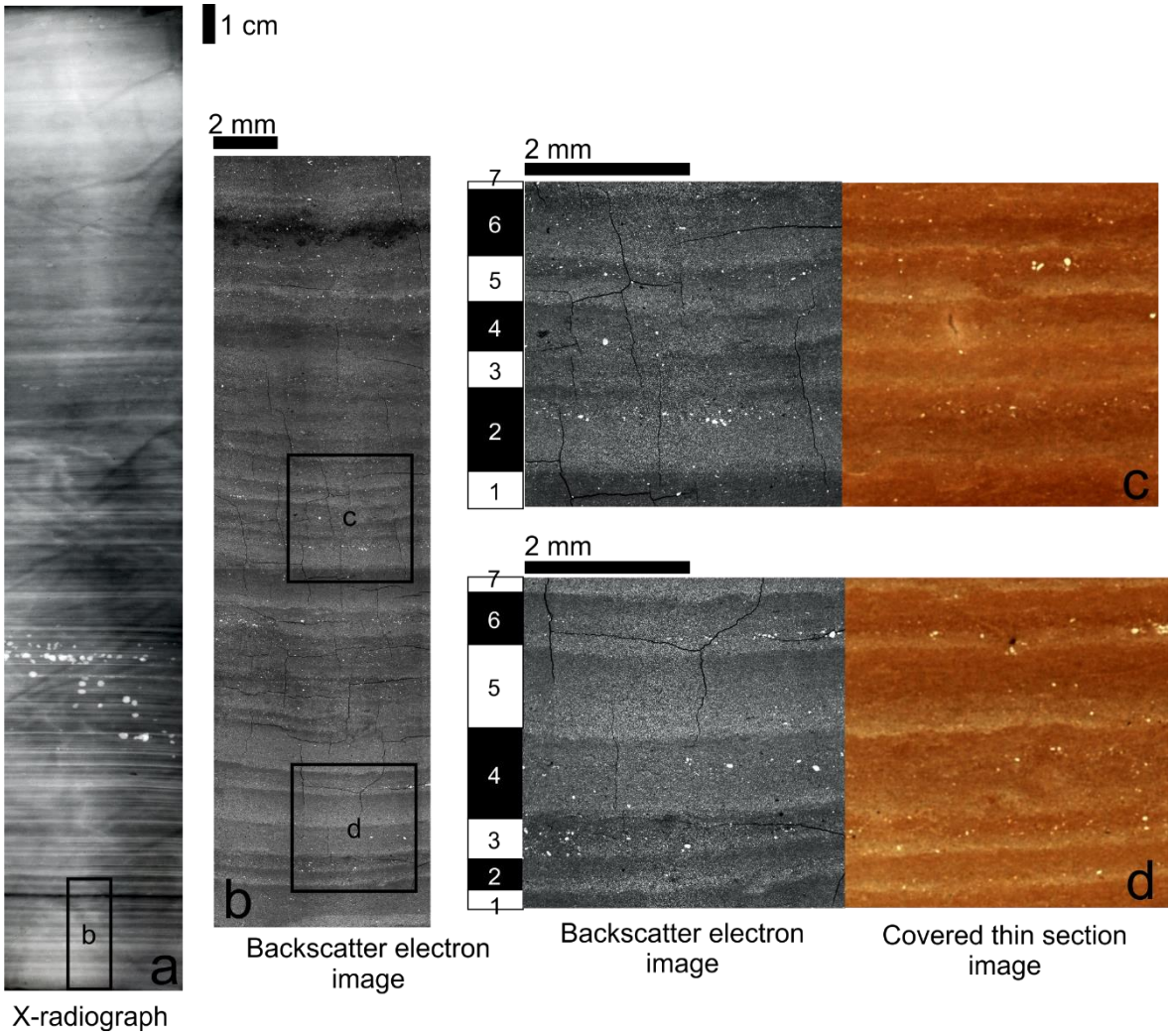

Figure 5.16: Example of distinct, relatively un-bioturbated mm-scale couplets found in Core 64. a) X-radiograph showing 25 cm of sediment; b) A backscatter electron image of a polished thin section showing bundles of distinct (c, d) interbedded with more bioturbated intervals one of which includes an organic-rich horizon; c) and d) A backscatter electron image and covered thin section image showing the detail of a few couplets. The alternating black and white bar to the left indicates different couplets.

5.12.4.3 Disturbed couplets from Core 68

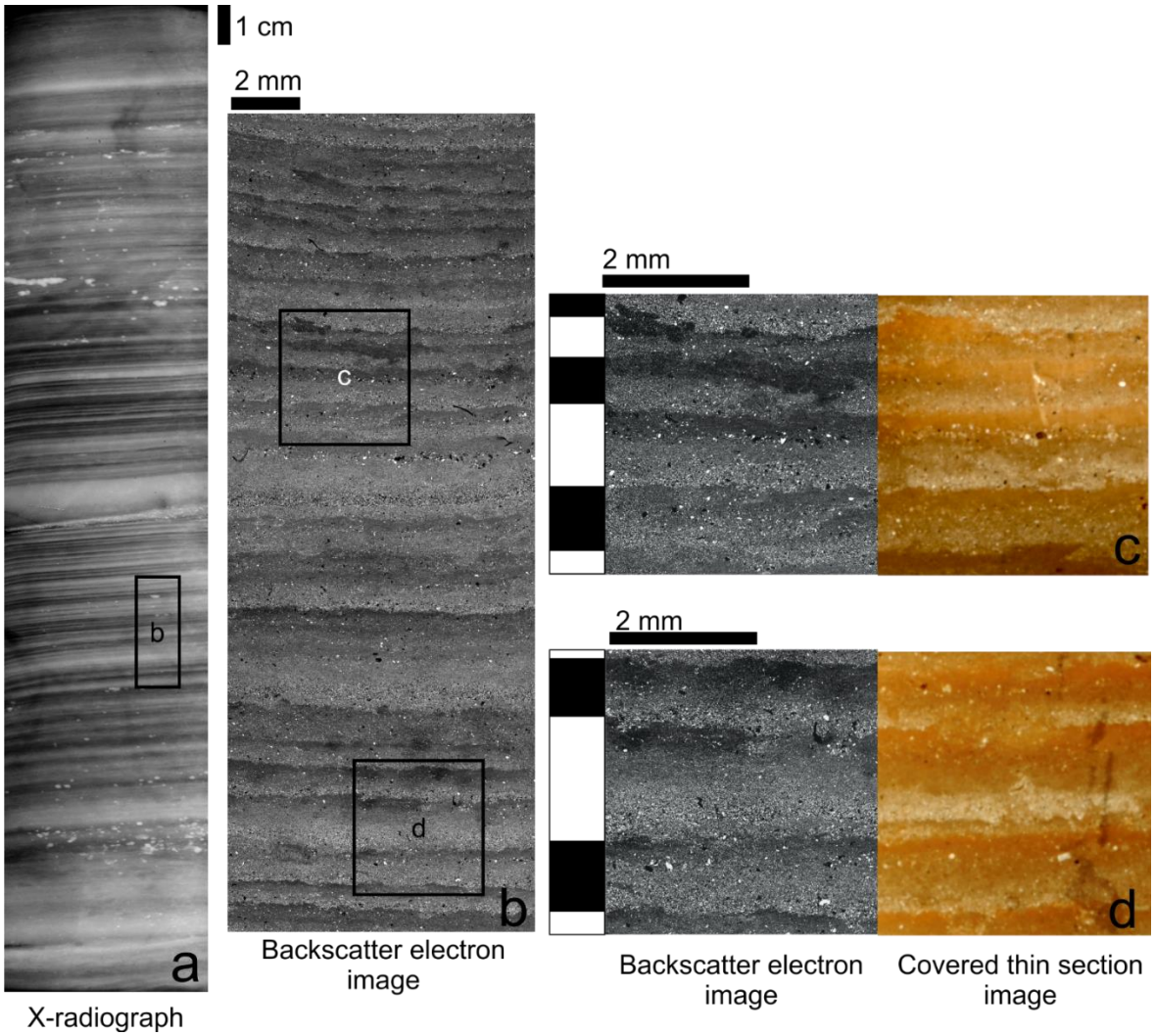

Figure 5.17: Distinct laminae with light bioturbation from Core 68. a) X-radiograph showing 25 cm of sediment; b) A backscatter electron image of a polished thin section showing ~25 laminae; c) and d) A backscatter electron image and covered thin section image showing the detail of a few laminae. The alternating black and white bar to the left indicates different laminae.

5.12.4.4 Indistinct couplets from Core 64

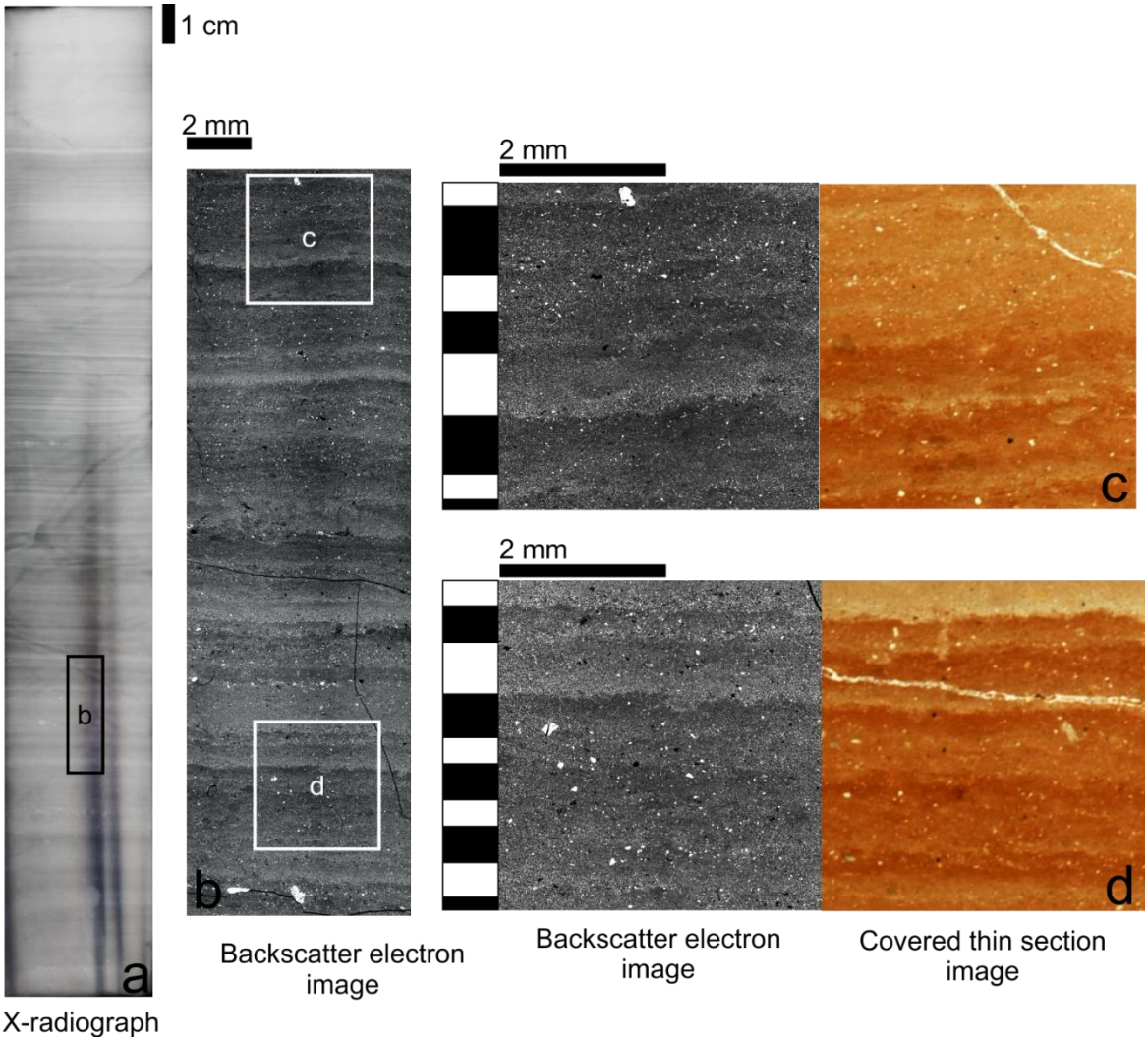

Figure 5.18: Indistinct bioturbated laminae in Core 64. a) X-radiograph showing 25 cm of sediment; b) A backscatter electron image of a polished thin section showing laminae; c) and d) A backscatter electron image and covered thin section image showing the detail of a few laminae. Note in (d) that laminae are more clearly observed in the optical photomicrograph. The alternating black and white bar to the left indicates different laminae.

5.12.4.5 Homogenised couplets from Core 64

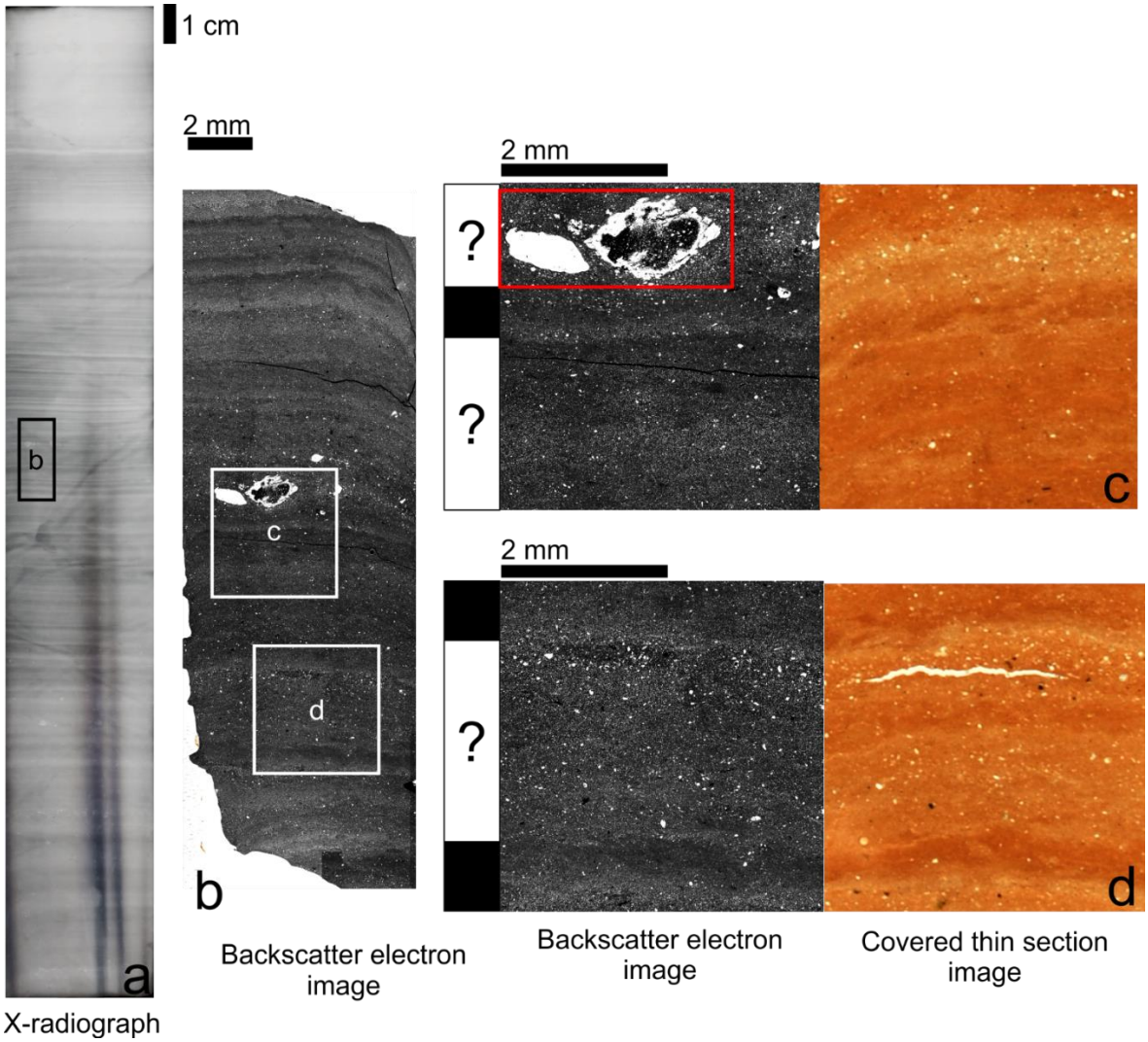

Figure 5.19: More pervasively bioturbated laminae in Core 64. a) X-radiograph showing 25 cm of sediment; b) A backscatter electron image of a polished thin section showing both laminated and homogenised sediment; c) and d) A backscatter electron image and covered thin section image showing the detail of some homogenised sediment. The alternating black and white bar to the left indicates different laminae, but it should be noted that there are potentially several undefinable laminae in the sections marked with question marks.

5.12.4.6 Early Holocene sediment

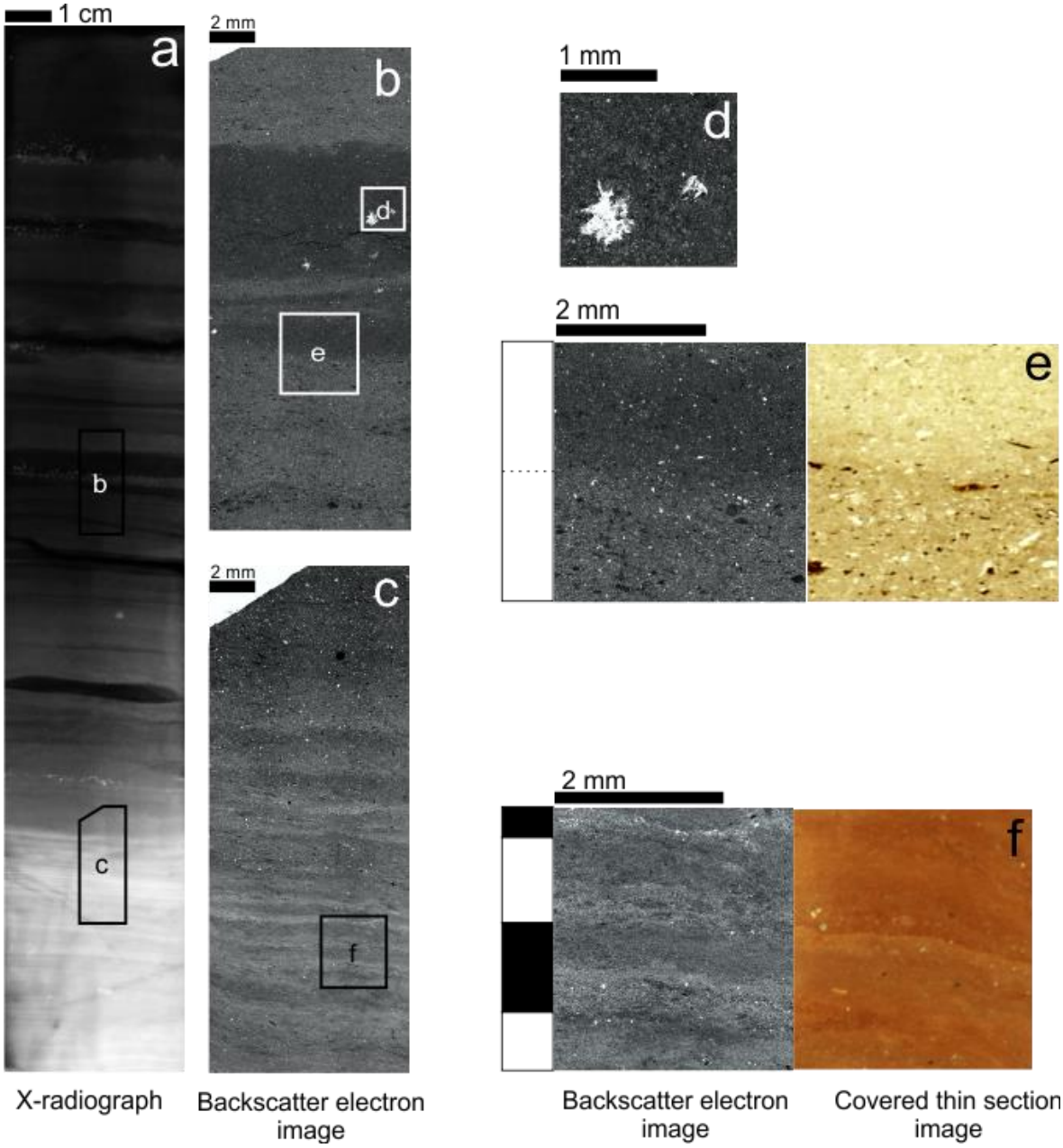

Figure 5.20: Sediment from the earliest Holocene in Core 67. a) X-radiograph showing 25 cm of sediment; b) and c) Backscatter electron image of polished thin sections showing both partially-laminated and unlaminated sediment; d) a backscatter electron image showing some post-sedimentation mineral growth of phosphoferrite; e) and f) A backscatter electron image and covered thin section image showing the detail of some early-Holocene sediment. The alternating black and white bar to the left indicates different laminae.

5.12.5 Details on varve counts

			Uncertainty	
Tie	Count 1	Count 2	+ve	-ve
A-B	81	82	1	0
B-C	100	101	0	0
C-D	98	98	0	0
D-E	104	105	1	0
E-F	107	107	0	0
G-H	64	64	0	0
H-I	79	80	1	0
I-J	75	77	2	0
J-K	77	78	1	0
K-L	81	82	1	0
L-M	21	21	0	0
TOT	887	895	7	0
% Error	0.78918			

Table 5.5: The tiepoints used in the Core 68 Younger Dryas varve sequence. Counts by two different researchers between each tiepoint are given, and the total uncertainty is given, calculated as the absolute number of disputed varves as a percentage of the total count (count 1).

Core 64			Uncertainty	
Tie	Count 1	Count 2	+ve	-ve
N-O	33	33	0	0
O-P	107	102	0	-5
P-Q	148	150	2	0
Q-R	84	83	1	-2
R-S	63	63	0	0
S-T	95	95	0	0
T-U	82	78	0	-4
U-V	76	76	0	0
TOT	688	680	3	-11
% Error	2.0349			

Table 5.6: The tiepoints used in the Core 64 Younger Dryas varve sequence. Counts by two different researchers between each tiepoint are given, and the total uncertainty is given, calculated as the absolute number of disputed varves as a percentage of the total count (count 1).

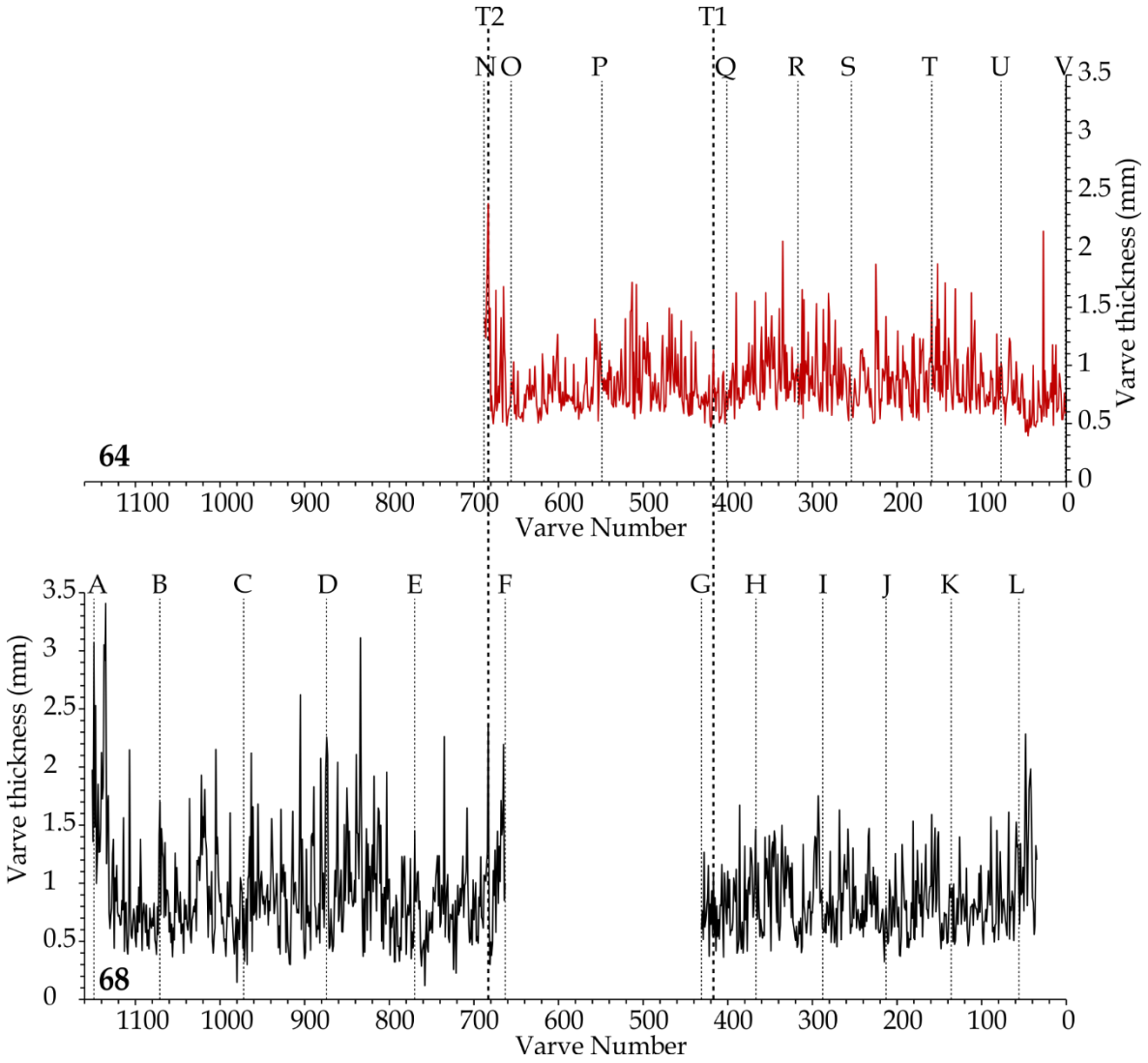

Figure 5.21: Varve thickness records for Cores 64 (red) and 68 (black) showing the counting intervals used for each core (A-V) and the two tiepoints used to correlate the records (T1, T2).

6. Strengthening of El Niño during the last deglaciation

In this chapter, selected varve thickness time series are used for spectral analysis in order to identify presence and drivers of interannual variability in varve thickness.

6.1 Abstract

Understanding the operation of interannual to multidecadal climatic oscillations during periods of abrupt climate change is imperative to further development of medium-term climate forecasting models. High-resolution palaeoclimate records from the Last Glacial Maximum to the onset of the Holocene show a series of abrupt warm and cool phases, and as such are ideal for the study of the drivers of interannual climate variability. The sedimentary archive of Windermere provides a number of varve sequences of several hundred years from the last centuries of Heinrich Stadial 1 (approximately 15 – 14.7 ka BP) prior to the onset of the Lateglacial Interstadial, and from the Younger Dryas (12.9 – 11.7 ka BP). Time series were produced from varve thickness measurements and were subject to spectral analysis using the REDFIT, multitaper, and wavelet techniques. Periods significant above the 95% confidence level were present in all time series, and in particular periods between 2.1 – 3.8 yr, interpreted as arising from interactions of the Quasi-Biennial Oscillation and/ or El Niño with the polar vortex. A composite time series from the pre-Interstadial (GS2) did not yield periodicities in the 4 – 7 yr "classical" El Niño band, whereas the Younger Dryas intervals showed strong power in this band. This is in keeping with evidence that the strength of El Niño variability was reduced during the Last Glacial Maximum but strengthened with Northern Hemisphere warming. As a test of the results, we reshuffled the data for a selection of time series. Periodicities < 5 yr appeared even in the synthetic time series and should be interpreted with some caution, but evidence for the absence of periodicities of 4 – 7 yr in the pre-Interstadial composite time series appears robust. Longer periods (>7 yr) are inconsistent but may represent known cycles (e.g. the Hale cycle, 22 yr, and longer-period El Niño variability, 12 – 14 yr).

6.2 Site description

Windermere is a north-south trending glacial ribbon lake in the southeast of the English Lake District (54.4° N, 2.9° W) (Figure 6.1), lying in a steep-sided pre-glacial river valley that has been overdeepened by successive glaciations (Pennington and Pearsall, 1973; Pinson et al., 2013). The lake has a present maximum water depth of 62 m and an elevation of 39 m above Ordnance Datum Newlyn. It has maximum dimensions of 17 km x 1.5 km and drains a catchment of 242 km^2 (Lowag et al., 2012; Miller et al., 2013). The catchment bedrock comprises the Ordovician Borrowdale Volcanic Group in the north and the Windermere Supergroup (Silurian mudstones and siltstones) in the south.

Windermere is separated into a north and South Basin by a bedrock high, with the South Basin draining westward into the River Leven (Wilson, 1987). Windermere has accumulated sediment since the retreat of the British-Irish Ice Sheet c. 17 ka (Ballantyne et al., 2009). The main sedimentary inputs into the lake are the Trout Beck in the northeast of the catchment (yellow outline; Figure 1), and the rivers Rothay and Brathay which are fed by several valleys in the north of the catchment (red outline; Figure 6.1)

The Lake District is situated adjacent to the Irish Sea, and during the present day is heavily influenced by weather systems originating from the Atlantic.

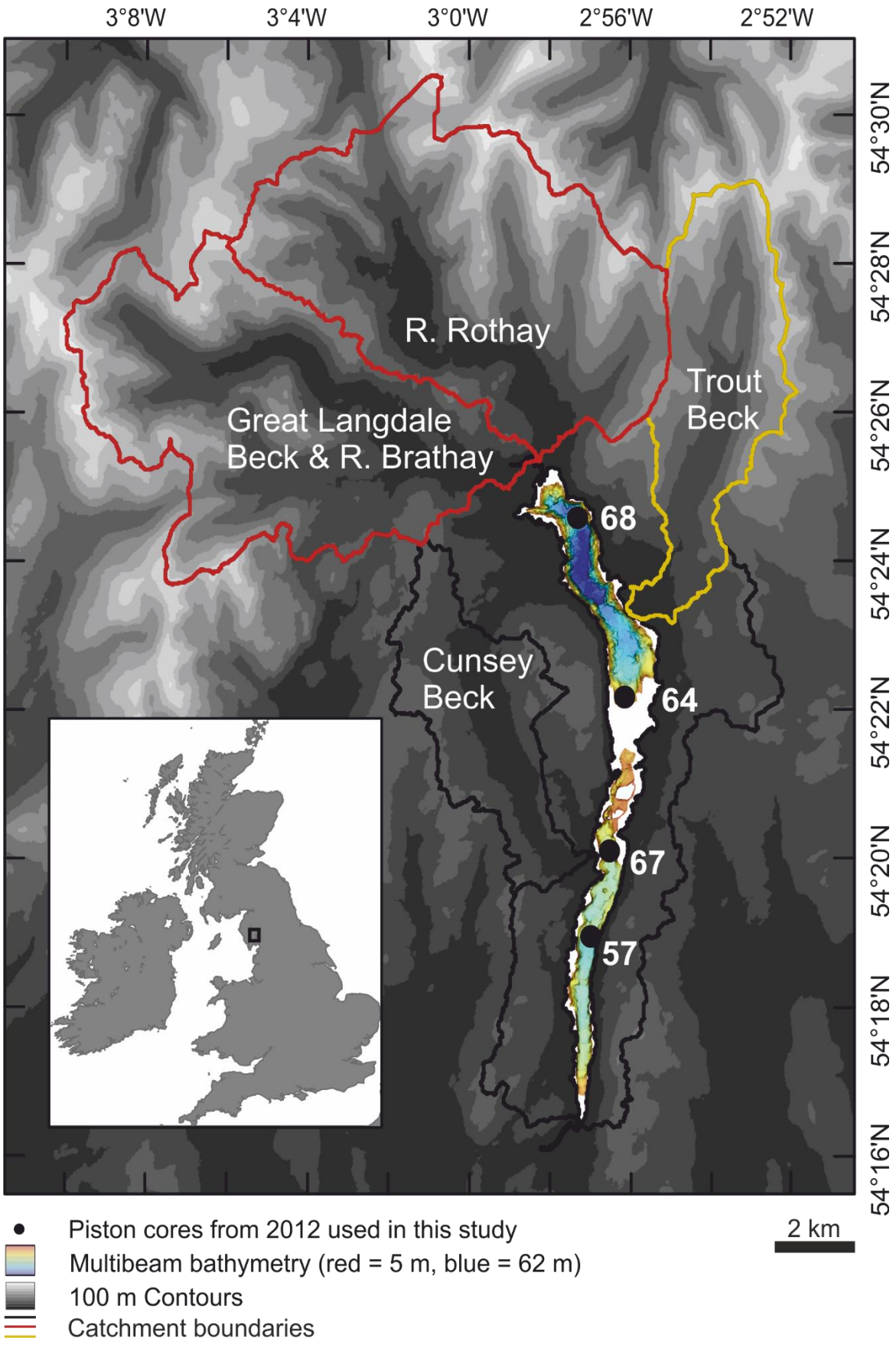

Figure 6.1 Map of the study area. The lake catchment of Windermere is shown in bold outlines (significant sub-catchments are shown in red and yellow). Significant fluvial inputs to the lake are named in the catchments. One hundred metre contours are shown as a greyscale colourmap. The

locations of Cores 57, 67, 64, and 68 are shown as filled black circles. Multibeam lake bathymetry is shown as a rainbow colour palette, where dark blue is deepest and red is shallowest.

6.3 Methods

6.3.1 Sediment selection and varve measurement

Varves thinner than ~20 mm were measured using the SEM from backscatter images of polished thin sections and from optical microscopy of covered thin sections, whilst thicker laminations were measured from CIS images of the split core. In some cases, several of the methods were used in parallel for cross-checking. Optical micrographs were examined alongside backscatter images and X-radiographs in order to identify continuously varved core sections. These sections were then inspected for ambiguous laminae (potential floods, multiple summer events etc.) and the longest (> 100 varves) sections chosen for spectral estimation. Any ambiguous laminae were inspected on the SEM and compared with X-ray radiography, ITRAX data, and other published varves (Francus et al., 2008; Larsen et al., 2011; Menounos and Clague, 2008) and either identified as varves or non-varves. The algorithm of Francus et al. (2002) was used to semi-automatically measure the mean thickness of each varve along three parallel vertical lines for each slide or split core image in the study and from this, varve thickness time series were created. Outliers such as turbidites were replaced with the local mean to avoid a spurious background spectrum (Weedon, 2003). Varve definitions were checked by two co-authors (AESK, RBP).

6.3.2 Spectral estimation

Varve sequences with evenly spaced data were analysed using REDFIT, Multitaper method, and Wavelet spectral estimation using PAST3.16 (Hammer et al., 2001), and sequences with unevenly spaced data underwent REDFIT analysis only (Table 6.1).

Varve sequence	Comments	REDFIT	Multitaper method	Wavelet
Core 68 YD mm-scale varves, core section F	Evenly spaced data, with 493 varves.	Yes	Yes	Yes

Core 68 YD mm-scale varves, core section G	Evenly spaced data, with 400 varves	Yes	Yes	Yes
Core 68 cm-scale varves	Evenly-spaced data, with 108 varves and 6 zero-padded data points	Yes	Yes	Yes
Core 57-67 composite cm-scale varve record	Evenly-spaced data, with 218 varves	Yes	Yes	Yes
Core 57 cm-scale varve record	Unevenly spaced data (sequence gaps closed), with 182 varves	Yes	No	No
Core 67 cm-scale varve record	Unevenly spaced data (sequence gaps closed), with 196 varves	Yes	No	No

Table 6.1: Varve sequences used and their treatment.

The REDFIT periodogram is based on a Lomb periodogram, but the dataset is split into overlapping segments which undergo individual Fourier transforms and are averaged to produce the final periodogram (Schulz and Mudelsee, 2002). A Hanning spectral window was used (which multiplies data points 1, 2, and 3 by 0.25, 0.5, 0.25 respectively) and which gives good frequency resolution and amplitude accuracy, and is effective at suppressing spectral leakage (Weedon, 2003).

A significant influence on peak location (assuming accurate thickness measurement with good sensitivity, and correct assessment of data stationarity) is the number of overlapping segments chosen. The number of segments chosen is a trade-off between spectrum smoothness and noise, where the reduction in noise results in wider spectral peaks due to averaging over a large number of periodograms. The analysis above used three segments overlapping by 50% (a greater overlap is in danger of the overlapping data points being non-independent) and the data oversampled by a factor of three to reduce noise.

The resulting spectra were fitted to an AR(1) red noise model and background level, 95% and 99% confidence levels were applied. Additionally, Monte Carlo 95% and 99% confidence levels were applied. Only spectral peaks which exceeded a 95% chance that they had arisen from a mathematically real cycle were considered for interpretation.

The multitaper method is designed for evenly-spaced data, and relies on a number (usually 4 – 8) of data tapers. The method here is based on (Lees and Park, 1995). The tapers are orthogonal prolate spheroidal (or Slepian) sequences. The time series is multiplied by the tapers where different weighting is given to different parts of the dataset by each taper, before generation of a series of periodograms. The periodograms are averaged to reduce noise. The multitaper method is effective at reducing spectral leakage and maintaining good frequency resolution, but tends to give flat peaks. The number of tapers trades confidence with smoothing. Five tapers were used, and an F-test applied to test for peak significance. Peaks associated with an F-value exceeding the 95% confidence limit were considered for interpretation (F-values which did not correspond with peaks were not considered).

The wavelet method of spectral estimation is a useful method for identifying significant frequencies through time, where the top of the plot shows high frequencies and the bottom shows low frequencies. For the wavelet method, the 'cone of influence' was applied to the plot, whereby all results outside the cone may be subject to data edge effects. Additionally, black contours were applied where $P<0.05$ (i.e. 95% probability of the frequency being significant). The P-value was determined by fitting to a red-noise model, determined by the MA(1) autocorrelation coefficient of each dataset. The method is based on (Torrence and Compo, 1998).

The Core 68 pre-Interstadial varve sequence was non-stationary, since the bottom eight varves were significantly thicker than those of the rest of the sequence. These data points were cut to reduce any damping of the power spectrum. However, the data set then needed to be lengthened in order to be a suitable length for confidence levels to be calculated. Therefore, the data set was zero-padded with six extra data points. Additionally, the data set was only long enough for one segment rather than the three used for the other datasets in the REDFIT spectral estimation, such that the resulting spectrum is less smoothed.

6.4 Results

The results for each spectral analysis suite are given in Figure 6.2 - Figure 6.8 below. The significant periods (in varve years) for each method and sequence are given in Table 6.2, and a summary figure is shown in Figure 6.9.

All of the sequences display peaks exceeding the 95% confidence level for a red-noise background at periods between 2 –4 years, and the Younger Dryas-age sequences also have periods between 4 – 7 years. Additionally, periods of 12 and 16 years are found in the upper Younger Dryas varves and 8.4, 11, and 35 years in the lower Younger Dryas sequence. In the pre-Interstadial sequences, a period of 13 years is seen from the wavelet analysis of the Core 57-67 composite.

Sequence	Confidence	REDFIT	Multitaper	Wavelet
68 Upper Younger Dryas age mm-scale	95%	2.1, 2.2, 3.1	2.8, (4.5?), 6, 16	2 – 4, 5.4, 8, 12
	99%	2.2, 2.8	2.14, 3.1, 3.5,	-
68 Lower Younger Dryas age mm-scale	95%	2.7, 3.7, 35	2.4, 2.5, 3.1, 3.6, 4.2, 5.1, 11.1, 35	Various between 2 – 6.2
	99%	-	8.4	-
64 Mid Younger Dryas	95%	-2.1, 2.5, 3.7, 7.1	2.3, 3.5, 3, 3.6, 22	-Various between 2 - 7
	99%	-	-	-
68 pre-Interstadial	95%	2.1, 3.5	2.7, 3.6, 6.0	2.5 – 3.5, ~5.6
	99%	6.2	-	-
57-67 composite	95%	2.1, 3.8	2.1, 2.3	2.1, ~3.5, ~13
	99%		2.7, 3.8	
57 cm-scale	95%	3.7	-	-
	99%	-	-	-
67 cm-scale	95%	3.3	-	-
	99%	-	-	-

Table 6.2: Significant periods for the spectral estimation methods and varve sequences used.

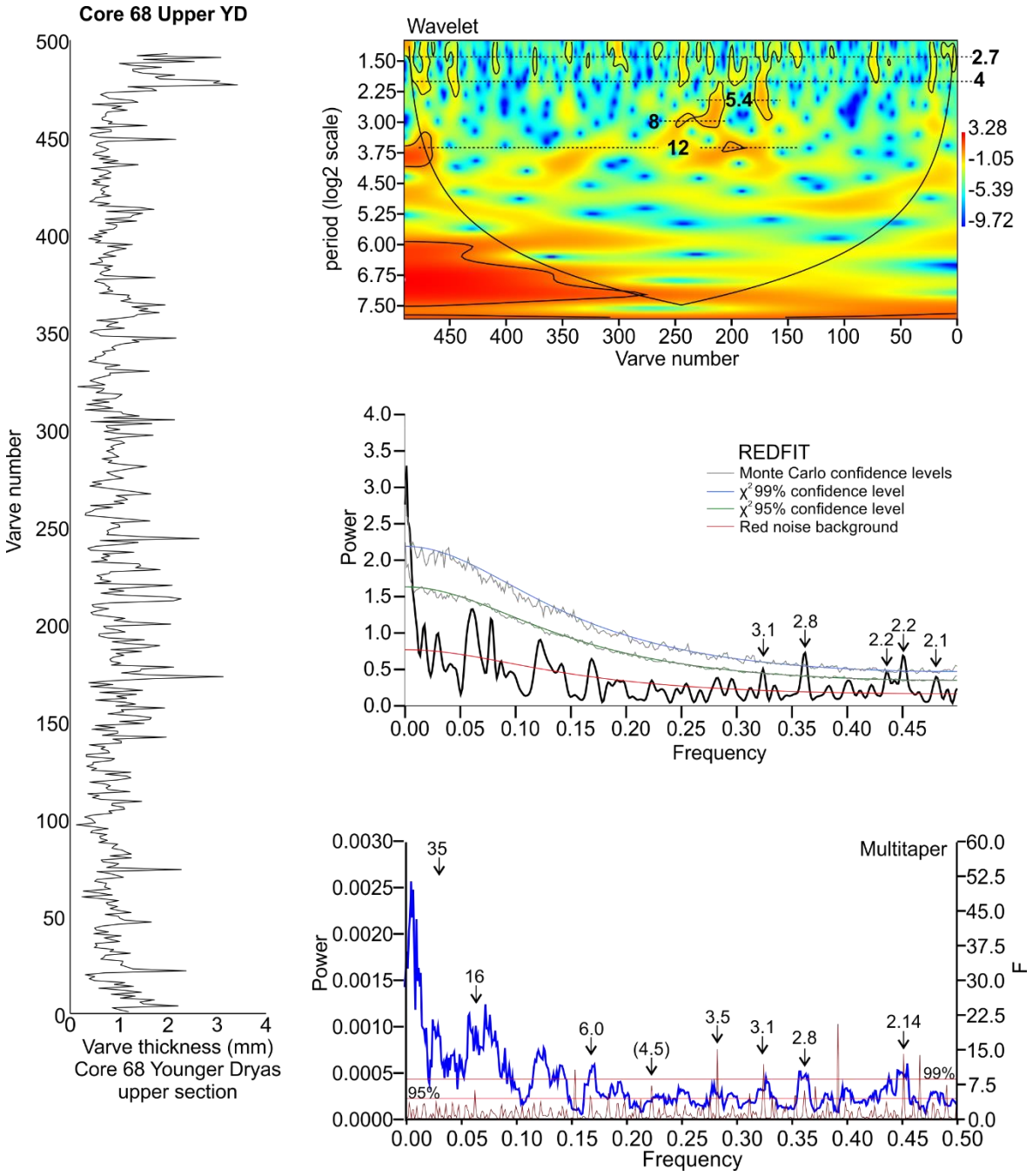

Figure 6.2: Spectral estimation results for the upper Younger Dryas-age mm-scale varve sequence in Core 68. Left: the varve thickness sequence. Top: Wavelet analysis with cone of influence and black contours showing P<0.05 significance. Middle: REDFIT power spectrum with chi-squared background (red), 95% (green) and 99% (blue) confidence levels, and Monte Carlo 95 and 99% confidence levels (grey). Bottom: Multitaper method spectrum (blue) with F-test peaks (brown) and 95% and 99% F-test confidence levels (red). For all spectral estimation panels, significant periods are given in varve years.

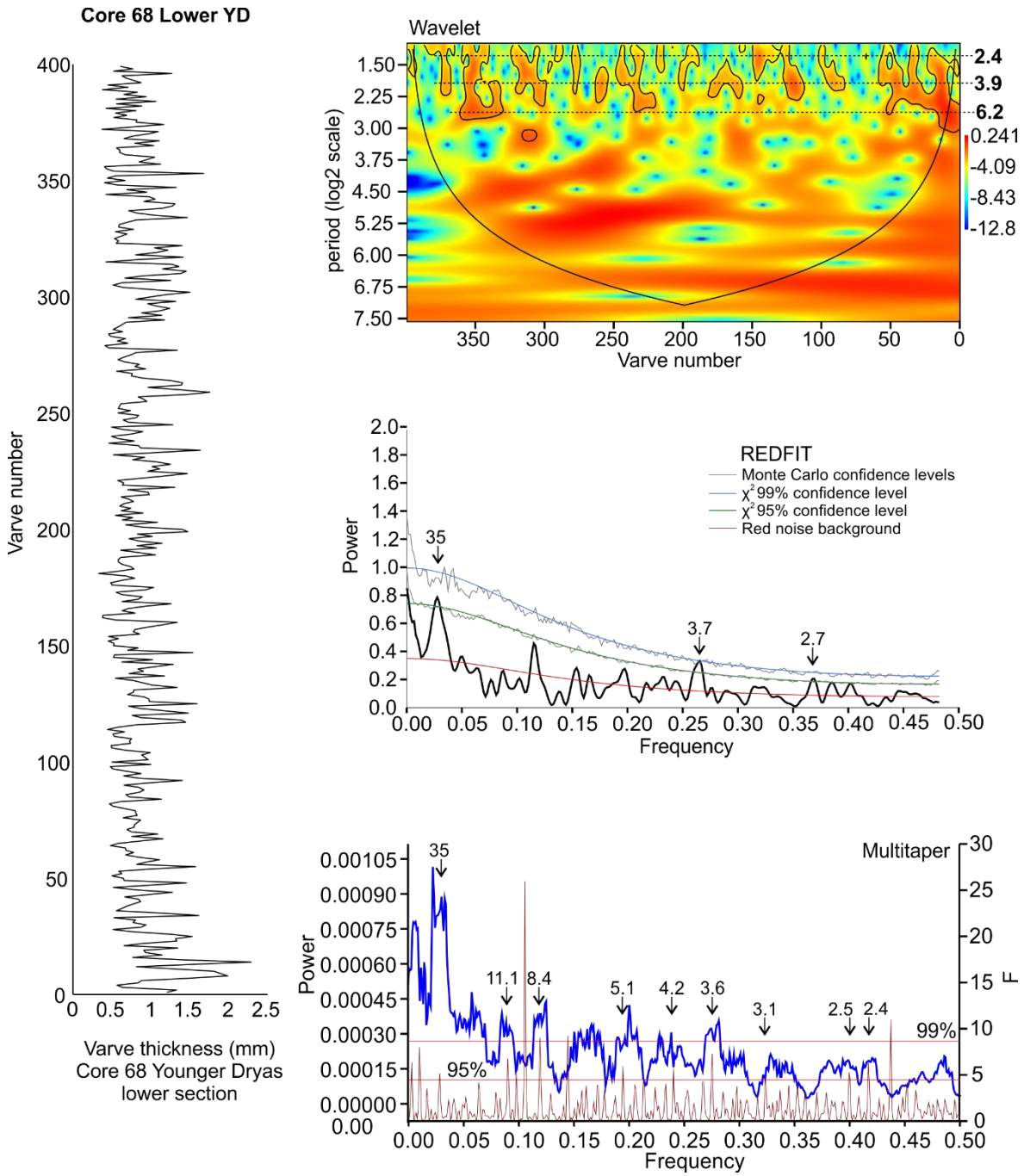

Figure 6.3: Spectral estimation results for the lower Younger Dryas-age mm-scale varve sequence in Core 68. Left: the varve thickness sequence. Top: Wavelet analysis with cone of influence and black contours showing P<0.05 significance. Middle: REDFIT power spectrum with chi-squared background (red), 95% (green) and 99% (blue) confidence levels, and Monte Carlo 95 and 99% confidence levels (grey). Bottom: Multitaper method spectrum (blue) with F-test peaks (brown) and 95% and 99% F-test confidence levels (red). For all spectral estimation panels, significant periods are given in varve years.

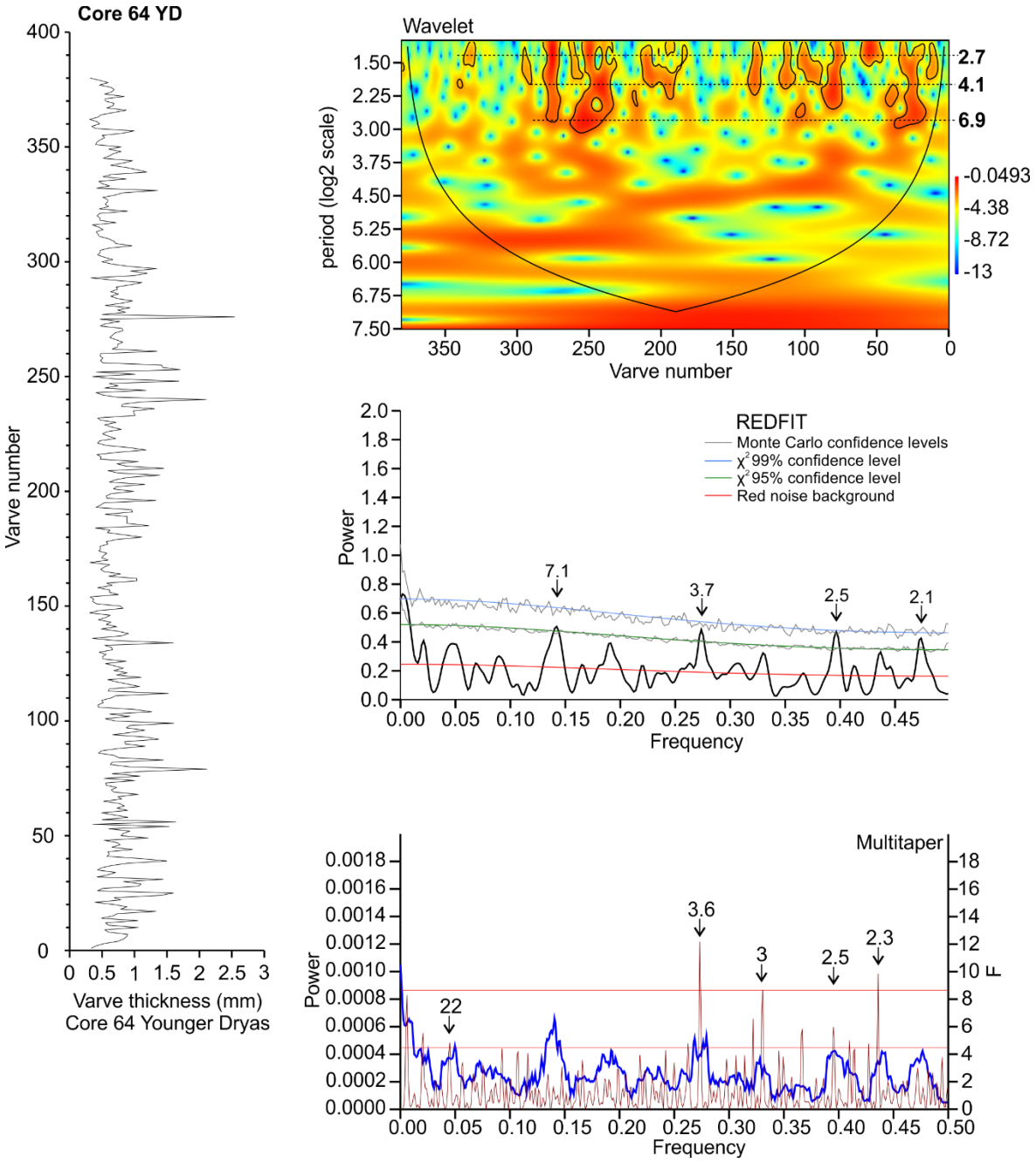

Figure 6.4: Spectral estimation results for the Younger Dryas-age mm-scale varve sequence in Core 64. Left: the varve thickness sequence. Top: Wavelet analysis with cone of influence and black contours showing P<0.05 significance. Middle: REDFIT power spectrum with chi-squared background (red), 95% (green) and 99% (blue) confidence levels, and Monte Carlo 95 and 99% confidence levels (grey). Bottom: Multitaper method spectrum (blue) with F-test peaks (brown) and 95% and 99% F-test confidence levels (red). For all spectral estimation panels, significant periods are given in varve years.

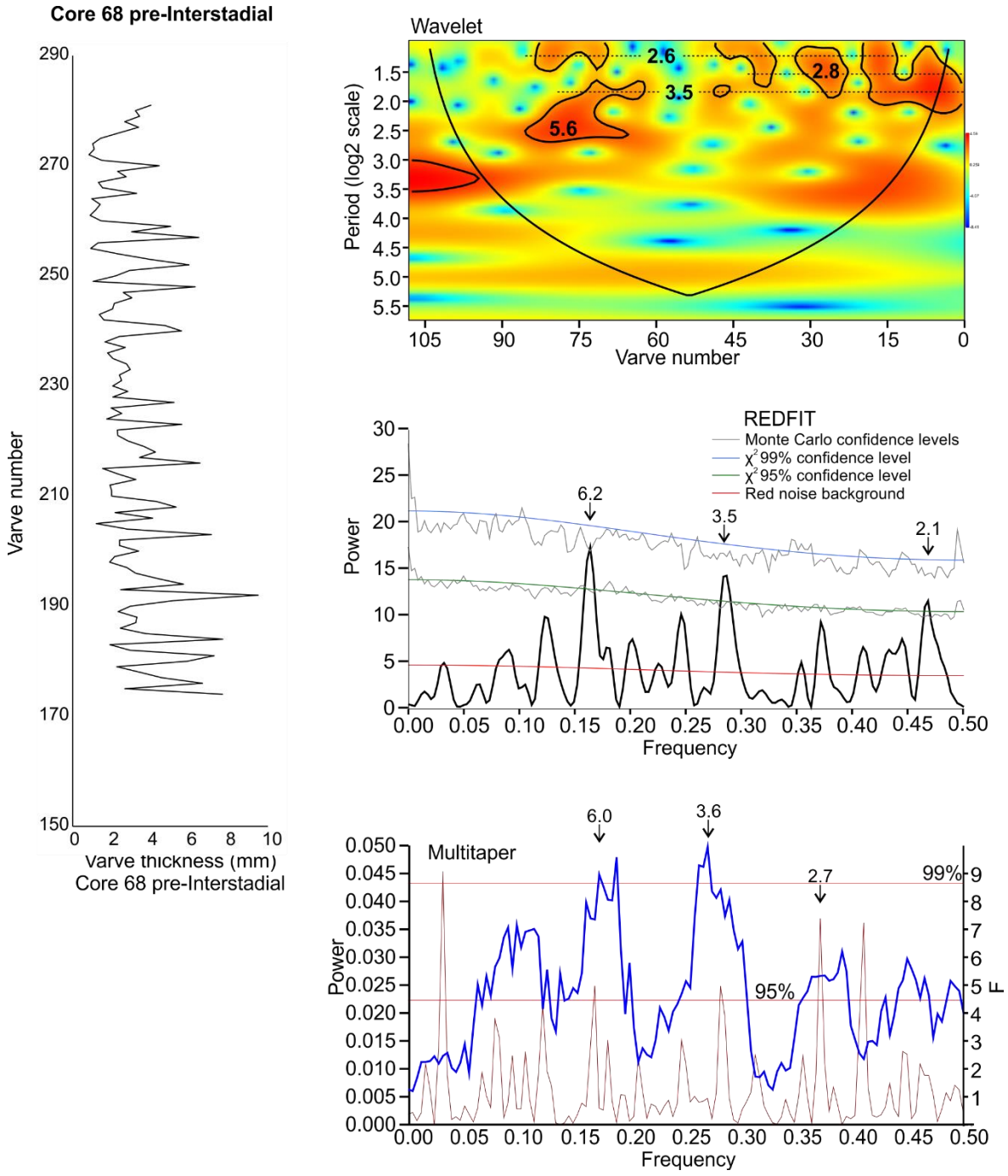

Figure 6.5: Spectral estimation results for the pre-Interstadial varve sequence in Core 68. Left: the varve thickness sequence. Top: Wavelet analysis with cone of influence and black contours showing P<0.05 significance. Middle: REDFIT power spectrum with chi-squared background (red), 95% (green) and 99% (blue) confidence levels, and Monte Carlo 95% and 99% confidence levels (grey). Bottom: Multitaper method spectrum (blue) with F-test peaks (brown) and 95% and 99% F-test confidence levels (red). For all spectral estimation panels, significant periods are given in varve years.

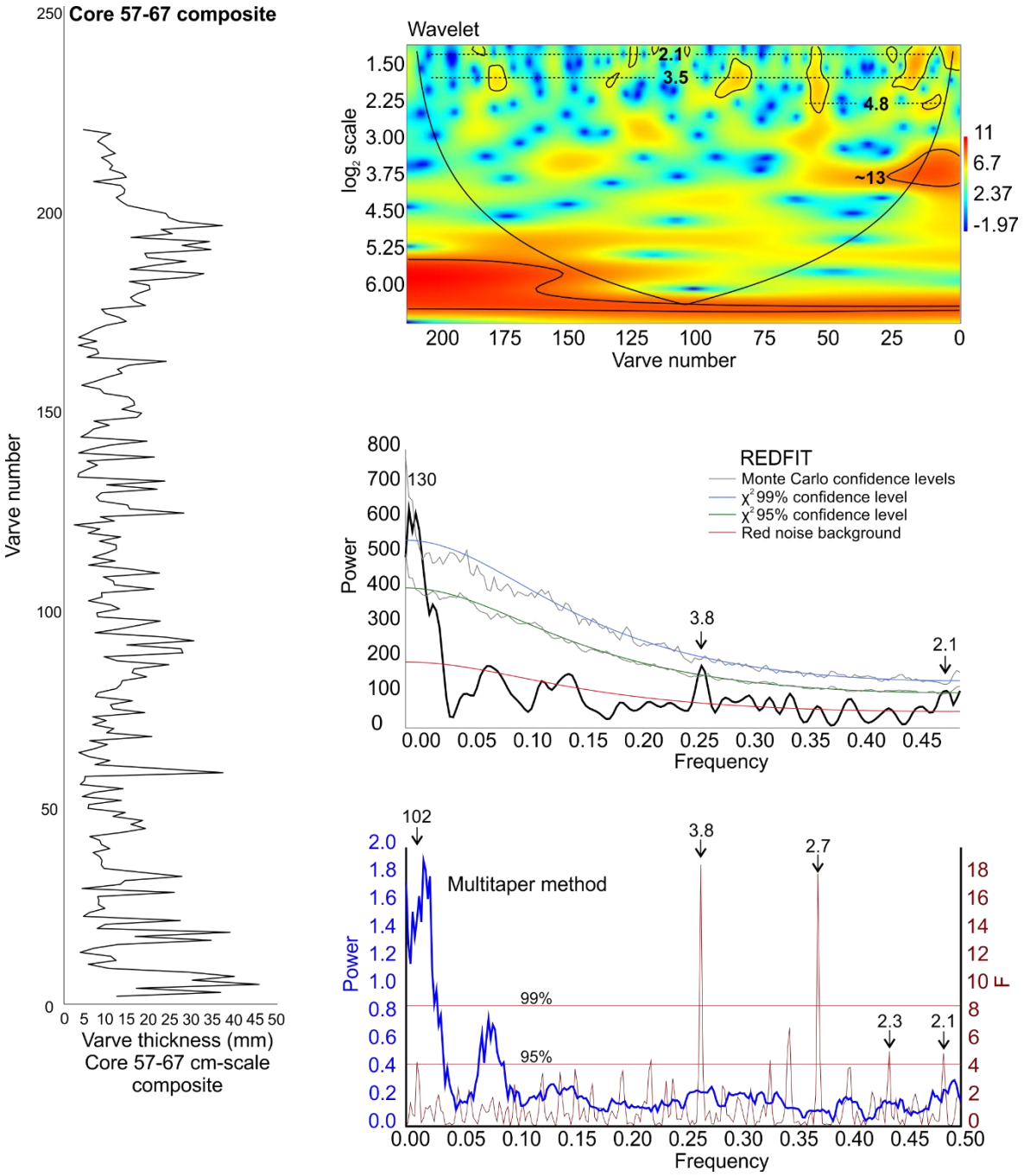

Figure 6.6: Spectral estimation results for the cm-scale varve Core 57-67 composite sequence. Left: the varve thickness sequence. Top: Wavelet analysis with cone of influence and black contours showing P<0.05 significance. Middle: REDFIT power spectrum with chi-squared background (red), 95% (green) and 99% (blue) confidence levels, and Monte Carlo 95 and 99% confidence levels (grey). Bottom: Multitaper method spectrum (blue) with F-test peaks (brown) and 95% and 99% F-test confidence levels (red). For all spectral estimation panels, significant periods are given in varve years.

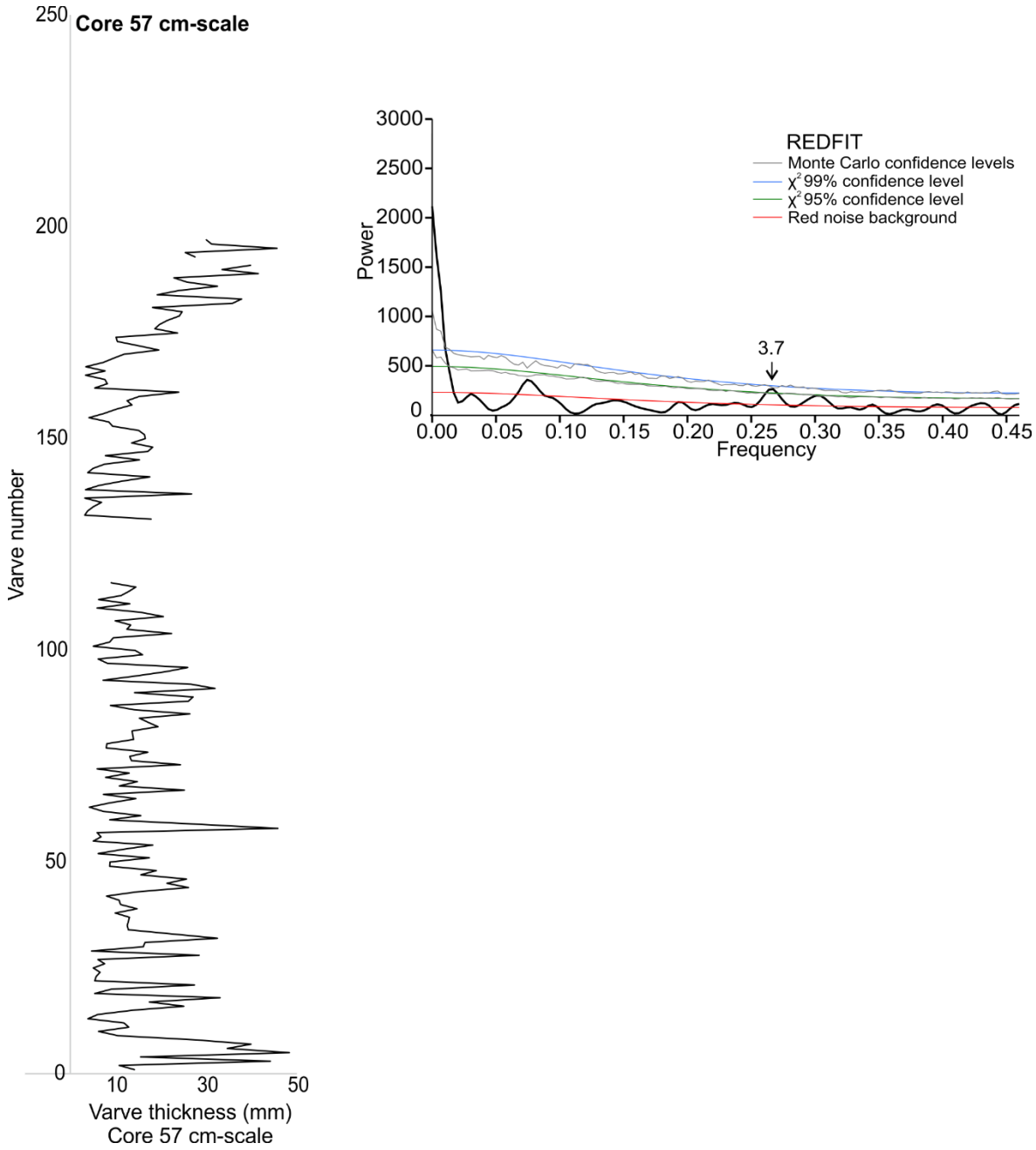

Figure 6.7: Spectral estimation results for the cm-scale varve sequence in Core 57. Left: the varve thickness sequence. Right: REDFIT power spectrum with chi-squared background (red), 95% (green) and 99% (blue) confidence levels, and Monte Carlo 95 and 99% confidence levels (grey). Significant periods are given in varve years.

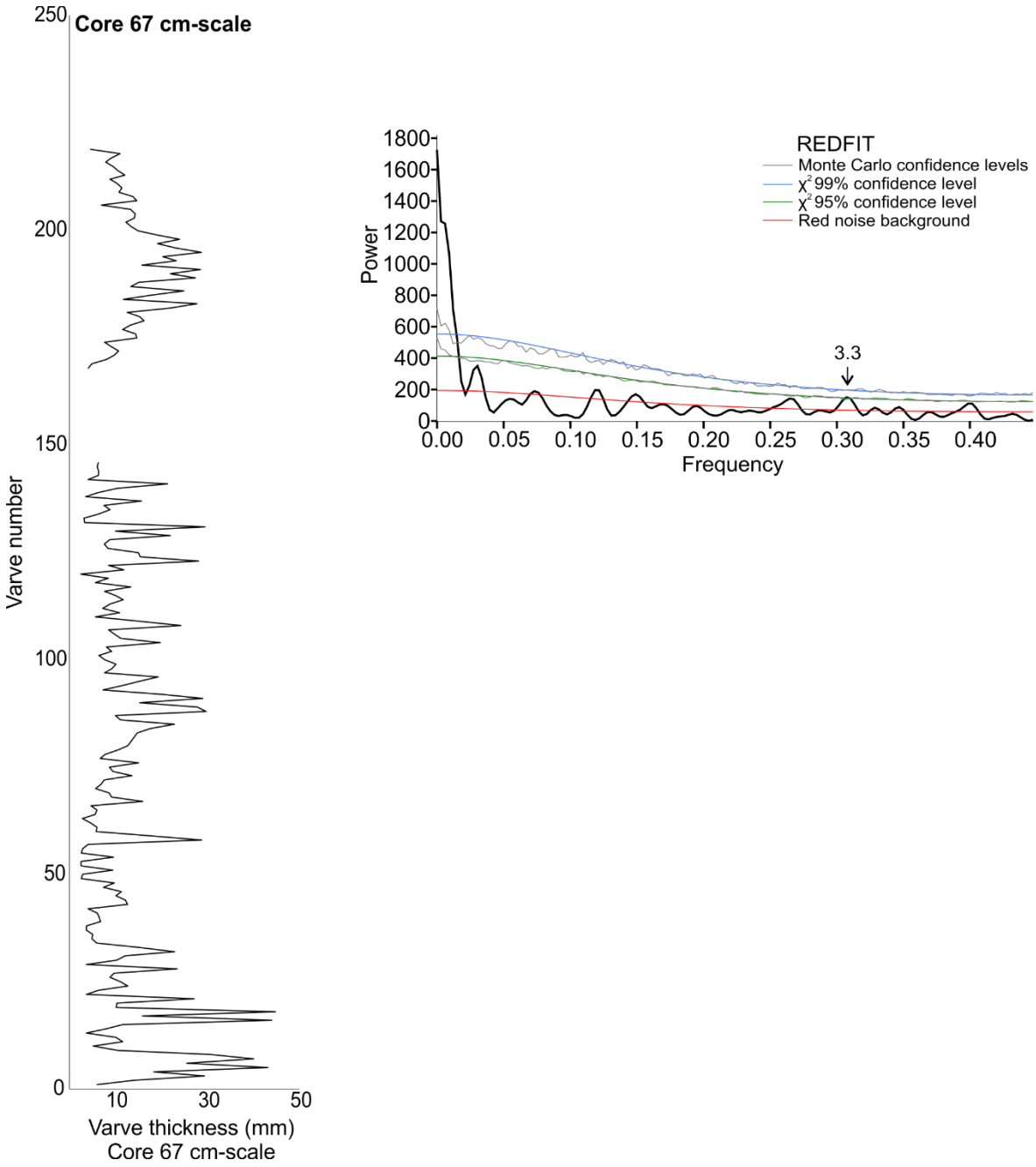

Figure 6.8: Spectral estimation results for the cm-scale varve sequence in Core 67. Left: the varve thickness sequence. Right: REDFIT power spectrum with chi-squared background (red), 95% (green) and 99% (blue) confidence levels, and Monte Carlo 95 and 99% confidence levels (grey). Significant periods are given in varve years.

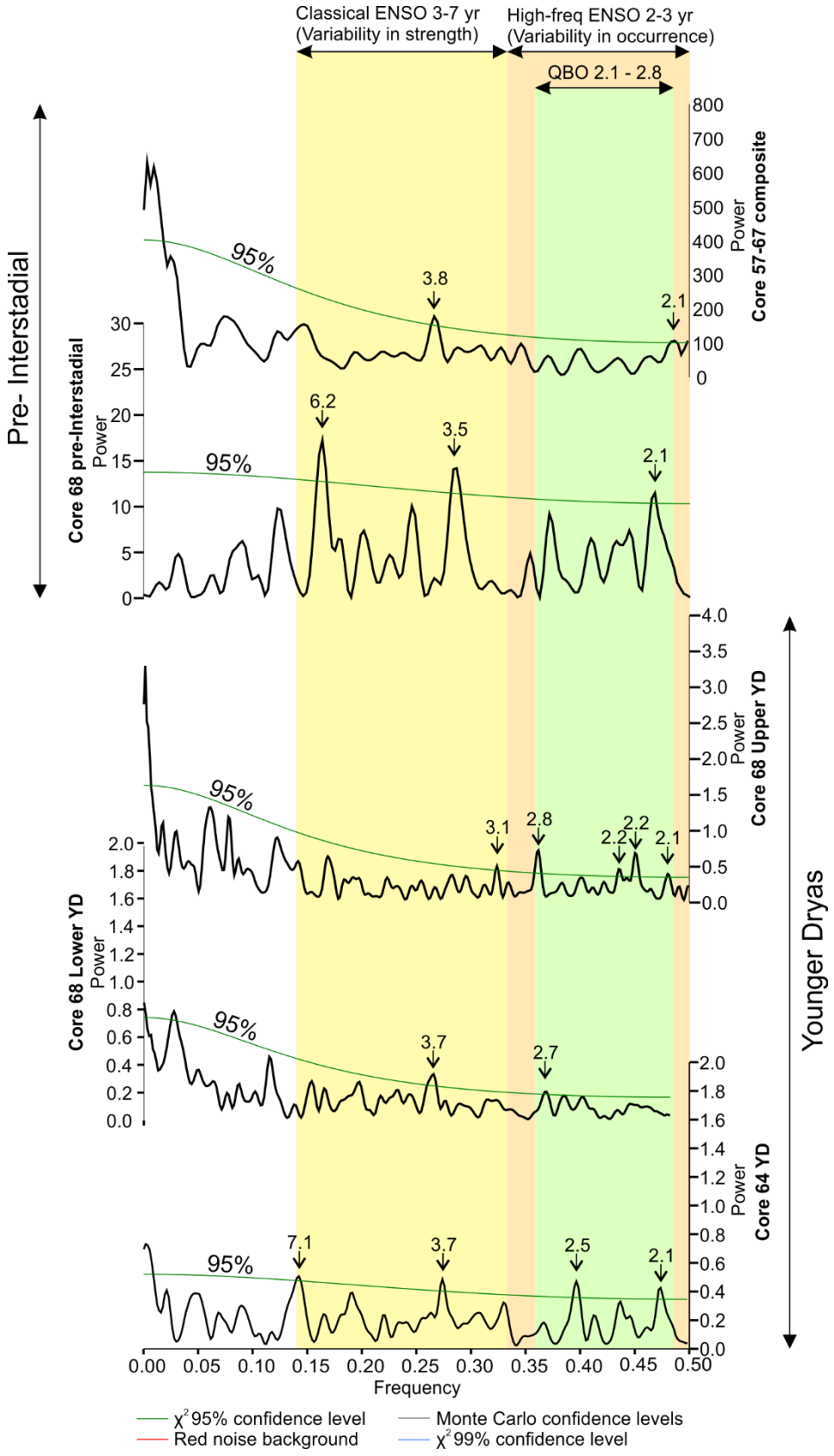

Figure 6.9: Summary of the periodicities present in the main varve sequences, with only the chi-squared 95% confidence limit from the REDFIT method shown for clarity. Different potential climate drivers are shown for certain periods: El Niño 'classical' 3 – 7 yr period (yellow); El Niño 'high-frequency' period (orange); Quasi-Biennial Oscillation (green).

6.5 Discussion

It must first be noted that no method of spectral estimation can produce the true spectrum of a time series. Each method produces a 'best estimate' with its own advantages and limitations. Therefore, even mathematically significant spectral peaks may not have arisen from real climatic processes. This discussion will treat all significant spectral peaks as if they have a climatic basis but the above caveat still holds.

6.5.1 Common climate drivers in the North Atlantic

Many of the statistically significant periods present in the spectra fall into frequency bands commonly seen in NH datasets ranging from sea surface temperature data (Mann and Park, 1996) to tree ring thickness (Cook et al., 1998).

6.5.1.1 El Niño – Southern Oscillation

El Niño is a sea surface temperature phenomenon where warm (El Niño) or cool (La Niña) water spreads from the eastern Equatorial Pacific westwards; the Southern Oscillation records a surface air pressure see-saw between east and west Pacific. Both phases of the El Niño-La Niña oscillation can have strong teleconnections around the world via the stratosphere; for example increased pressure from the poles to 50^{o}N in European late winter during the El Niño phase promotes cold dry conditions over Northern Europe (Ineson and Scaife, 2008). The high-frequency periodicity of ENSO is typically 2.1 – 3. yr, and reflects the interannual variability in the occurrence of El Niño years and La Niña years, whereas the 3 – 7 yr 'classical' periodicity reflects variability in the strength of such events (Allan, 2000; Ribera and Mann, 2002) There also exists decadal- scale variability within the modern ENSO records, of 12 – 14 yr (Jevrejeva et al., 2004).

6.5.1.2 Quasi-Biennial Oscillation

The Quasi-Biennial Oscillation is a phenomenon comprising alternate bands of westerly and easterly wind which propagate downward through the stratosphere, with a complete oscillation taking between 2 and 3 years (Baldwin et al., 2001; Ebdon, 1960). In the stronger easterly phase, cold anomalies in Northern European winters are more common through polar vortex disruption (Holton and Tan, 1980; Thompson and Wallace, 2001), although its

effect on European summer is more tenuous. The mean period for the QBO is 2.3 yr, but observations over the 1953 – 2008 period indicate an association with El Niño whereby the QBO period to varies from 2.1 yr in El Niño years to 2.7 – 2.8 yr in La Niña years (Camp and Tung, 2007; Taguchi, 2010).

ENSO- and QBO- band variability is commonly seen in the North Atlantic Oscillation (NAO) index (Thompson et al., 2002) (an index of the pressure 'see-saw' between Iceland and the Azores in the modern day, and which is a good indicator of European weather patterns), due to wave transmission via the stratosphere to high latitudes affecting the tropospheric North Atlantic by interaction with the polar vortex (Jevrejeva et al., 2004). Although in pre-Holocene times the NAO may not have existed due to the presence of expanded sea ice and a more southern polar front, or large Northern Hemisphere ice sheets, it is likely that a similar pressure see-saw operated in the Atlantic region. It has been shown that ENSO, or ENSO-like variability, existed in the LGM and the post-LGM Pleistocene, but that ENSO variability was amplified at the LGM but damped in the mid-Holocene (Koutavas et al., 2002; Koutavas and Joanides, 2012; Rittenour et al., 2000)

6.5.2 Pre-Interstadial sequences

The pre-Interstadial varves (Core 57, Core 67, Core 57-67 composite, and Core 68 cm-scale) formed in a proglacial environment, as the Lake District ice cap retreated from the Windermere catchment. The main control on varve thickness was glacial melt, itself controlled by melting degree-days, a function of summer temperature. The regional environment of the time consisted of retreating ice sheets.

Assessments of past El Niño variability using planktonic foraminifer palaeotemperature proxies in deep sea cores from the Equatorial Pacific have yielded conflicting results, with some advocating strengthened (Koutavas et al., 2002; Koutavas and Joanides, 2012) and others reduced (Leduc et al., 2009; Martínez et al., 2003) El Niño activity at the Last Glacial Maximum. A more comprehensive recent investigation based on single foram analysis finds reduced El Niño variability corresponding to the reduced LGM equatorial Pacific zonal SST (Ford et al., 2015). An isotope-enabled earth system model reconstruction gives results consistent with the foram studies, confirming reduced ENSO variability at the LGM (21 ka), questioning the validity of total variance temperature reconstructions such as those

of Koutavas and Joanides, (2012) but validating those based on thermocline dynamics (Zhu et al., 2017).

Continued existence of the ENSO signal throughout the Lateglacial Interstadial through to the Holocene is evidenced (Rittenour et al., 2000; Zhou et al., 2001). We would therefore expect to detect an ENSO-like signal in the pre-Interstadial varve time series. However, periods between 4 – 7 yr in the Core 57-67 composite are non-existent. There is evidence from a New England varve sequence that shows a near absence of 3.5 – 5.5 yr periodicities between ~15.2 - ~13.5 cal ka BP (Rittenour et al., 2000), attributed to astronomical forcing causing reduced ENSO variability (Clement et al., 1999). The presence of some more ENSO-like signals in the Core 68 record appears to contradict this finding, although it must be noted that the site of Core 68 was fed by six tributary valleys, and in the modern day there are smaller up-catchment lakes which may have a ponding effect, such that the Core 68 signal is more complex and may not reflect simple climate variation. Additionally, the Core 68 record is shorter, starting later than the South Basin cores.

6.5.3 Younger Dryas sequences

The Younger Dryas varves (Core 68 and Core 64) formed in an ice distal environment. In Scotland, the large ice cap, which re-nucleated at the onset of the Younger Dryas, had started to retreat by ~12.5. ka, and had fully disappeared by 12.2 ka (Ballantyne, 2012; Bromley et al., 2014). Although ice was also present in the catchment for at least the early part of the YD (Brown, 2009; McDougall, 2013, 2001; Sissons, 1980; Wilson, 2004; Wilson and Clark, 1998), it is also likely to have fully melted well before the onset of the Holocene.

On a smoothed scale, increased varve thickness seems to be a function of regional temperature controlling sea ice extent, which controls how much warm moist air reaches the UK for precipitation.

The Younger Dryas sequence significant periods fall mostly between 2 – 4 yr. In the lower YD, longer periods include 6 and 35 yr. In the Core 64 (mid-YD) record, periods of 7 and 22 yr exist, and in the upper YD record of Core 68, periods of 6, 8, 12, and 16 yr are present.

The periods of 2.1 – 2.8 yr are commonly attributed to the quasi-biennial oscillation (QBO). In the modern day, the eastward phase of the QBO coincides with a weakened Atlantic jet stream and colder winters in Northern Europe and the eastern USA. During the Younger Dryas, sea ice expansion had pushed the polar front southwards (Isarin et al., 1998). It is

unclear if and how this affected the QBO, although the prevalence of these short periodicities may indicate that the QBO continued to operate in some capacity during the Younger Dryas.

The periodicities between 3 and 7 yr are within the ENSO band. It is thought that ENSO, or a similar mechanism, was in operation in the Younger Dryas, and exerted some control on interannual precipitation conditions in Europe (Zhou et al., 2001). The presence of longer-period ENSO-band periodicities (3.5 - 7 yr) in the lower Younger Dryas time series suggests that interannual variability of ENSO event magnitude had become amplified again (in contrast with the pre-Interstadial time series). A loss of power in the time-evolutive spectrum in the upper Younger Dryas (in particular in the 3 – 7 yr band) may indicate a return to damped interannual variability into the Holocene (Clement et al., 1999; Rittenour et al., 2000). However, since the position of the polar front changed so significantly throughout this period, that it is impossible to pinpoint whether these changes in 3.5 – 7 yr variability reflect changes in ENSO or just changes in how ENSO teleconnections and QBO-related winds might have interacted with northern European weather systems.

6.5.4 Validation

In order to scrutinise further the significant peaks found in the varve sequences, the thickness data for the four evenly-spaced sequences were re-shuffled before undergoing further spectral analysis using the REDFIT method. After re-shuffling the data, the spectra for the four sequences lose most of the power from the lower-frequency peaks (in effect, becoming more 'whitened'). In all four sequences, periods in the 2 – 4 yr band are still common. However, significant periods also appear in all four sequences between 4 and 7 years (especially 4 – 5) despite this period not being significant in the original 57-67 composite sequence. In the longer period band (> 7 yr), the reshuffled Younger Dryas sequences have significant periods at 22 – 26 yr and in the pre-Interstadial sequences at 10 - 12 yr. In the original spectra, the YD sequences have their longer periods at 12, 16, and 35 yr, unlike the reshuffled spectra. The pre-Interstadial original spectrum for Core 68 does not have significant periods longer than ~6 yr (unlike the reshuffle), and in the 57-67 composite the original and reshuffled significant periods are ~13 and ~10 yr respectively.

In summary, the reshuffled datasets show that many of the higher-frequency (<5 yr) significant peaks could still have arisen by chance (as might be expected), and should be

interpreted with some caution, but that the absence of any 4 – 7 yr peaks in the Core 57 - 67 composite spectrum is most probably real.

- Shorter periods- common, noise- but in nature the 'noise' at these periods can still be caused by real cycles

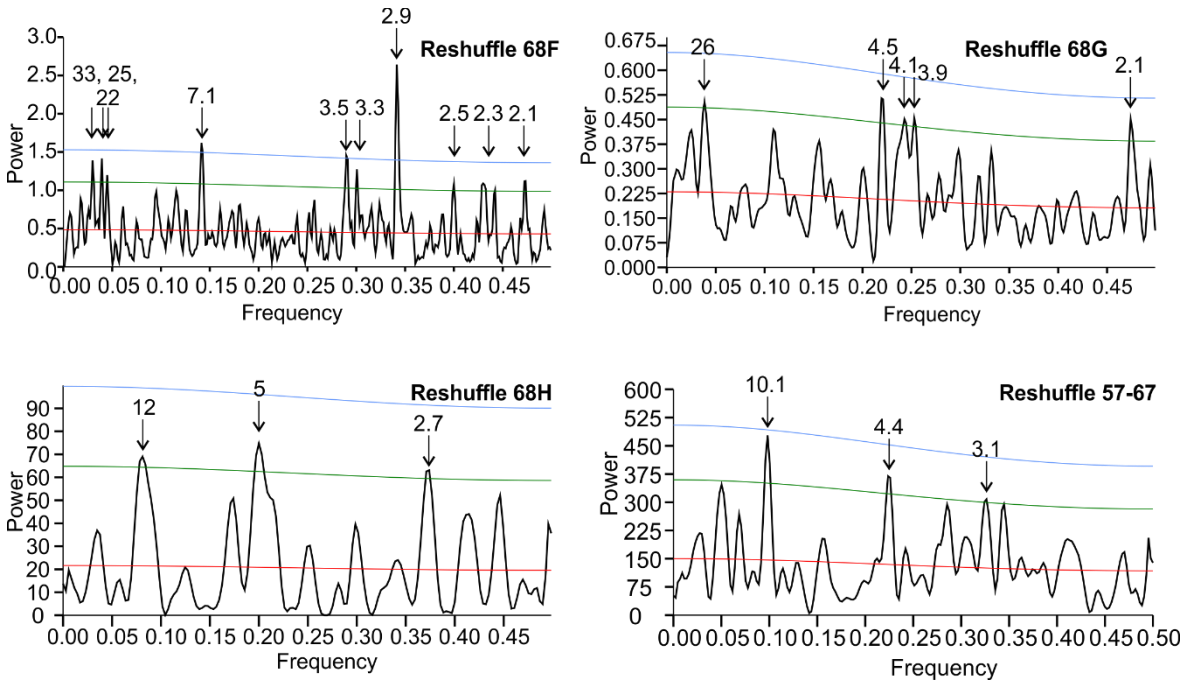

Figure 6.10: REDFIT spectra for selected reshuffled varve thickness sequences, with chi-squared background (red), 95% (green) and 99% (blue) confidence levels. Significant periods are given in varve years. .

6.6 Conclusions

Several varve thickness timeseries underwent spectral estimation using the REDFIT, Multitaper, and wavelet methods in order to identify which, if any, interannual to decadal climate oscillations were influencing controls on sedimentation in the pre-Interstadial periods and the Younger Dryas. Significant peaks were common in all the records from 2.1 – 3.8 yr, which may be interpreted as arising from interactions of the QBO and/ or El Niño with the polar vortex. Periodicities from 4 – 7 yr, which reflect interannual variability in the strength of ENSO events, are present in the Younger Dryas-age time series but not the pre-Interstadial, which supports evidence that the strength of El Niño variability was damped at this time. Longer periods (>7 yr) are present in some records and may represent known cycles (e.g. the Hale cycle, 22 yr, and longer-period El Niño variability, 12 – 14 yr), although

superposition of noise could also have produced these peaks. Reshuffling the data for a selection of the time series shows that periodicities < 5 yr are common even in a synthetic timeseries and should be interpreted with some caution, although evidence for the absence of periodicities 4 – 7 yr in the pre-Interstadial composite time series appears robust.

.

7. Conclusions

In this chapter, the main findings of this thesis are summarised, the overall deglacial history of Windermere is discussed, and recommendations of further work are made, based on the limitations of this research.

7.1 Restatement of Study Objectives

The overarching objective was to use the cores to develop new insights into the deglaciation of Windermere and place this in the context of the deglacial history of the British and Irish Ice Sheet and North Atlantic climate change. To this end, several sub-objectives have been identified:

- To provide a chronology and develop age models for the cores using the full range of available methods including radiocarbon dating, tephra, varve counts, and palaeomagnetic methods.
- To construct a new palaeomagnetic secular variation (PSV) record from the four main Windermere cores with a view to updating the UK PSV curve of Turner and Thompson (1981).
- To analyse and synthesise the overall stratigraphy and sedimentology of the deglacial sediments in order to reconstruct and correlate the key climatic transitions and processes operating during deglaciation.
- To develop varve chronologies in order to improve understanding of the timing of the different phases of the Lateglacial period.
- To analyse time series of varves and develop records of seasonal through centennial scale and examine evidence for variations in the drivers of interannual variability during deglaciation.

By synthesis of all available data, to produce a new model for the deglaciation of Windermere and relate this to the overall deglacial history of the North Atlantic region.

7.2 Summary of key findings

A series of coring campaigns in Windermere has yielded several sediment cores which contain sediment ranging from post-LGM to the modern day, and which record sedimentological changes throughout this period. The Holocene is covered in a separate thesis, Fielding 2017.

The results from Chapters 2 to 7 are summarised below.

In Chapter 2, the overall stratigraphy of the cores is discussed. The methods used to analyse the cores are also detailed.

In Chapter 3, the palaeomagnetic signal of the sediments is discussed. Although the whole core sequence was measured, only the Holocene sediments had magnetite as the primary magnetisation carrier and thus reliable directional results. These results have facilitated the construction of the first Holocene PSV curve for the UK since 1981. This curve (WINPSV-12K) may now be used in geomagnetic models and as a dated stratigraphic tool for other palaeoclimatic archives in the region. Comparison of WINPSV-12K with other PSV records from the northern North Atlantic (NNA) region shows many similarities on timescales of 1 – 3 kyr, and comparison of NNA records with those from the North East Pacific and East Asia reveals behaviour of the high-latitude flux lobes of the Earth's magnetic field trough the Holocene.

In Chapter 4, the sediment sequences from the bases of the cores up to the Lateglacial Interstadial are examined. The South Basin cores exhibit cm-scale varves, and seismic reflection profiles through South Basin depocenters indicate that a potential further ~2200 yr varved sedimentation may be present below the recovered cores (although the number is likely fewer). The ice in the Windermere valley at this time is interpreted to form a southern lobe of the Lake District Ice Cap. Varve thickness measurements through the pre-Interstadial interval show that Cores 57, 67, and 64 likely shared the same sediment source (the Trout Beck Valley), and that the location of Core 64 remained ice-proximal until ~75 yr before the onset of the Interstadial. The location of Core 68 was fed by the catchments to the north of the lake (Langdales, Grasmere, and Rydal) which comprised six tributary valleys and thus more complex sedimentation. Varve thickness measurements show that the location of Core 68 stopped being proximal to its ice source before that of Core 64, thus the Trout Beck and the 'Northern' ice masses acted independently and the Lak District Ice Cap separated from the 'Northern' ice mass before the Trout Beck ice mass. Varve

sedimentology also shows that the cessation of varves in Cores 57, 67, and 64 occurred within 23-61 vyr of the vegetation of the lake catchment (as evidenced by higher bioturbation and inwashed coarse silt clasts in the varves), whereas in Core 68 it was ~100 yr as there would have been more high-elevation ice present in the 'Northern' catchments at the valley heads.

In Chapter 5, the Younger Dryas- age varves are examined. Most of these varves have been removed by erosion in Cores 57 and 67, so the focus is on Cores 64 and 68. In Core 68, varves are usually definable, whereas in Core 64 most of the varves are thinner and more bioturbated, likely due to the greater lakebed depth of Core 68. Varve thickness increases are hypothesised to represent possible locations of the Mid-Younger Dryas Transition, as cold, dry, storm tracks shifted north with the retreating polar front and precipitation-bearing air moved over the UK. The latest Younger Dryas sediments are typified by much thicker (~3.5 mm) varves with instances of moderate to heavy bioturbation, interpreted as representing the onset of warmer conditions and heightened nival melt. The smoothed composite varve thickness record appears to broadly co-vary with NGRIP $\delta^{18}O$ data after 12200 yr BP, showing that the UK and Greenland may have formed part of a regional climate system as sea ice retreated to a more modern-day scenario, but the lack of dating precision on the Windermere varves makes proof impossible.

In Chapter 6, varve thickness sequences from the Younger Dryas and the pre-Interstadial sediments were selected for spectral analysis using the REDFIT, Multitaper, and wavelet methods. Significant periods shorter than 4 yr were common in all of the records (associated with the QBO and high-frequency El Niño), whereas the period of 4 – 7 yr was absent in the South Basin pre-Interstadial composite sequence. This is in keeping with a weakened El Niño signal from the LGM to ~14 ka. Reshuffling the data showed that periodicities < 5 yr are common in the reshuffled time series and should thus be interpreted with caution in the natural data sets; however, the data reshuffle also verified the absence of the 4 – 7 yr periods in the pre-Interstadial composite.

7.3 Deglacial History of Windermere

Glaciolacustrine sedimentation in Windermere started to occur in the Mystery Interval, likely > 17 ka. The presence of seven recessional moraines in the South Basin represents several still-stands during recession. Following this, approximately 250 vyr before the onset of the Lateglacial Interstadial, ice retreated rapidly up the North Basin within a few decades. Sedimentation in the northern part of the North Basin was controlled by the 'Northern Catchments', but sedimentation further south was controlled by the Trout Beck Valley. Within ~250 yr of the onset of sedimentation in the northernmost part of the lake, the catchment had become vegetated and glacial and nival sedimentation had ceased in all but the most northerly part of the lake.

Vegetation heralded the onset of the Lateglacial Interstadial from ~14.7 ka until ~12.9 ka (not Windermere-specific dates). The Lateglacial Interstadial was characterised by catchment vegetation, and inwash of *Ellerbeckia* sp. From Cunsey Beck. Lake overturn was present.

The climate returned to the near-glacial conditions of the Younger Dryas at ~12.9 ka (not a Windermere-specific date). The early Younger Dryas conditions at Windermere were cold and stormy, but as the regional sea ice extent decreased, the Atlantic storm tracks moved north and the windiness decreased. Warmer, precipitation-bearing air masses moved over the UK at around 683 vyr after the onset of the Younger Dryas. The onset of the Holocene saw an increase in precipitation and also vegetation and lake biota, and an end to paraglacial conditions in the lake catchment.

7.4 Future Work

7.4.1 The Lateglacial Interstadial

The Windermere core suite underwent detailed sediment analysis, which has yielded myriad results. However, a period that was studied in somewhat less depth was the Lateglacial Interstadial. Some of the major features of the period were identified and interpreted (e.g. the *Ellerbeckia* sp. diatoms), but further study would be highly beneficial. For example, a thorough species assemblage construction and analysis from both deep-

water and shallow-water depocentres would build on Pennington's work (e.g. organic content, diatoms, Chironomids, pollen etc.). Given the time-consuming nature of these studies (in particular Chironomid separation and identification), a thorough investigation of the Lateglacial Interstadial in Windermere could be carried out as a separate PhD project.

7.4.2 Further coring

A coring campaign in April 2012 yielded several piston and gravity cores. These were augmented by coring campaigns in May 2014 (gravity cores) and August 2014 (Livingstone cores). Whilst these three core suites yielded a trove of data, they only represent one lake. Other countries have pursued systematic lake and ice coring programmes, or have at least benefitted from extensive lake research, whilst the UK has a paucity of post-LGM to early Holocene lake data despite a number of promising water bodies. In comparison to these other areas (e.g. Canada, Greenland, Iceland, Scandinavia, Germany, Siberia, and the Carpathians), further lake coring in the UK could bring a wealth of new deglacial and palaeomagnetic data to the post-LGM debates. The Lake District itself hosts many deep lakes as well as scores of tarns, whilst the Scottish Highlands host plenty of promising lochs that may yield extensive varve sequences similar to that of Windermere.

Secondly, the piston cores taken in April 2012 in the Windermere coring campaign were not taken with overlapping sections so that core-gaps existed and composite sections could not be produced. Despite producing much useful data, this problem has prevented a full, continuous chronology from being produced from any singly site. Furthermore, a lack of multiple cores and overlap at individual sites has limited the scope for further investigations of the current cores. This study provides the basis and motivation for a second coring campaign in Windermere, in the South Basin focussed on the 50 m deep cm-varve depocentre from HS1, and in the North Basin aimed at recovering complete Younger Dryas laminated sections. Such an endeavour would cement Windermere as a key palaeoclimate archive in the Northern Hemisphere.

Appendix A: Radiometric Results and age models

A.1 Radiocarbon

The radiocarbon dates were calibrated using Calib 7.1 (Stuiver and Reimer, 1993) and the Intcal13 calibration curve (Reimer et al., 2013). The radiocarbon results are reported in Table 7.1, with ages given as reported conventional radiocarbon age, reported age uncertainty, the calibrated median probability age, and both the 1σ and 2σ calibrated ages. Additionally a column indicates whether each date is reliable (Y/N). Only dates which were thought to be reliable (i.e. not within a mass transport deposit, or not unreasonably young or old with respect to surrounding dates and both visual and instrumental stratigraphic markers) were used in the construction of age models.

The radiocarbon results verified the stratigraphic inference that the organic-rich upper layer was the Holocene, and strengthened the inference that the terrigenous laminated clays and silts directly below were formed during the Younger Dryas (Figure 2.2). Most of the dates which were taken from the stratigraphic unit defined by Pennington as the Windermere Interstadial (Coope and Pennington, 1977) are thought to be too old due to carbon reservoir effects during this time period (and indeed Pennington's own dates may also suffer from this), coming out as 16 – 18 cal ka BP. The BIIS is thought to have covered the Lake District at 18 cal ka BP, and the main evidence for the Lake District being ice-free at 17 cal ka BP is the dates of Pennington (Coope and Pennington, 1977). One date from near the top of this more organic-rich unit in Core 68 comes is reported as 13497 $\pm$ 77 (2σ) cal a BP which is in keeping with the widely-reported age of the start of the Younger Dryas of 12.9 cal ka BP so this date has been accepted.

Sections of sediment containing mass transport deposits (MTDs) were removed from the depth records prior to the construction of a 'normal sedimentation' age model.

It should be noted that the radiocarbon results could have been interpreted with greater confidence had the microfossils in question been fine organic particles, such as blossoms. Since blossoms degrade quickly in the environment (i.e. within the year) and are only preserved when in sediment, the use of blossoms would have strengthened the assumption that preservation in sediment occurred immediately after the fossil died. The use of leaf fragments and seeds leaves open the possibility that the fossils could have stayed within the catchment area for some time prior to sedimentation. Theoretically there is potential for

some of the dates to be 'ground-truthed' in future by the radiocarbon dating of some blossom microfossils at some of the sampled depths.

Core	Depth, cm	Sample no., SUERC	Type	Mass, mg	Reported age, 14C y BP	Error, 14C y BP	Median Probability age, cal y BP	Min. 2σ	Max. 2σ	Min. 1σ	Max. 1σ	Reliable?	Reason for unreliability
										689	745		
57	29.2	62197	Leaf	20	817	37	728	678	790	753	758	N	Too close to core top
57	72.3	64862	Wood	4200	1739	37	1651	1554	1732	1609	1703	Y	
								2737	2809				
57	86.0	62199	Leaf	90	2646	37	2765	2813	2844	2745	2780	Y	
								5912	6026				
								6047	6065				
								6077	6116				
57	143.6	62194	Bulk	11000	5227	37	5974	6152	6175	5925	5997	Y	
								8588	8791				
								8829	8865				
								8884	8897	8600	8725		
57	176.6	62208	Bulk	5120	7885	39	8688	8915	8972	8740	8748	Y	
								1083	1160				
67	48.1	62198	Twig	20	1260	35	1214	1172	1282	1179	1262	Y	
								2068	2079	2135	2182		
67	80.2	52714	Leaf	120	2181	35	2199	2110	2315	2237	2304	Y	
										5056	5144		
										5155	5188		
										5214	5224		
										5234	5244		
67	160.4	55686	Leaf	170	4505	35	5168	5044	5301	5260	5288	Y	
								7955	8069				
67	211.2	55684	Leaf	80-	7209	39	8018	8086	8157			Y	

67	228.5	55685	Seed	70	8302	38	9324	9140 9202	9178 9434	9273 9337	9334 9405	Y	
67	257.2	62213	Bulk	10360	10119	43	11750	11409 11476 11599	11435 11553 12003	11620 11686 11892	11681 11826 11929	Y	
67	481	64861	Bulk	9800	14089	44	17134	16943	17376	17027	17230	N	Unreliable carbon reservoir
64	36.0	62195	Leaf	110	972	38	863	793 945	939 953	800 826 901	813 865 931	N	Too close to core top
64	85.0	62194	Leaf	230	2456	37	2544	2363 2628	2620 2705	2384 2432 2565 2586 2632	2387 2539 2568 2617 2699	Y	
64	129.4	62203	Leaf	70	4046	40	4519	4423 4765	4617 4784	4440 4508	4485 4570	Y	
64	170.1	62204	Bulk	10300	5790	35	6591	6491	6673	6549	6654	Y	
64	206.5	62196	Leaf, root	70	8166	38	9103	9013 9160	9153 9255	9021 9184	9135 9191	N	Mass transport deposit
64	219.2	62209	Bulk	13100	10008	45	11489	11280 11660	11653 11709	11355 11387 11520	11378 11507 11609	Y	
68	72.0	64854	Bulk	5000	1114	37	1020	934 1109 1133 1160	1088 1125 1143 1172	975	1057	Y	

68	120.7	64859	Bulk	8000	1708	35	1614	1548	1702	1561 1669	1626 1691	Y	
68	171.4	52708	Leaf	10	2242	37	2232	2153 2288	2277 2342	2161 2178 2301	2169 2244 2330	Y	
68	237.7	52709	Leaf	10	3499	35	3771	3649 3690	3659 3866	3720 3810	3802 3831	Y	
68	329	52710	Leaf	30	5124	37	5862	5748 5843	5830 5939	5762 5887	5809 5923	Y	
68	377.1	62207	Bulk	10600	6468	36	7375	7295 7306	7296 7439	7329 7368 7412	7359 7395 7428	Y	
68	428.2	52711	Leaf & root	20	8653	39	9600	9539	9688	9545 9649	9629 9651	Y	
68	454.4	62206	Bulk	11900	9061	40	10225	10180	10260	10205	10241	Y	
68	493	52712	Bulk	11420	9308	40	10515	10302 10384 10620	10316 10603 10652	10436 10488	10458 10574	N	Mass transport deposit
68	521.7	52713	Bulk	45000	9708	39	11160	10881 11082	10929 11225	11127	11202	Y	
68	531	52713	Bulk	5300	11121	46	13002	12839	13087	12950	13072	N	Old carbon contamination?
68	658	64860	Bulk	10100	11662	41	13497	13422	13574	13451 13506	13498 13545	Y	
68	683	64858	Bulk	9800	15188	46	18459	18316	18603	18384	18603	N	Unreliable carbon reservoir

								4651 4702	4670 4758			
LWB1A	50-54	62215	Bulk	3900	4527	36	4838	4808	4873	2824	4860	Y
										10294	10429	
LWB1B	102-106	62224	Bulk	4120	9222	41	10382	10258	10503	10465	10482	Y
LWB1B	131-135	62214	Bulk	3300	9806	43	11223	11171	11271	11202	11241	Y
										9143 9244	9172 9325	
LWB2B	135-139	62216	Bulk	3800	8279	40	9285	9133	9416	9345	9401	Y
										10741	10810	
								10704	10896	10846	10866	
LWB2B	161-165	62217	Bulk	3800	9542	42	10910	10917	11088	10953	11069	Y
										11410 11479	11431 11482	
								11396	11829	11493	11551	
LWB3	199-201	62223	Bulk	7800	10084	43	11658	11878	11949	11600	11770	Y
LWB3	251-252	62218	Bulk	10200	12095	47	13950	13781	14100	13848	14034	?
LWB3	264-265	62219	Bulk	11900	13746	53	16604	16355	16870	16467	16739	N

Appendix A

Table 7.1**:** Radiocarbon dating table showing all samples and their locations within the cores, the reported radiocarbon age and uncertainty, and calibrated median probability, 1-sigma and 2-sigma ages. Additionally the reliability of each date is shown, where only 'reliable' dates were included when constructing age models

A.2 ^{210}Pb and ^{37}Cs

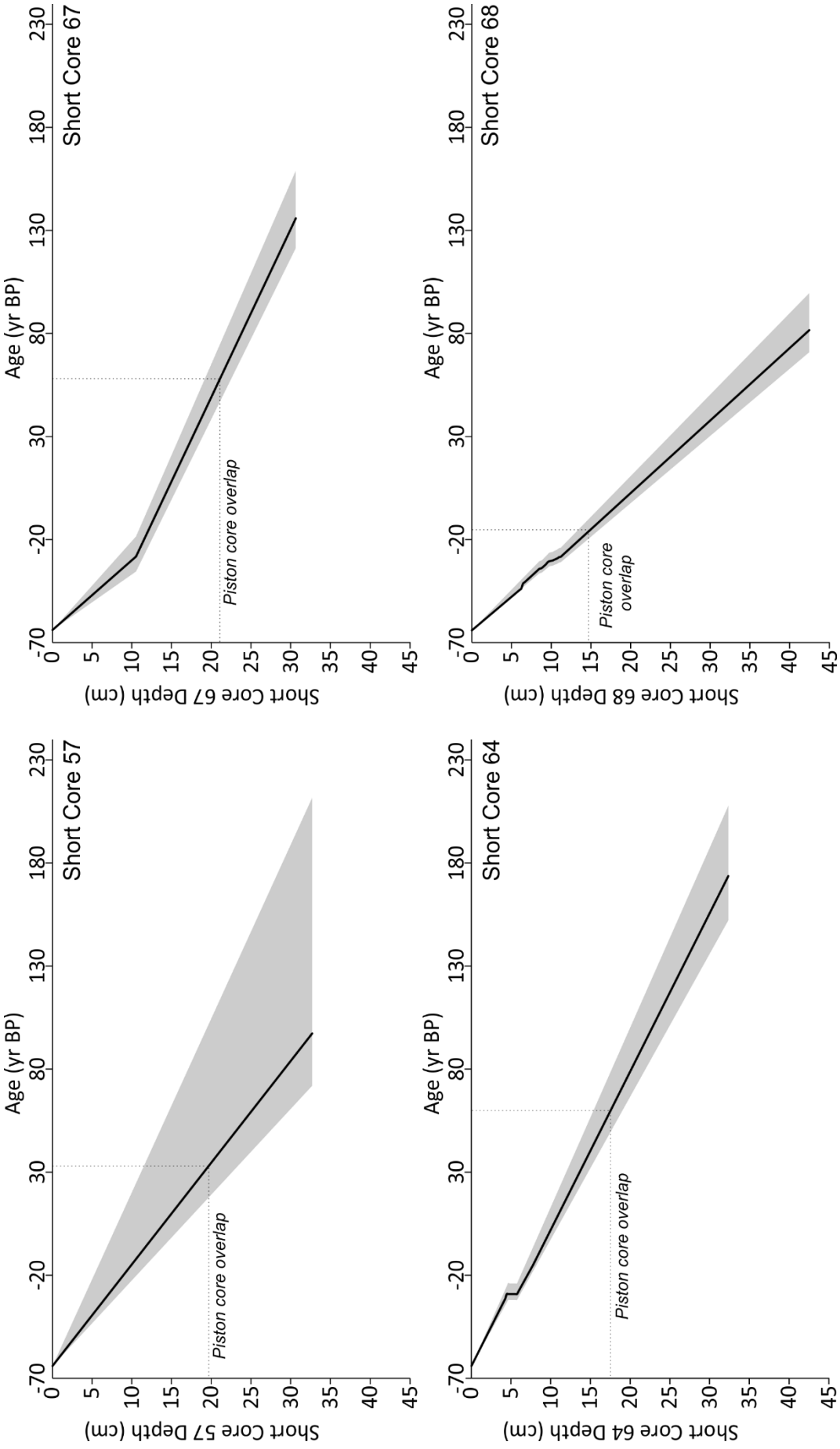

Appendix A

Figure 7.1 ^{210}Pb-decay based age-depth models for the Windermere short gravity cores. The age-depth model was validated using ^{137}Cs bomb-testing peaks in the sediment. More details on age model validation may be found in (Fielding, 2017).

Appendix B: Tephra Results

Only two definitive shards were found. One was in the top 10 cm of 68G, and the other was in the bottom 10 cm of 64C. The shard in 68G was found in a section of varve deformation including some detachments so might not have been in situ, although it would almost certainly have been deposited during the Younger Dryas. If it were in situ it would be amongst varves aged approximately 12.3-12.4 cal ka BP, making it possible that it could have come from the Vedde event if the shard had dispersed downwards through the sediment. The shard found in 64C was within the Lateglacial Interstadial sediment that has poorer age control, but is likely to be between 13.9 and 14.7 cal ka BP, which is in the age range of both the Penifiler and Borrobol tephras. The paucity of shards precluded taking any 1 cm samples or performing geochemical fingerprinting.

None of the ashes mentioned above has yet been found in the Lake District, although the estimated dispersal envelopes for each tephra do include, or pass very close to, the Lake District (Figure 7.2)(Bronk Ramsey et al., 2015). In fact, no Lateglacial Icelandic tephras have been reported south of Scotland in Great Britain. It is possible that regional wind patterns during the Lateglacial skirted towards the north of the British Isles then dispersed upon reaching mainland Europe, although the most likely explanation for the lack of shards is the size and complexity of the catchment.

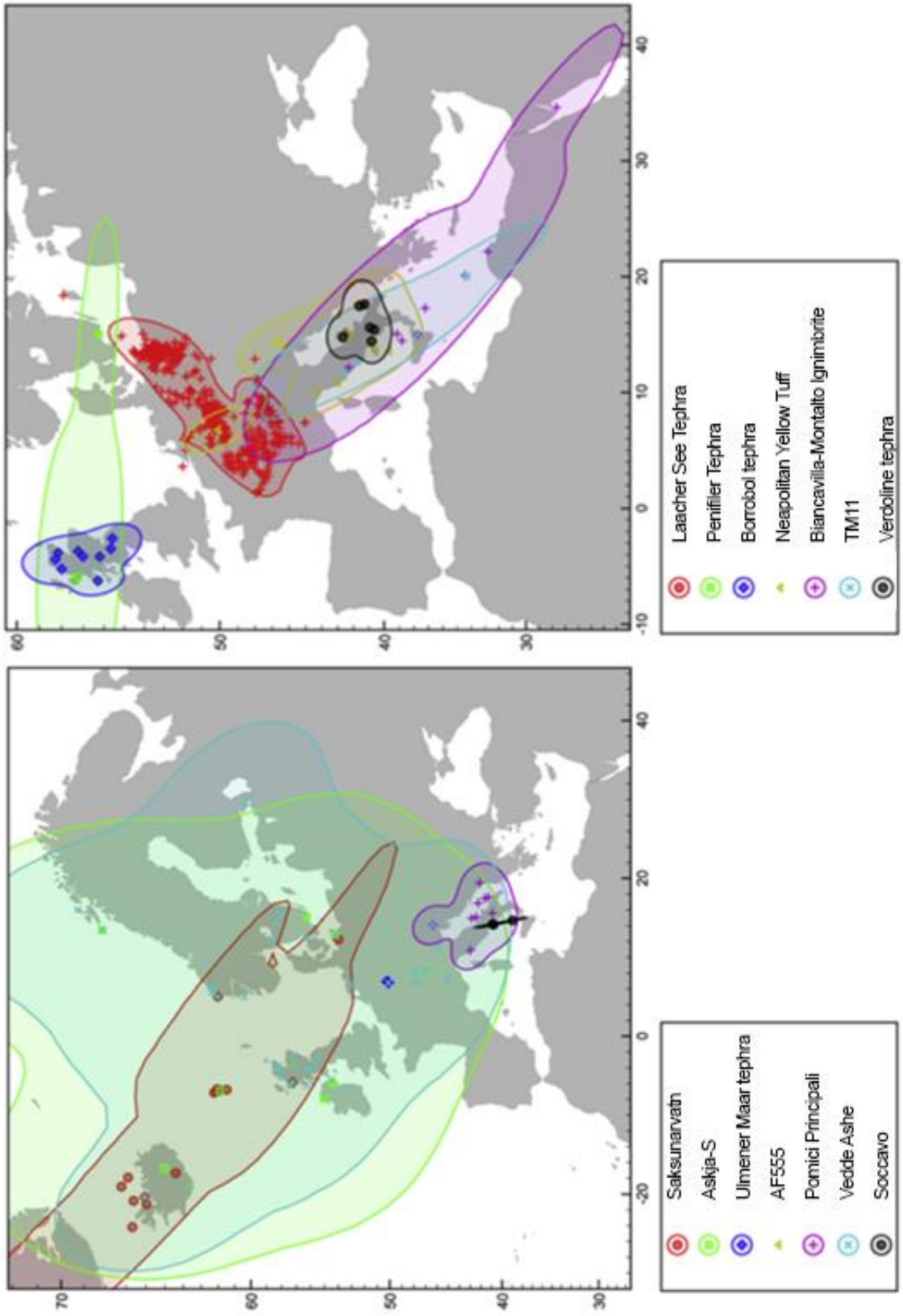

Figure 7.2 Locations of tephra discovery sites (markers) and estimated tephra dispersal envelopes for eruptions from 10 - 12.5 cal ka BP (left) and 12.5 – 20 cal ka BP (right). *Reprinted from QSR 118, Bronk Ramsey et al., Improved age estimates for key Late Quaternary European tephra horizons in the RESET lattice, Page 24, Copyright (2015), with permission from Elsevier.*

Appendix C: Sediment Facies Summary

A summary of the major sediment facies in the cores are given below.

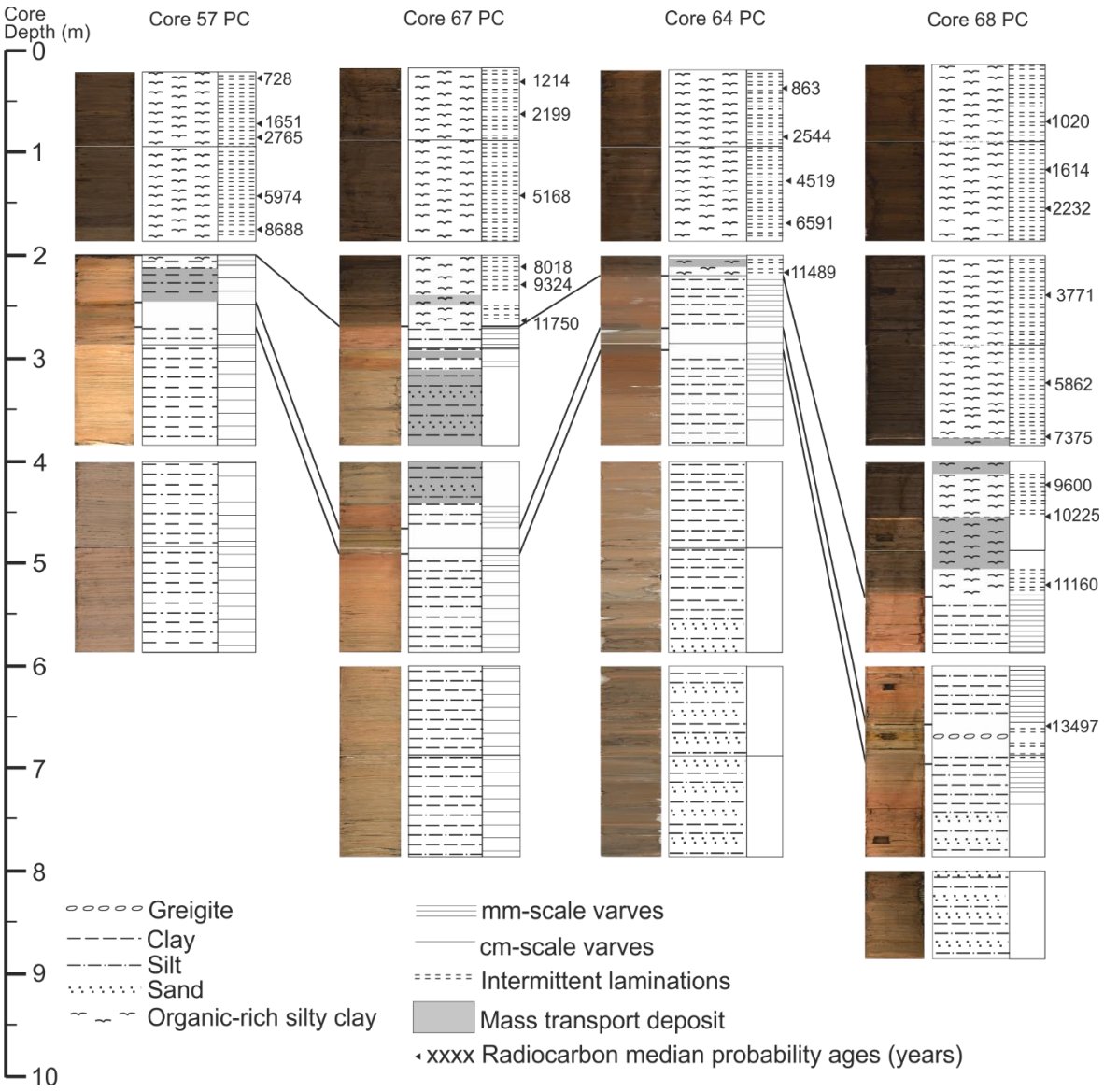

Figure 7.3: Core image (left) and lithostratigraphy (right) of Windermere Cores 57, 67, 64, and 68. Lithostratigraphic tie-points between the cores are included. Sediment ages given are median-probability radiocarbon dates in cal y BP calculated with Calib 7.1 (Stuiver and Reimer, 1993) using the Intcal13 calibration curve (Reimer et al., 2013).

C.1 Organic-rich Sediments

This unit lies above the topmost tiepoint in Figure 7.3. The top part of the long cores is characterised by dark brown, wet sediment with occasional macrofossils present such as leaves, twigs, seeds, roots etc. There are visible mm- to cm-scale laminations present throughout this unit. Mass transport deposits (MTDs) are present in the bottom of this unit, the smallest a couple of cm, and the largest in Core 68 that are 20 and 52 cm thick.

The organic-rich sediment will not be described in detail since this is outside the scope of this thesis. A companion thesis (Fielding, 2017) focusses on the sedimentology and stratigraphy of the Holocene sections of the cores (57A - B; 67A - C; 64A - C; 68A – E).

C.2 Transition Sediments from Silt and Clay to Organic-rich

The transition sediments are shown in Figure 7.4. In Figure 7.3 these sediments are found around the topmost tiepoint. The base of the organic-rich sediments in long Cores 67, 64, and 68 exhibit cm-scale laminations, which vary in colour from yellowish grey to dark brown. These base-organic sediments are almost all paler than the overlying unit and X-radiographs show the majority of the laminations to be denser than the overlying unit, although the yellow laminations are the least dense. The sediment largely comprises pelletised mud, indicative of burrowing organisms. This unit shows a decrease in terrigenous-type elements in the ITRAX data up-core, such as silica (Si), titanium (Ti), iron (Fe), and potassium (K). Many diatoms are present in this unit, including *Ellerbeckia* sp.

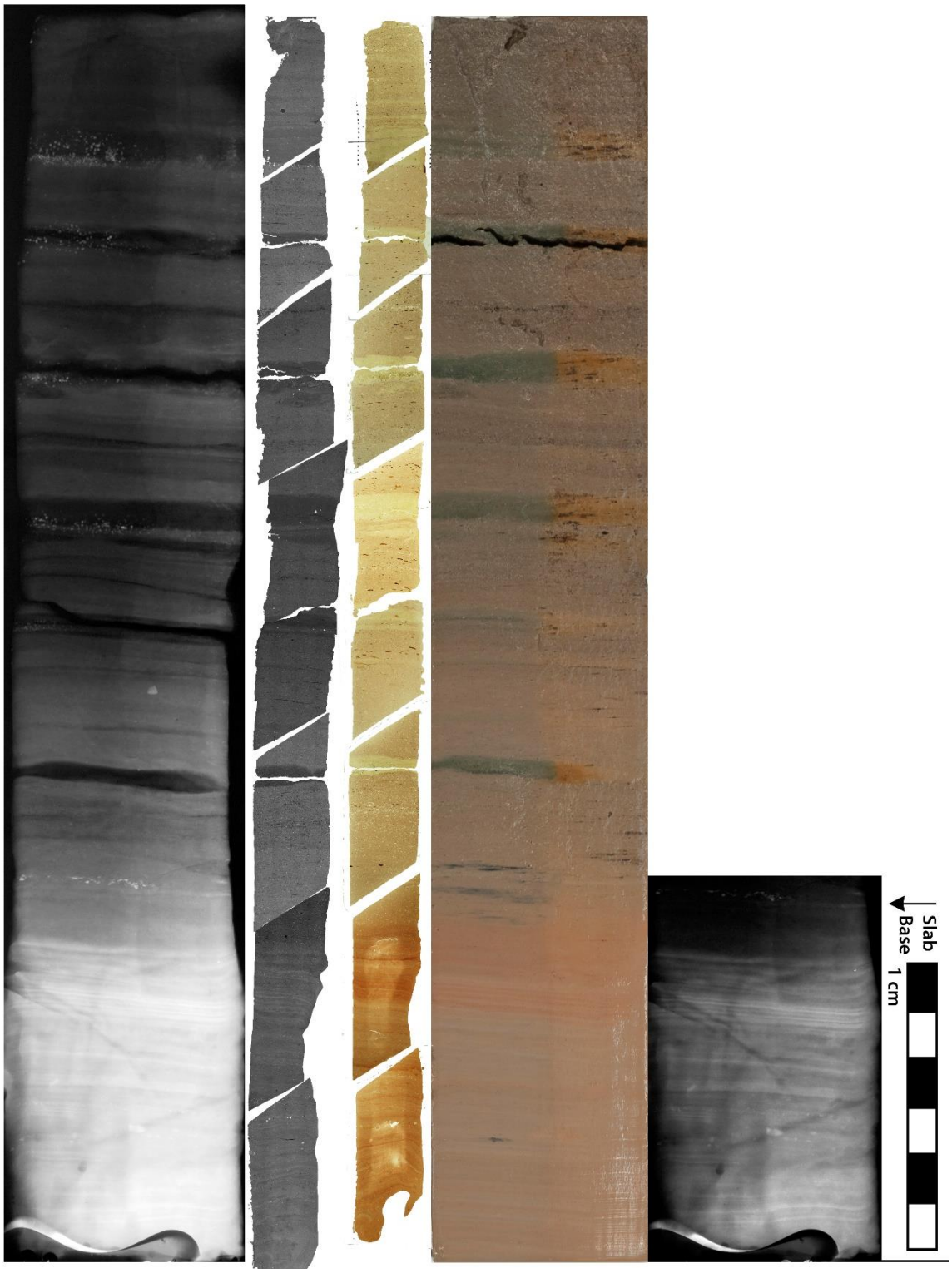

Figure 7.4 Transition sediments macro-scale visualisation. Far left: X-radiograph of slab. Left: X-Scanning electron microscope backscatter image. Centre: covered thin sections. Right: Slab photograph. Far right: X-radiograph segment with different brightness and contrast to show the detail of some denser sediment. This example comes from Core 67.

C.3 Millimetre-scale Laminated Sediments

The sediments directly below the laminated 'transition' sediments are dominated by silt and clay with negligible organic material (Figure 7.5; between top and middle tiepoints in Figure 7.3). The unit is horizontally laminated with alternating greyish silt bases fining into pinkish clay, and with a mean clay-silt couplet thickness of ~1 mm in Core 68, and ~0.5 mm in Core 64. X-radiograph results show that this unit is much denser than the organic units are. Some beds are thicker, around 1 cm. The grains at the bases of the thicker laminations can be seen with the naked eye, usually fine sand or coarse silt fining upwards to clay at the top of the lamination.

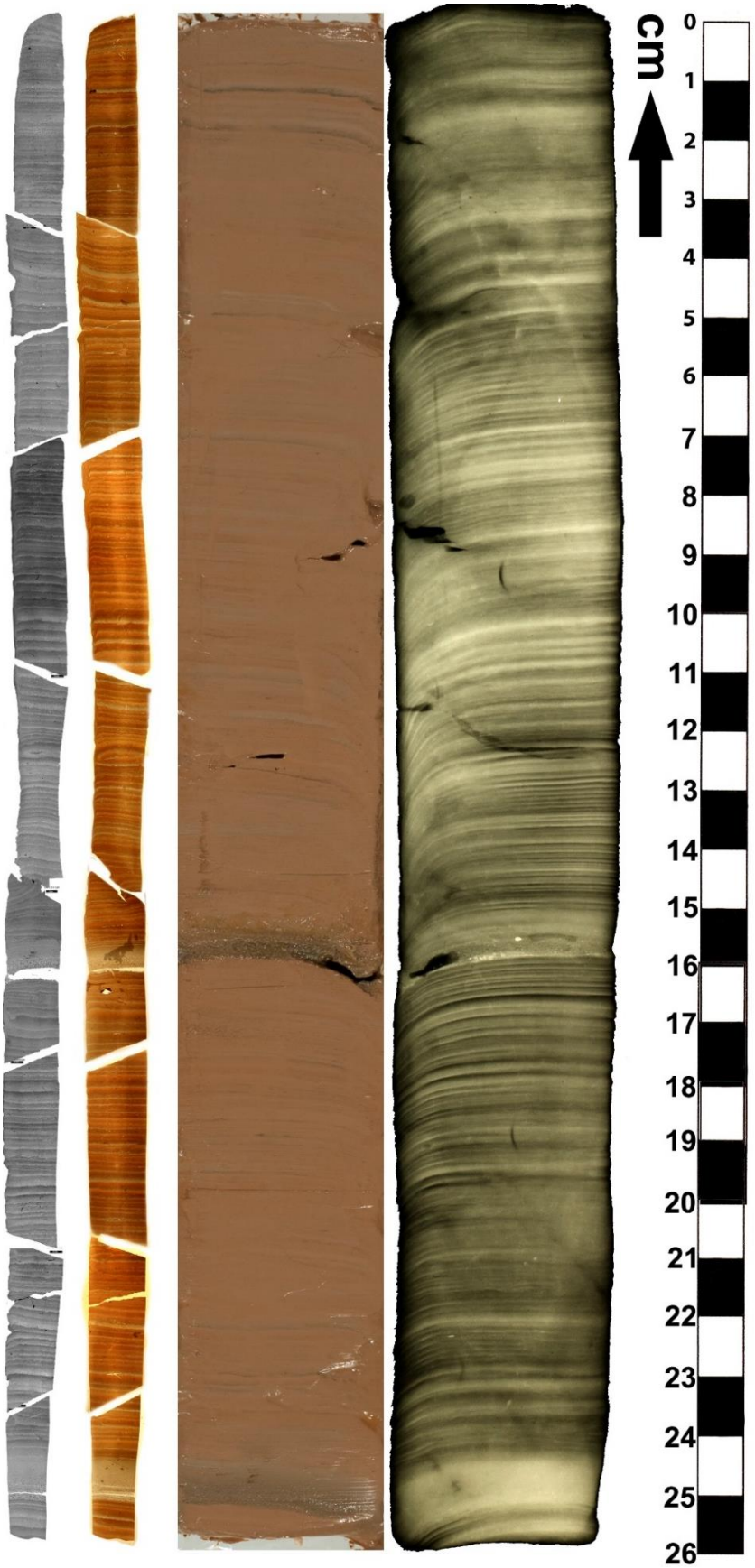

Figure 7.5 Millimetre-scale laminated sediment, macro-scale visualisation. Far left: Backscatter electron images. Left: Covered thin section photographs. Right: Slab photograph. Far right: X-radiograph.

C.4 Intermediate-organic Sediments

The sediments directly below the mm-scale laminated clays and silts differ in each core. In Figure 7.3, this unit lies between the middle and bottom tiepoint. However each core shares a decrease in terrigenous-type elements and a decrease in density (as seen in X-radiograph evidence, Figure 7.6), and an increase in organic material (although in far smaller amounts than the topmost mud unit). This unit also does not exhibit any regular clay-silt couplet laminations, although Core 68 exhibits cm-scale organic laminations similar to the 'transition sediments' above, and Core 67 exhibits several siliceous laminations which upon further investigation are found to be diatom mats of *Ellerbeckia* sp.

The increased presence of microfossils in all of these units, the increased bioturbation in the laminations bounding this unit, and the increased porosity of the sediment suggests that this sedimentary unit was deposited in a more oxygenated and warmer environment than the silt-clay laminations.

Cores 57 and 68 both contain diagenetic iron inclusions (some of which are several millimetres in diameter), tentatively identified as Greigite (Fe_3S_4) due to the iron and sulphur ratios found in EDS spot analysis.

The LWB cores have a well-preserved intermediate-organic unit which will be used in future for a pollen study.

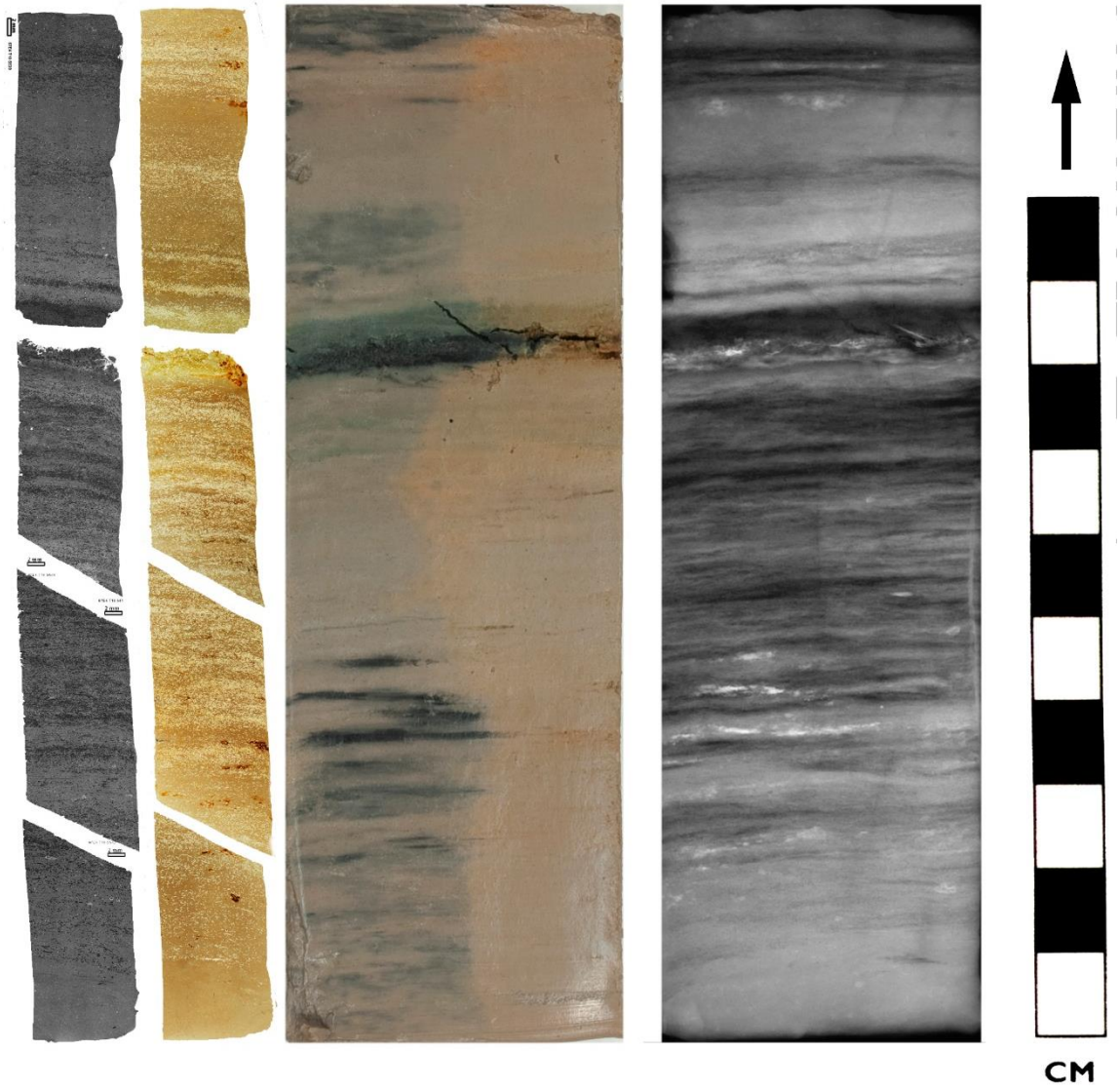

Figure 7.6 Intermediate-organic sediment macro-visualisation from Core 67. Each core shows a different characterisation for this unit. Far left: BSEI. Left: Covered thin section photographs. Right: Slab photograph. Far right: X-radiograph.

C.5 Centimetre-scale Laminated Sediments

Towards the bottom of the long cores from the South Basin (57 and 67), and possibly at the very bottom of LWB1D, are clay-silt couplet laminations but on a centimetre scale, mainly between 0.5 and 5 cm for a whole clay-silt couplet. This unit is found below the bottom tiepoint in Figure 7.3, and in Cores 57 and 67 extend to the bottoms of the cores. This unit is also high in terrigenous type elements in the ITRAX data, and in particular there is somewhat heightened calcium (Ca) in comparison with the mm-scale lamination unit (see Chapter 4).

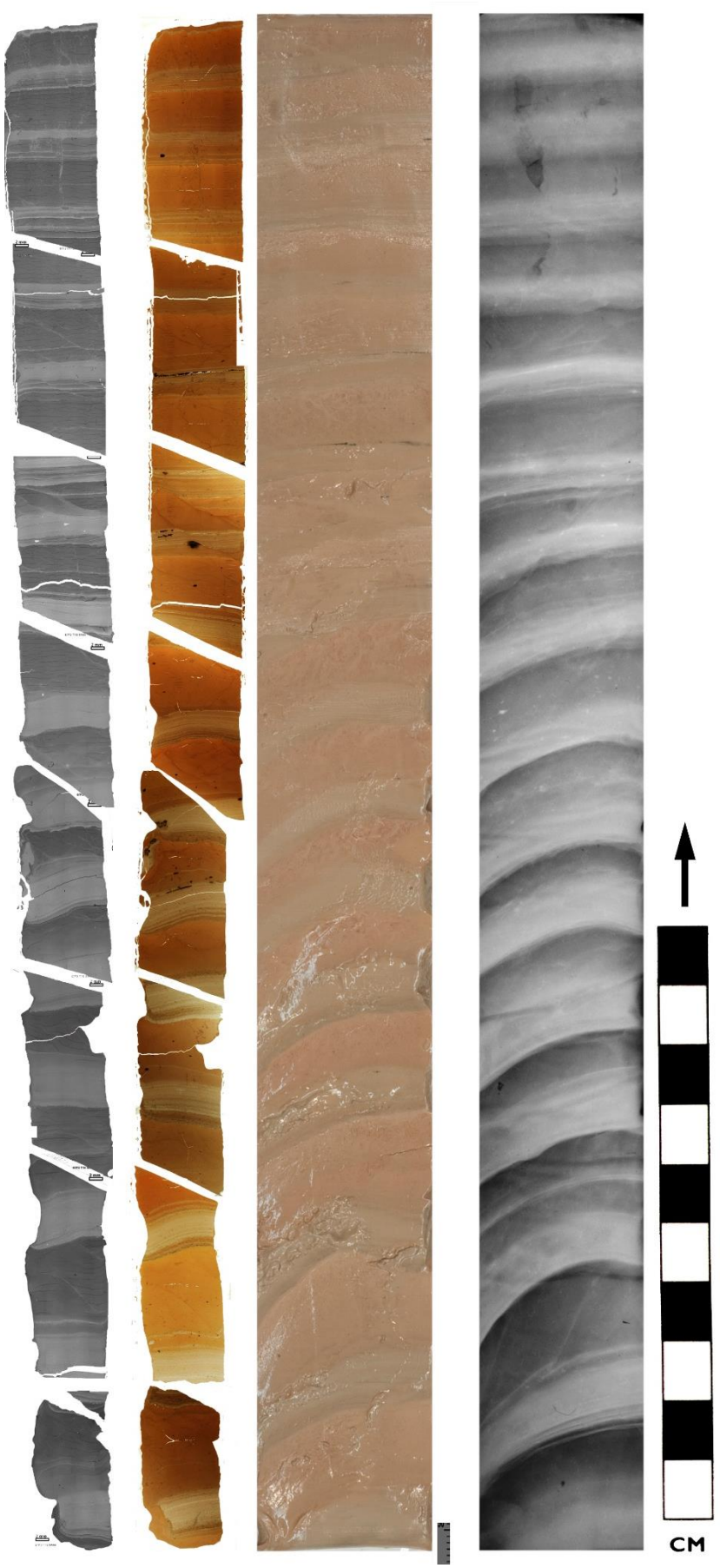

Figure 7.7: Centimetre-scale lamination macro-scale visualisation from Core 67. Far left: BSEI. Left:

Appendix C

Covered thin section photographs. Right: Slab photograph. Far right: Slab X-radiograph.

C.6 Basal Sediments (North Basin Only)

The basal units of the long North Basin cores (64 and 68) are high in terrigenous-type elements in the ITRAX data and particularly higher in Ca (see Chapter 4). Visual and X-radiographic inspection shows the presence of some layers but they do not appear to be regular silt-clay couplets, rather pulses of greyer, coarser silt than seen in the South Basin unit.

The basal sediments of Core 64 comprise thick (decimetre) layers of silt interspersed with thinner (0.5 - 2 cm) layers of clay. The silt layers are made up of several sub-laminations up to a few millimetres thick, with each sub-lamination being relatively well-sorted and ranging from fine to coarse silt. There are occasional very fine sand clasts. Although the backscatter images show the silt layers to be very similar in atomic number, the transmitted light slide images do show some degree of colour change. In slab 64G3, the silt sub-laminations lie mostly conformably (Figure 7.8), but in slab 64E3 (2 m above section G3), there is more cross-bedding within the sub-laminations. Slab 64E3 also has much more frequent clay layers. In section 64H (the deepest core section in Core 64), the clay layers are more than 20 cm apart.

The basal sediments of Core 68 are different. Section J (~9 – 10 m) of Core 68 exhibits widespread faulting and water-escape features, and was not sampled after splitting due to the sediment being so sandy and compacted. Section I (~8 – 9 m) has multiple thin (<1 mm to several mm) sand layers interspersed with clay layers, also <1 mm to several mm. A massive sand bed at the top of the section can be seen in Figure 7.9. There is much more distortion in the layers than in Core 64.

The basal sediments of Core 68 exhibit characteristics of a higher-energy depositional environment than Core 64 (e.g. presence of sand layers, and increased sediment distortion), and possibly also a more complex environment.

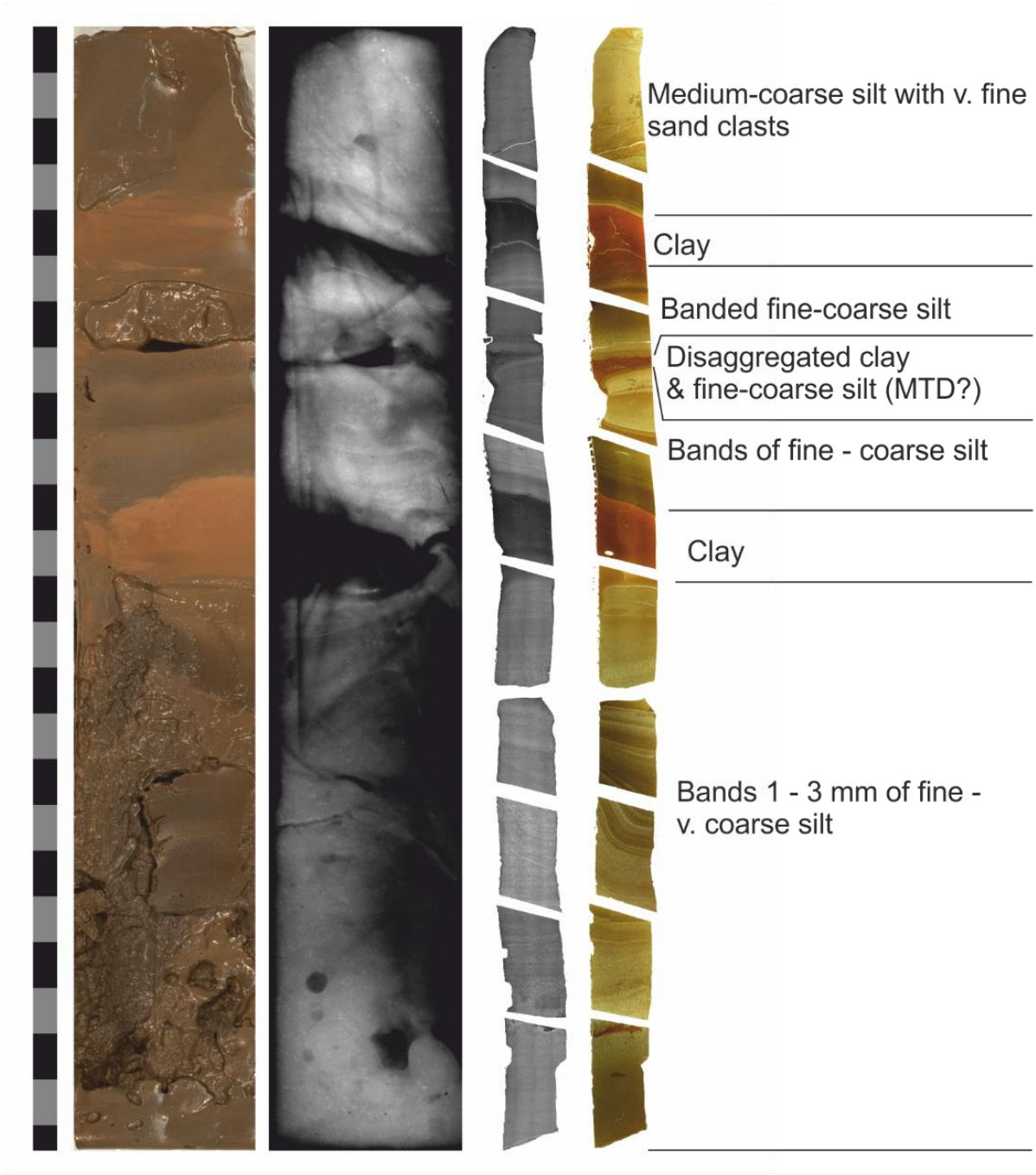

Figure 7.8 Example of basal sediments from Core 64, section G3. From the left: Slab photograph, X-radiograph, BSEI, Optical microscope slides, sediment description, ITRAX measurements. The basal sediment in this section comprises thick (multi-cm) layers of banded silts ranging from fine to very coarse and intermittent clay layers. Clay layers may be clearly seen in the ITRAX data as decreased levels of Si and Ca, and increased levels of K.

Appendix C

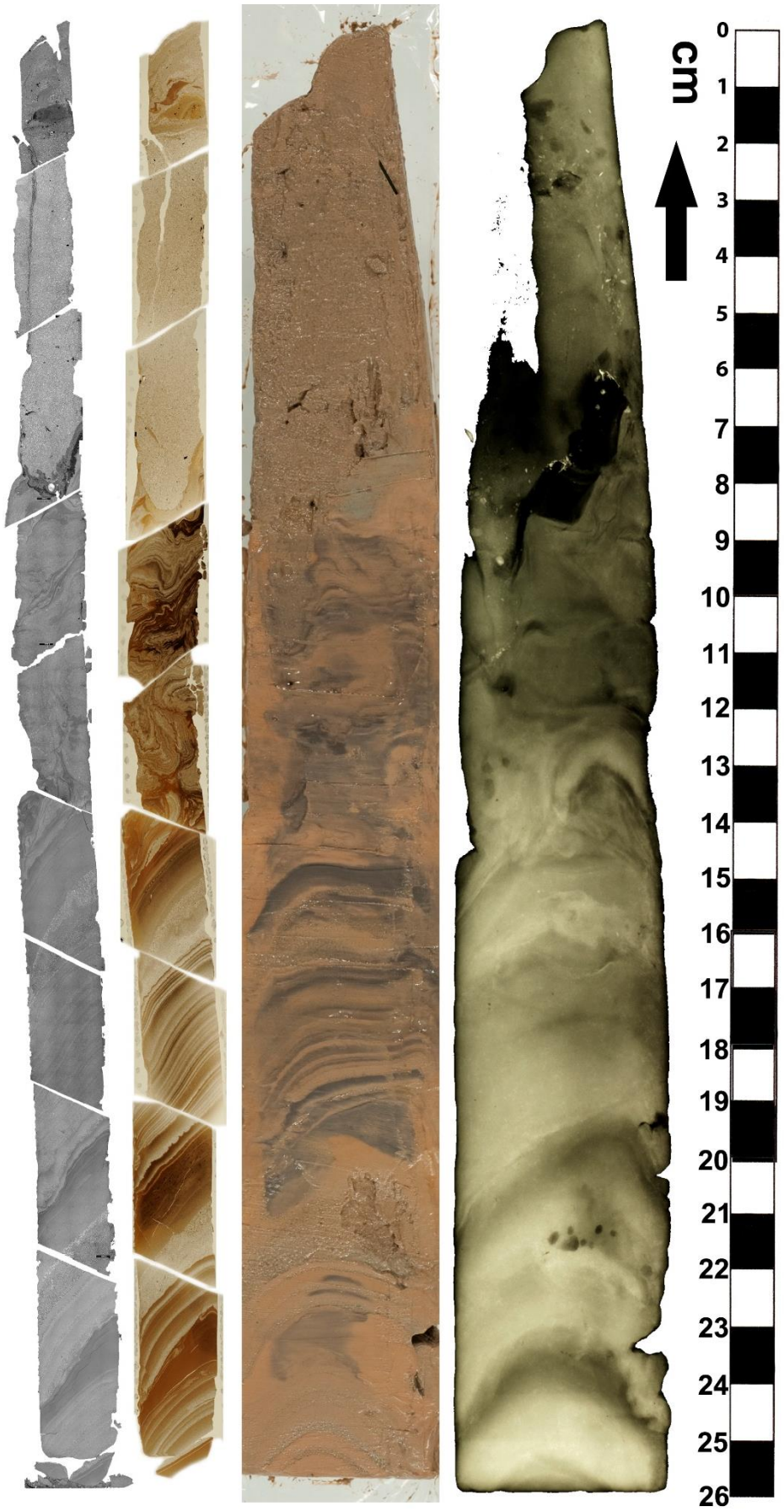

Figure 7.9: Basal irregular deposits visualisation from Core 68. Far left: BSEI. Left: covered thin section photographs. Right: Slab photograph. Far right: Slab X-radiograph.

C.7 Mass Transport Deposits

All four long cores contain at least one MTD. In Core 68, there are two mass movement deposits in the overlying organic-rich sediment

Core 64 contains small-scale MTDs at the base of the topmost organic-rich unit. In addition, the mm-scale laminated sediment appears truncated.

Core 67 contains a small MTD in the base of the topmost organic-rich unit. The mm-scale laminated sediment is also bisected by a larger (~1 m) MTD, which has removed most of this unit.

Core 57 contains a MTD within the mm-scale laminated unit, comprising a cohesive block of cm-scale laminated clay and silt and truncating the intermediate-organic unit. There also does not appear to be any 'transition'-type sediment at the base of the organic-rich unit, implying that this may have been removed by a mass-transport event that may have had a deposit in the core section gap.

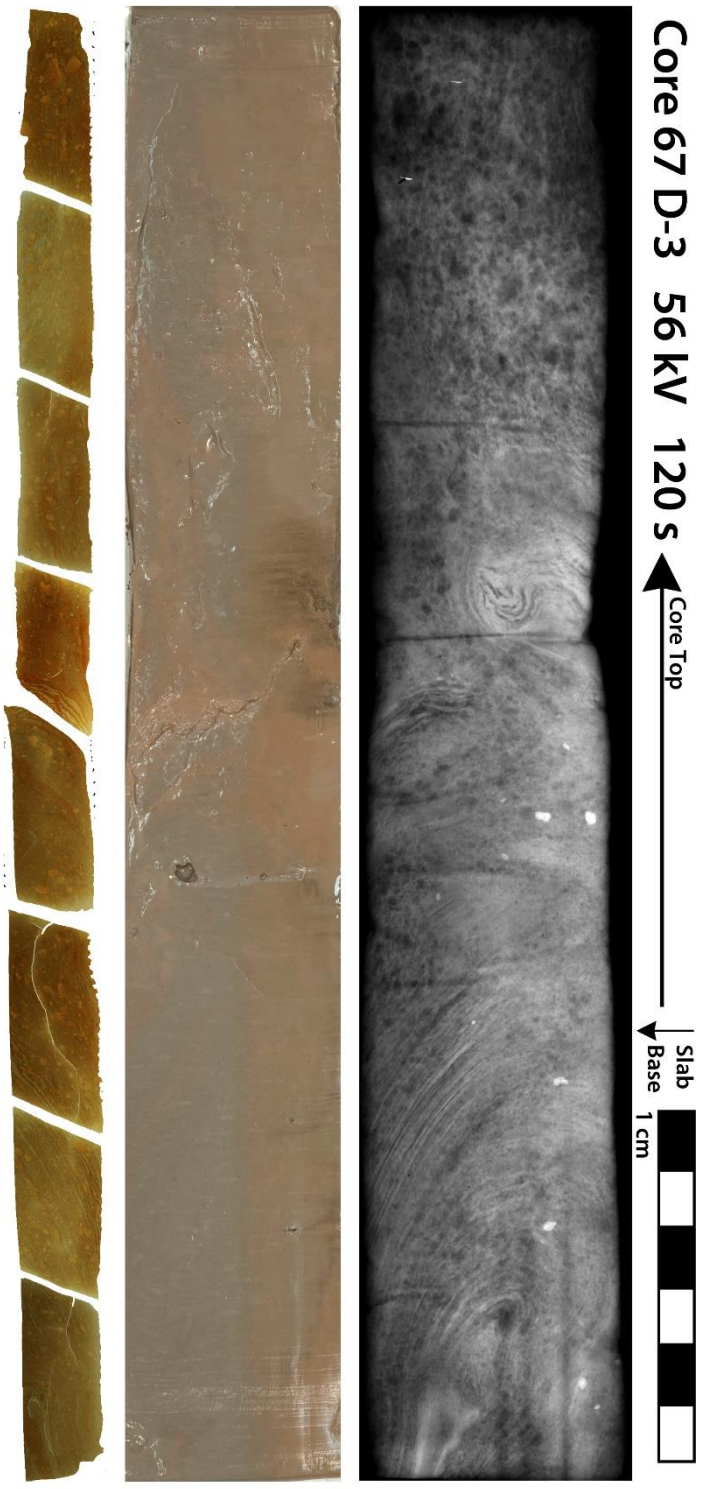

Figure 7.10 Part of the mass transport deposit in Core 67. Far left: Backscatter images. Left: covered thin section images. Right: Slab photograph. Far right: X-radiograph.

Appendix D: Examples of Other Published Varves

D.1 Proglacial varves and varves from glaciated catchments

Bendle et al., (2017). Lago Buenos Aires, Patagonia.	 *Reused under a Creative Commons Attribution Licence (CC BY). DOI: 10.1016/j.quascirev.2017.10.013*
Lamoureux & Chutko (2008) Lake R, Colin Archer Peninsula, northwest Devon Island, Nunavut. *G = glacially-derived component; N = nivally-derived component*	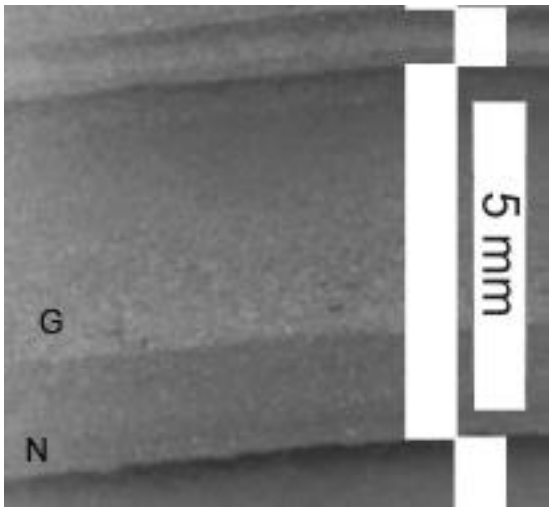 *© Canadian Science Publishing or its licensors*

Appendix D

Amann et al 2014 Lake Oeschinen, Swiss Alps. *White = coarse component, black = clay component*	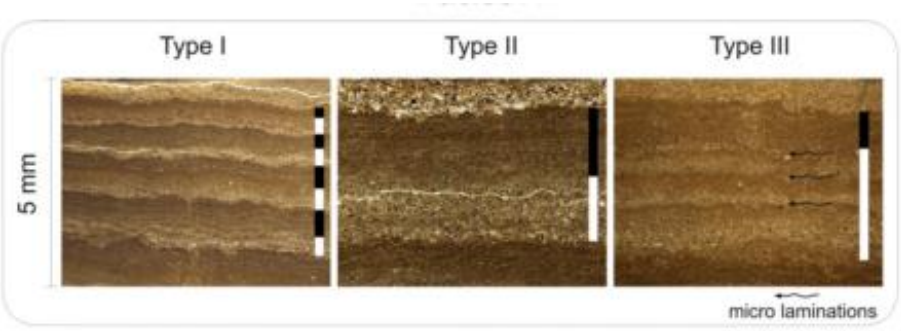 *Reprinted by permission from Springer Nature: Springer, Journal of Paleolimnology, Quantitative high-resolution warm season rainfall recorded in varved sediments of Lake Oeschinen, northern Swiss Alps: Calibration and validation AD 1901-2008, Amann, B., Mauchle, F., Grosjean, Martin, © 2014*
Menounos & Clague, 2008 Cheakamus Lake, British Columbia, Canada *Black lines indicate varve boundaries*	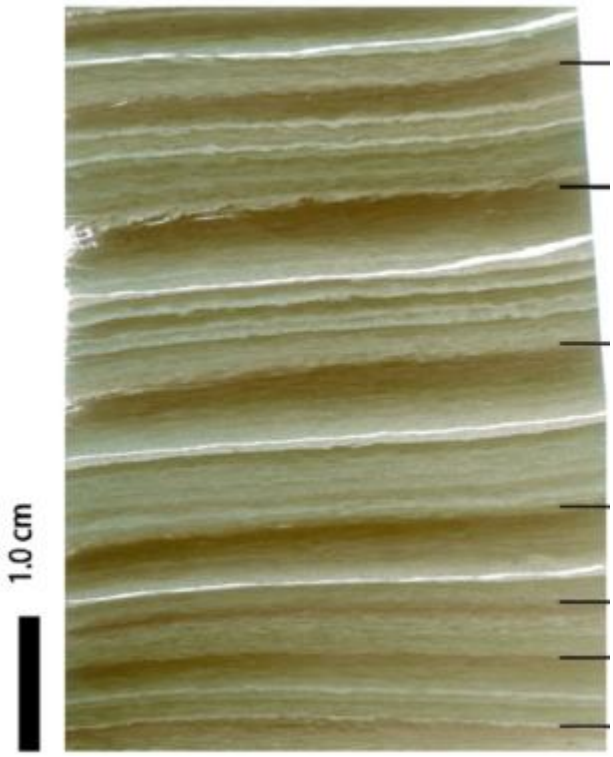 *Reprinted from Quaternary Science Reviews, 27 (7-8), Menounos, B., Clague, J., Reconstructing hydro-climatic events and glacier fluctuations over the past millennium from annually laminated sediments of Cheakamus Lake, southern Coast Mountains, British Columbia, Canada, p. 701-713., Copyright (2008), with permission from Elsevier*

D.2 Varves from snowmelt-dominated catchments

(Kaufman et al., 2011) Shadow Bay, Lake Chaeukuktuli, Alaska *Grey bar = 1 varve*	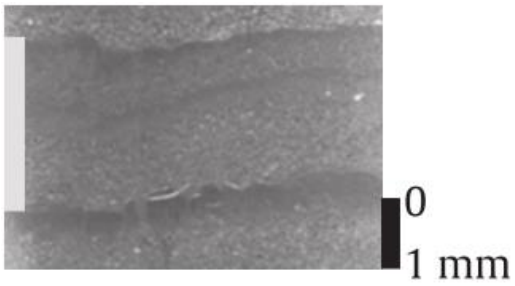 *Kaufman, C. A., Lamoureux, S.F., Kaufman, D.S., 2011. Long-term river discharge and multidecadal climate variability inferred from varved sediments, southwest Alaska. Quat. Res. 76, 1–9. doi:10.1016/j.yqres.2011.04.005*
Hambley & Lamoureux (2006) Nicolay Lake, Cornwall Island, Nunavut, Canada *Grey bars = varves* *SC = split clay cap* *N = nival unit* *P = pluvial unit; S = slump unit*	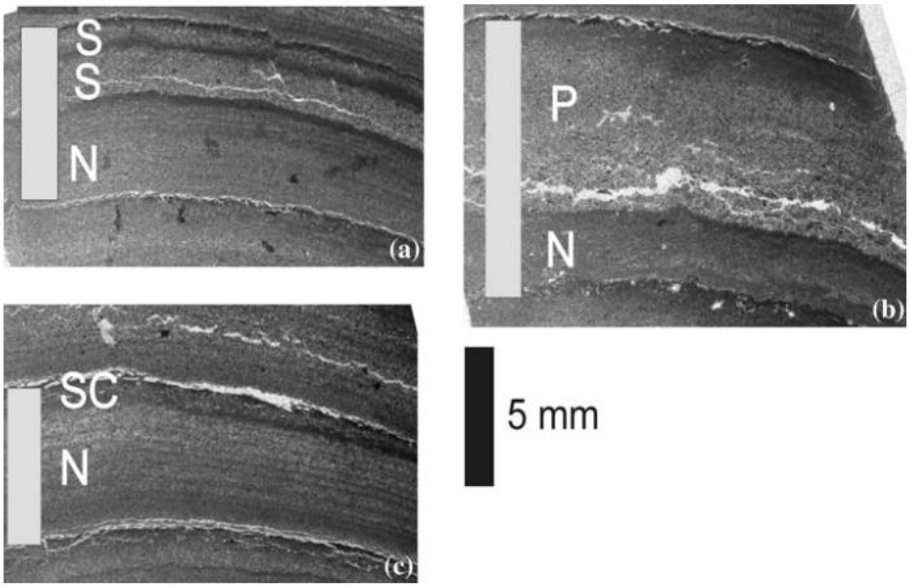 *Reprinted by permission from Springer Nature: Springer Journal of Paleolimnology. Recent summer climate recorded in complex varved sediments, Nicolay Lake, Cornwall Island, Nunavut, Canada. Hambley, G. W., Lamoureux, S. F., © (2006)*

Appendix D

Francus et al., 2008 South Sawtooth Lake *In macroscopic view, clay caps are pale*	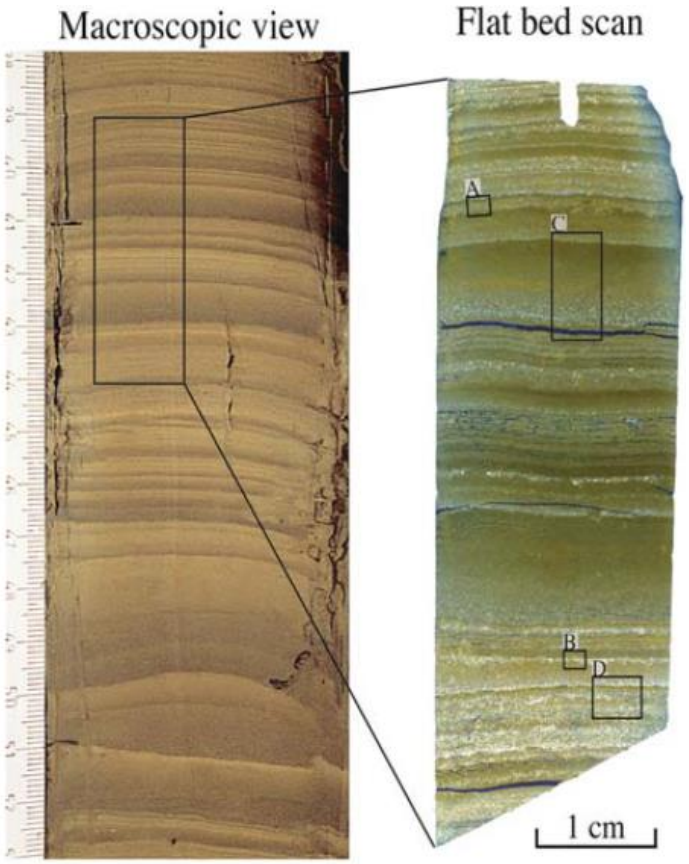 *Reprinted by permission from Springer Nature: Springer Journal of Paleolimnology. Limnological and sedimentary processes at Sawtooth Lake, Canadian High Arctic, and their influence on varve formation. Francus, P., Bradley, R. S., Lewis, T., Abbott, M., Retelle, M., Stoner, J. S.© (2008)*

List of References

Allan, R.J., 2000. ENSO and Climatic Variability in the Past 150 years, in: Diaz, H.F., Markgraf, V. (Eds.), El Nino and the Southern Oscillation. Cambridge University Press, pp. 3–55.

Amann, B., Mauchle, F., Grosjean, M., 2014. Quantitative high-resolution warm season rainfall recorded in varved sediments of Lake Oeschinen, northern Swiss Alps: Calibration and validation AD 1901-2008. J. Paleolimnol. 51, 375–391. doi:10.1007/s10933-013-9761-3

Antevs, E., 1928. The last glaciation: with special reference to the ice retreat in northeastern North America. Geogr. Soc. 17.

Antevs, E., 1922. The Recession of the last ice sheet in New england. Am. Geogr. Soc. 11.

Ashley, G., 1975. Rhythmic sedimentation in glacial Lake Hitchcock, Massachusetts-Connecticut, in: A.V, J., McDonald, B.C. (Eds.), Glaciofluvial and Glaciolacustrine Sedimentation. Society of Economic Paleontologists and Mineralogists, pp. 304–320.

Ashley, G., 1972. Rhythmic sedimentation in glacial lake Hitchcock, Massachusetts-Connecticut. Amherst, Massachusetts, Univ. Massachusetts, Geol. Dep. 148.

Asikainen, C.A., Francus, P., Brigham-Grette, J., 2007. Sedimentology, clay mineralogy and grain-size as indicators of 65 ka of climate change from El'gygytgyn Crater Lake, Northeastern Siberia. J. Paleolimnol. 37, 105–122. doi:10.1007/s10933-006-9026-5

Avery, R.S., Xuan, C., Kemp, A.E.S., Bull, J.M., Cotterill, C.J., Fielding, J.J., Pearce, R.B., Croudace, I.W., 2017. A new Holocene record of geomagnetic secular variation from Windermere, UK. Earth Planet. Sci. Lett. 477, 108–122. doi:10.1016/j.epsl.2017.08.025

Bader, J., Mesquita, M.D.S., Hodges, K.I., Keenlyside, N., Østerhus, S., Miles, M., 2011. A review on Northern Hemisphere sea-ice, storminess and the North Atlantic Oscillation: Observations and projected changes. Atmos. Res. 101, 809–834. doi:10.1016/j.atmosres.2011.04.007

Bakke, J., Lie, Ø., Heegaard, E., Dokken, T., Haug, G.H., Birks, H.H., Dulski, P., Nilsen, T., 2009. Rapid oceanic and atmospheric changes during the Younger Dryas cold period. Nat. Geosci. 2, 202–205. doi:10.1038/ngeo439

Baldwin, M., Gray, L., Dunkerton, T., Hamilton, K., Haynes, P., Randel, W., Holton, J., Alexander, M., Hirota, I., Horinouchi, T., Jones, D., Kinnersly, J., Marquardt, C., Sato, K., Takahashi, M., 2001. The Quasi-biennial Oscillation. Rev. Geophys. 39, 181.

Ballantyne, C.K., 2012. Chronology of glaciation and deglaciation during the loch lomond (younger dryas) stade in the scottish highlands: Implications of recalibrated 10Be exposure ages. Boreas 41, 513–526. doi:10.1111/j.1502-3885.2012.00253.x

Ballantyne, C.K., Stone, J.O., Fifield, L.K., 2009. Glaciation and deglaciation of the SW Lake District, England: implications of cosmogenic 36Cl exposure dating. Proc. Geol. Assoc. 120, 139–144. doi:10.1016/j.pgeola.2009.08.003

Barletta, F., St-Onge, G., Stoner, J.S., Lajeunesse, P., Locat, J., 2010. A high-resolution Holocene paleomagnetic secular variation and relative paleointensity stack from

eastern Canada. Earth Planet. Sci. Lett. 298, 162–174. doi:10.1016/j.epsl.2010.07.038

Barnola, J., Raynaud, D., Korotkevich, Y., Lorius, C., 1987. Vostok ice core provides 160,000-year record of atmospheric CO2. Nature 329, 408–414.

Barr, I.D., Roberson, S., Flood, R., Dortch, J., 2017. Younger Dryas glaciers and climate in the Mourne Mountains, Northern Ireland. J. Quat. Sci. 32, 104–115. doi:10.1002/jqs.2927

Batt, C.M., Brown, M.C., Clelland, S.-J., Korte, M., Linford, P., Outram, Z., 2017. Advances in archaeomagnetic dating in Britain: New data, new approaches and a new calibration curve. J. Archaeol. Sci. 85, 66–82. doi:10.1016/j.jas.2017.07.002

Beerling, D.J., Royer, D.L., 2011. Convergent Cenozoic CO2 history. Nat. Geosci. 4, 418–420. doi:10.1038/ngeo1186

Bendle, J.M., Palmer, A.P., Thorndycraft, V.R., Matthews, I.P., 2017. High-resolution chronology for deglaciation of the Patagonian Ice Sheet at Lago Buenos Aires (46.5°S) revealed through varve chronology and Bayesian age modelling. Quat. Sci. Rev. 177, 314–339. doi:10.1016/j.quascirev.2017.10.013

Berger, A., Loutre, M.F., 1991. Insolation values for the climate of the last 10 million years. Quat. Sci. Rev. 10, 297–317. doi:10.1016/0277-3791(91)90033-Q

Besonen, M.R., Patridge, W., Bradley, R.S., Francus, P., Stoner, J.S., Abbott, M.B., 2008. A record of climate over the last millennium based on varved lake sediments from the Canadian High Arctic. The Holocene 18, 169–180. doi:10.1177/0959683607085607

Björck, S., Walker, M.J.C., Cwynar, L.C., Johnsen, S., Knudsen, K.L., Lowe, J.J., Wohlfarth, B., 1998. An event stratigraphy for the last termination in the North Atlantic region based on the Greenland ice-core record: a proposal by the INTIMATE group. J. Quat. Sci. 13, 283–292. doi:10.1002/(SICI)1099-1417(199807/08)13:4<283::AID-JQS386>3.0.CO;2-A

Blass, A., Anselmetti, F., Ariztegui, D., 2003. 60 years of glaciolacustrine sedimentation in Steinsee (Sustenpass, Switzerland) compared with historic events and instrumental meteorological data. Lake Syst. from Ice Age to … 96, 59–72.

Bloxham, J., Gubbins, D., 1985. The secular variation of Earth's magnetic field. Nature 317, 777–779.

Blystad, P., Selsing, L., 1989. Some erroneous radiocarbon dates of lacustrine sediments. Nor. Geol. Tidsskrif 69, 201–208.

Bond, G.C., Lotti, R., 1995. Iceberg Discharges into the North Atlantic on Millennial Time Scales During the Last Glaciation. Science (80-.). 267, 1005–1010. doi:10.1126/science.267.5200.1005

Bouvier, V., Johnson, M.D., Påsse, T., 2015. Distribution, genesis and annual-origin of De Geer moraines in Sweden: insights revealed by LiDAR. Gff 137, 319–333. doi:10.1080/11035897.2015.1089933

Bradwell, T., Fabel, D., Stoker, M., Mathers, H., McHargue, L., Howe, J., 2008. Ice caps existed throughout the Lateglacial Interstadial in northern Scotland. J. … 23, 401–407. doi:10.1002/jqs

Brauer, A., Haug, G.H., Dulski, P., Sigman, D.M., Negendank, J.F.W., 2008. An abrupt wind

shift in western Europe at the onset of the Younger Dryas cold period. Nat. Geosci. 1, 520–523. doi:10.1038/ngeo263

Broecker, W., Putnam, A.E., 2012. How did the hydrologic cycle respond to the two-phase mystery interval? Quat. Sci. Rev. 57, 17–25. doi:10.1016/j.quascirev.2012.09.024

Bromley, G.R.M., Putnam, A.E., Rademaker, K.M., Lowell, T. V., Schaefer, J.M., Hall, B., Winckler, G., Birkel, S.D., Borns, H.W., 2014. Younger Dryas deglaciation of Scotland driven by warming summers. Proc. Natl. Acad. Sci. 111, 6215–6219. doi:10.1073/pnas.1321122111

Bronk Ramsey, C., Albert, P.G., Blockley, S.P.E., Hardiman, M., Housley, R.A., Lane, C.S., Lee, S., Matthews, I.P., Smith, V.C., Lowe, J.J., 2015. Improved age estimates for key Late Quaternary European tephra horizons in the RESET lattice. Quat. Sci. Rev. 118, 18–32. doi:10.1016/j.quascirev.2014.11.007

Bronk Ramsey, C., Staff, R.A., Bryant, C.L., Brock, F., Kitagawa, H., van der Plicht, J., Schlolaut, G., Marshall, M.H., Brauer, A., Lamb, H.F., Payne, R.L., Tarasov, P.E., Haraguchi, T., Gotanda, K., Yonenobu, H., Yokoyama, Y., Tada, R., Nakagawa, T., 2012. A complete terrestrial radiocarbon record for 11.2 to 52.8 kyr B.P. Science (80-.). 338, 370–374. doi:10.1126/science.1226660

Brothers, R.J., Kemp, A.E.S., Maltman, A.J., 1996. Mechanical development of vein structures due to the passage of earthquake waves through poorly-consolidated sediments. Tectonophysics 260, 227–244. doi:10.1016/0040-1951(96)00088-1

Brown, M.C., Donadini, F., Korte, M., Nilsson, A., Korhonen, K., Lodge, A., Lengyel, S.N., Constable, C.G., 2015. GEOMAGIA50.v3: 1. general structure and modifications to the archeological and volcanic database, Earth, Planets and Space. doi:10.1186/s40623-015-0232-0

Brown, M.C., Korte, M., 2016. A simple model for geomagnetic field excursions and inferences for palaeomagnetic observations. Phys. Earth Planet. Inter. 254, 1–11. doi:10.1016/j.pepi.2016.03.003

Brown, V., 2009. Reconstructing the LochLomond Stadial glaciers and climate in the south-west English Lake District. University of Durham.

Brown, V.H., Evans, D.J.A., Vieli, A., Evans, I.S., 2013. The Younger Dryas in the English Lake District: Reconciling geomorphological evidence with numerical model outputs. Boreas 42, 1022–1042. doi:10.1111/bor.12020

Brown, V.H., Evans, D.J. a., Evans, I.S., 2011. The Glacial Geomorphology and Surficial Geology of the South-West English Lake District. J. Maps 7, 221–243. doi:10.4113/jom.2011.1187

Camp, C.D., Tung, K.-K., 2007. The Influence of the Solar Cycle and QBO on the Late-Winter Stratospheric Polar Vortex. J. Atmos. Sci. 64, 1267–1283. doi:10.1175/JAS3883.1

Carr, S., 2001. A glaciological approach for the discrimination of Loch Lomond Stadial glacial landforms in the Brecon Beacons, South Wales. Proc. Geol. Assoc. 112, 253–262. doi:10.1016/S0016-7878(01)80005-5

Chiverrell, R.C., Thomas, G.S.P., 2010. Extent and timing of the Last Glacial Maximum (LGM) in Britain and Ireland: a review. J. Quat. Sci. 25, 535–549. doi:10.1002/jqs.1404

Chutko, K.J., Lamoureux, S.F., 2008. Identification of coherent links between interannual sedimentary structures and daily meteorological observations in Arctic proglacial lacustrine varves: potentials and limitations. Can. J. Earth Sci. 45, 1–13. doi:10.1139/E07-070

Clark, C.D., Hughes, A.L.C., Greenwood, S.L., Jordan, C., Sejrup, H.P., 2012. Pattern and timing of retreat of the last British-Irish Ice Sheet. Quat. Sci. Rev. 44, 112–146. doi:10.1016/j.quascirev.2010.07.019

Clark, P.U., Dyke, A.S., Shakun, J.D., Carlson, A.E., Clark, J., Wohlfarth, B., Mitrovica, J.X., Hostetler, S.W., McCabe, a M., 2009. The Last Glacial Maximum. Science 325, 710–4. doi:10.1126/science.1172873

Clark, P.U., Shakun, J.D., Baker, P.A., Bartlein, P.J., Brewer, S., Brook, E., Carlson, A.E., Cheng, H., Kaufman, D.S., Liu, Z., Marchitto, T.M., Mix, A.C., Morrill, C., Otto-Bliesner, B.L., Pahnke, K., Russell, J.M., Whitlock, C., Adkins, J.F., Blois, J.L., Clark, J., Colman, S.M., Curry, W.B., Flower, B.P., He, F., Johnson, T.C., Lynch-Stieglitz, J., Markgraf, V., McManus, J., Mitrovica, J.X., Moreno, P.I., Williams, J.W., 2012. Global climate evolution during the last deglaciation. Proc. Natl. Acad. Sci. 109, E1134–E1142. doi:10.1073/pnas.1116619109

Clement, a. C., Seager, R., Cane, M. a., 1999. Orbital controls on the El Niño/Southern Oscillation and the tropical climate. Paleoceanography 14, 441. doi:10.1029/1999PA900013

Cockburn, J.M.H., Lamoureux, S.F., 2008. Hydroclimate controls over seasonal sediment yield in two adjacent High Arctic watersheds. Hydrol. Process. 22, 2013–2027. doi:10.1002/hyp.6798

Cockburn, J.M.H., Lamoureux, S.F., 2007. Century-scale variability in late-summer rainfall events recorded over seven centuries in subannually laminated lacustrine sediments, White Pass, British Columbia. Quat. Res. 67, 193–203. doi:10.1016/j.yqres.2006.10.003

Constable, C., Korte, M., Panovska, S., 2016. Persistent high paleosecular variation activity in southern hemisphere for at least 10000 years. Earth Planet. Sci. Lett. 453, 78–86. doi:10.1016/j.epsl.2016.08.015

Cook, E.R., DArrigo, R.D., Briffa, K.R., 1998. A reconstruction of the North Atlantic Oscillation using tree-ring chronologies from North America and Europe. The Holocene 8, 9–17. doi:10.1191/095968398677793725

Cook, T.L., Bradley, R.S., Stoner, J.S., Francus, P., 2009. Five thousand years of sediment transfer in a high arctic watershed recorded in annually laminated sediments from Lower Murray Lake, Ellesmere Island, Nunavut, Canada. J. Paleolimnol. 41, 77–94. doi:10.1007/s10933-008-9252-0

Coope, G.R., Pennington, W., 1977. The Windermere Interstadial of the late Devensian. Philos. Trans. R. Soc. London. B 280, 337–339.

Croudace, I.W., Rindby, a., Rothwell, R.G., 2006. ITRAX: description and evaluation of a new multi-function X-ray core scanner. Geol. Soc. London, Spec. Publ. 267, 51–63. doi:10.1144/GSL.SP.2006.267.01.04

Cuven, S., Francus, P., Lamoureux, S., 2011. Mid to Late Holocene hydroclimatic and geochemical records from the varved sediments of East Lake, Cape Bounty, Canadian High Arctic. Quat. Sci. Rev. 30, 2651–2665. doi:10.1016/j.quascirev.2011.05.019

References

Cuven, S., Francus, P., Lamoureux, S.F., 2010. Estimation of grain size variability with micro X-ray fluorescence in laminated lacustrine sediments, Cape Bounty, Canadian High Arctic. J. Paleolimnol. 44, 803–817. doi:10.1007/s10933-010-9453-1

Day, R., Fuller, M., Schmidt, V.A., 1977. Hysteresis properties of titanomagnetites: grain-size and compositional dependence. Phys. Earth Planet. Inter. 13, 260–267.

de Geer, G., 1912. A Geochronology of the last 12000 Years. Proc. Int. Geol. Congr. Stock. 1, 241–257.

De Geer, G., 1937. A New Varve connection between four continents. Ark. Mat. Astron. Och Fys. 25 B.

Dean, J., Kemp, A., Bull, D., Pike, J., 1999. Taking varves to bits: Scanning electron microscopy in the study of laminated sediments and varves. J. Paleolimnol. 22, 121–136.

Denton, G.H., Broecker, W.S., Alley, R.B., 2006. The Mystery Interval 17.5 to 14.5 kyrs ago. PAGES News 14, 14–16.

Desloges, J.R., 1994. Varve Deposition and the Sediment Yield Record at Three Small Lakes of the Southern Canadian Cordillera. Arct. Alp. Res. 26, 130–140.

Desloges, J.R., Gilbert, R., 1994. Sediment source and hydroclimatic inferences from glacial lake sediments: the postglacial sedimentary record of Lillooet Lake, British Columbia. J. Hydrol. 159, 375–393. doi:10.1016/0022-1694(94)90268-2

Ebdon, R.A., 1960. Notes on the wind flow at 50 mb in tropical and subtropical regions in January 1957 and in 1958. Q. J. R. Meteorol. Soc. 86, 540–542.

Ehlers, J., Gibbard, P., Hughes, P.D., 2011. Quaternary Glaciations- Extent and Chronology. Elsevier Ltd.

Fielding, J.J., 2017. A High-resolution environmental and climate record of change in the Holocene sediments of Windermere, UK. University of Southampton.

Ford, H.L., Ravelo, A.C., Polissar, P.J., 2015. Reduced El Nino-Southern Oscillation during the Last Glacial Maximum. Science (80-.). 347, 255–258. doi:10.1126/science.1258437

Francus, P., 2002. Paleoclimate studies of minerogenic sediments using annually resolved textural parameters. Geophys. Res. Lett. 29, 59-1-59–3. doi:10.1029/2002GL015082

Francus, P., Bradley, R.S., Lewis, T., Abbott, M., Retelle, M., Stoner, J.S., 2008. Limnological and sedimentary processes at Sawtooth Lake, Canadian High Arctic, and their influence on varve formation. J. Paleolimnol. 40, 963–985. doi:10.1007/s10933-008-9210-x

Francus, P., Keimig, F., Besonen, M., 2002. An algorithm to aid varve counting and measurement from thin-sections. J. Paleolimnol. 28, 283–286. doi:10.1023/A:1021624415920

Francus, P., Ridge, J.C., Johnson, M.D., 2013. The rise of varves. Gff. doi:10.1080/11035897.2013.833548

Frumkin, A., Bar-Yosef, O., Schwarcz, H.P., 2011. Possible paleohydrologic and paleoclimatic effects on hominin migration and occupation of the Levantine Middle Paleolithic. J. Hum. Evol. 60, 437–451. doi:10.1016/j.jhevol.2010.03.010

Gammon, P., Neville, L.A., Patterson, R.T., Savard, M.M., Swindles, G.T., 2017. A log-normal spectral analysis of inorganic grain-size distributions from a Canadian boreal lake core: Towards refining depositional process proxy data from high latitude lakes. Sedimentology 64, 609–630. doi:10.1111/sed.12281

Gilbert, R., Crookshanks, S., Hodder, K.R., Spagnol, J., Stull, R.B., 2006. The record of an extreme flood in the sediments of montane Lillooet Lake, British Columbia: Implications for paleoenvironmental assessment. J. Paleolimnol. 35, 737–745. doi:10.1007/s10933-005-5152-8

Golledge, N.R., 2010. Glaciation of Scotland during the Younger Dryas stadial: A review. J. Quat. Sci. 25, 550–566. doi:10.1002/jqs.1319

Group, N. dating, 2006. Greenland Ice Core Chronology 2005 (GICC05). IGBP PAGES/World Data Cent. Paleoclimatology Data Contrib. Ser. # 2006-118. NOAA/NCDC Paleoclimatology Program, Boulder CO, USA.

Gubbins, D., Jones, A.L., Finlay, C.C., 2006. Fall in Earth's magnetic field is erratic. Science (80-.). 312, 900–902.

Haltia-Hovi, E., Nowaczyk, N., Saarinen, T., 2010. Holocene palaeomagnetic secular variation recorded in multiple lake sediment cores from eastern Finland. Geophys. J. Int. 180, 609–622. doi:10.1111/j.1365-246X.2009.04456.x

Hambley, G.W., Lamoureux, S.F., 2006. Recent summer climate recorded in complex varved sediments, Nicolay Lake, Cornwall Island, Nunavut, Canada. J. Paleolimnol. 35, 629–640. doi:10.1007/s10933-005-4302-3

Hammer, Ø., Harper, D.A.T., Ryan, P.D., 2001. Paleontological Statistics Software Package for Education and Data Analysis. Palaeontol. Electron. 4.

Hardy, D., 1996. Climatic influences on streamflow and sediment flux into Lake C2, northern Ellesmere Island, Canada. J. Paleolimnol. 16, 133–149. doi:10.1007/BF00176932

Hodder, K., 2009. Flocculation: a key process in the sediment flux of a large, glacier-fed lake. Earth Surf. Process. Landforms 34, 1151–1163. doi:10.1002/esp

Hodder, K.R., Gilbert, R., 2007. Evidence for flocculation in glacier-fed Lillooet Lake, British Columbia. Water Res. 41, 2748–62. doi:10.1016/j.watres.2007.02.058

Hodder, K.R., Gilbert, R., Desloges, J.R., 2007. Glaciolacustrine varved sediment as an alpine hydroclimatic proxy. J. Paleolimnol. 38, 365–394. doi:10.1007/s10933-006-9083-9

Hodell, D.A., Nicholl, J.A., Bontognali, T.R.R., Danino, S., Dorador, J., Dowdeswell, J.A., Einsle, J., Kuhlmann, H., Martrat, B., Mleneck-Vautravers, M.J., Rodríguez-Tovar, F.J., Röhl, U., 2017. Anatomy of Heinrich Layer 1 and its role in the last deglaciation. Paleoceanography 32, 284–303. doi:10.1002/2016PA003028

Hoek, W., 2008. The last glacial-interglacial transition. Episodes 31, 226–229.

Holton, J.R., Tan, H.-C., 1980. The influence of the equatorial Quasi-Biennial Oscillation on the global circulation at 50 mb. J. Atmos. Sci. 37, 2200–2208.

Hughen, K. a., Overpeck, J.T., Anderson, R.F., 2000. Recent warming in a 500-year palaeotemperature record from varved sediments, Upper Soper Lake, Baffin Island,

Canada. The Holocene 10, 9–19. doi:10.1191/095968300676746202

Hughes, A.L.C., Clark, C.D., Jordan, C.J., 2014. Flow-pattern evolution of the last British Ice Sheet. Quat. Sci. Rev. 89, 148–168. doi:10.1016/j.quascirev.2014.02.002

Hughes, A.L.C., Greenwood, S.L., Clark, C.D., 2011. Dating constraints on the last British-Irish Ice Sheet: a map and database. J. Maps 7, 156–184. doi:10.4113/jom.2011.1145

Hughes, A.L.C., Gyllencreutz, R., Lohne, Ø.S., Mangerud, J., Svendsen, J.I., 2016. The last Eurasian ice sheets - a chronological database and time-slice reconstruction, DATED-1. Boreas 45, 1–45. doi:10.1111/bor.12142

Hughes, P.D., 2009. Loch Lomond Stadial (Younger Dryas) glaciers and climate in Wales. Geol. J. 44, 375–391. doi:10.1002/gj

Hutchinson, I., James, T.S., Reimer, P.J., Bornhold, B.D., Clague, J.J., 2004. Marine and limnic radiocarbon reservoir corrections for studies of late- and postglacial environments in Georgia Basin and Puget Lowland, British Columbia, Canada and Washington, USA. Quat. Res. 61, 193–203. doi:10.1016/j.yqres.2003.10.004

Ineson, S., Scaife, a. a., 2008. The role of the stratosphere in the European climate response to El Niño. Nat. Geosci. 2, 32–36. doi:10.1038/ngeo381

Isarin, R.F.B., Renssen, H., Vandenberghe, J., 1998. The impact of the North Atlantic Ocean on the Younger Dryas climate in northwestern and central Europe. J. Quat. Sci. 13, 447–453. doi:10.1002/(sici)1099-1417(1998090)13:5<447::aid-jqs402>3.0.co;2-b

Jackson, A., Jonkers, R.T., Walker, M.R., 2000. Four centuries of geomagnetic secular variation from historical records. Phil. Trans. R. Soc. Lond. A 358, 957–990. doi:10.1029/2002RG000115

Jackson, M., Solheid, P., 2010. On the quantitative analysis and evaluation of magnetic hysteresis data. Geochemistry, Geophys. Geosystems 11, 1–25. doi:10.1029/2009GC002932

Jevrejeva, S., Moore, J.C., Grinsted, A., 2004. Oceanic and atmospheric transport of multiyear El Niño-Southern Oscillation (ENSO) signatures to the polar regions. Geophys. Res. Lett. 31, 1–4. doi:10.1029/2004GL020871

Johnsen, S.J., Clausen, H.B., Dansgaard, W., Fuhrer, K., Gundestrup, N., Hammer, C.U., Iversen, P., Jouzel, J., Stauffer, B., Steffensen, J.P., 1992. Irregular glacial interstadials recorded in a new Greenland ice core. Nature 359, 311–313. doi:10.1038/359311a0

Jones, R.T., Marshall, J.D., Crowley, S.F., Bedford, A., Richardson, N., Bloemendal, J., Oldfield, F., 2002. A high resolution, multiproxy Late-glacial record of climate change and intrasystem responses in northwest England. J. Quat. Sci. 17, 329–340. doi:10.1002/jqs.683

Kaiser, K.F., 1994. Two Creeks Interstade Dated through Dendrochronology and AMS. Quat. Resarch 42, 288–298.

Kaufman, C. a., Lamoureux, S.F., Kaufman, D.S., 2011. Long-term river discharge and multidecadal climate variability inferred from varved sediments, southwest Alaska. Quat. Res. 76, 1–9. doi:10.1016/j.yqres.2011.04.005

Kawamura, K., Parrenin, F., Lisiecki, L., Uemura, R., Vimeux, F., Severinghaus, J.P., Hutterli, M. a, Nakazawa, T., Aoki, S., Jouzel, J., Raymo, M.E., Matsumoto, K., Nakata,

H., Motoyama, H., Fujita, S., Goto-Azuma, K., Fujii, Y., Watanabe, O., 2007. Northern Hemisphere forcing of climatic cycles in Antarctica over the past 360,000 years. Nature 448, 912–6. doi:10.1038/nature06015

Kemp, A.E.S., Pearce, R.B., Pike, J., Marshall, J.E.A., 1998. Microfabric and microcompositional studies of Pliocene and Quaternary sapropels from the Eastern Mediterranean. Proc. Ocean Drill. Progr. Sci. Results 160, 349–364.

Kirschvink, J.L., 1980. The least-squares line and plane and the analysis of paleomagnetic data. Geophys. J. R. Astron. Soc. 62, 699–718. doi:10.1111/j.1365-246X.1980.tb02601.x

Knight, J., 2001. Glaciomarine deposition around the Irish Sea basin: Some problems and solutions. J. Quat. Sci. 16, 405–418. doi:10.1002/jqs.630

Korte, M., Constable, C., Donadini, F., Holme, R., 2011. Reconstructing the Holocene geomagnetic field. Earth Planet. Sci. Lett. 312, 497–505. doi:10.1016/j.epsl.2011.10.031

Korte, M., Donadini, F., Constable, C.G., 2009. Geomagnetic field for 0-3 ka: 2. A new series of time-varying global models. Geochemistry, Geophys. Geosystems 10. doi:10.1029/2008GC002297

Koutavas, A., Joanides, S., 2012. El Niño-Southern Oscillation extrema in the Holocene and Last Glacial Maximum. Paleoceanography 27, 1–15. doi:10.1029/2012PA002378

Koutavas, A., Lynch-stieglitz, J., Marchitto, T.M., Sachs, J.P., 2002. El Niño – Like Pattern in Ice Age Tropical Pacific Sea Surface Temperature. Science (80-.). 297, 226–230.

Lane, C.S., Brauer, A., Martín-Puertas, C., Blockley, S.P.E., Smith, V.C., Tomlinson, E.L., 2015. The Late Quaternary tephrostratigraphy of annually laminated sediments from Meerfelder Maar, Germany. Quat. Sci. Rev. 122, 192–206. doi:10.1016/j.quascirev.2015.05.025

Lane, C.S., Brauer, a., Blockley, S.P.E., Dulski, P., 2013. Volcanic ash reveals time-transgressive abrupt climate change during the Younger Dryas. Geology 41, 1251–1254. doi:10.1130/G34867.1

Lapointe, F., Francus, P., Lamoureux, S.F., Saïd, M., Cuven, S., 2012. 1750 years of large rainfall events inferred from particle size at East Lake, Cape Bounty, Melville Island, Canada. J. Paleolimnol. 48, 159–173. doi:10.1007/s10933-012-9611-8

Larsen, D.J., Miller, G.H., Geirsdóttir, Á., Thordarson, T., 2011. A 3000-year varved record of glacier activity and climate change from the proglacial lake Hvítárvatn, Iceland. Quat. Sci. Rev. 30, 2715–2731. doi:10.1016/j.quascirev.2011.05.026

Lear, C.H., Billups, K., Rickaby, R.E.M., Diester-Haass, L., Mawbey, E.M., Sosdian, S.M., 2016. Breathing more deeply: Deep ocean carbon storage during the mid-Pleistocene climate transition. Geology G38636.1. doi:10.1130/G38636.1

Leduc, G., Vidal, L., Cartapanis, O., Bard, E., 2009. Modes of eastern equatorial Pacific thermocline variability: Implications for ENSO dynamics over the last glacial period. Paleoceanography 24, 1–14. doi:10.1029/2008PA001701

Leemann, A., Niessen, F., 1994. Varve formation and the climatic record in an Alpine proglacial lake: calibrating annually- laminated sediments against hydrological and meteorological data. The Holocene 4, 1–8. doi:10.1177/095968369400400101

Lees, J.M., Park, J., 1995. Multiple-taper Spectral-analysis - A Stand-alone C-subroutine.

Comput. Geosci. 21, 199–236. doi:10.1016/0098-3004(94)00067-5

Leonard, E., 1997. relationship between glacial activity and sediment production: evidence from a 4450-year varve record of neoglacial sedimentation in Hector Lake, Alberta, Canada. J. Paleolimnol. 17, 319–330.

Levi, S., Banerjee, S.K., 1976. On the possibility of obtaining relative paleointensities from lake sediments. Earth Planet. Sci. Lett. 29, 219–226. doi:10.1016/0012-821X(76)90042-X

Lewis, T., Braun, C., Hardy, D.R., Francus, P., Bradley, R.S., 2005. An Extreme Sediment Transfer Event in a Canadian High Arctic Stream An Extreme Sediment Transfer Event in a Canadian High Arctic Stream. Arctic 37, 477–482. doi:10.1657/1523-0430(2005)037

Lewis, T., Francus, P., Bradley, R.S., Kanamaru, K., 2010. An automated system for the statistical analysis of sediment texture and structure at the micro scale. Comput. Geosci. 36, 1374–1383. doi:10.1016/j.cageo.2010.03.018

Lewis, T., Lafrenière, M.J., Lamoureux, S.F., 2012. Hydrochemical and sedimentary responses of paired High Arctic watersheds to unusual climate and permafrost disturbance, Cape Bounty, Melville Island, Canada. Hydrol. Process. 26, 2003–2018. doi:10.1002/hyp.8335

Linick, T.W., Damon, P.E., Donahue, D.J., Jull, A.J.T., 1989. Accelerator mass spectrometry: The new revolution in radiocarbon dating. Quat. Int. 1, 1–6. doi:10.1016/1040-6182(89)90004-9

Lisiecki, L.E., Raymo, M.E., 2005. A Pliocene-Pleistocene stack of 57 globally distributed benthic δ 18 O records. Paleoceanography 20, n/a-n/a. doi:10.1029/2004PA001071

Livingstone, S.J., Roberts, D.H., Davies, B.J., Evans, D.J.A., Ó Cofaigh, C., Gheorghiu, D.M., 2015. Late Devensian deglaciation of the Tyne Gap Palaeo-Ice Stream, northern England. J. Quat. Sci. 30, n/a-n/a. doi:10.1002/jqs.2813

Lohne, Ø.S., Mangerud, J., Birks, H.H., 2013. Precise 14 C ages of the Vedde and Saksunarvatn ashes and the Younger Dryas boundaries from western Norway and their comparison with the Greenland Ice Core (GICC05) chronology. J. Quat. Sci. 28, 490–500. doi:10.1002/jqs.2640

Lowag, J., Bull, J.M., Vardy, M.E., Miller, H., Pinson, L.J.W., 2012. High-resolution seismic imaging of a Younger Dryas and Holocene mass movement complex in glacial lake Windermere, UK. Geomorphology 171–172, 42–57. doi:10.1016/j.geomorph.2012.05.002

Lowe, J.J., Rasmussen, S.O., Björck, S., Hoek, W.Z., Steffensen, J.P., Walker, M.J.C., Yu, Z.C., 2008. Synchronisation of palaeoenvironmental events in the North Atlantic region during the Last Termination: a revised protocol recommended by the INTIMATE group. Quat. Sci. Rev. 27, 6–17. doi:10.1016/j.quascirev.2007.09.016

Mackereth, F.J.H., 1971. On the variation in direction of the horizontal component of remanent magnetisation in lake sediments. Earth Planet. Sci. Lett. 12, 332–338. doi:10.1016/0012-821X(71)90219-6

Mann, M.E., Park, J., 1996. Joint Spatiotemporal Modes of Surface Temperature and Sea Level Pressure Variability in the Northern Hemisphere during the Last Century. J. Clim. 9, 2137–2162.

Martínez, I., Keigwin, L., Barrows, T.T., Yokoyama, Y., Southon, J., 2003. La Niña-like conditions in the eastern equatorial Pacific and a stronger Choco jet in the northern Andes during the last glaciation. Paleoceanography 18, 1–18. doi:10.1029/2002PA000877

Maslin, M.A., Ridgwell, A.J., 2005. Mid-Pleistocene revolution and the "eccentricity myth." Geol. Soc. London, Spec. Publ. 247, 19–34. doi:10.1144/gsl.sp.2005.247.01.02

Masson-Delmotte, V., 2005. GRIP Deuterium Excess Reveals Rapid and Orbital-Scale Changes in Greenland Moisture Origin. Science (80-.). 309, 118–121. doi:10.1126/science.1108575

Matthews, I.P., Birks, H.H., Bourne, A.J., Brooks, S.J., Lowe, J.J., Macleod, A., Pyne-O'Donnell, S.D.F., 2011. New age estimates and climatostratigraphic correlations for the borrobol and penifiler tephras: Evidence from Abernethy Forest, Scotland. J. Quat. Sci. 26, 247–252. doi:10.1002/jqs.1498

Mazaud, A., Channell, J.E.T., Stoner, J.S., 2012. Relative paleointensity and environmental magnetism since 1.2Ma at IODP site U1305 (Eirik Drift, NW Atlantic). Earth Planet. Sci. Lett. 357–358, 137–144. doi:10.1016/j.epsl.2012.09.037

McCarroll, D., Stone, J.O., Ballantyne, C.K., Scourse, J.D., Fifield, L.K., Evans, D.J.A., Hiemstra, J.F., 2010. Exposure-age constraints on the extent, timing and rate of retreat of the last Irish Sea ice stream. Quat. Sci. Rev. 29, 1844–1852. doi:10.1016/j.quascirev.2010.04.002

McDougall, D., 2013. Glaciation style and the geomorphological record: evidence for Younger Dryas glaciers in the eastern Lake District, northwest England. Quat. Sci. Rev. 73, 48–58. doi:10.1016/j.quascirev.2013.05.002

McDougall, D. a., 2001. The geomorphological impact of Loch Lomond (Younger Dryas) Stadial plateau icefields in the central Lake District, northwest England. J. Quat. Sci. 16, 531–543. doi:10.1002/jqs.624

Médail, F., Diadema, K., 2009. Glacial refugia influence plant diversity patterns in the Mediterranean Basin. J. Biogeogr. 36, 1333–1345. doi:10.1111/j.1365-2699.2008.02051.x

Menounos, B., 2006. Anomalous early 20th century sedimentation in proglacial Green Lake, British Columbia, Canada. Can. J. Earth Sci. doi:10.1139/e06-016

Menounos, B., Clague, J.J., 2008. Reconstructing hydro-climatic events and glacier fluctuations over the past millennium from annually laminated sediments of Cheakamus Lake, southern Coast Mountains, British Columbia, Canada. Quat. Sci. Rev. 27, 701–713. doi:10.1016/j.quascirev.2008.01.007

Merrill, R.T., McFadden, P.L., 2003. The geomagnetic axial dipole field assumption. Phys. Earth Planet. Inter. 139, 171–185. doi:10.1016/j.pepi.2003.07.016

Miller, H., 2014. Lake bed environments, modern sedimentation and the glacial and post-glacial history of Windermere, UK. University of Southampton.

Miller, H., Bull, J.M., Cotterill, C.J., Dix, J.K., Winfield, I.J., Kemp, A.E.S., Pearce, R.B., 2013. Lake bed geomorphology and sedimentary processes in glacial lake Windermere, UK. J. Maps 1–14. doi:10.1080/17445647.2013.780986

Miller, H., Cotterill, C.J., Bradwell, T., 2014a. Glacial and paraglacial history of the

Troutbeck Valley, Cumbria, UK: integrating airborne LiDAR, multibeam bathymetry, and geological field mapping. Proc. Geol. Assoc. 125, 31–40. doi:10.1016/j.pgeola.2013.04.007

Miller, H., Croudace, I.W., Bull, J.M., Cotterill, C.J., Dix, J.K., Taylor, R.N., 2014b. A 500 year sediment lake record of anthropogenic and natural inputs to windermere (English Lake District) using double-spike lead isotopes, radiochronology, and sediment microanalysis. Environ. Sci. Technol. 48, 7254–7263. doi:10.1021/es5008998

Miller, H., Winfield, I.J., Fletcher, J.M., Ben James, J., van Rijn, J., Bull, J.M., Cotterill, C.J., 2014c. Distribution, characteristics and condition of Arctic charr (Salvelinus alpinus) spawning grounds in a differentially eutrophicated twin-basin lake. Ecol. Freshw. Fish n/a-n/a. doi:10.1111/eff.12122

Mitchell, G.H., 1956. The Geological History of the Lake District. Proc. Yorksh. Geol. Soc. 30, 407–463. doi:10.1144/pygs.30.4.407

Mitchell, W.A., 1996. Significance of snowblow in the generation of Loch Lomond Stadial (Younger Dryas) glaciers in the western Pennines, northern England. J. Quat. Sci. 11, 233–248. doi:10.1002/(SICI)1099-1417(199605/06)11:3<233::AID-JQS240>3.0.CO;2-Q

Mullins, C.E., 1977. Magnetic Susceptibility of the Soil and Its Significance in Soil Science - a Review. J. Soil Sci. 28, 223–246. doi:10.1111/j.1365-2389.1977.tb02232.x

Muschitiello, F., Wohlfarth, B., 2015. Time-transgressive environmental shifts across Northern Europe at the onset of the Younger Dryas. Quat. Sci. Rev. 109, 49–56. doi:10.1016/j.quascirev.2014.11.015

Nilsson, a., Holme, R., Korte, M., Suttie, N., Hill, M., 2014. Reconstructing Holocene geomagnetic field variation: new methods, models and implications. Geophys. J. Int. 198, 229–248. doi:10.1093/gji/ggu120

O'Sullivan, P.E., 1983. Annually-laminated lake sediments and the study of Quaternary environmental changes--a review. Quat. Sci. Rev. 1, 245–313.

Ojala, A.E.K., Francus, P., Zolitschka, B., Besonen, M., Lamoureux, S.F., 2012. Characteristics of sedimentary varve chronologies – A review. Quat. Sci. Rev. 43, 45–60. doi:10.1016/j.quascirev.2012.04.006

Ojala, A.E.K., Saarinen, T., 2002. Palaeosecular variation of the Earth's magnetic field during the last 10000 years based on the annually laminated sediment of Lake Nautajärvi, central Finland. The Holocene 12, 391–400. doi:10.1191/0959683602hl551rp

Ólafsdóttir, S., Geirsdóttir, Á., Miller, G.H., Stoner, J.S., Channell, J.E.T., 2013. Synchronizing holocene lacustrine and marine sediment records using paleomagnetic secular variation. Geology 41, 535–538. doi:10.1130/G33946.1

Palmer, A.P., Rose, J., Lowe, J.J., MacLeod, A., 2010. Annually resolved events of Younger Dryas glaciation in Lochaber (Glen Roy and Glen Spean), western Scottish Highlands. J. Quat. Sci. 25, 581–596. doi:10.1002/jqs.1370

Palmer, A.P., Rose, J., Lowe, J.J., Walker, M.J.C., 2008. Annually laminated Late Pleistocene sediments from Llangorse Lake, South Wales, UK: a chronology for the pattern of ice wastage. Proc. Geol. Assoc. 119, 245–258. doi:10.1016/S0016-7878(08)80304-5

Palmer, a. P., Rose, J., Rasmussen, S.O., 2012. Evidence for phase-locked changes in climate

between Scotland and Greenland during GS-1 (Younger Dryas) using micromorphology of glaciolacustrine varves from Glen Roy. Quat. Sci. Rev. 36, 114–123. doi:10.1016/j.quascirev.2011.12.003

Pennington, W., 1977. The Late Devensian flora and vegetation of Britain. Philos. Trans. R. Soc. London. B 280, 247–271. doi:Frequency based selection occurs when the relative fitness of an allele changes dependent on its frequency, and the frequency of other alleles, within the population.

Pennington, W., 1947. Studies of the Post-Glacial History of British Vegetation. VII. Lake Sediments: Pollen Diagrams from the Bottom Deposits of the North Basin of Windermere. Philos. Trans. R. Soc. Lond. B. Biol. Sci. 233, 137–175. doi:10.1098/rstb.1947.0008

Pennington, W., 1943. Lake sediments: the bottom deposits of the north basin of Windermere, with special reference to the diatom succession. New Phytol. 42, 1–27.

Pennington, W., Pearsall, W.H., 1973. Glaciation-the shaping of the landscape, in: The Lake District: A Landscape History. Collins: London.

Philippsen, B., 2013. The freshwater reservoir effect in radiocarbon dating. Herit. Sci. 1, 24. doi:10.1186/2050-7445-1-24

Pike, J., Kemp, A.E.S., 1996. Preparation and analysis techniques for studies of laminated sediments. Geol. Soc. London, Spec. Publ. 116, 37–48. doi:10.1144/GSL.SP.1996.116.01.05

Pinson, L.J.W., Vardy, M.E., Dix, J.K., Henstock, T.J., Bull, J.M., Maclachlan, S.E., 2013. Deglacial history of glacial lake windermere, UK: implications for the central British and Irish Ice Sheet. J. Quat. Sci. 28, 83–94. doi:10.1002/jqs.2595

Rasmussen, S.O., Andersen, K.K., Svensson, A.M., Steffensen, J.P., Vinther, B.M., Clausen, H.B., Siggaard-Andersen, M.L., Johnsen, S.J., Larsen, L.B., Dahl-Jensen, D., Bigler, M., Röthlisberger, R., Fischer, H., Goto-Azuma, K., Hansson, M.E., Ruth, U., 2006. A new Greenland ice core chronology for the last glacial termination. J. Geophys. Res. Atmos. 111, 1–16. doi:10.1029/2005JD006079

Rasmussen, T.L., Thomsen, E., Moros, M., 2016. North Atlantic warming during Dansgaard-Oeschger events synchronous with Antarctic warming and out-of-phase with Greenland climate. Sci. Rep. 6, 12. doi:10.1038/srep20535

Reading, H., 1996. Sedimentary environments: processes, facies and stratigraphy. Wiley-Blackwell, Malden.

Reimer, P., Bard, E., Bayliss, A., Beck, J.W., Blackwell, P.G., Buck, C.B.R.C.E., Cheng, H., Edwards, R.L., Friedrich, M., Grootes, P.M., Guilderson, T.P., Haflidason, H., Hajdas, I., Hatté, C., Heaton, T.J., Hoffmann, D.L., Hogg, A.G., Hughen, K.A., Kaiser, K.F., Kromer, B., Manning, S.W., Niu, M., Reimer, R.W., Richards, D.A., Scott, E.M., Southon, J.R., Staff, R.A., Turney, C.S.M., Plicht, J. van der, 2013. IntCal13 and Marine13 Radiocarbon Age Calibration Curves 0–50,000 Years cal BP. Radiocarbon 55, 1869–1887. doi:10.2458/azu_js_rc.55.16947

Rein, B., Jäger, K., Kocot, Y., Grimm, K., Sirocko, F., 2007. 10. Holocene and Eemian varve types of Eifel maar lake sediments. Dev. Quat. Sci. 7, 141–156. doi:10.1016/S1571-0866(07)80035-2

References

Renssen, H., Lautenschlager, M., Schuurmans, C.J.E., 1996. The atmospheric winter circulation during the Younger Dryas stadial in the Atlantic/European sector. Clim. Dyn. 12, 813–824. doi:10.1007/s003820050145

Renssen, H., Mairesse, A., Goosse, H., Mathiot, P., Heiri, O., Roche, D.M., Nisancioglu, K.H., Valdes, P.J., 2015. Multiple causes of the Younger Dryas cold period. Nat. Geosci. 8, 946–949. doi:10.1038/ngeo2557

Ribera, P., Mann, M.E., 2002. Interannual variability in the NCEP Reanalysis 1948 – 1999. Geophys. Res. Lett. 29, 10–13.

Ridge, J.C., Balco, G., Bayless, R.L., Beck, C.C., Carter, L.B., Dean, J.L., Voytek, E.B., Wei, J.H., 2012. The new north american varve chronology: A precise record of southeastern laurentide ice sheet deglaciation and climate, 18.2-12.5 KYR BP, and correlations with greenland ice core records. Am. J. Sci. 312, 685–722. doi:10.2475/07.2012.01

Ritchie, J., McHenry, J.R., 1990. Application of Radioactive Fallout Cesium-137 for Measuring Soil Erosion and Sediment Accumulation Rates and Patterns : A Review. J. Environ. Qual. 19, 215–233. doi:10.2134/jeq1990.00472425001900020006x

Rittenour, T.M., Brigham-Grette, J., Mann, M.E., 2000. El Niño-Like Climate Teleconnections in New England During the Late Pleistocene. Science (80-.). 288, 1039–1042. doi:10.1126/science.288.5468.1039

Robbins, J.A., 1978. Geochemical and geophysical applications of radioactive lead. Biogeochem. lead Environ. 285–393.

Rohling, E., Fenton, M., Jorissen, F., Bertrand, P., Ganssen, G., Caulet, J.P., 1998. Magnitudes of sea-level lowstands of the past 500,000 years. Nature 394, 162–165.

Saarinen, T., 1999. Palaeomagnetic dating of late Holocene sediments in Fennoscandia. Quat. Sci. Rev. 18, 889–897. doi:10.1016/S0277-3791(99)00003-7

Sagnotti, L., MacRì, P., Lucchi, R., Rebesco, M., Camerlenghi, A., 2012. A Holocene paleosecular variation record from the northwestern Barents Sea continental margin. Geochemistry, Geophys. Geosystems 12, 1–24. doi:10.1029/2011GC003810

Sagnotti, L., Smedile, A., De Martini, P.M., Pantosti, D., Speranza, F., Winkler, A., Carlo, P. Del, Bellucci, L.G., Gasperini, L., 2011. A continuous palaeosecular variation record of the last four millennia from the Augusta Bay (Sicily, Italy). Geophys. J. Int. 184, 191–202. doi:10.1111/j.1365-246X.2010.04860.x

Sanchez Goñi, M.F., Harrison, S.P., 2010. Millennial-scale climate variability and vegetation changes during the Last Glacial: Concepts and terminology. Quat. Sci. Rev. 29, 2823–2827. doi:10.1016/j.quascirev.2009.11.014

Schiefer, E., 2006. Contemporary sedimentation rates and depositional structures in a montane lake basin, southern Coast Mountains, British Columbia, Canada. Earth Surf. Process. Landforms 31, 1311–1324. doi:10.1002/esp

Schiefer, E., Menounos, B., Slaymaker, O., 2006. Extreme sediment delivery events recorded in the contemporary sediment record of a montane lake, southern Coast Mountains, British Columbia. Can. J. Earth Sci. 43, 1777–1790. doi:10.1139/e06-056

Schulz, M., Mudelsee, M., 2002. REDFIT: Estimating red-noise spectra directly from unevenly spaced paleoclimatic time series. Comput. Geosci. 28, 421–426.

doi:10.1016/S0098-3004(01)00044-9

Shakun, J.D., Carlson, A.E., 2010. A global perspective on Last Glacial Maximum to Holocene climate change. Quat. Sci. Rev. 29, 1801–1816. doi:10.1016/j.quascirev.2010.03.016

Shinn, R.A., Barron, E.J., 1989. Climate Sensitivity to Continental Ice Sheet Size and Configuration. J. Clim. doi:10.1175/1520-0442(1989)002<1517:CSTCIS>2.0.CO;2

Sissons, J., 1980. The Loch Lomond Advance in the Lake District, northern England. Trans. R. Soc. Edinburgh … 71, 13–27.

Smith, N.D., Ashley, G., 1985. Proglacial Lacustrine Environment, in: Ashley, G.M., Shaw, J., Smith, N.D. (Eds.), Glacial Sedimentary Environments. Society of Economic Paleontologists and Mineralogists (SEPM), pp. 135–215.

Smith, N.D., Syvitski, J.P.M., 1982. Sedimentation in a Glacier-Fed Lake: The Role of Pelletization on Deposition of Fine-Grained Suspensates. J. Sediment. Petrol. Vol. 52, 503–513.

Smith, S. V., Bradley, R.S., Abbott, M.B., 2004. A 300 year record of environmental change from Lake Tuborg, Ellesmere Island, Nunavut, Canada. J. Paleolimnol. 32, 137–148. doi:10.1023/B:JOPL.0000029431.23883.1c

Snowball, I., Sandgren, P., 2002. Geomagnetic field variations in northern Sweden during the Holocene quantified from varved lake sediments and their implications for cosmogenic nuclide production rates. The Holocene 12, 517–530. doi:10.1191/0959683602hl562rp

Snowball, I., Zillén, L., Ojala, A., Saarinen, T., Sandgren, P., 2007. FENNOSTACK and FENNORPIS: Varve dated Holocene palaeomagnetic secular variation and relative palaeointensity stacks for Fennoscandia. Earth Planet. Sci. Lett. 255, 106–116. doi:10.1016/j.epsl.2006.12.009

Southon, J., Noronha, A.L., Cheng, H., Edwards, R.L., Wang, Y., 2012. A high-resolution record of atmospheric 14C based on Hulu Cave speleothem H82. Quat. Sci. Rev. 33, 32–41. doi:10.1016/j.quascirev.2011.11.022

Steffensen, J.P., Andersen, K.K., Bigler, M., Clausen, H.B., Dahl-Jensen, D., Fischer, H., Goto-Azuma, K., Hansson, M., Johnsen, S.J., Jouzel, J., Masson-Delmotte, V., Popp, T., Rasmussen, S.O., Röthlisberger, R., Ruth, U., Stauffer, B., Siggaard-Andersen, M.-L., Sveinbjörnsdóttir, A.E., Svensson, A., White, J.W.C., 2008. High-resolution Greenland ice core data show abrupt climate change happens in few years. Science 321, 680–4. doi:10.1126/science.1157707

Stone, P., Millward, D., Young, B., Merritt, J.W., Clarke, S.M., McCormac, M., Lawrence, D.J.D., 2010. Mineralization in the Lake District, in: British Regional Geology: Northern England. British Geological Survey, Keyworth, Nottingham.

Stoner, J.S., Channell, J.E.T., Mazaud, A., Strano, S.E., Xuan, C., 2013. The influence of high-latitude flux lobes on the Holocene paleomagnetic record of IODP Site U1305 and the northern North Atlantic. Geochemistry, Geophys. Geosystems 14, 4623–4646. doi:10.1002/ggge.20272

Stoner, J.S., Jennings, A., Kristjánsdóttir, G.B., Dunhill, G., Andrews, J.T., Hardardóttir, J., 2007. A paleomagnetic approach toward refining Holocene radiocarbon-based

chronologies: Paleoceanographic records from the north Iceland (MD99-2269) and east Greenland (MD99-2322) margins. Paleoceanography 22, n/a-n/a. doi:10.1029/2006PA001285

Stuiver, M., Reimer, P.J., 1993. Extended 14C data base and revised CALIB 3.0 14C age calibration program. Radiocarbon 35, 215–230.

Taguchi, M., 2010. Observed connection of the stratospheric quasi-biennial oscillation with El Niño-Southern Oscillation in radiosonde data. J. Geophys. Res. Atmos. 115, 1–12. doi:10.1029/2010JD014325

Tauxe, L., 1993. Sedimentary records of relative paleointenstiy of the geomagnetic field: theory and practice. Rev. Geophys. 31, 319–354.

Tauxe, L., Steindorf, J.L., Harris, A., 2006. Depositional remanent magnetization: Toward an improved theoretical and experimental foundation. Earth Planet. Sci. Lett. 244, 515–529. doi:10.1016/j.epsl.2006.02.003

Thiagarajan, N., Subhas, A. V, Southon, J.R., Eiler, J.M., Adkins, J.F., 2014. Abrupt pre-Bølling-Allerød warming and circulation changes in the deep ocean. Nature 511, 75–8. doi:10.1038/nature13472

Thompson, D., Baldwin, M., Wallace, J., 2002. Stratospheric connection to Northern Hemisphere wintertime weather: Implications for prediction. J. Clim. 1421–1428.

Thompson, D.J.W., Wallace, J.M., 2001. Regional Climate impacts of the northern hemisphere annular mode. Science (80-.). 293, 85–89.

Thompson, R., Turner, G., 1979. British geomagnetic master curve 10,000-0 yr BP for dating European sediments. Geophys. Res. Lett. 6, 249–252.

Tolonen, K., Jaakkola, T., 1983. History of lake acidification and air pollution studied on sediments in South Finland. Ann. Bot. Fenn. 20, 57–78.

Tomkins, J.D., Lamoureux, S.F., Antoniades, D., Vincent, W.F., 2008. Sedimentary pellets as an ice-cover proxy in a High Arctic ice-covered lake. J. Paleolimnol. 41, 225–242. doi:10.1007/s10933-008-9255-x

Tomkins, M.D., Dortch, J.M., Hughes, P.D., 2016. Schmidt Hammer exposure dating (SHED): Establishment and implications for the retreat of the last British Ice Sheet. Quat. Geochronol. 33, 46–60. doi:10.1016/j.quageo.2016.02.002

Torrence, C., Compo, G.P., 1998. A Practical Guide to Wavelet Analysis. Bull. Am. Meteorol. Soc. 79, 61–78. doi:10.1175/1520-0477(1998)079<0061:APGTWA>2.0.CO;2

Trenberth, K.E., Shea, D.J., 2005. Relationships between precipitation and surface temperature. Geophys. Res. Lett. 32, 1–4. doi:10.1029/2005GL022760

Turner, G.M., Howarth, J.D., de Gelder, G.I.N.O., Fitzsimons, S.J., 2015. A new high-resolution record of Holocene geomagnetic secular variation from New Zealand. Earth Planet. Sci. Lett. 430, 296–307. doi:10.1016/j.epsl.2015.08.021

Turner, G.M., Thompson, R., 1982. Detransformation of the British geomagnetic secular variation record for Holocene times. Geophys. J. R. Astron. Soc. 70, 789–792. doi:10.1111/j.1365-246X.1981.tb04879.x

Turner, G.M., Thompson, R., 1981. Lake sediment record of the geomagnetic secular

variation in Britain during Holocene times. Geophys. J. Int. 65, 703–725. doi:10.1111/j.1365-246X.1981.tb04879.x

van der Hammen, T., 1951. Late-glacial flora and periglacial Phenomena in the Netherlands.

Vardy, M.E., Pinson, L.J.W., Bull, J.M., Dix, J.K., Henstock, T.J., Davis, J.W., Gutowski, M., 2010. 3D seismic imaging of buried Younger Dryas mass movement flows: Lake Windermere, UK. Geomorphology 118, 176–187. doi:10.1016/j.geomorph.2009.12.017

Vigliotti, L., 2006. Secular variation record of the Earth's magnetic field in Italy during the Holocene: Constraints for the construction of a master curve. Geophys. J. Int. 165, 414–429. doi:10.1111/j.1365-246X.2005.02785.x

Walczak, M.H., Stoner, J.S., Mix, A.C., Jaeger, J., Rosen, G.P., Channell, J.E.T., Heslop, D., Xuan, C., 2017. A 17,000 yr paleomagnetic secular variation record from the southeast Alaskan margin: Regional and global correlations. Earth Planet. Sci. Lett. 473, 177–189. doi:10.1016/j.epsl.2017.05.022

Walker, M., Johnsen, S., Rasmussen, S.O., Popp, T., Steffensen, J.-P., Gibbard, P., Hoek, W., Lowe, J., Andrews, J., Bjorck, S., Cwynar, L.C., Hughen, K., Kershaw, P., Kromer, B., Litt, T., Lowe, D.J., Nakagawa, T., Newnham, R., Schwander, J., 2009. Formal definition and dating of the GSSP (Global Stratotype Section and Point) for the base of the Holocene using the Greenland NGRIP ice core, and selected auxiliary records. J. Quat. Sci. 24, 3–17. doi:10.1002/jqs.1227

Walker, M.J.C., Coope, G.., Sheldrick, C., Turney, C.S.., Lowe, J.., Blockley, S.P.., Harkness, D.., 2003a. Devensian Lateglacial environmental changes in Britain: a multi-proxy environmental record from Llanilid, South Wales, UK. Quat. Sci. Rev. 22, 475–520. doi:10.1016/S0277-3791(02)00247-0

Walker, M.J.C., Coope, G.R., Lowe, J.J., 1993. The Devensian (Weichselian) Lateglacial palaeoenvironmental record from Gransmoor, East Yorkshire, England. A contribution to the "North Atlantic seaboard programme" of IGCP-253, "Termination of the Pleistocene." Quat. Sci. Rev. 12, 659–680. doi:10.1016/0277-3791(93)90006-8

Walker, M.J.C., Coope, G.R., Sheldrick, C., Turney, C.S.M., Lowe, J.J., Blockley, S.P.E., Harkness, D.D., 2003b. Devensian Lateglacial environmental changes in Britain : a multi-proxy environmental record from Llanilid , South Wales , UK.

Wang, Y.J., 2001. A High-Resolution Absolute-Dated Late Pleistocene Monsoon Record from Hulu Cave, China. Science (80-.). 294, 2345–2348. doi:10.1126/science.1064618

Weedon, G.P., 2003. Spectral Estimation, in: Time Series Analysis and Cyclostratigraphy Examining Stratigraphic Records of Environmental Cycles. Cambridge University Press, pp. 59–106.

Wilson, C., 1987. The outflow of Windermere, Cumbria : a re-appraisal. Geol. J. 22, 219–224.

Wilson, P., 2004. Description and implications of valley moraines in upper Eskdale, Lake District. Proc. Geol. Assoc. 115, 55–61.

Wilson, P., Clark, R., 1998. Characteristics and implications of some Loch Lomond Stadial moraine ridges and later landforms, eastern Lake District, northern England. Geol. J. 2, 73–87.

Wilson, P., Lord, T., 2014. Towards a robust deglacial chronology for the northwest England

sector of the last British-Irish Ice Sheet. North West Geogr. 14, 1–11.

Wilson, P., Lord, T., Rodés, Á., 2013. Deglaciation of the eastern Cumbria glaciokarst, northwest England, as determined by cosmogenic nuclide (10Be) surface exposure dating, and the pattern and significance of subsequent environmental changes. Cave Karst Sci. 40, 22–27.

Wohlfarth, B., 1996. The chronology of the last termination: A review of radiocarbon-dated, high-resolution terrestrial stratigraphies. Quat. Sci. Rev. 15, 267–284. doi:10.1016/0277-3791(96)00001-7

Wohlfarth, B., Muschitiello, F., L. Greenwood, S., Andersson, A., Kylander, M., Smittenberg, R.H., Steinthorsdottir, M., Watson, J., Whitehouse, N.J., 2016. Hässeldala - a key site for Last Termination climate events in northern Europe. Boreas. doi:10.1111/bor.12207

Wu, J.Y., Wang, Y.J., Cheng, H., Edwards, L.R., 2009. An exceptionally strengthened East Asian summer monsoon event between 19.9 and 17.1 ka BP recorded in a Hulu stalagmite. Sci. China, Ser. D Earth Sci. 52, 360–368. doi:10.1007/s11430-009-0031-1

Wu, Y., Li, S., Lücke, A., Wünnemann, B., Zhou, L., Reimer, P., Wang, S., 2010. Lacustrine radiocarbon reservoir ages in Co Ngoin and Zigê Tangco, central Tibetan Plateau. Quat. Int. 212, 21–25. doi:10.1016/j.quaint.2008.12.009

Xuan, C., Channell, J.E.T., 2009. UPmag: MATLAB software for viewing and processing u channel or other pass-through paleomagnetic data. Geochemistry, Geophys. Geosystems 10, 1–12. doi:10.1029/2009GC002584

Xuan, C., Channell, J.E.T., Hodell, D.A., 2016. Quaternary magnetic and oxygen isotope stratigraphy in diatom-rich sediments of the southern Gardar Drift (IODP Site U1304, North Atlantic). Quat. Sci. Rev. 142, 74–89. doi:10.1016/j.quascirev.2016.04.010

Zachos, J.C., Dickens, G.R., Zeebe, R.E., 2008. An early Cenozoic perspective on greenhouse warming and carbon-cycle dynamics. Nature 451, 279–83. doi:10.1038/nature06588

Zheng, Y., Zheng, H., Deng, C., Liu, Q., 2014. Holocene paleomagnetic secular variation from East China Sea and a PSV stack of East Asia. Phys. Earth Planet. Inter. 236, 69–78. doi:10.1016/j.pepi.2014.07.001

Zhou, W., Head, M.J., An, Z., De Deckker, P., Liu, Z., Liu, X., Lu, X., Donahue, D., Jull, A.J.T., Beck, J.W., 2001. Terrestrial evidence for a spatial structure of tropical-polar interconnections during the Younger Dryas episode. Earth Planet. Sci. Lett. 191, 231–239. doi:10.1016/S0012-821X(01)00416-2

Zhu, J., Liu, Z., Brady, E., Otto-Bliesner, B., Zhang, J., Noone, D., Tomas, R., Nusbaumer, J., Wong, T., Jahn, A., Tabor, C., 2017. Reduced ENSO variability at the LGM revealed by an isotope-enabled Earth system model. Geophys. Res. Lett. 44, 6984–6992. doi:10.1002/2017GL073406

Zolitschka, B., 2007. Varved Lake Sediments 3105–3114. doi:10.1016/B0-444-52747-8/00065-X

Zolitschka, B., 1996. Recent sedimentation in a high arctic lake, northern Ellesmere Island, Canada. J. Paleolimnol. 16, 169–186.

Zolitschka, B., Brauer, a., Negendank, J.F.W., Stockhausen, H., Lang, a., 2000. Annually

dated late Weichselian continental paleoclimate record from the Eifel, Germany. Geology 28, 783–786. doi:10.1130/0091-7613(2000)28<783:ADLWCP>2.0.CO

Zolitschka, B., Francus, P., Ojala, A.E.K., Schimmelmann, A., 2015. Varves in lake sediments – a review. Quat. Sci. Rev. 117, 1–41. doi:10.1016/j.quascirev.2015.03.019